

6. SITE 1052¹

Shipboard Scientific Party²

HOLE 1052A

Position: 29°57.0906'N, 76°37.5966'W
Date occupied: 1500 hr, 30 January 1997
Spud hole: 1800 hr, 30 January 1997
Date departed: 1200 hr, 31 January 1997
Time on hole: 21 hr (21 hr)
Seafloor (drill pipe measurement from rig floor, mbrf): 1356.0
Distance between rig floor and sea level (m): 11.5
Water depth (drill pipe measurement from sea level, m): 1344.5
Total depth (drill pipe measurement from rig floor, mbrf): 1530.5
Penetration (m): 174.5
Number of cores (including cores having no recovery): 21
Total core recovered (m): 159.63
Core recovery (%): 91.5
Oldest sediment cored:
Depth (mbsf): 174.5
Lithology: claystone
Age: late Paleocene

HOLE 1052B

Position: 29°57.0791'N, 76°37.6098'W
Date occupied: 1200 hr, 31 January 1997
Spud hole: 1300 hr, 31 January 1997
Date departed: 2045 hr, 31 January 1997
Time on hole: 8.75 hr (8 hr, 45 min)
Seafloor (drill pipe measurement from rig floor, mbrf): 1356.5
Distance between rig floor and sea level (m): 11.5
Water depth (drill pipe measurement from sea level, m): 1345.0
Total depth (drill pipe measurement from rig floor, mbrf): 1476.0
Penetration (m): 119.5
Number of cores (including cores having no recovery): 14
Total core recovered (m): 115.65
Cored section (m): 119.5
Core recovery (%): 96.8
Oldest sediment cored:
Depth (mbsf): 119.5

Lithology: nannofossil ooze with spicules
Age: middle Eocene

HOLE 1052C

Position: 29°57.0798'N, 76°37.6104'W
Date occupied: 2045 hr, 31 January 1997
Spud hole: 2115 hr, 31 January 1997
Date departed: 2200 hr, 31 January 1997
Time on hole: 1.25 hr (1 hr, 15 min)
Seafloor (drill pipe measurement from rig floor, mbrf): 1356.5
Distance between rig floor and sea level (m): 11.5
Water depth (drill pipe measurement from sea level, m): 1345.0
Total depth (drill pipe measurement from rig floor, mbrf): 1375.5
Penetration (m): 19.0
Number of cores (including cores having no recovery): 2
Total core recovered (m): 19.91
Cored section (m): 19.0
Core recovery (%): 104.8
Oldest sediment cored:
Depth (mbsf): 19.0
Lithology: nannofossil ooze
Age: early late Eocene

HOLE 1052D

Position: 29°57.0773'N, 76°37.6123'W
Date occupied: 2200 hr, 31 January 1997
Spud hole: 2215 hr, 31 January 1997
Date departed: 0200 hr, 1 February 1997
Time on hole: 4 hr (4 hr)
Seafloor (drill pipe measurement from rig floor, mbrf): 1354.0
Distance between rig floor and sea level (m): 11.5
Water depth (drill pipe measurement from sea level, m): 1342.5
Total depth (drill pipe measurement from rig floor, mbrf): 1373.0
Penetration (m): 19.0
Number of cores (including cores having no recovery): 2
Total core recovered (m): 19.41
Cored section (m): 19.0
Core recovery (%): 102.2
Oldest sediment cored:
Depth (mbsf): 19.0

¹Norris, R.D., Kroon, D., Klaus, A., et al., 1998. *Proc. ODP, Init. Repts.*, 171B: College Station, TX (Ocean Drilling Program).

²Shipboard Scientific Party is given in the list preceding the Table of Contents.

Lithology: nannofossil ooze
Age: early late Eocene

HOLE 1052E

Position: 29°57.0794'N, 76°37.6094'W
Date occupied: 0200 hr, 1 February 1997
Spud hole: 0700 hR, 1 February 1997
Date departed: 0430 hr, 6 February 1997
Time on hole: 122.5 hr (5 day, 2 hr, 30 min)
Seafloor (drill pipe measurement from rig floor, mbrf): 1355.0
Distance between rig floor and sea level (m): 11.5
Water depth (drill pipe measurement from sea level, m): 1343.5
Total depth (drill pipe measurement from rig floor, mbrf): 2039.8
Penetration (m): 684.8
Number of cores (including cores having no recovery): 58
Total core recovered (m): 327.90
Cored section (m): 544.8
Core recovery (%): 60.2
Oldest sediment cored:
 Depth (mbsf): 684.80
 Lithology: claystone with carbonate; clayey siltstone with carbonate
 Age: Albian
Comments: 0.0 to 140.0 mbsf drilled.

HOLE 1052F

Position: 29°57.0794'N, 76°37.6098'W
Date occupied: 0430 hr, 6 February 1997
Spud hole: 0930 hr, 6 February 1997
Date departed: 1930 hr, 6 February 1997
Time on hole: 15 hr (15 hr)
Seafloor (drill pipe measurement from rig floor, mbrf): 1353.5
Distance between rig floor and sea level (m): 11.5
Water depth (drill pipe measurement from sea level, m): 1342.0
Total depth (drill pipe measurement from rig floor, mbrf): 1482.0
Penetration (m): 128.5
Number of cores (including cores having no recovery): 14
Cored section (m): 128.5
Total core recovered (m): 129.12
Core recovery (%): 100.5
Oldest sediment cored:
 Depth (mbsf): 128.5
 Lithology: nannofossil ooze
 Age: middle Eocene

Principal results: Site 1052 is the shallowest site of the depth transect on the upper part of the Blake Nose. The site is presently at ~1345 meters below sea level (mbsl) and is within the depth range of modern intermediate waters. Multichannel seismic (MCS) profile Line TD-5 suggests that the lower to middle Eocene interval is substantially thinner at Site 1052 than at the deeper sites. Conversely, the upper Eocene sequence was expected to be thicker here than at the downdip sites. The principal objectives were

to extend the depth transect up the slope of the Blake Nose for studies of Eocene intermediate water structure as well as to recover a sequence of upper Eocene strata that could be used to improve the chronology of this interval. We hoped to recover a continuous upper Eocene section that might include debris from the upper Eocene tektite strewn field. In addition, the site was chosen to recover a thick Cretaceous section that was deposited at water depths as much as 1500 m shallower than those cored at Site 1049. Recovery of the Cretaceous sequence was expected to include an expanded Maastrichtian and Aptian–Albian sequence for comparison with age-equivalent strata at Site 1049. Of particular interest is the upper Aptian laminated claystone (black shale) interval that we found at Site 1049. We hoped to identify this black shale at Site 1052 and use it to study the vertical structure of the oxygen minimum zone.

Virtually all of these goals were met at Site 1052. The middle and upper Eocene section proved to have well-preserved calcareous and siliceous microfossils, a very clean magnetostratigraphic signature, clearly defined cyclostratigraphy, and no unconformities between the top of Chron 19r (~41.6 Ma) and the top of the recovered section (~35 Ma). We recovered Chron C16n.1n, in which the upper Eocene tektite strewn field is believed to occur, although we have not yet been able to identify the tektite layers. The completeness of the middle and upper Eocene section, as shown by detailed chronostratigraphy, will enable us to document the oceanic changes associated with the transition from the warm early Eocene to a cool late Eocene world in the low-latitude Atlantic Ocean. Our cores contain a thick sequence of Danian and Maastrichtian strata that include a mostly complete Cretaceous/Tertiary (K/T) boundary sequence. Drilling at the site also penetrated a thick section of lower Cenomanian and upper Albian rocks. These include laminated claystones that appear to represent low-oxygen environments near the shelf-slope break. The mid-Cretaceous section contains a diverse assortment of calcareous microfossils as well as ammonites that retain the iridescent luster of their aragonitic shells. The calcareous microfossils are extremely well preserved and are ideal for meaningful stable-isotope studies. To recover the beautifully preserved mid-Cretaceous assemblages was one of the main objectives of Leg 171B. Shore-based studies will document sea-surface and deep-water conditions during the mid-Cretaceous warm period. Our one disappointment was not recovering the updip correlative section of the upper Aptian black shale sequence found at Site 1049.

Six holes were drilled at Site 1052. We divided the section into five lithologic units based on variations in microfossil and siliciclastic content, sedimentary structures, and color. Lithologic Unit I consists mainly of nannofossil or calcareous ooze with varying amounts of foraminifers and siliceous microfossils and is subdivided into three subunits. The uppermost unit is a <5-m-thick layer of foraminifer sands and manganese nodules that is present across the entire Blake Nose transect. Foraminifers in this surficial layer range in age from Oligocene to Holocene and include substantial numbers of early and middle Miocene-aged taxa. The manganeseiferous foraminifer sands rest on pale yellow middle Eocene siliceous nannofossil ooze. As at Sites 1050 and 1051, a dramatic color change from pale yellow to light greenish gray occurs within the upper part of the Eocene ooze sequence at Site 1052. The Eocene section is generally well magnetized and contains an excellent record of cyclic variations in color and magnetic susceptibility as well as a clear magnetic polarity stratigraphy. The youngest Eocene sediments belong to Magnetochron C15r, planktonic foraminifer Zone P16, and the upper part of calcareous nannofossil Zone CP15b. There do not appear to be any substantial hiatuses within the Eocene section above Chron 19r, suggesting a long-term average sedimentation rate of about 2.6–2.8 cm/k.y.

Lithologic Unit II is divided into an ~33-m-thick interval of pale green upper lower to middle Eocene nannofossil chalk and foraminifer chalk with chert layers and chert nodules, and an ~38.4-m-thick interval composed of upper lower to middle Eocene dark greenish gray to grayish green porcellanitic calcareous claystone. Recovery in the calcareous claystones was poor, and drilling-induced fragmentation is severe throughout because of the presence of chert layers. An extremely condensed section occurs at the base of this unit, where upper Paleocene to middle Eocene

microfossils are mixed in a 5-m-thick interval of foraminifer packstones, claystones, and chert. The unconformity partly represents the updip continuation of hiatuses present in the upper Paleocene and middle Eocene sequences at Site 1051, with the addition of the updip pinch-out of all of the lower Eocene and a large part of the middle Eocene. We did not recover most of the upper Paleocene at Site 1052. We suspect that the lithified layers tended to jam in the bit and caused us to wash away the softer interbeds. Still, it is apparent that the highly condensed sections of upper Paleocene and lower Eocene rocks on the Blake Nose, such as those at Sites 1049 and 1052, tend to contain much more chert than the relatively expanded sections, such as those cored at Sites 1050 and 1051.

Lithologic Unit III is characterized by an alternation of dark greenish gray lower to upper Paleocene calcareous claystones and lighter greenish gray nannofossils with clay. The color grades downhole to light greenish gray. The top of this unit is defined at the lowest occurrence of chert, but the nature of the contact is not known because of poor recovery. The base of the unit is the K/T boundary, where the color changes from more uniform light gray to variable, mostly olive tones. All told, the Danian and lower part of the upper Paleocene are represented by nearly 100 m of section. Microfossils tend to be moderately preserved throughout most of the section, although preservation improves markedly in the lower Danian. The lowest part of the Paleocene appears to include a small portion of the early Danian planktonic foraminifer Zone P α , but the boundary ejecta bed was not recovered. However, some green spherules and quartz grains occur within burrows in the lowermost Paleocene sediment.

Lithologic Unit IV includes an 87-m-thick interval that contains mostly greenish gray to light greenish gray Maastrichtian clayey nannofossil chalk and an 89-m-thick light greenish gray Maastrichtian nannofossil chalk to nannofossil chalk with clay. The uppermost Cretaceous is present (calcareous nannofossil Zone CC26b). We suspect that only a short section of the K/T boundary was not recovered. The entire Maastrichtian section exhibits meter-scale color cycles and slump deposits. Parts of the unit are faulted; however, the faults appear to be contained within this lithologic unit because major displacements that cut across older and younger strata are not evident on MCS Line TD-5. The middle part of the Maastrichtian appears to be relatively complete and almost completely recovered. Therefore, this section should be useful for studies of the climate history and biotic turnovers associated with the middle Maastrichtian. The base of the Maastrichtian is associated with a series of slump beds that contain reworked Coniacian nannofossils and rest directly on Cenomanian limestones and interbedded siltstones.

Lithologic Unit V includes hemipelagic Cenomanian to upper Albian sediments with a greater amount of terrigenous components than the overlying sediment. The seismic profile of MCS Line TD-5 shows that the Cenomanian–Albian sequence consists of two sets of clinoforms built over, and located northeast of, a buried reef complex. The lower Cenomanian is a thin drape over a much thicker package of upper Albian clinoforms. Neither the planktonic foraminifer nor the nannofossil stratigraphy identifies a substantial unconformity between the Albian and Cenomanian rocks.

The Cenomanian includes dominant dark olive-gray calcareous silty claystone to clay-rich siltstone. The sediment color varies from olive gray to black, and the darker intervals have a greater abundance of terrigenous components. An interval of small slumps and glauconite beds separates the Cenomanian from upper Albian deposits. The Albian sequence consists of green massive claystone, alternating with dark greenish black laminated claystones. The laminated claystones are rich in pyrite and contain clay with varying amounts of calcareous nannofossils, fine-silt-sized quartz, fish remains, well-preserved ammonites, and organic debris. Total organic carbon (TOC) content is always <1 wt%, and even the darkest laminated claystones are poor source rocks because they are dominated by humic material. Indeed, gas content is uniformly extremely low throughout the rocks at Site 1052 and consists mostly of methane. Interbedded with the laminated claystones are lithified, coarser grained intervals that contain foraminifers, shallow-water limestone fragments, and quartz. The color varies from light olive gray in the limestones to dark olive gray in

the more laminated rocks. The laminated claystones are more abundant and thicker toward the top of the Albian section. Near the bottom of Hole 1052E, the Albian sequence becomes dominated by slightly to moderately bioturbated dark (dark olive-gray) sandy siltstones that are clearly of middle- or outer shelf environments. These sandstones were probably deposited near storm wave base, as suggested by the occurrence of well-sorted grainstones and structures associated with sand waves. Apparently, the entire upper Albian clinoform stack represents a deepening-upward package.

Albian and Cenomanian rocks all have normal polarities consistent with the Cretaceous Long Normal Chron C34n. Rocks of this age were generally recovered in long, coherent sections of core that allowed us to collect high-quality data on the inclinations associated with the natural remanent magnetization of the rocks. Calculation of paleolatitude from these data suggests that the Blake Nose was located at 23°N during the late Albian and early Cenomanian. These results are based on more than 700 data points and are statistically well constrained. The calculated paleolatitude is much less than the previously published estimates of North American paleolatitude of 30°N for the Blake Nose during the Hauterivian to Santonian. Apparently, previous reconstructions have placed the mid-Cretaceous North American pole ~1000 km too far south with respect to the southeastern United States.

BACKGROUND AND OBJECTIVES

Background

Site 1052 is the shallowest site of the depth transect on the upper part of the Blake Nose. The Paleogene section at Site 1052 is relatively condensed compared with the other sites. However, recovery of the Paleocene to upper Eocene section extends the depth transect into water depths of ~1345 mbsl, equivalent to the depth of modern intermediate waters. Site 1052 sediments yield calcareous microfossils that allow studies of the vertical hydrographic structure of the Paleogene oceans and, in particular, the chemistry of intermediate-water masses. The location of this site was chosen particularly to recover a thick Cretaceous section that is buried by the Cenozoic sediments at much shallower depth than at any of the other sites along the depth transect—except for Site 1049. The Cretaceous sequence includes an expanded Aptian–Albian sequence that can be compared with the age-equivalent Site 1049 sequence.

Objectives

MCS profile Line TD-5 (Fig. 3, “Introduction” chapter, back-pocket foldout, this volume) suggests that the lower to middle Eocene interval is much thinner at Site 1052 than at the deeper sites. Also, upper Eocene sediments that are present were not found at the deeper sites. Drilling at this site was expected to recover sediments that, although more condensed, are necessary to extend the depth transect up the slope of the Blake Nose in order to study Eocene intermediate-water structure. An additional goal was to recover sediments belonging to the upper Eocene that could be used to describe the timing of the onset of Antarctic glaciation and debris from the upper Eocene tektite strewn field. We believed that climate-controlled color and lithologic cycles would be pronounced at Site 1052 because of its more landward position and possibly higher clay content, compared with the deeper water sites. The lithologic cycles should provide a high-quality cyclostratigraphy that could enhance both the magneto-chronology and biochronology and improve correlation among sites along the depth transect. The correlation of the adjacent Site 1052 holes would also allow the planning of post-cruise, high-resolution sampling.

Drilling at Site 1052 provides the possibility to recover a substantial Mesozoic sequence. The MCS line suggests that the Maastrichtian–Paleocene sequence is of nearly uniform thickness across the

Blake Nose. The Maastrichtian–Paleocene sequence covers unconformably a thick Albian–Cenomanian sequence. We hoped to recover a continuous Aptian–Albian sequence and to compare its lithology with the Aptian–Albian section at Site 1049 and the Albian–Cenomanian interval at Site 1050. Of particular interest is the black shale layer of early Albian age that we recovered at Site 1049. We hoped to identify this black shale at Site 1052 and to use its distribution to examine the expansion of the oxygen minimum zone into intermediate waters.

OPERATIONS

Site 1052

After the 15-nmi transit from Site 1051, we deployed a beacon at the Global Positioning System (GPS) coordinates of Site 1052 (proposed site BN-5Alt) at 1500 hr on 30 January 1997. After assembling the advanced hydraulic piston corer/extended core barrel (APC/XCB) bottom-hole assembly (BHA) with a rebuilt polycrystalline diamond coring (PDC) XCB bit (similar to the one used at Site 1051), we ran the drill string in to 1329 meters below rig floor (mbrf).

Hole 1052A

Once the top drive was picked up and an XCB core barrel was dropped, the driller slowly lowered the bit until he made contact with the seafloor at a depth of 1356.0 mbrf (based on a reduction in drill-string weight). Cores 171B-1052A-1X and 2X were taken to 13.2 mbsf to penetrate the 5-m-thick hard surficial crust. We then initiated APC coring and proceeded to 129.7 mbsf. Cores 4H through 15H were oriented using the tensor tool. When Core 15H did not fully stroke, we switched to XCB coring. At 174.5 mbsf, we encountered a hard layer that effectively prevented further penetration with the XCB. If we wanted to penetrate any deeper at this site, we realized we would have to use the rotary core barrel (RCB) system. The drill string was then pulled out of the hole, and the bit cleared the seafloor at 1200 hr on 31 January.

Hole 1052B

We offset the ship 30 m to the southwest and spudded Hole 1052B with the XCB at 1300 hr. Based on a reduction in drill-string weight, the driller estimated the seafloor to be at 1356.5 mbrf. Because the driller did not observe the hard layer that we had found at all of the previous sites, we retrieved the XCB barrel after penetrating only to 5 mbsf. We then took APC Cores 171B-1052B-2H through 14H to 119.5 mbsf (Table 1). The bit cleared the seafloor at 2045 hr on 31 January.

Hole 1052C

Because we did not find the surficial hard layer at Hole 1052B, we felt that it was possible to take a near-mudline piston core without undue hazard to the drilling equipment. We also wanted to obtain slightly younger Eocene sediments that we suspected might contain upper Eocene tektites. Because there appeared to be local variability in the bottom topography on the precision depth recorder (PDR), we did not offset the ship. The driller observed a reduction in drill-string weight at 1356.5 mbrf and attempted an APC core at this depth. It was a full stroke that recovered nearly 10 m, so it was most likely taken below the true seafloor. A second piston core was taken from 9.5 to 19.0 mbsf. The bit cleared the seafloor at 2200 hr on 31 January.

Hole 1052D

Without offsetting the vessel, we shot the first APC core at 2215 hr, 31 January, ~2 m above the inferred mudline. Because the first core was full, we could not determine the seafloor depth by the recovery. We then took a second piston core from 9.5 to 19.0 mbsf. After recovering the second piston core, we tripped the bit to the surface to switch over to rotary coring to reach the deeper objectives at this site. The bit cleared the seafloor at 2330 hr on 31 January.

Hole 1052E

After the bit cleared the rig floor at 0200 hr on 1 February, we inspected the PDC XCB bit and found that it had lost most of its PDC cutting elements. It was returned to the Ocean Drilling Program (ODP) for refurbishing. The APC/XCB BHA was laid down and a new RCB bit (9⁷/₈-in RBI C-3) was assembled with a mechanical bit release so that we could remotely release the bit to log this hole.

We spudded Hole 1052E at 0700 hr on 1 February and drilled without coring to 140 mbsf. After we retrieved the wash barrel and a core barrel was deployed, we started rotary coring at ~1100 hr on 1 February. The RCB had no trouble penetrating the hard formation that had stymied XCB coring in Hole 1052A. However, the recovery from 140 to 252 mbsf was poor (30%) because of the interbedded hard and soft sediments. Below this interval, core recovery improved as the sediments became more homogeneous and lithified. We recovered a nearly complete K/T boundary section in Core 171B-1052E-19R (309.7–319.3 mbsf).

The K/T boundary was recovered mainly by chance. When the core barrel for Core 19R was retrieved, it was empty. The driller assumed that there was no recovery and dropped another core barrel to prepare for coring the next interval. While the core barrel was on the way down the pipe, a decision was made to drop a bit deplugger to ensure that the bit throat was clear. Before this could be done, we had to recover the core barrel that had just been dropped. When we recovered the core barrel, it contained ~1 m of core, which coincidentally turned out to contain part of the K/T boundary sequence. We then decided to drop a second core barrel, which recovered an additional ~1 m of core. We suspect that both of these sections of core fell out of the Core 171B-1052E-19R core barrel. Finally, a bit deplugger was dropped, latched in, and recovered, and we resumed RCB coring. Core recovery continued to improve with depth, and when we reached the total depth of 684.8 mbsf, the average recovery for the hole had improved to 60% (Table 1).

In preparation for logging, we circulated 20 bbl of high-viscosity mud and made a wiper trip by pulling the drill pipe up to 213 mbsf and then lowering it back to the bottom of the hole. After washing and reaming with the drill bit from 674 to 685 mbsf, we circulated another 20 bbl of mud. The bit was released, and the bottom of the drill string was raised to 222 mbsf for logging.

Once the Schlumberger equipment was rigged up, the triple-combo was run into the hole at 1045 hr on 5 February. The triple-combo was able to log from the bottom of the hole (685 mbsf) to 222 mbsf. A second logging pass was made over the section containing the K/T boundary (335–222 mbsf). The data appear to be of high quality. Caliper readings indicated good, smooth borehole conditions with the borehole diameter mostly about 10–11 in. Vessel heave was ~1 m during logging (the wireline heave compensator was not available for this leg).

We then ran the Formation MicroScanner (FMS) with the sonic tool. The FMS string was also able to log from total depth to 222 mbsf. As with the first log, a second pass was made over the K/T boundary. The deviation at the bottom of the hole was 1°. Our last

Table 1. Site 1052 coring summary.

Core, interval (cm)	Date (1997)	Time (UTC)	Depth (mbsf)	Length cored (m)	Length recovered (m)	Recovery (%)	Core, interval (cm)	Date (1997)	Time (UTC)	Depth (mbsf)	Length cored (m)	Length recovered (m)	Recovery (%)
171B-1052A-							16R	2 Feb	0350	280.90-290.50	9.6	8.22	85.60
1X	30 Jan	1845	0.00-3.50	3.5	0.86	24.60	17R	2 Feb	0500	290.50-300.10	9.6	9.85	102.60
2X	30 Jan	1930	3.50-13.20	9.7	8.48	87.40	18R	2 Feb	0555	300.10-309.70	9.6	2.69	28.00
3H	30 Jan	2005	13.20-22.70	9.5	9.48	99.80	19R	2 Feb	0900	309.70-319.30	9.6	2.08	21.70
4H	30 Jan	2045	22.70-32.20	9.5	9.92	104.40	20R	2 Feb	1000	319.30-328.90	9.6	9.87	102.80
5H	30 Jan	2120	32.20-41.70	9.5	9.79	103.10	21R	2 Feb	1100	328.90-338.60	9.7	7.29	75.20
6H	30 Jan	2155	41.70-51.20	9.5	9.72	102.30	22R	2 Feb	1210	338.60-348.30	9.7	5.41	55.80
7H	30 Jan	2230	51.20-60.70	9.5	10.00	105.30	23R	2 Feb	1310	348.30-357.90	9.6	6.45	67.20
8H	30 Jan	2305	60.70-70.20	9.5	9.71	102.20	24R	2 Feb	1430	357.90-367.50	9.6	4.70	49.00
9H	30 Jan	2335	70.20-79.70	9.5	9.66	101.70	25R	2 Feb	1540	367.50-377.10	9.6	1.39	14.50
10H	31 Jan	0020	79.70-89.20	9.5	9.67	101.80	26R	2 Feb	1705	377.10-386.70	9.6	9.94	103.50
11H	31 Jan	0055	89.20-98.70	9.5	9.87	103.90	27R	2 Feb	1810	386.70-396.30	9.6	8.68	90.40
12H	31 Jan	0130	98.70-108.20	9.5	9.54	100.40	28R	2 Feb	1900	396.30-405.90	9.6	3.86	40.20
13H	31 Jan	0200	108.20-117.70	9.5	9.72	102.30	29R	2 Feb	1955	405.90-415.50	9.6	8.65	90.10
14H	31 Jan	0230	117.70-127.20	9.5	9.92	104.40	30R	2 Feb	2055	415.50-425.10	9.6	8.75	91.10
15H	31 Jan	0305	127.20-129.70	2.5	2.49	99.60	31R	2 Feb	2225	425.10-434.70	9.6	9.88	102.90
16X	31 Jan	0400	129.70-136.00	6.3	5.27	83.70	32R	2 Feb	2315	434.70-444.30	9.6	0.00	0.00
17X	31 Jan	0500	136.00-145.70	9.7	6.49	66.90	33R	3 Feb	0115	444.30-453.90	9.6	1.65	17.20
18X	31 Jan	0530	145.70-155.30	9.6	9.08	94.60	34R	3 Feb	0220	453.90-463.60	9.7	2.08	21.40
19X	31 Jan	0645	155.30-162.90	7.6	9.08	119.50	35R	3 Feb	0310	463.60-473.20	9.6	5.08	52.90
20X	31 Jan	0845	162.90-168.40	5.5	0.52	9.5	36R	3 Feb	0455	473.20-482.80	9.6	9.36	97.50
21X	31 Jan	1035	168.40-174.50	6.1	0.36	5.90	37R	3 Feb	0645	482.80-492.40	9.6	9.66	100.60
Coring totals:				174.50	159.63	91.48	38R	3 Feb	0830	492.40-502.00	9.6	8.69	90.50
171B-1052B-							39R	3 Feb	1045	502.00-510.60	8.6	9.38	109.10
1X	31 Jan	1330	0.00-5.00	5.00	0.04	0.80	40R	3 Feb	1330	510.60-520.30	9.7	6.28	64.70
2H	31 Jan	1410	5.00-14.50	9.5	9.86	103.80	41R	3 Feb	1600	520.30-529.90	9.6	9.25	96.40
3H	31 Jan	1430	14.50-24.00	9.5	9.88	104.00	42R	3 Feb	1830	529.90-539.50	9.6	8.47	88.20
4H	31 Jan	1500	24.00-33.50	9.5	9.73	102.40	43R	3 Feb	2100	539.50-549.10	9.6	10.04	104.60
5H	31 Jan	1530	33.50-43.00	9.5	9.86	103.80	44R	3 Feb	2300	549.10-558.70	9.6	9.00	93.80
6H	31 Jan	1600	43.00-52.50	9.5	9.37	98.60	45R	4 Feb	0105	558.70-568.30	9.6	2.40	25.00
7H	31 Jan	1630	52.50-62.00	9.5	9.47	99.70	46R	4 Feb	0415	568.30-578.00	9.7	7.38	76.10
8H	31 Jan	1700	62.00-62.50	0.5	0.43	86.00	47R	4 Feb	0625	578.00-587.60	9.6	9.43	98.20
9H	31 Jan	1730	62.50-72.00	9.5	9.49	99.90	48R	4 Feb	0800	587.60-597.30	9.7	9.83	101.30
10H	31 Jan	1805	72.00-81.50	9.5	9.71	102.20	49R	4 Feb	0925	597.30-606.90	9.6	7.11	74.10
11H	31 Jan	1840	81.50-91.00	9.5	9.76	102.70	50R	4 Feb	1115	606.90-616.60	9.7	3.85	39.70
12H	31 Jan	1910	91.00-100.50	9.5	9.52	100.20	51R	4 Feb	1250	616.60-621.70	5.1	2.74	53.70
13H	31 Jan	1935	100.50-110.00	9.5	8.82	92.80	52R	4 Feb	1435	621.70-627.20	5.5	5.98	108.70
14H	31 Jan	2000	110.00-119.50	9.5	9.71	102.20	53R	4 Feb	1615	627.20-636.80	9.6	8.20	85.40
Coring totals:				119.50	115.65	96.7	54R	4 Feb	1815	636.80-646.40	9.6	3.62	37.70
171B-1052C-							55R	4 Feb	2005	646.40-656.00	9.6	9.65	100.50
1H	31 Jan	2130	0.00-9.50	9.5	9.98	105.10	56R	4 Feb	2215	656.00-665.60	9.6	1.38	14.40
2H	31 Jan	2155	9.50-19.00	9.5	9.93	104.50	57R	4 Feb	2350	665.60-675.20	9.6	9.91	103.20
Coring totals:				19.00	19.91	104.79	58R	5 Feb	0135	675.20-684.80	9.6	7.40	77.10
171B-1052D-							Coring totals:				544.80	327.90	60.19
1H	31 Jan	2230	0.00-9.50	9.5	9.51	100.10	Drilled:				140.00		
2H	31 Jan	2305	9.50-19.00	9.5	9.90	104.20	Total:				684.80		
Coring totals:				19.00	19.41	102.16	171B-1052F-						
171B-1052E-							1H	6 Feb	0940	0.00-9.50	9.50	9.43	99.30
			*****Drilled from 0.0 to 140.0 mbsf*****				2H	6 Feb	1030	9.50-19.00	9.50	9.95	104.70
1R	1 Feb	1140	140.00-146.40	6.4	2.18	34.10	3H	6 Feb	1055	19.00-28.50	9.50	10.15	106.80
2R	1 Feb	1200	146.40-156.00	9.6	1.77	18.40	4H	6 Feb	1130	28.50-38.00	9.50	9.95	104.70
3R	1 Feb	1300	156.00-165.60	9.6	3.49	36.40	5H	6 Feb	1210	38.00-47.50	9.50	9.99	105.20
4R	1 Feb	1415	165.60-175.20	9.6	0.18	1.90	6H	6 Feb	1240	47.50-57.00	9.50	9.83	103.50
5R	1 Feb	1535	175.20-184.80	9.6	0.76	7.90	7H	6 Feb	1315	57.00-66.50	9.50	6.34	66.70
6R	1 Feb	1700	184.80-194.40	9.6	0.73	7.60	8H	6 Feb	1400	66.50-76.00	9.50	9.73	102.40
7R	1 Feb	1750	194.40-204.00	9.6	0.08	0.80	9H	6 Feb	1430	76.00-81.00	5.00	5.77	115.40
8R	1 Feb	1900	204.00-213.60	9.6	6.42	66.90	10H	6 Feb	1510	81.00-90.50	9.50	9.45	99.50
9R	1 Feb	2015	213.60-223.20	9.6	2.39	24.90	11H	6 Feb	1535	90.50-100.00	9.50	9.34	98.30
10R	1 Feb	2130	223.20-232.80	9.6	7.72	80.40	12H	6 Feb	1600	100.00-109.50	9.50	9.78	102.90
11R	1 Feb	2220	232.80-242.40	9.6	2.02	21.00	13H	6 Feb	1625	109.50-119.00	9.50	9.87	103.90
12R	1 Feb	2330	242.40-252.00	9.6	5.94	61.90	14H	6 Feb	1655	119.00-128.50	9.50	9.54	100.40
13R	2 Feb	0050	252.00-261.70	9.7	4.07	42.00	Coring totals:				128.50	129.12	100.48
14R	2 Feb	0145	261.70-271.30	9.6	1.74	18.10							
15R	2 Feb	0240	271.30-280.90	9.6	2.88	30.00							

Note: An expanded version of this coring summary table that includes lengths and depths of sections and comments on sampling is included on CD-ROM (back pocket, this volume).

LITHOSTRATIGRAPHY

Description of Lithologic Units

logging run was the geological high-sensitivity magnetic tool–natural gamma-ray spectrometry tool (GHMT-NGT). The GHMT was also able to log the complete section, and a second pass was made over the K/T boundary region.

After the logging equipment was rigged down, we pulled the drill string up to 100 mbsf and displaced the hole with 35 bbl of 10.5 lb/gal mud. After retrieving the drill string, securing the drilling equipment, retrieving the beacon, and retracting the thrusters and hydrophones, we began the transit to Site 1053 at 1930 hr on 6 February.

Site 1052 is the most shoreward site of the Blake Nose depth transect (see “Operations” section, this chapter). It was drilled into a set of thick clinoforms that overlie the Lower Cretaceous carbonate platform reflectors on MCS Line TD-5 (Fig. 3, “Introduction” chapter, back-pocket foldout, this volume). Consequently, more proximal

lithofacies were anticipated than at previous Sites 1049, 1050, and 1051. Six holes were drilled at Site 1052. We divided the section into five lithologic units based on variations in microfossil and siliciclastic content, sedimentary structures, and color (Table 2; Fig. 1). Composition was estimated from smear slides (see Section 5 on CD-ROM, back pocket, this volume). The composite section for Site 1052 is 684.6 m thick (Fig. 2).

Unit I

Description: Foraminifer ooze with clay, clayey ooze with foraminifers and fish debris, manganese nodules and coatings, nannofossil or calcareous ooze with varying amounts of foraminifers and siliceous microfossils, and siliceous nannofossil ooze

Intervals: 171B-1052A-1X-1, 0 cm, through 15H-CC; 171B-1052B-1X-1, 0 cm, through 14H-CC; 171B-1052C-1H-1, 0 cm, through 2H-CC; 171B-1052D-1H-1, 0 cm, through 2H-CC; 171B-1052F-1H-1, 0 cm, through 171B-1052F-14H-CC

Depth: 0–129.7 mbsf, Hole 1052A; 0–119.5 mbsf, Hole 1052B; 0–19.0 mbsf, Hole 1052C; 0–19.0 mbsf, Hole 1052D; 0–128.5 mbsf, Hole 1052F

Thickness: 129.7 m, Hole 1052A; 119.5 m, Hole 1052B; 19.0 m, Hole 1052C; 19.0 m, Hole 1052D; 128.5 m, Hole 1052F

Age: Pleistocene to middle Eocene

Lithologic Unit I is divided into three subunits. The uppermost, Subunit IA, is a <5-m-thick layer with Mn nodules similar to sediments at Sites 1049, 1050, and 1051, which were also assigned to Subunit IA. Subunit IB is ~22 m thick and is composed of pale yellow middle Eocene nannofossil ooze with varying amounts of foraminifers and siliceous microfossils. As at Sites 1050 and 1051, a distinctive color change from pale yellow to light greenish gray marks the top of Subunit IC in Sections 171B-1052A-4H-4, 51 cm, and 171B-1052B-4H-2, 148 cm. Subunit IC is ~102 m thick and consists of nannofossil ooze to siliceous nannofossil ooze. Site 1052 contains no equivalent to the chalk that was designated Subunit ID at Site 1051.

Subunit IA

Description: Calcareous ooze with foraminifers, foraminifer ooze with clay nannofossil foraminifer ooze, clayey ooze with foraminifers and fish debris, and Mn nodules

Intervals: 171B-1052A-1X-1, 0 cm, to 2X-2, 128 cm; 171B-1052B-1X-1, 0 cm, to 2H-1, 49 cm; 171B-1052C-1H-1, 0–52 cm; 171B-1052D-1H-1, 0–80 cm; 171B-1052F-1H-1, 0–70 cm

Depth: 0–4.8 mbsf, Hole 1052A; 0–5.5 mbsf, Hole 1052B; 0–0.5 mbsf, Hole 1052C; 0–0.8 mbsf, Hole 1052D; 0–0.70 cm, Hole 1052F

Thickness: 4.8 m, Hole 1052A; 5.5 m, Hole 1052B; 0.5 m, Hole 1052C; 0.8 m, Hole 1052D; 0.7 m, Hole 1052F

Age: ?Pleistocene

Subunit IA is composed primarily of a very pale brown (10YR 8/2) calcareous ooze with clay, foraminifers, and nannofossil foraminifer ooze. This ooze contains numerous indurated carbonate nodules with thin Mn coatings on their upper surfaces, representing periods of nondeposition on the seafloor. In addition, Subunit IA contains a drilling slurry of light brownish gray (10YR 6/2) clayey ooze with foraminifers and fish debris (scales, vertebrae, and unspecified phosphatic debris), isolated Mn nodules ~5 cm in diameter, and yellow (10YR 8/8) foraminifer ooze with nannofossils (Fig. 3). Subunit IA most likely corresponds to the Mn oxide layer recovered at the top of Sites 1049, 1050, and 1051, where it was also designated as lithologic Subunit IA. The base of Subunit IA is placed at the first downhole occurrence of pale yellow nannofossil ooze.

Subunit IB

Description: Nannofossil ooze with varying amounts of foraminifers and siliceous microfossils to siliceous nannofossil ooze

Intervals: 171B-1052A-2H-2, 128 cm, to 4H-4, 51 cm; 171B-1052B-2H-1, 49 cm, to 4H-2, 148 cm; 171B-1052C-1H-1, 52 cm, through

2H-CC; 171B-1052D-1H-1, 80 cm, through 2H-CC; 171B-1052F-1H-1, 70 cm, to 4H-1, 59 cm

Depth: 4.8–27.7 mbsf, Hole 1052A; 5.5–26.7 mbsf, Hole 1052B; 0.5–19.0 mbsf, Hole 1052C; 0.8–19.0 mbsf, Hole 1052D; 0.7–29.1 mbsf, Hole 1052F

Thickness: 22.9 m, Hole 1052A; 21.2 m, Hole 1052B; 18.5 m, Hole 1052C; 18.2 m, Hole 1052D; 28.4 m, Hole 1052F

Age: middle Eocene

Subunit IB is a middle Eocene nannofossil ooze with siliceous microfossils (diatoms, radiolarians, and sponge spicules) to siliceous nannofossil ooze. The base of lithologic Subunit IB is defined by a sharp change in color from pale yellow (5Y 8/1–8/2) to the light greenish gray (5G 8/1 to 10GY 8/1) of the underlying lithologic Subunit IC. In general, bedding is poorly defined, and the sediment appears homogeneous. Burrow-mottled intervals occur sporadically. Pyrite flecks are disseminated throughout the sediment. Drilling slurry occurs in the upper few centimeters of most cores; otherwise, lithologic Subunit IB sediment has been only slightly disturbed by drilling.

Nine ash layers occur in Subunit IB, and their depths are listed in Table 3.

Subunit IC

Description: Nannofossil ooze to nannofossil ooze with siliceous microfossils to siliceous nannofossil ooze

Intervals: 171B-1052A-4H-4, 51 cm, through 15H-CC; 171B-1052B-4H-2, 148 cm, through 14H-CC; 171B-1052F-4H-1, 59 cm through 14H-CC.

Depth: 27.7–129.7 mbsf, Hole 1052A; 26.7–119.5 mbsf, Hole 1052B; 29.1–128.5 mbsf, Hole 1052F

Thickness: 102.0 m, Hole 1052A; 92.8 m, Hole 1052B; 100.1 m, Hole 1052F

Age: middle Eocene

The top of Subunit IC is defined by a sharp color change from the overlying pale yellow (5Y 8/1–8/2) Subunit IB sediment to the varying shades of greenish gray (5G 8/1 to 10GY 8/1) sediment of Subunit IC. The darker greenish gray sediment is slightly richer in siliceous microfossils, whereas the lighter greenish gray sediment is richer in calcareous material. Subunit IC contains middle Eocene nannofossil ooze, siliceous nannofossil ooze, and calcareous chalk. The sediment is slightly to moderately bioturbated; burrows include *Zoophycos* and undifferentiated burrows. Pyrite occurs as flecks, burrow linings, and burrow fill throughout. The sediment remains a soft ooze to the base of the unit, except for 5- to 10-cm-thick hard, generally evenly spaced, calcareous chalk beds that occur through an ~7-m interval at ~60 mbsf in Holes 1052A, 1052B, and 1052F (Fig. 4). This interval is characterized by reduced recovery and drilling disturbance. Eighteen ash layers occur in Subunit IC and are listed in Table 3. The lower boundary of Subunit IC is placed at the first downhole occurrence of chert.

Unit II

Description: Nannofossil chalk and foraminifer chalk with chert layers and porcellanitic calcareous claystone

Intervals: 171B-1052A-16X-1, 0 cm, through 21X-CC; 171B-1052E-1R-1, 0 cm, to 7R-CC, 8 cm.

Depth: 129.7–174.5 mbsf, Hole 1052A; 140.0–204.0 mbsf, Hole 1052E

Thickness: 44.8 m, Hole 1052A (base of unit not recovered); 64.0 m, Hole 1052E (top of unit not recovered)

Age: middle Eocene to late Paleocene

Lithologic Unit II is compositionally similar to the overlying unit but differs by being more lithified and containing chert. It is divided into two subunits. The upper Subunit IIA is an ~33-m-thick interval with very pale green (10GY 8/1) nannofossil chalk and foraminifer chalk with chert layers and chert nodules. Subunit IIB is ~38.4 m

Table 2. Summary of lithologic units from the six holes drilled at Site 1052.

Lithologic unit/ subunit	Hole 1052A	Hole 1052B	Hole 1052C	Hole 1052D	Hole 1052E	Hole 1052F	Age	Lithology
IA	Interval 1X-1, 0 cm, to 2X-2, 128 cm 0-4.78 mbsf	Interval 1X-1, 0-4 cm 0-5.49 mbsf	Interval 1H-1 0-52 cm 0-0.8 mbsf	Interval 1H-1 0-80 cm 0-0.8 mbsf	Drilled without coring	Interval 1H-1, 0-70 cm 0-0.7 mbsf	Pleistocene? to late Eocene	Mn oxide nodules; calcareous ooze with foraminifers; foraminifer ooze with clay; clayey ooze with foraminifers and fish debris
IB	Interval 2X-2, 128 cm, to 4H-4, 51 cm 4.78-27.7 mbsf	Interval 2H-1, 49 cm, to 4H-2, 148 cm 5.49-26.68 mbsf	Interval 1H-1, 52 cm, to 2H-CC 0.52-19.0 mbsf	Interval 1H-1, 80 cm, to 2H-CC 0.8-19.0 mbsf	Drilled without coring	Interval 1H-1, 70 cm, to 4H-1, 59 cm 0.7-29.09 mbsf	late Eocene	Nannofossil ooze with siliceous microfossils to siliceous nannofossil ooze
IC	Interval 4H-4, 51 cm, to 15H-CC 27.7-129.7 mbsf	Interval 4H-2, 148 cm, to 14H-CC 26.68-119.5 mbsf	Not recovered (end of hole)	Not recovered (end of hole)	Drilled without coring		late to middle Eocene	Nannofossil ooze to siliceous nannofossil ooze
IIA	Interval 16X-1, 0 cm, to 19X-CC 129.7-162.9 mbsf	Not recovered (end of hole)			Interval 1R-1, 0 cm, to 3R-CC 140.0-165.6 mbsf	Not recovered (end of hole)	middle Eocene	Nannofossil and foraminifer chalk with chert layers and nodules; zeolitic nannofossil chalk
IIB	Interval 20X-1, 0 cm, to 21X-CC 162.9-174.5 mbsf				Interval 4R-1, 0 cm, to 7R-CC 165.6-204.0 mbsf		middle to early Eocene	Porcellanitic calcareous claystone, cherty claystone, claystone
III	Not recovered (end of hole)				Interval 8R-1, 0 cm, to 17R-CC 204.0-301.6 mbsf		late to early Paleocene	Nannofossil claystone; calcareous claystone with zeolite; nannofossil, foraminifer, and calcareous chalk with clay
IVA					Interval 18R-3 0 cm, to 27R-2, 38 cm 301.6-388.6 mbsf		late Maastrichtian	Clayey nannofossil chalk; nannofossil chalk with clay
IVB					Interval 27R-2, 38 cm, to 36R-3, 122 cm 388.6-477.4 mbsf		late Maastrichtian	Nannofossil chalk; nannofossil chalk with clay
VA					Interval 36R-3, 122 cm, to 40R-1, 124 cm 477.4-511.8 mbsf		Cenomanian to late Albian	Silty claystone; clayey siltstone with nannofossils
VB					Interval 40R-1, 124 cm, to 53R-5, 30 cm 511.8-633.5 mbsf		late Albian	Laminated black shale; clayey limestone with foraminifers and quartz; silty claystone
VC					Interval 53R-5, 30 cm, to 58R-CC, 20 cm 633.5-684.6 mbsf		late Albian	Clayey siltstone; silty claystone; siltstone with carbonate grains; bioclastic and lithic grainstone

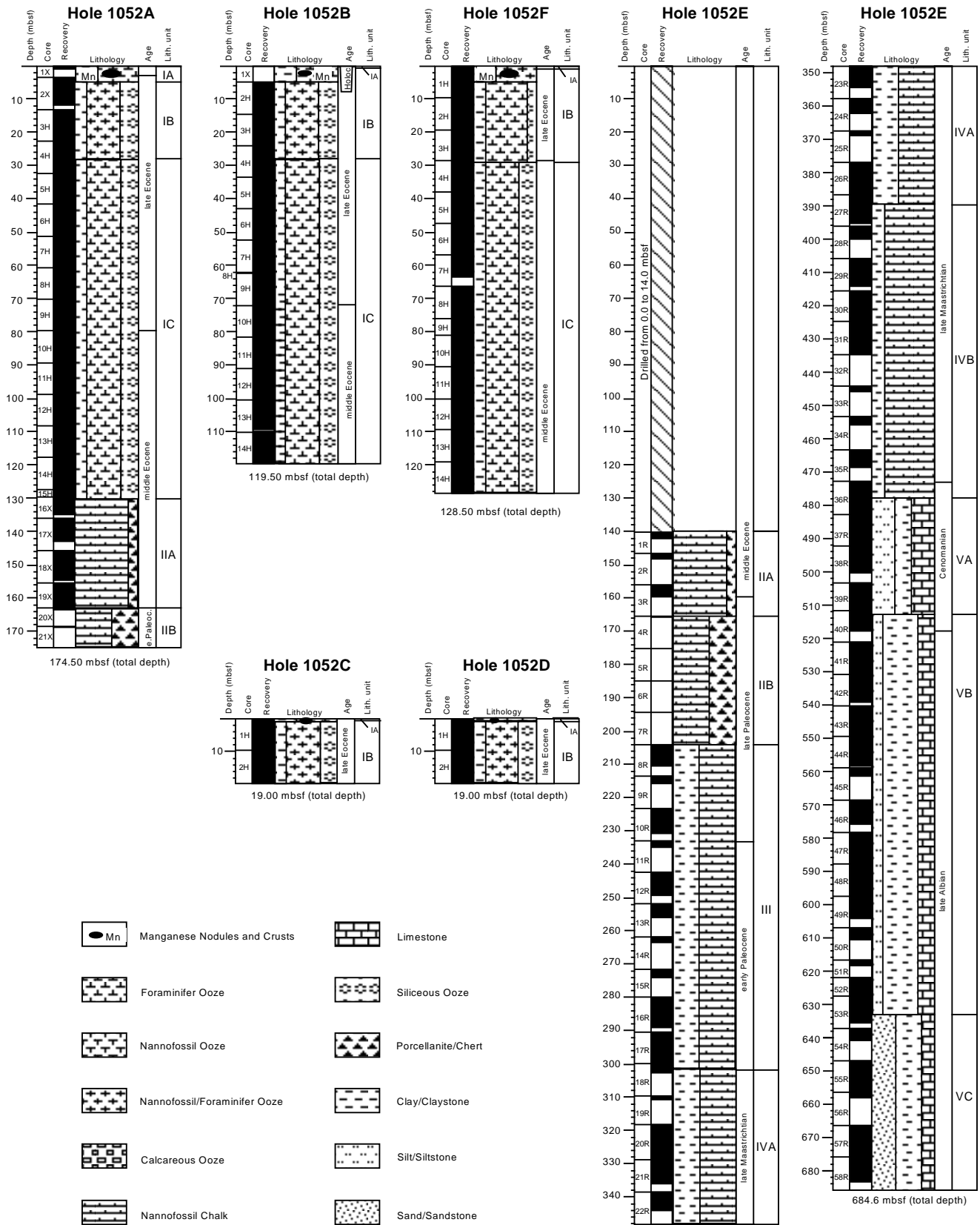


Figure 1. Summary of lithology, core recovery, and age for sediment recovered from the six holes (1052A–1052F) at Site 1052.

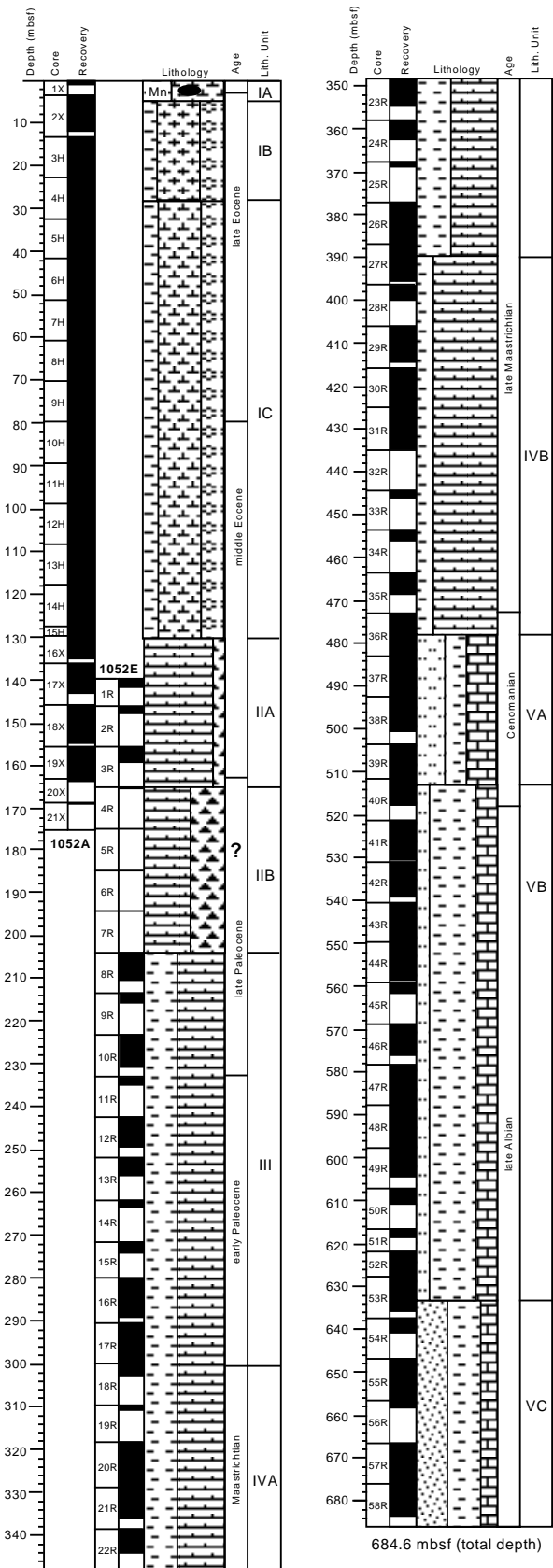


Figure 2. Composite section from Holes 1052A and 1052E. Symbols are the same as in Figure 1.

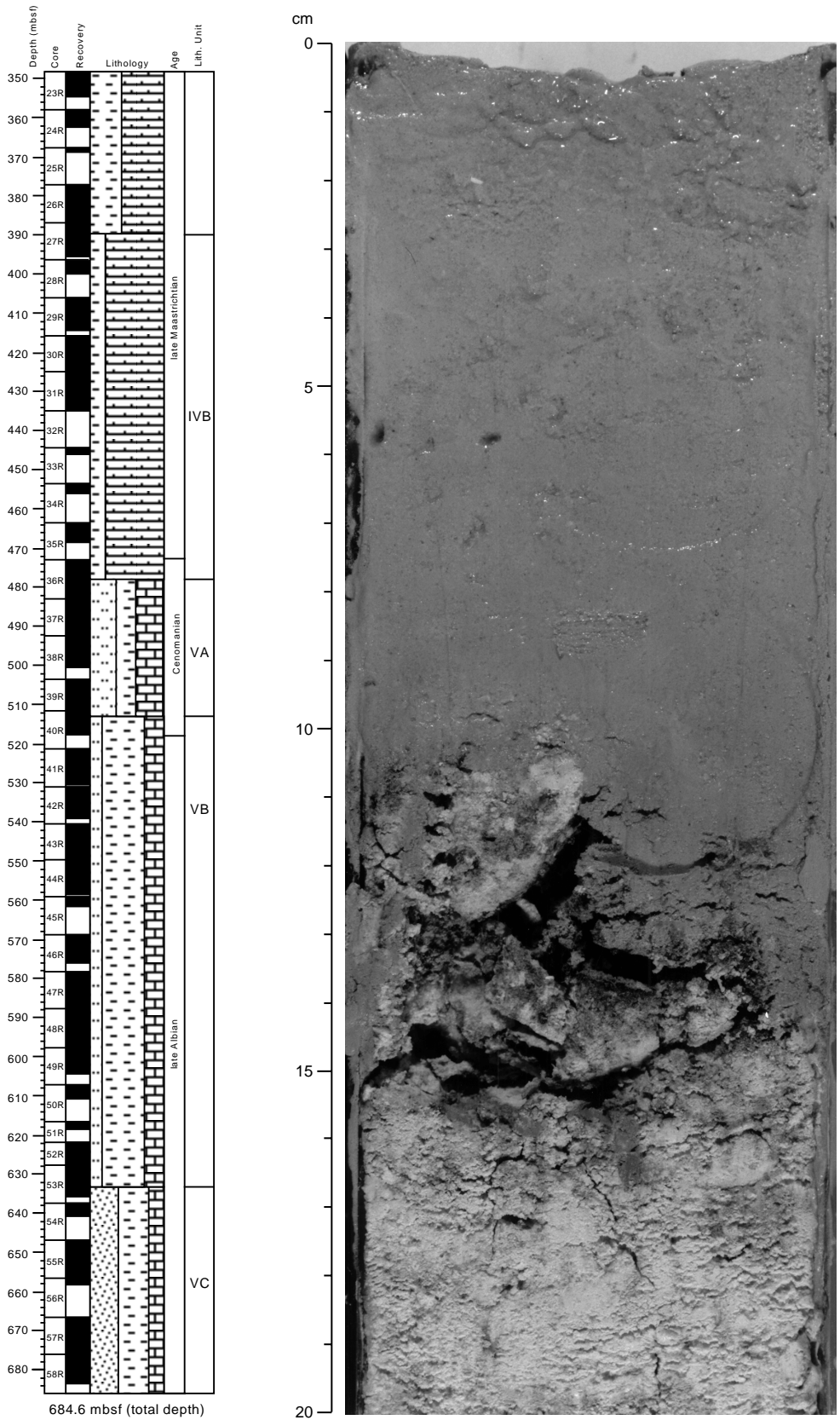


Figure 3. Interval 171B-1052A-2X-1, 0–20 cm. Drilling slurry of brownish clayey ooze with foraminifers and fish debris overlies a partly indurated, pale yellow calcareous ooze with clay in lithologic Subunit IA.

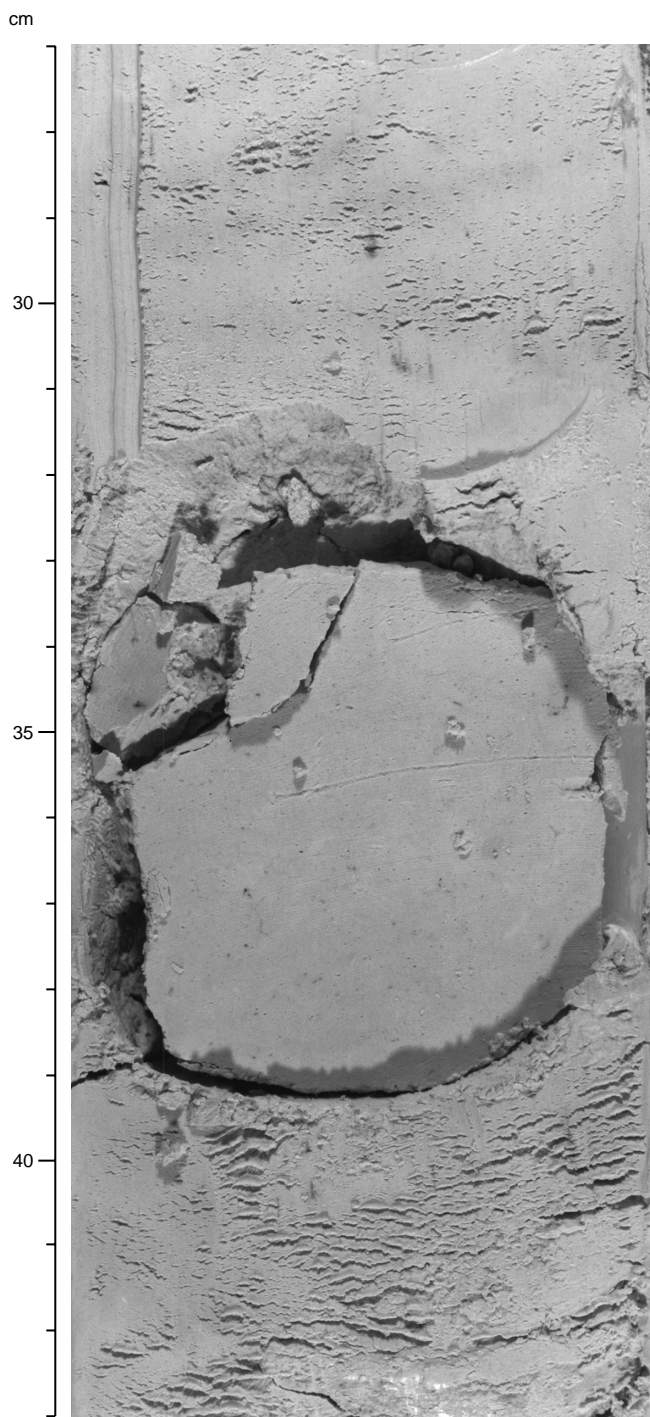


Figure 4. Interval 171B-1052A-7H-4, 27–43 cm. Piece of calcareous chalk with nannofossils in calcareous nannofossil ooze with foraminifers. At least five chalk layers occur over the same 7-m interval in lithologic Subunit IC in Holes 1052A, 1052B, and 1052F.

thick and contains more chert than the overlying subunit. It is composed of dark greenish gray to grayish green (5GY 6/1 to 5GY 5/1) porcellanitic calcareous claystone.

Subunit IIA

Description: Nannofossil chalk and foraminifer chalk with chert layer and nodules and zeolitic nannofossil chalk

Table 3. Ash layers recovered at Site 1052.

Core, section, interval (cm)	Depth (mbsf)	Lithologic subunit	
171B-1052A-3H-5, 78	19.8		
3H-CC, 5	23.6		
171B-1052B-2H-3, 88-91	8.9		
2H5, 63-68	11.65		
3H-4, 90-95	19.9-19.95		
3H-7, 25-27	23.75-23.77		
171B-1052C-2H-1, 84-90	10.34-10.36	IB	
171B-1052F-2H-4, 13-16	14.13-14.16		
3H-3, 65-67	22.65-22.67		
4H-1, 124-125	29.74-29.75		
5H-3, 69-73	41.63-41.73		
8H-3, 85	70.35		
8H-5, 78	73.28		
10H-5, 19	87.19		
11H-6, 92-101	98.29-99.01		
171B-1052A-4H-5, 6	28.76		IC
5H-5, 59	38.79		
6H-6, 62	49.8		
8H-5, 95-97	67.65		
10H-4, 70-71	84.9-84.91		
11H-5, 101-108	96.21-96.28		
171B-1052B-4H-3, 87	27.87		
6H-6, 54	51.04		
9H-3, 109	66.59		
9H-5, 87	69.37		
11H-2, 32-33	83.32-83.33		
12H-3, 71-76	94.71-94.76		
171B-1052E-13R-3, 4-5	255.04-255.05	III	

Intervals: 171B-1052A-16X-1, 0 cm, through 19X-CC; 171B-1052E-1R-1, 0 cm, through 3R-CC
 Depth: 129.7–162.9 mbsf, Hole 1052A; 140.0–165.6 mbsf, Hole 1052E
 Thickness: 33.2 m, Hole 1052A; 25.6 m, Hole 1052E
 Age: late early Eocene to middle Eocene

The top of lithologic Subunit IIA is placed at the first downhole occurrence of chert. The dominant lithology in Subunit IIA is a pale green (10GY 8/1) nannofossil chalk with foraminifers that grades downhole into a foraminifer chalk with zeolite. Some intervals, ranging from a few millimeters to 1.5 m in thickness, are highly enriched in calcispheres. Drilling-induced biscuiting and fragmentation of the cores are common throughout Subunit IIA. Bioturbation varies from slight to moderate. Hardgrounds and/or firmgrounds were found at Sections 171B-1052A-18X-4, 10 cm (150.30 mbsf), and 171B-1052E-2R-1, 85 cm (147.25 mbsf; Fig. 5).

Subunit IIB

Description: Porcellanitic calcareous claystone, cherty claystone, and claystone
 Intervals: 171B-1052A-20X-1, 0 cm, through 21X-CC; 171B-1052E-4R-1, 0 cm, through 7R-CC
 Depth: 162.9–174.5 mbsf, Hole 1052A; 165.6–204.0 mbsf, Hole 1052E
 Thickness: 11.6 m, Hole 1052A; 38.4 m, Hole 1052E
 Age: late early Eocene to middle Eocene

The dominant lithology in Subunit IIB is a greenish gray (10GY 5/1) porcellanite calcareous claystone that grades into cherty claystone and chert. Recovery in Subunit IIB was poor, and drilling-induced fragmentation is severe throughout. The base of Subunit IIB was not recovered from Hole 1052A. In Hole 1052E, the base of this subunit is placed at the transition to claystone.

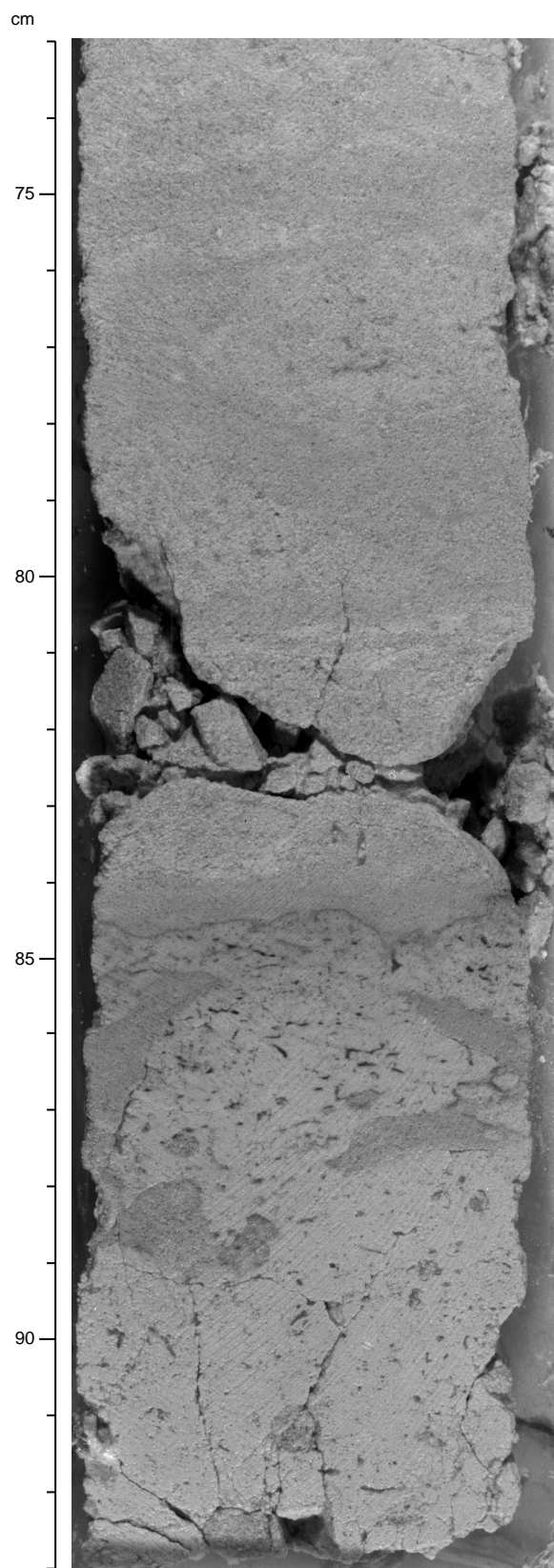


Figure 5. Interval 171B-1052E-2R-1, 73–93 cm. Greenish hardground with borings in white foraminifer chalk in lithologic Subunit IIA. Burrows extend down to 92 cm and are filled with coarser grained, dark green sediment.

Unit III

Description: Nannofossil claystone and calcareous claystone with zeolite, calcareous claystone, nannofossil and calcareous chalk with clay, and foraminifer chalk

Interval: 171B-1052E-8R-1, 0 cm, to 18R-2, 58 cm

Depth: 204.0–301.6 mbsf, Hole 1052E

Thickness: 97.6 m, Hole 1052E

Age: early to late Paleocene

Lithologic Unit III is characterized by an alternation of dark greenish gray (5GY 5/1 to 5GY 4/1) calcareous claystones and lighter greenish gray (5GY 6/1) nannofossils with clay. The color grades downhole into light greenish gray (10Y 7/1). The scale of alternation varies from centimeters to meters. The top of this unit is defined at the lowest occurrence of chert, but the nature of the contact is not known because of poor recovery. The base of the unit is the K/T boundary (Fig. 6), where the color changes from uniform light gray in the Paleocene sediment to variable, mostly olive tones in the Maastrichtian. The K/T boundary ejecta layer was not recovered at Site 1052, although some green spherules and quartz grains occur within burrows in lowermost Paleocene sediment of interval 171B-1052E-18R-2, 52–58 cm. The whole of lithologic Unit III is thoroughly burrowed with common, pyrite-lined *Chondrites*, *Planolites*, and *Zoophycos*. Only one altered ash layer was recovered at 255.04–255.05 mbsf. The uppermost interval in this unit is zeolite rich and alternates on a centimeter scale with dark intervals richer in zeolite and pyrite. Carbonate content increases downhole (see “Organic Geochemistry” section, this chapter). Some soft-sediment deformation by slumping and debris flow occurs in intervals 171B-1052E-16R-5, 111–150 cm, and 16R-6, 0–20 cm (Fig. 7). Drilling disturbance is slight, with limited fragmentation and biscuiting.

Unit IV

Description: Clayey nannofossil chalk, nannofossil chalk with clay, and nannofossil chalk

Interval: 171B-1052E-18R-3, 0 cm, to 36R-3, 122 cm

Depth: 301.6–477.4 mbsf, Hole 1052E

Thickness: 175.8 m, Hole 1052E

Age: Maastrichtian.

Lithologic Unit IV is divided into two subunits. Subunit IVA is an ~87-m-thick interval that contains mostly greenish gray (5GY 6/1) to light greenish gray (10GY 7/1) clayey nannofossil chalk and nannofossil chalk with clay. Subunit IVB is ~89 m thick and contains mostly light greenish gray (5Y 7/1 to 5GY 7/1) to very light greenish gray (5GY 8/1) nannofossil chalk to nannofossil chalk with clay. Both subunits exhibit meter-scale alternations between darker and lighter sediment and contain meter-scale slump deposits. The upper contact of Unit IV is placed at the K/T boundary, and the lower contact is placed at the base of a slump that separates Maastrichtian chalk from Cenomanian limestone with interbedded siltstone.

Subunit IVA

Description: Clayey nannofossil chalk and nannofossil chalk with clay

Interval: 171B-1052E-18R-3, 0 cm, to 27R-2, 38 cm

Depth: 301.6–388.6 mbsf, Hole 1052E

Thickness: 87.0 m, Hole 1052E

Age: late Maastrichtian

Greenish gray (5GY 6/1) to light greenish gray (10GY 7/1) nannofossil chalk with clay to clayey nannofossil chalk with meter-scale alternations between lighter (relatively carbonate-rich) and darker (relatively carbonate-poor) intervals form most of Subunit IVA. Color transitions are gradational, and pyrite occurs throughout. The abundance of clay minerals estimated from smear slides is greater than carbonate measurements support (Section 5 on CD-ROM, back pocket,

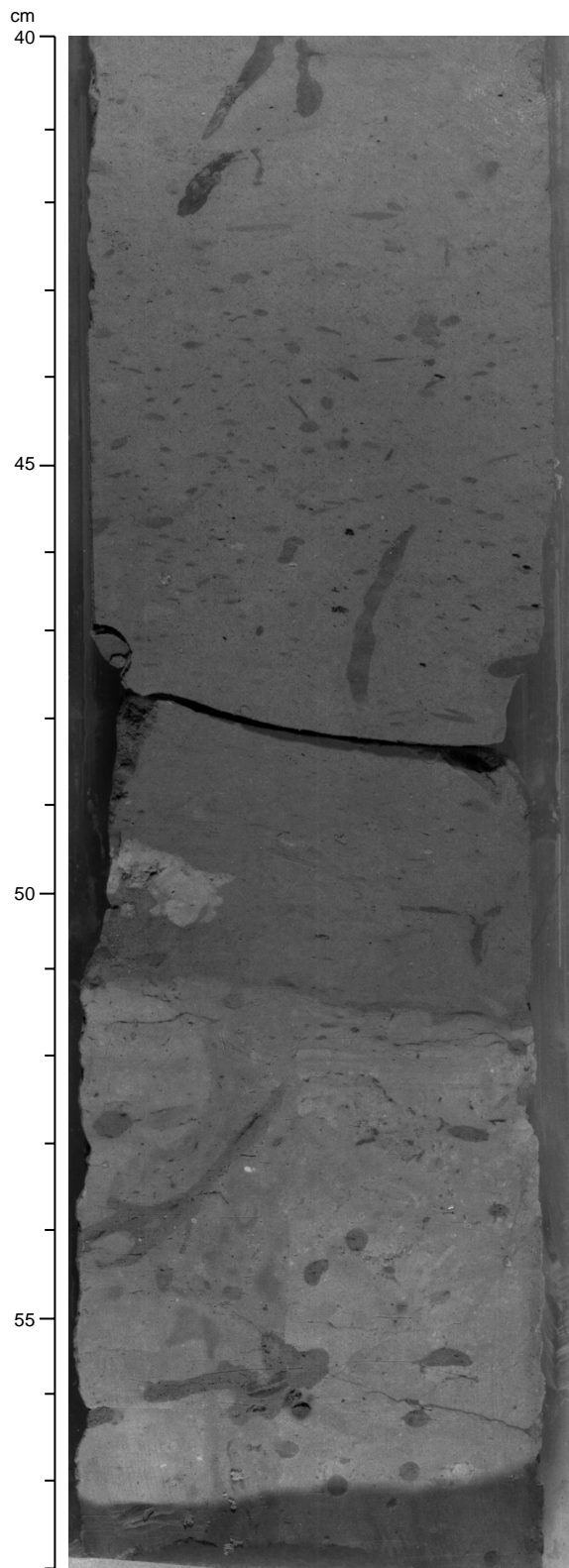


Figure 6. Close-up photo of interval 171B-1052-18R-2, 40–58 cm. Light-colored bed at 51–58 cm contains earliest Paleocene planktonic foraminifers and nanofossils, as well as green spherules in burrow fillings.

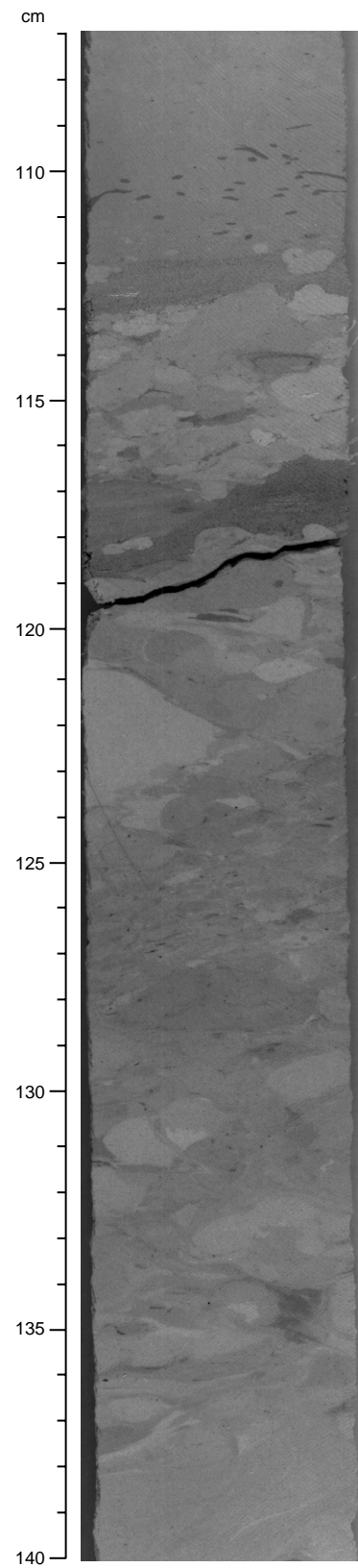


Figure 7. Interval 171B-1052E-16R-5, 107–140 cm. An intraformational soft-mud-cobble conglomerate at 111–136 cm, is underlain by slumped nanofossil claystone in interval 16R-6, 0–20 cm, in lithologic Unit III.

this volume; also see “Organic Geochemistry” section, this chapter), suggesting that much of the clay-sized components found in smear slides is carbonate, rather than phyllosilicates. Drilling disturbance is limited to biscuiting and slight fragmentation, but faulting along slickensided surfaces is common. Recovery was poor in the upper portion of the subunit. Sediments range from laminated to heavily bioturbated, with moderately to heavily bioturbated intervals predominating. Identified traces are *Zoophycos*, *Teichichnus*, *Planolites*, *Chondrites*, and *Phycoides*. In Core 171B-1052E-21R, *Chondrites* and *Phycoides* seem to occur preferentially in light intervals. However, it is not clear to what extent bioturbation varies systematically between light and dark intervals. Foraminifer packstone occurs in intervals 171B-1052E-23R-1, 0–150 cm, and Sections 23R-3, 123 cm, to 23R-4, 80 cm. A fold is centered at Section 23R-1, 50 cm (Fig. 8), suggesting that the limestone in which it occurs is a slump deposit. The lower limestone contains ripple cross-lamination, planar bedding, and glauconitic rip-up clasts. It may have been formed through current reworking.

The K/T boundary (Section 171B-1052E-18R-2, 0 cm; 301.6 mbsf) separates the relatively uniform gray clayey chinks of Subunit IVA from the more variable olive chinks and claystones of lithologic Unit III (Fig. 6). Part of the K/T boundary sequence may have been lost because of poor recovery in the top of the Cretaceous section (Cores 19R and 20R, ~305–320 mbsf). Logging results suggest a gradational change over this interval punctuated by a sharp, negative inflection in gamma ray, weight percent potassium, and magnetic susceptibility at the boundary. The presence of spherules in burrows within the basal Paleocene suggests that the ejecta bed may be present at Site 1052 but was not recovered. Alternatively, the inflection in the logs could record the somewhat granular green chalk present in Section 171B-1052E-18R-3 (see “Downhole Logging” section, this chapter).

The base of Subunit IVA is placed at the top of an 83-cm-thick, generally homogeneous, light gray bed (interval 27R-2, 40–123 cm) with a sharp upper contact and several tiers of burrows that extend through the bed and into the underlying sediment. Many of the burrows are filled with green sediment piped in from the overlying unit (Figs. 8–10). The burrowed bed occurs immediately above a 2.5-m-thick slump deposit (Fig. 9C, D) to which it may be genetically related (see “Discussion,” this section).

Subunit IVB

Description: Nannofossil chalk to nannofossil chalk with clay
Interval: 171B-1052E-27R-2, 38 cm, to 36R-3, 122 cm
Depth: 388.6–477.4 mbsf, Hole 1052E
Thickness: 88.8 m, Hole 1052E
Age: early–late Maastrichtian.

Subunit IVB is dominated by light greenish gray (5Y 7/1 to 5GY 7/1) to very light greenish gray (5GY 8/1) nannofossil chalk to nannofossil chalk with clay. Subunit IVB has many similarities with Subunit IVA, including subtle meter-scale alternations between lighter (relatively carbonate-rich) and darker (relatively carbonate-poor) intervals, fabrics that range from laminated to heavily burrow mottled by the same types of traces, pyrite throughout, and only slight drilling disturbance despite variable recovery. Differences between Subunits IVB and IVA are that Subunit IVB is generally lighter in color and more carbonate rich; laminated to slightly bioturbated intervals constitute >50% of the recovered sediment, rather than being a minor fabric as in Subunit IVA; inoceramid shell fragments are repeatedly observed in Subunit IVB but are not seen in Subunit IVA; slickensided fault planes are largely absent in Subunit IVB; and apparent slump deposits are more common in Subunit IVB than in Subunit IVA, with beds of redeposited material occupying intervals 171B-1052E-27R-2, 123 cm, to 27R-4, 100 cm; 29R-2, 75–149 cm; 31R-2, 17–47 cm; 33R-1, 105 cm, to 33R-2, 11 cm; 33R-2, 60 cm, to 34R-1, 109 cm; and 36-1, 52–135 cm.

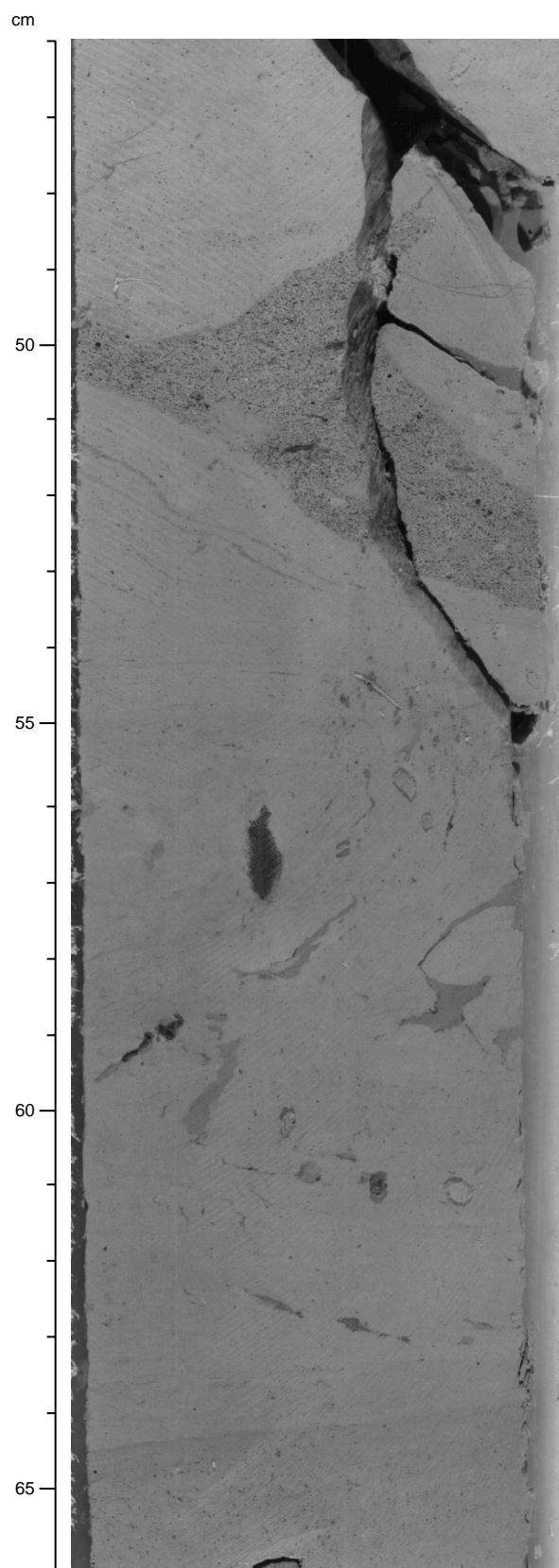


Figure 8. Interval 171B-1052E-23R-1, 46–66 cm. Sediment deformation by slumping in lithologic Subunit IVA has a fold axis centered at Section 23R-1, 50 cm, and affects the sediment throughout the interval.

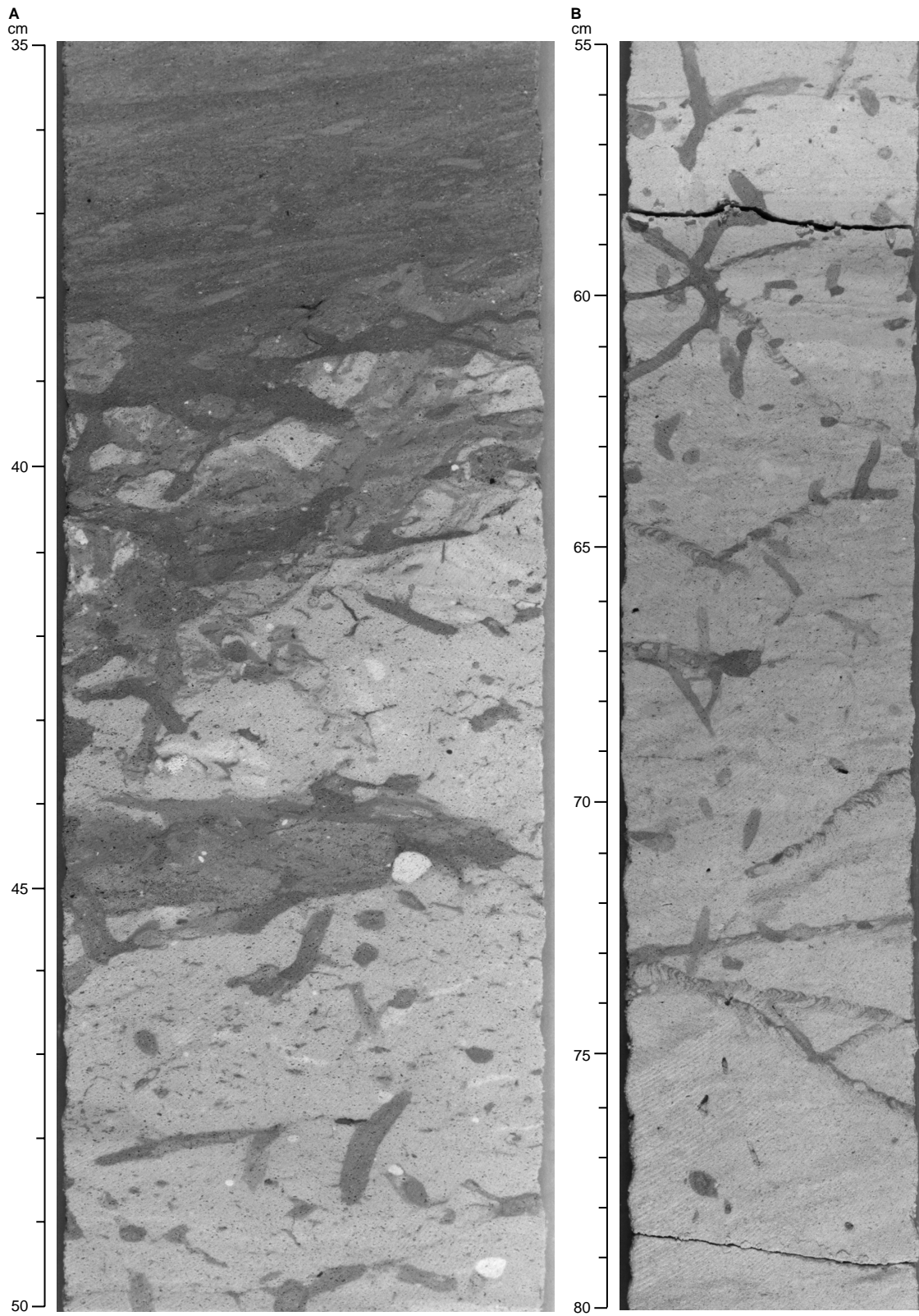


Figure 9. **A.** Interval 171B-1052E-27R-1, 35–50 cm. Contact between Subunits IVA and IVB in Section 27R-2, 40 cm. **B.** Interval 171B-1052E-27R-1, 55–80 cm. In the bed below the contact shown in A, *Planolites* is concentrated in the upper part, whereas *Zoophycos* burrows are concentrated in the lower part.

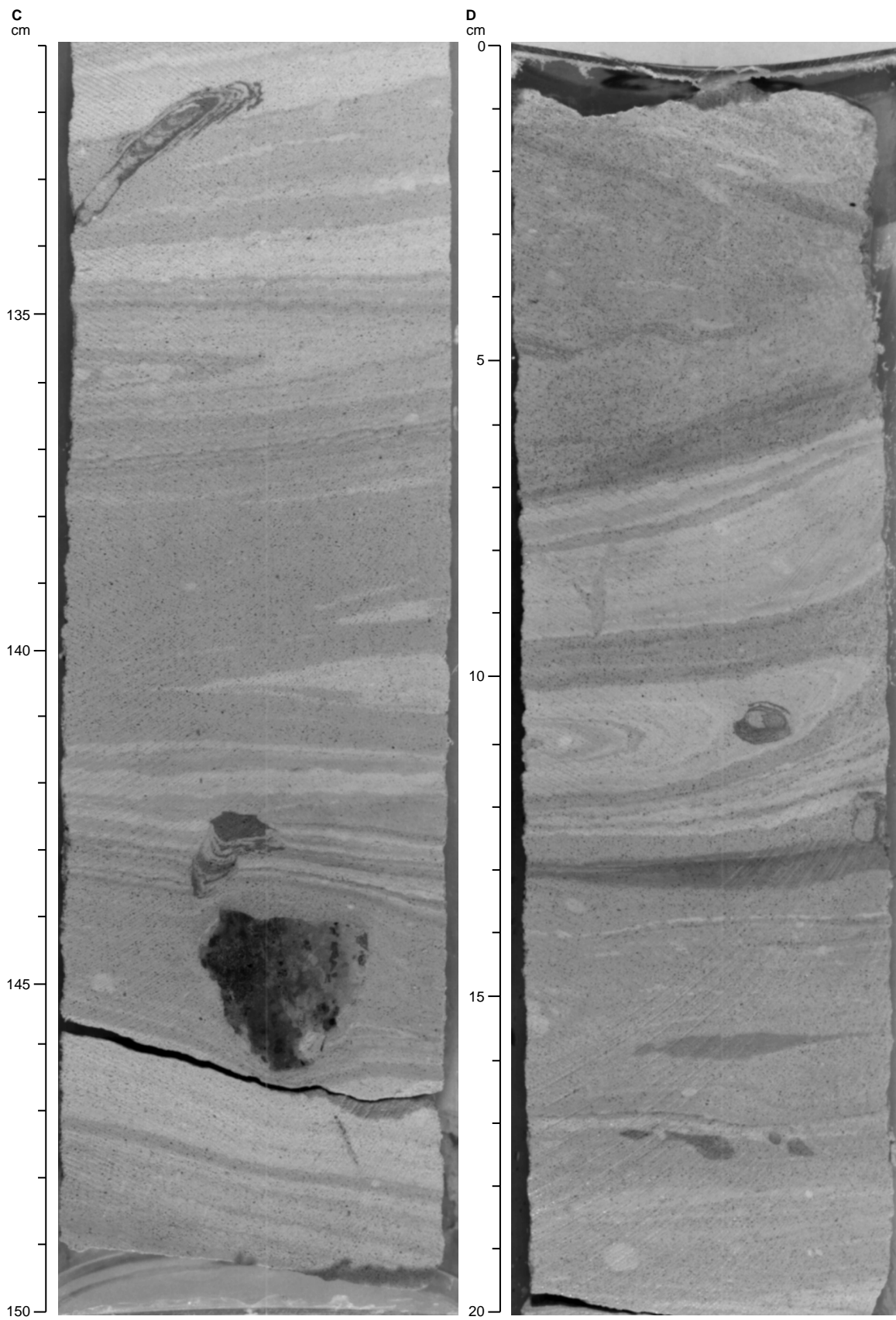


Figure 9 (continued). **C.** Interval 171B-1052E-27R-2, 131–150 cm. The upper portion of the slump below the contact shows *Zoophycos* spreiten piping sediment from at least 100 cm above, as well as transported reef debris. **D.** Interval 171B-1052E-27R-3, 0–20 cm. A slump fold occurs in the limestone bed at interval 171B-1052E-27R-2, 123 cm, to 27R-4, 100 cm.

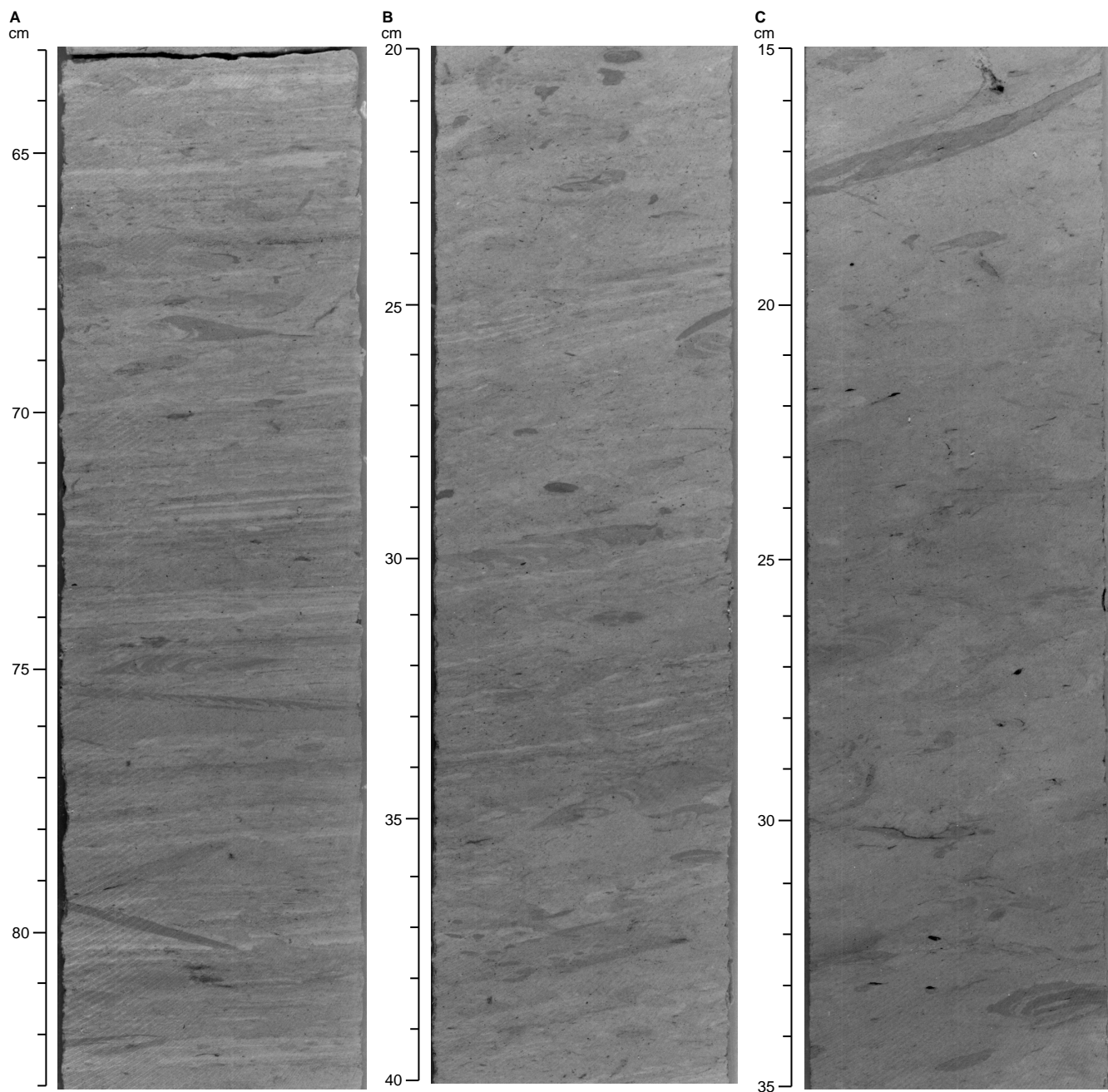


Figure 10. Lithologic Subunits IVA and IVB. **A.** Interval 171B-1052E-28R-2, 63–83 cm. Slightly bioturbated sediments are typical of Core 28R. **B.** Interval 171B-1052E-27R-1, 20–40 cm. Moderately bioturbated sediments are typical of the lower portions of Sections 27R-CC through 27R-5. **C.** Interval 171B-1052E-27R-1, 15–35 cm. Heavily bioturbated sediments are typical of Cores 27R and 26R.

The upper contact of Subunit IVB is placed at a burrowed interval (Section 171B-1052E-27R-2, 38 cm) developed above an 85-cm-thick, very light greenish gray (5GY 8/1) to white (N9), generally homogeneous foraminifer packstone, with green sediment brought down from above by burrowing organisms. Trace fossil tiering is apparent. *Planolites* and unidentified single and branching burrows (*Thalassinoides*?) as much as 1 cm across are common in interval 27R-2, 38–53 cm, and are rare immediately below to 64 cm; *Zoophycos* spreiten are common from 70 to 93 cm in Section 27R-2, although they occur as high as 56 cm and as low as Section 27R-3, 11 cm (in the underlying slump deposit); and open, unidentified, millimeter-scale simple tubes are rare in interval 27R-2, 72–98 cm, and are common from 98 to 110 cm (Fig. 9A–C). The burrowed foraminifer packstone rests on ~2.5 m of foraminifer limestone that is inter-

preted as a slump deposit (Fig. 9C, D). The slumped and burrowed interval separates lithology typical of Subunit IVA from lithology typical of Subunit IVB, but it is unclear how much time is represented by the sediment between the youngest pelagic sediment of Subunit IVB and the oldest pelagic sediment of Subunit IVA (see “Discussion” section, this chapter). The contact between Subunit IVB and lithologic Unit V is placed at the base of a slump deposit containing Coniacian–Maastrichtian microfossils and lying on top of Cenomanian limestones with interbedded siltstones.

Unit V

Description: Dark olive silty claystone, calcareous claystone, black shale, and calcite-cemented quartz foraminifer sandstone

Interval: 171B-1052E-36R-3, 122 cm, to 58R-CC, 20 cm
 Depth: 477.4–684.8 mbsf, Hole 1052E
 Thickness: 207.4 m, Hole 1052E
 Age: Cenomanian to late Albian

Lithologic Unit V includes hemipelagic sediments with more terrigenous components than in the overlying sediment. The top of the unit is placed at the last downhole occurrence of large-scale slumping. The bottom of the unit was not reached, as the hole was terminated when a series of coarse sandstones was recovered. This unit comprises dark olive silty claystone, calcareous claystone, black shale, and medium to coarse, moderately well- to well-sorted sandstone. It is divided into three subunits: the lower subunit includes the interval with sandstone, the middle subunit contains the dark laminated claystone beds, and the upper subunit is dominantly calcareous claystone and quartz silt claystone. We use the term “black shale” for the laminated, clay-rich lithofacies with organic matter contents >0.5% that characterize lithologic Subunit VB.

Subunit VA

Description: Dark olive silty claystone and calcareous claystone
 Interval: 171B-1052E-36R-3, 122 cm, to 40R-1, 124 cm
 Depth: 477.4–511.8 mbsf, Hole 1052E
 Thickness: 34.4 m, Hole 1052E
 Age: Cenomanian to late Albian

Lithologic Subunit VA includes dominant dark olive-gray calcareous silty claystone to clay-rich siltstone. Bedding is on the centimeter to decimeter scale, with bedding contacts commonly obscured by heavy bioturbation (Fig. 11). *Zoophycos*, *Teichichnus*, *Planolites*, *Phycoides*, and *Chondrites* burrows are common, as are many unidentified trace fossils. The sediment color varies from olive gray to black, and the darker intervals have a greater abundance of terrigenous components. Many beds are enriched with foraminifers and, to a lesser extent, quartz silt. They are generally heavily bioturbated, but locally faint outlines of wavy laminae are visible in the clayey foraminifer limestones. These foraminifer-rich intervals are weakly bioturbated and appear to be graded, but whether this is a primary depositional feature or is generated by bioturbation is difficult to distinguish. A thin section from one of these beds (Sample 171B-1052E-39R-7, 56–58 cm) indicates that it is a calcisphere packstone with minor planktonic foraminifers and larger, sand- to granule-sized grains replaced by calcite. The matrix is dominantly calcareous clay and silt. In the core, the calcisphere packstones are commonly calcite cemented, and where they are, the finer grained enclosing sediment drapes around them. This feature appears to be a product of early diagenesis and suggests that these coarser grained beds were cemented before the main body of sediment underwent compaction. The top of the subunit bears numerous clay-filled, subparallel, subhorizontal veins, which apparently are dewatering sheet structures associated with the large slump deposit at the base of the overlying unit. Minor slump features appear as centimeter- to decimeter-scale folds in Cores 171B-1052E-36R, 37R, and 39R.

The calcareous component contains rare to common nannofossils, rare to abundant foraminifers, and calcite grains of uncertain origin. Fragments of bivalves are rare but appear throughout the subunit. Gastropod shells and ammonite fragments occur near the base. Calcispheres locally constitute one-half of the calcareous fraction. Traces of rhombohedral dolomite are dispersed in the claystone. The terrigenous component is dominantly clay in the fine fraction and subrounded to rounded quartz grains in the silt to fine-sand fraction. Minor but persistent coarse terrigenous components include microcline feldspar and heavy minerals. Zircon, twinned tourmaline, and biotite flakes dominate the heavy-mineral fraction. Blue chlorite(?) flakes are rare but persistent components. Chlorite is green in the underlying subunits. Authigenic components include rare to common glauconite pellets, rare to abundant zeolite, pyrite as brassy burrow fill, black burrow fill, disseminated framboids, and rare, well-formed dolomite rhombs. The zeolite occurs as tiny, thin, elongate blades and

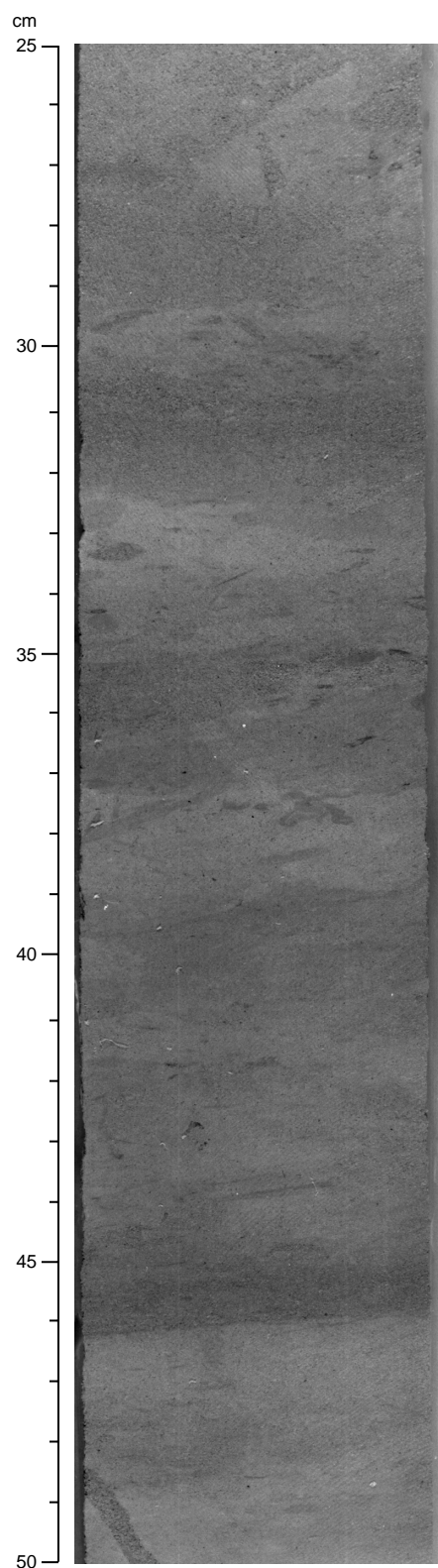


Figure 11. Interval 171B-1052E-36R-4, 25–50 cm. Alternations of darker to lighter sediment in lithologic Subunit VA. Contacts are locally sharp (46–47 cm) with faint grading, but more commonly are gradational because of heavy bioturbation. The darker sediment is enriched in silt- to clay-sized terrigenous components such as clay, quartz, rare feldspar, and heavy minerals. The lighter intervals are enriched in calcareous, pelagic, biogenic components, dominantly calcispheres.

is probably of the clinoptilolite-heulandite series, based on X-ray diffraction (XRD) data from Site 390 (T. Pletsch, pers. comm., 1997).

Subunit VB

Description: Black shale, calcareous claystone, silty claystone, clayey limestone with foraminifers and quartz, and clayey siltstone
Interval: 171B-1052E-40R-1, 124 cm, to 53R-5, 30 cm
Depth: 511.34 to 633.50 mbsf, Hole 1052E
Thickness: 122.16 m, Hole 1052E
Age: late Albian

Lithologic Subunit VB is a remarkably thick upper Albian sequence of claystone alternating with laminated dark claystone (referred to previously as black shale) and minor, lighter colored limestone. The claystones contain variable amounts of pelagic calcareous microfossils, neritic shell debris, and siliciclastic components (mainly quartz, feldspar, and mica). The laminated black shales are rich in pyrite and contain clay with varying amounts of calcareous nannofossils, fine-silt-sized quartz, fish remains, and organic debris (Fig. 12). Lithified, coarser grained intervals contain foraminifers, shallow-water limestone fragments, and quartz. The color varies from light olive gray in the limestones to very dark olive gray in the black shales. Drilling disturbance is slight to moderate and recovery was high. The upper boundary of lithologic Subunit VB is defined by the first occurrence (FO) of black shale in Section 171B-1052E-40R-1, 124 cm (511.84 mbsf). The lower boundary is defined as the last downhole occurrence of laminated black shale in Section 53R-5, 0 cm (633.20 mbsf). A general increase in silt-sized siliciclastic components occurs downhole. Quartz, feldspar, mica, and heavy minerals, such as tourmaline and apatite, occur throughout but increase in abundance and grain size with depth. Bioturbation is moderate to strong throughout Subunit VB (e.g., *Chondrites*, *Planolites*, *Teichichnus*, and *Zoophycos*). Except for rare *Chondrites*, there is no bioturbation in the laminated intervals. Many black shale intervals have a sharp lower contact, gradational upper contact, and weakly bioturbated interval in the middle. Well-preserved ammonites, gastropods, and bivalves (pyritized or aragonitic) are present throughout Subunit VB.

Cores 171B-1052E-40R through 42R show cyclic alternation of light-colored, strongly bioturbated, lithified, coarse-grained clayey siltstones with moderately bioturbated silty claystones and dark, laminated black shales (Fig. 13). Fifteen such cycles were observed. Laminated black shales also occur in Cores 171B-1052E-43R, 44R, 45R, and 53R. The laminated intervals become lighter in color, contain more silt-sized components, and are less abundant downhole.

Subunit VC

Description: Dark clayey siltstone, dark silty claystone, dark siltstone with carbonate grains, medium-fine- to coarse-grained bioclastic and lithic grainstone, and lithic and peloid grainstone with bioclasts
Interval: 171B-1052E-53R-5, 30 cm, to 58R-CC, 20 cm
Depth: 633.2–684.8 mbsf, Hole 1052E
Thickness: 52.2 m, Hole 1052E
Age: late Albian

Lithologic Subunit VC is dominated by slight to moderately bioturbated dark olive-gray sandy siltstones, which are wavy laminated on a centimeter scale. Scattered throughout the dark siltstone intervals are flattened, but otherwise complete and well-preserved, aragonitic ammonite shells (Fig. 14). Fragments of larger ammonite shells and belemnites also occur throughout the subunit. Minor lithology types include several quartz and bioclast-rich grainstone intervals (intervals 171B-1052E-57R-3, 132–127 cm, and 57R-4, 78–50 cm) and more intensely bioturbated sandier intervals (intervals 171B-1052E-57R-3, 27–48 cm; 57R-3, 77–92 cm; 57R-4, 91–97 cm; and 57R-CC).

Two intervals at Sections 171B-1052E-55R-7, 50 cm, to 56R-1, 137 cm, and 58R-1, 83 cm, to 58R-2, 105 cm, consist of gray, cross-

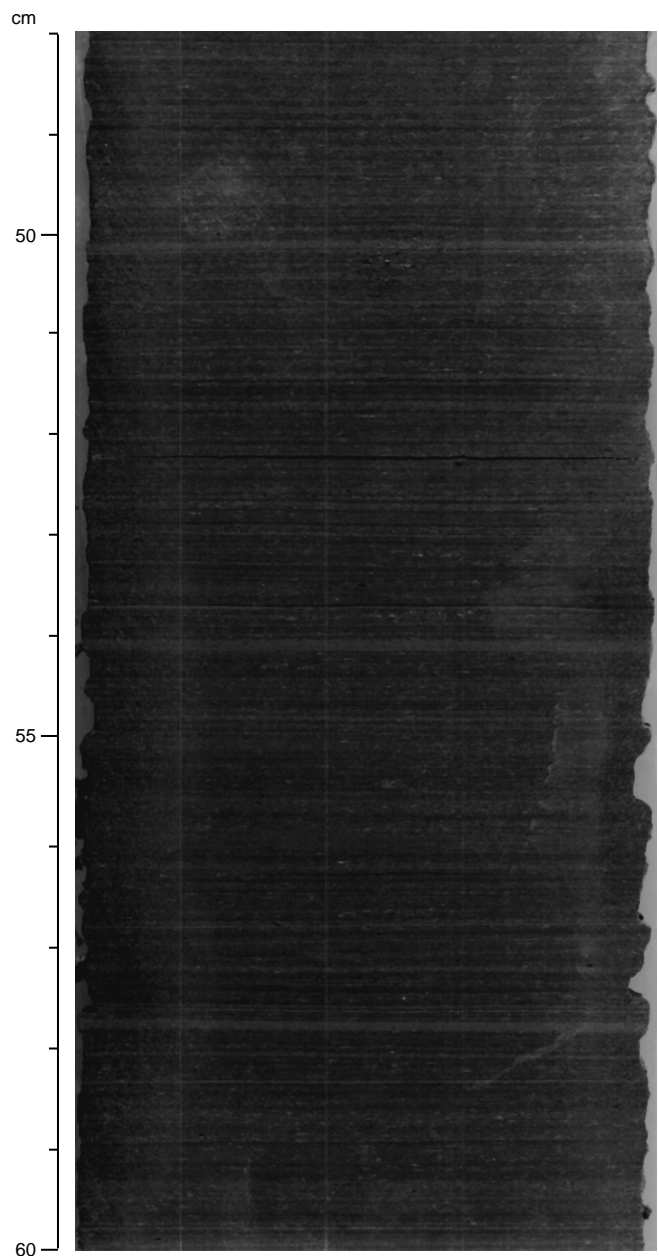


Figure 12. Interval 171B-1052E-40R-4, 48–60 cm (563.10–563.22 mbsf). Distinct, fine lamination within an upper Albian black shale in lithologic Subunit VB.

bedded, very coarse to medium-fine-grained calcite-cemented sandstone containing rounded lithic, bioclast, and peloidal grains. The texture is a well-sorted grainstone. Interval 171B-1052E-56R-1, 73–139 cm, is a massive, medium- to coarse-grained grainstone, with some dark rip-up clasts within the interval at 77–80 cm. Interval 171B-1052E-56R-1, 53–72 cm (Fig. 15), consists of ripple-laminated, medium- to fine-grained peloid grainstone with lithic grains. The ripples appear unidirectional on the cut face and are interpreted as climbing ripples. Interval 171B-1052E-56R-1, 0–53 cm, is a moderately sorted, coarse-grained bioclast grainstone with a sparry calcite matrix (Fig. 16). This interval is cross-bedded, with 2- to 3-cm-thick poorly delimited, inversely graded foresets that dip 15°–20° (Fig. 17). Dominant grains are miliolids, benthic foraminifers, and red algae. In some laminae, as much as 30% of the grains are subrounded to rounded quartz grains. Darker laminae contain more glauconite,

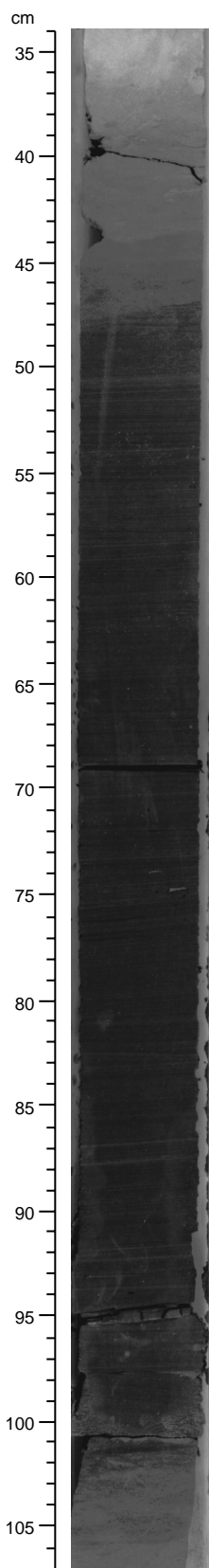


Figure 13. Interval 171B-1052E-40R-3, 34–107 cm (513.84–514.67 mbsf). Alternation of lithified, light, coarse-grained limestone with darker marlstone and dark, laminated black shale in lithologic Subunit VB.

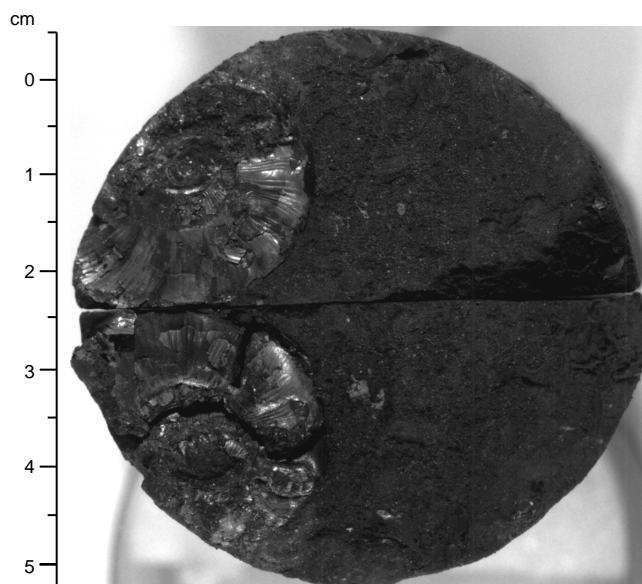


Figure 14. Interval 171B-1052E-55R-1, 140 cm (647.8 mbsf). Part and counterpart of the aragonite shell of an ammonite in lithologic Subunit VC. The ruler is for scale only.

biotite, lithic fragments, and as much as 50% quartz. A massive, crudely cross-bedded, very coarse-grained to medium-fine-grained peloid bioclast grainstone with miliolids and lithic fragments is present in Sections 171B-1052E-58R-1, 83 cm, through 58R-2, 105 cm (Fig. 18). Minor components in all grainstone layers include echinoid, bivalve, and red algae bioclasts. The cross-bedded intervals in intervals 171B-1052E-56R-1, 0–53 cm, and 58R-1, 83 cm, to 58R-2, 105 cm are interpreted as sand waves, as suggested by the dipping, inversely graded foreset laminae. Inverse grading may be caused by avalanching along the foreset slope of the sand waves. (Figs. 18, 19).

Discussion

More than 100 m of mixed carbonate-siliciclastic sediment with common lithic grains, feldspars, and pelagic and neritic components was recovered at the base of Hole 1052E. Although we anticipated more proximal sedimentary facies at Site 1052 than at the previous sites, we expected the sediments to be more compositionally mature. The sedimentary facies at the bottom of the section at Site 1052 indicate deposition in shallow water (i.e., middle- or outer shelf environments). Lithologic Subunit VC was probably deposited near storm wave base, as suggested by the occurrence of well-sorted grainstones, which indicate oscillating currents, and by the occurrence of mega-ripples (sand waves), interpreted as offshore bars. However, given the passive continental margin setting and the ongoing drift stage of the adjacent Atlantic basin, deposition of this compositionally immature mixed siliciclastic sediment remains surprising, even in such a shallow marine environment. There are at least two possible scenarios for the deposition of these mixed siliciclastic, pelagic, and neritic sediments: (1) the depositional environment was close to an unroofing source area with subsequent rapid transport and burial of the unstable grains on the shelf or (2) the shoreward continental area experienced an arid climate that prevented chemical weathering of the unstable grains before burial. Hallam (1984) proposed that most of the eastern American seaboard was humid, rather than arid, during the mid-Cretaceous, which makes a climatically controlled supply of unstable grains unlikely.

Lower Cretaceous siliciclastic sediment also occurs in the lower continental rise hills at Deep Sea Drilling Project (DSDP) Site 603. At Site 603, the thick package of turbidites roughly correlates with

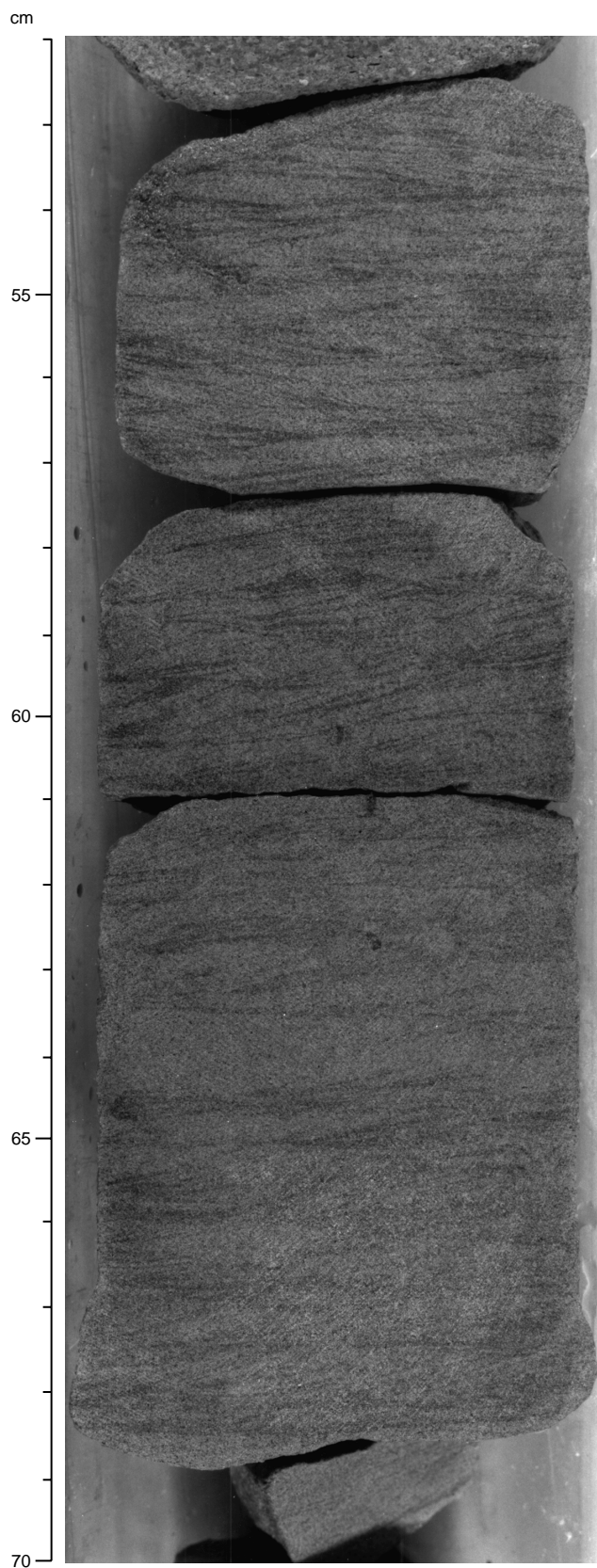


Figure 15. Interval 171B-1052E-56R-1, 52–70 cm (656.5–656.7 mbsf). Small-scale, ripple-laminated, fine-grained grainstone in lithologic Subunit VC. Ripples are unidirectional and faintly climbing.

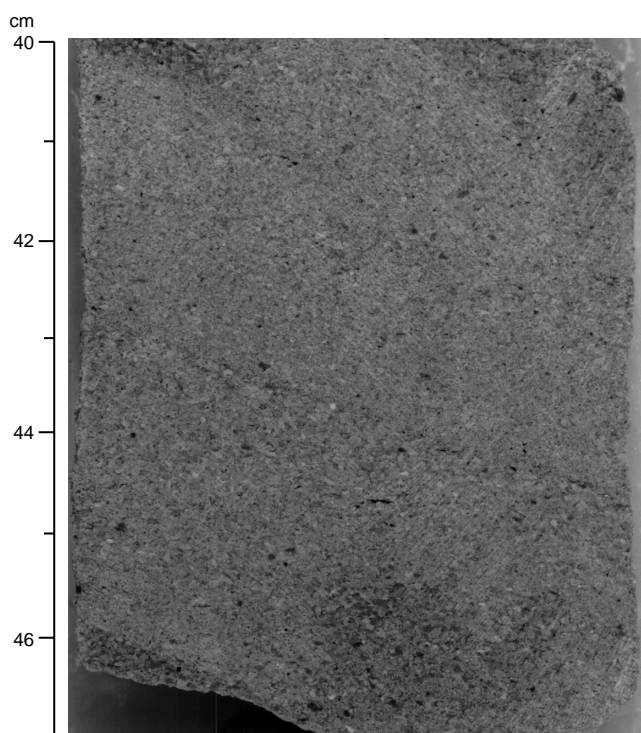


Figure 16. Interval 171B-1052E-56R-1, 40–47 cm (656.4–656.5 mbsf). Inversely graded foreset beds dipping 15° in lithologic Subunit VC are indicative of mega-cross-bedding in a longshore sand bar.

poorly dated Lower Cretaceous deltaic sediment of the Potomac Group in the Salisbury Embayment near Maryland (Sarti and von Rad, 1987; Holmes et al., 1987; Glaser, 1969). This sediment is, however, older than any sediment recovered at Site 1052. Most of the turbidite deposition at Site 603 occurred during the Hauterivian and Barremian, with an enhanced pulse of neritic input during a middle Aptian sea-level drop (Sarti and von Rad, 1987). Turbidite deposition stopped during the Aptian–Albian sea-level highstand and did not recur.

Deltaic sediment along the southeast Atlantic seaboard (e.g., the Cape Fear Formation in North and South Carolina) is apparently younger (Santonian) than siliciclastic sediment at Site 1052 (Christopher et al., 1979; Sohl and Owens, 1991). Deltaic sediment would indicate humid conditions and a steady, perhaps rapid, rate of sediment supply to the Blake Nose. As the presence of unstable minerals in this upper Albian sediment probably indicates a fairly high rate of sediment supply, rapid unroofing is indicated for the igneous and metamorphic terrains of the Piedmont and the Blue Ridge. A decrease of coarse-grained terrigenous sediment components upsection in Unit V at Site 1052 suggests either a decrease in morphotectonic activity onshore or trapping of sediment in nearshore areas during a sea-level highstand.

The middle part of the mixed carbonate-siliciclastic succession of lithologic Unit V includes several black shale intervals (Subunit VB). The lower black shales contain common detrital material including terrestrial organic debris. The increase upsection in black shale frequency and thickness probably reflects a deepening-upward trend during deposition of lithologic Subunit VB and culminates in Core 171B-1052E-40R, which displays distinct laminae (Fig. 12) and has a lower siliciclastic content than black shales deeper in the section. This trend may be interpreted as a response to the generally transgressive global sea level in the late Albian (Haq et al., 1987). The lack of macrobenthic fossils, such as bivalves or trace fossils other than *Chondrites*, within the black shales indicates dysoxic to anoxic

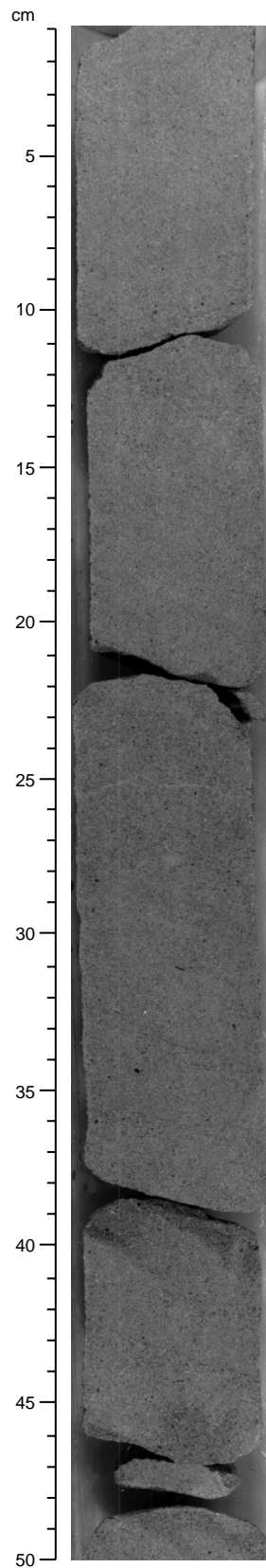


Figure 17. Interval 171B-1052E-56R-1, 1–50 cm (656–656.5 mbsf). Inversely graded, foreset laminae with a 15°–30° dip of coarse-grained grainstone in lithologic Subunit VC are interpreted as the mega-cross-bedding of a longshore bar.

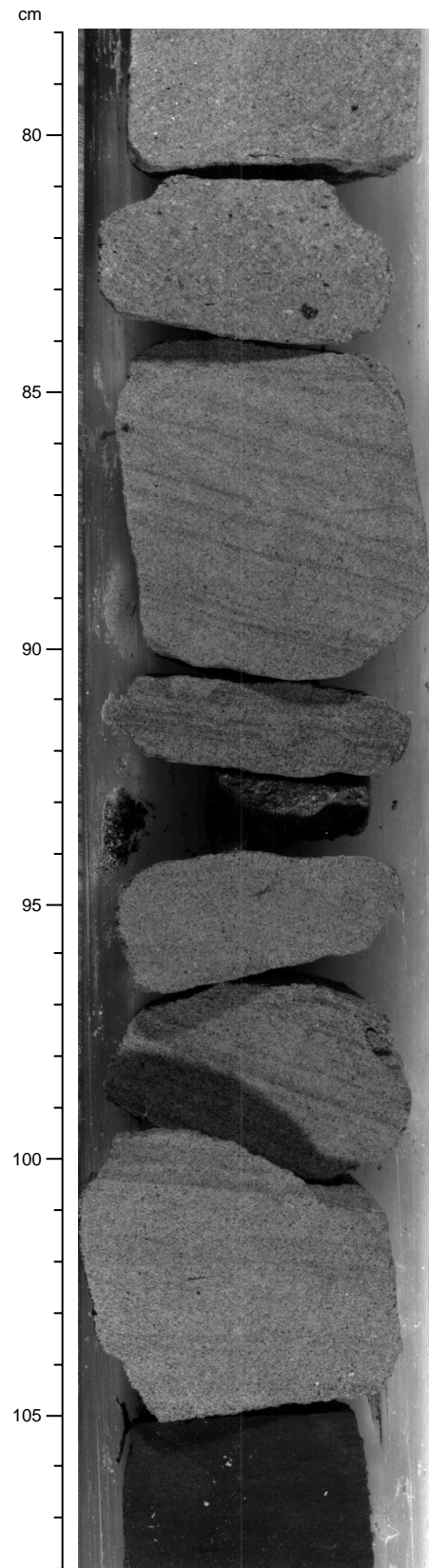


Figure 18. Interval 171B-1052E-58R-2, 78–108 cm (677.5–677.8 mbsf). Very coarse-grained grainstone with peloids and bioclasts (miliolids and red algae) in lithologic Subunit VC.

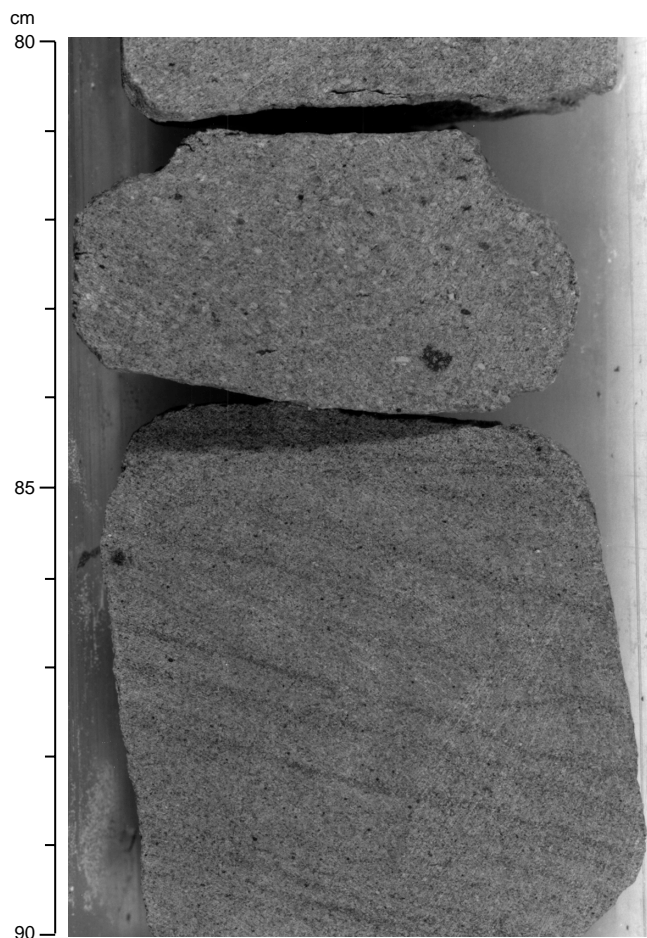


Figure 19. Close-up photo of interval 171B-1052E-58R-2, 80–90 cm (677.5–677.6 mbsf). Very coarse-grained grainstone with peloids and bioclasts (miliolids and red algae) in lithologic Subunit VC.

bottom-water conditions. The rare occurrence of *Chondrites* traces in this sequence can be interpreted as short oxygenation events within anoxic periods.

Black shales in Cores 171B-1052E-40R through 42R can be correlated biostratigraphically with time-equivalent, organic-rich sediments in Tethyan basins that formed during Oceanic Anoxic Event 1d (OAE 1d; Erbacher and Thurow, 1997; see “Biostratigraphy” section, this chapter). This anoxic event coincides with one of the major Cretaceous drowning events of carbonate platforms and has been interpreted as a result of enhanced productivity caused by leaching of nutrients from flooded lowlands during transgressions and/or increased runoff from land. The observed cyclic alternation of black shale, marl, and limestone intervals seems to match similar bundles observed in black shales attributed to OAE 1d in the Vocontian Basin of southeast France (Niveau Breistroffer; Bréhéret, 1994). Whether the laminated intervals of Cores 171B-1052E-43R through 53R are correlative with transgressive periods also remains questionable.

Lithologic Subunit VA was deposited in a hemipelagic environment with fine-grained terrigenous input including clay, silt-sized quartz and feldspar, and heavy minerals. The low abundance of siliclastic silt and sand indicates that this environment was either in deeper water, well removed from the coastline, or both. The stratigraphic succession is cyclic at the centimeter to decimeter scale. Dominantly biogenic sediment alternates with dominantly terrigenous sediment. The duration of the sedimentary cycles is still uncertain. Fairly rapid sedimentation rates are indicated by minor slump

features. Normal hemipelagic sedimentation was interrupted by currents that transported foraminifers or winnowed the fines from them to form porous foraminifer limestone beds. Current activity did not recur with any regularity, as the foraminifer limestones are irregularly spaced in the core. The beds were cemented before substantial sediment compaction.

In contrast to lithologic Unit V, pelagic sedimentation predominated during deposition of Unit IV. The frequency of slump deposits decreases and the incidence of slickensided surfaces increases upward through the unit. The concentration of hard, slump-derived limestones in the base of the unit and of fractures in the top of the unit may explain why recovery was generally poor in both the lower and upper portions of lithologic Unit IV, but good to excellent in the middle portion (Cores 171B-1052E-28R through 26R).

In the Basque region of France and Spain, the extinction of inoceramids is associated with an increase in the intensity of bioturbation (MacLeod, 1994). In Hole 1052E, Subunit IVB is less intensely bioturbated, on average, than Subunit IVA, and inoceramids were observed in Subunit IVB but not in Subunit IVA. The transition between slightly bioturbated and heavily bioturbated fabrics appears gradual within the pelagic sediments of Cores 171B-1052E-28R through 26R (Fig. 10), and subsequent study will determine the relationship between sedimentary fabric and the stratigraphic distribution of inoceramids. A large slump deposit capped by a distinctive burrowed bed (the contact between Subunits IVA and IVB) interrupts the record. Similar burrowed intervals are present in light-colored, homogeneous, sandy limestones above slumps within lithologic Unit IV; however, the time represented by these intervals is not clear. If the homogenized interval represents a massive bed of winnowed foraminifers created during emplacement of the underlying slump, pelagic deposition could have been relatively continuous. Alternatively, the surfaces may represent a long period of nondeposition during which extensive burrowing erased the primary fabrics. The burrows could be interpreted as those active at the time of renewed deposition of the upper surface, or a slump contact could represent a hardground. Emplacement of a mass flow during an interval when background deposition ceased (i.e., when sedimentation patterns changed) is possible, especially if the hiatus was long.

The K/T boundary is biostratigraphically complete, although the section lacks the distinctive spherule layer found at Site 1049. The bioturbated light grey chalk present immediately above the Maastrichtian green chalks at Site 1052 is a distinctive unit that is similar to, and perhaps correlative with, white nannofossil ooze of similar age at Site 1049 that directly overlies dark grey nannofossil ooze and the spherule bed. The presence of scattered dark green spherules within burrows in the light grey chalk at Site 1052 suggests that the spherule bed was deposited but not recovered during coring, or that it was largely slumped into deeper water before deposition of Paleocene sediments.

The Paleocene and Eocene strata are similar to sediments of equivalent age at other Leg 171B sites. However, a major hiatus is present between the Paleocene and Eocene sections at Site 1052 that is not found at deeper water sites on the Blake Nose. We recognized an ~1.5-m.y. hiatus between the Eocene and the middle Eocene at Sites 1051 and 1050. At Site 1052, a condensed interval represents ~13 m.y. of deposition and has cut out, or greatly thinned, the upper Paleocene, lower Eocene, and part of the middle Eocene sequences. The rocks are interbedded silicified foraminifer claystone, porcellanitic calcareous claystone, and cherty claystone that retain a rough age progression from the bottom to the top of the section. The retention of at least a crude succession of nannofossil zones in these rocks suggests that the area was exposed to winnowing by bottom currents for a prolonged period before the resumption of pelagic ooze deposition in the middle Eocene.

The depositional environment of lithologic Units I through III is similar to that of the equivalent units at Sites 1049 through 1051 and is not discussed further here.

BIOSTRATIGRAPHY

Calcareous Nannofossils

The following discussion of the calcareous nannofossil biostratigraphy at Site 1052 is based predominantly upon the examination of samples from Holes 1052A and 1052E. These two holes form a composite section that spans the upper Albian–upper Eocene (Fig. 20). Calcareous nannofossil datums and their depths are listed in Table 4.

The upper 160 m of sediment consists of upper to middle Eocene calcareous oozes with well-preserved calcareous nannofossil assemblages. The presence of *Isthmolithus recurvus* in the upper 15–20 m of sediment in Holes 1052B, 1052C, and 1052D indicates the late Eocene Subzone CP15b. The occurrence of *I. recurvus* is sporadic and rare in this sequence, suggesting that more detailed examination may extend this subzone downward in the sequence.

Core 171B-1052A-10H through Section 171B-1052A-19X-5 consist predominantly of sediment from the upper part of the middle Eocene (Zone CP14). The thickness of Subzone CP14b (~33 m) suggests a relatively low sediment accumulation rate of 10 m/m.y. Alternatively, this zone may be truncated by one or more disconformities. The fact that the top of Subzone CP14b and the top of planktonic foraminifer Zone P14 are nearly coincident at this site (Fig. 20) suggests that the upper part of CP14b is missing, as these two biostratigraphic events were separated by 1.3 m.y. in the Berggren et al. (1995) time scale.

The base of the middle Eocene is marked by a sequence of foraminifer packstones separated by glauconitic hardgrounds. Although cored in both Holes 1052A and 1052E, neither hole contains a complete record of this complex interval. In addition, reworking of older nannofossils is pervasive, so assigned ages are the youngest that are consistent with the assemblages. Given this convention, at least four distinct ages can be recognized within this <5-m interval. The upper part of the foraminifer packstone interval contains *Nannotetrina fulgens* and rare specimens of *Reticulofenestra umbilica*. The latter include specimens with a major axis of 14–16 μm . This size and presence of *N. fulgens* indicates the earliest part of Subzone CP14a. The next youngest interval (represented in Sample 171B-1052E-3R-1, 68–69 cm) contains *N. fulgens* but not *R. umbilica* (s.s.), indicating Subzone CP13c. This overlies an interval (represented by Sample 171B-1052E-3R-2, 66–67 cm) containing *N. fulgens* and *Chiasmolithus gigas*, denoting Subzone CP13b. Finally, the base of the foraminifer packstone contains assemblages with *Discoaster subloadoensis* and *Rhabdosphaera inflata*, definitive of middle Eocene Subzone CP12b. Reworked specimens throughout this complex include species indicative of both upper Paleocene (such as *Heliolithus kleinpellii* and *Fasciculithus tympaniformis*) and lower Eocene (including *Discoaster lodoensis* and *Tribrachiatus orthostylus*). This middle Eocene sequence lies disconformably on the mid-Paleocene in Sample 171B-1052E-3R-2, 0–1 cm.

A thick sequence of pelagic and hemipelagic calcareous sediments of mid-Maastrichtian through mid-Paleocene age occur below the disconformity. Differentiation of the boundary of Zones CP3 and CP2 is difficult at this site because of the rarity and sporadic occurrence of *Ellipsolithus macellus*. A proxy species, *E. bollii*, was used to approximate this boundary. *E. bollii* is believed to be the first descendant of *E. macellus* and speciates from the ancestor very early in Zone CP3. Thus, the boundary marked in Figure 20 and used in Table 4 is probably too young. Despite this fact, Zone CP3 is quite thick (more than 110 m) and contains well-preserved nannofossils throughout, suggesting its usefulness for calibrating zonal subdivisions that are currently informal. By contrast, Zones CP1 and CP2 are relatively thin, reflecting a general lack of siliceous microfossils and the low calcareous microplankton productivity that followed the K/T extinction event.

The Maastrichtian lies in apparent conformity below the lowest Danian, as reflected by the presence of *Micula prinsii*, *Pseudomicula*

quadrata, and *Cylindralithus oweinae*. Approximately 170 m of Maastrichtian sediment was cored with moderately to well-preserved calcareous nannofossils throughout. Although the upper Maastrichtian (Section 171B-1052A-18R-3 through Core 171B-1052A-29R) contains the expected mid-latitude assemblages, the lower Maastrichtian is characterized by a paucity of the index species *Reinhardtites levis*. This species, whose last occurrence (LO) marks the top of the lower Maastrichtian, is abnormally rare and sporadic in this section. It is only slightly more common than other obviously reworked species such as *Aspidolithus parvus constrictus*. In addition, there is conclusive evidence of allochthonous calcareous nannofossils in this sequence. Angular coarse sand- to granule-sized clasts of green, smectitic claystone occur in Sections 171B-1052A-27R-2 and 33R-CC. These green clasts contain rare calcareous nannofossils, including *M. decussata* (early form), *Lithastrinus moratus*, and *L. septenarius*, indicating a Coniacian age (Zones CC13 and CC14) for this material. Finally, lithologic examination indicates that some of the sequence (Core 171B-1052E-27R through Section 171B-1052E-36R-1) is slumped (see “Lithostratigraphy” section, this chapter). Thus, it is possible that Zone CC24 (i.e., the lower Maastrichtian of Gradstein et al., 1995) is absent at this site and that the entire Maastrichtian sequence was deposited between 65 and 69.4 Ma.

The Maastrichtian lies disconformably on a thick (~211 m) sequence that spans the upper Albian–lower Cenomanian. The sequence is marked by rhythmically bedded, light-colored limestones and dark-colored calcareous claystones that are especially well developed in the lower Cenomanian interval. Calcareous nannofossil preservation is moderate to poor in the limestones, but good to very good in the claystones. Samples from the finely laminated dark calcareous claystones can be described only as stunningly beautiful. There are no apparent disconformities in the sequence, making it nearly unique for its completeness and preservation across the boundary of the Lower and Upper Cretaceous.

Planktonic Foraminifers

The 682-m sequence at Site 1052 ranges from early late Eocene (Zone P16) to late Albian in age and is capped by a thin sequence of Pleistocene to Holocene nannofossil foraminifer ooze (Fig. 20). Major hiatuses occur between middle Eocene Zone P12 and upper Paleocene Subzone P3b and between the lower Maastrichtian (upper *Globotruncana gansseri*–*G. falsostuarti* Zone) and the lower Cenomanian (*Rotalipora greenhornensis* Zone).

Zonal assignments for all holes are summarized in Figure 20 and Table 5, and distribution charts for Holes 1052A and 1052E are presented in Tables 6 and 7. A list of foraminifer datums used to calculate the sediment accumulation rates is included in Table 5.

Foraminifers are abundant and well preserved in nearly all samples of Eocene nannofossil and siliceous ooze and chalk, rare and poorly preserved in the upper Paleocene claystone, moderately to poorly preserved in a lower Paleocene chalk spanning Subzone P1b through Zone P2, and very well preserved in a lowermost Danian chalk from Zone P α . The middle to upper Maastrichtian chalk sequence yields foraminifers that are abundant and consistently well preserved. Preservation and abundance vary with changes in lithification of the nannofossil chalk and siltstones in the lower Maastrichtian, Cenomanian, and Albian intervals of siltstone, depending upon the degree of sediment lithification. The Albian laminated claystones yield abundant and remarkably well-preserved assemblages—particularly in finely laminated intervals—probably as a result of a high clay content.

The cap of foraminifer ooze (upper ~60 cm) in Holes 1052A and 1052D contains a number of Pleistocene–Holocene species (e.g., *Globorotalia truncatulinoidea*, *Globoquadrina dehiscens*, *G. sacculifer*) and reworked species from the middle Miocene (e.g., *Globigerinoides mitra*), early Oligocene (e.g., *Paragloborotalia nana* and *P. opima*), and middle Eocene.

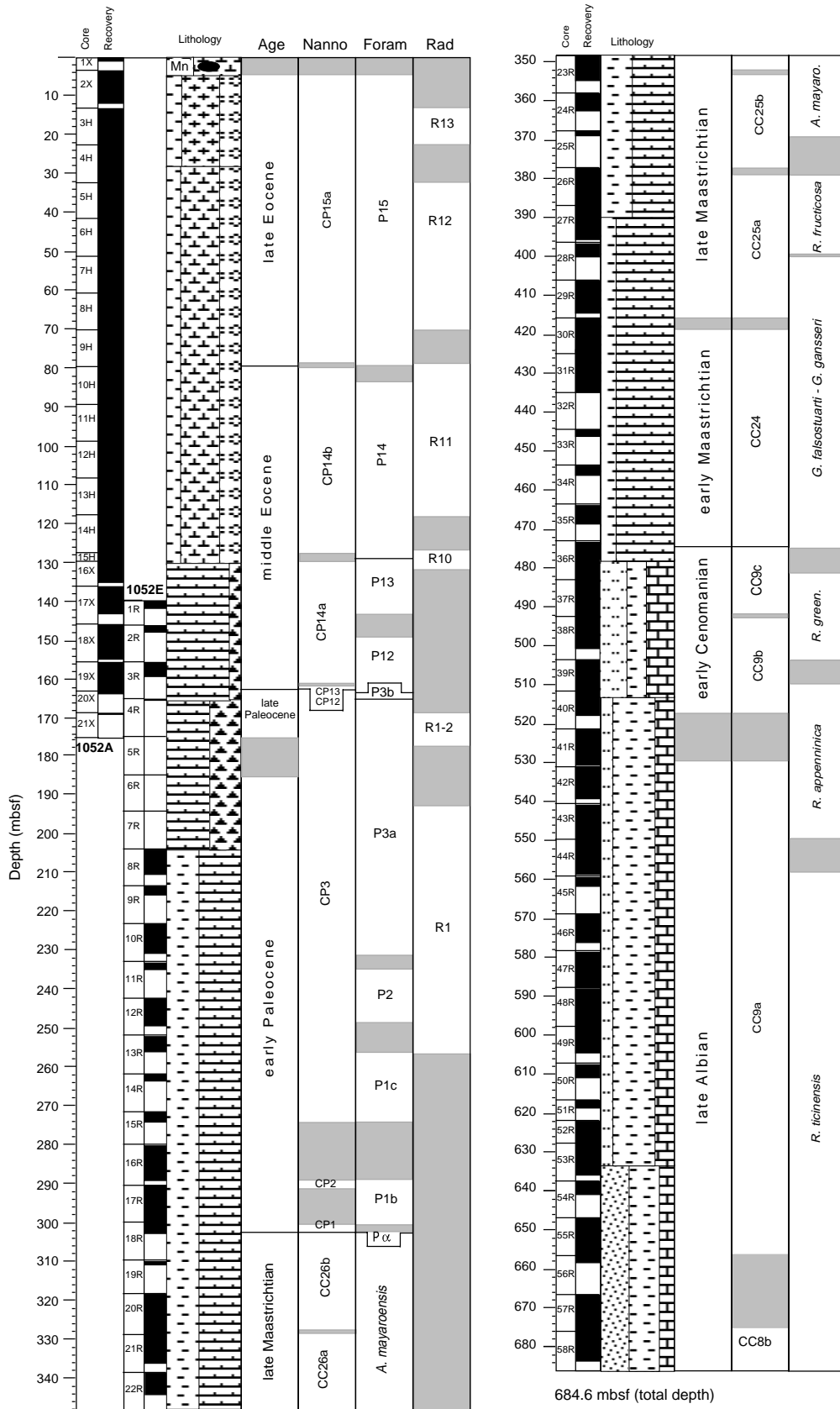


Figure 20. Distribution of biostratigraphic units and ages in the composite section of Holes 1052A and 1052E. Shaded areas indicate uncertainty caused by sample spacing or poor preservation.

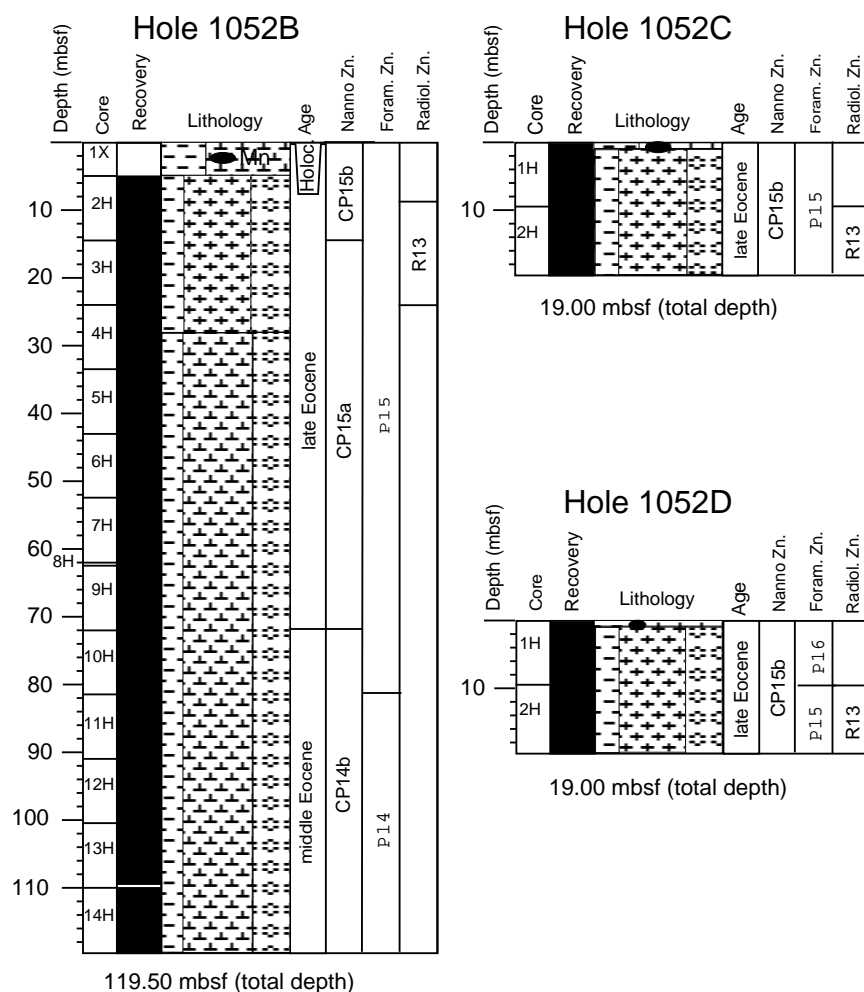


Figure 20 (continued). Distribution of biostratigraphic units and ages in the composite sections of Holes 1052B, 1052C, and 1052D.

Upper Eocene Zone P16 was recovered only from Hole 1052D. The base of this zone is identified in Section 171B-1052D-1H-CC by the presence of *Cribohantkenina inflata* and *Turborotalia cunialensis*. Transitional forms of these two species (i.e., *Hantkenina* aff. *C. inflata*, lacking multiple areal apertures, and *Turborotalia cocoaensis* trans. to *T. cunialensis*) were identified in the first section of core (1H-1) from Holes 1052A, 1052B, and 1052C, suggesting that the youngest Eocene sediments at these holes correlate with the top of Zone P15.

The base of Zone P15 is defined by the FO of *Porticulasphaera semiinvoluta* in Section 171B-1052A-9H-CC (79.82 mbsf). This species is a reliable marker, as it consistently occurs in low to moderate abundance throughout its range. The FO of *Hantkenina alabamensis* occurs in lower Zone P15, and the LO of *Subbotina linaperta* occurs in the middle of this zone. Zone P14 extends to the LO of *Orbulinoides beckmanni* in Sample 171B-1052A-15H-2, 64–66 cm (129.34 mbsf). The LO of *Morozovella spinulosa* is identified within uppermost Zone P14 in Core 171B-1052A-10H, which is slightly lower than the lowermost Zone P15 extinction noted by Berggren et al. (1995). The LO of *Acarinina bullbrooki* also is in this sample.

The *Orbulinoides beckmanni* Zone (Zone P13) spans about a 20-m thickness to the FO of the nominate species in Section 171B-1052A-17X-CC (142.4 mbsf). The nominate taxon of this zone consistently occurs in low abundance throughout its range. The LO of *Hantkenina dumblei* occurs at the base of this zone, as was observed at Sites 1050 and 1051. Zone P13 was observed only in the first core catcher from Hole 1052E.

A hiatus between middle Eocene Zone P12 and upper Paleocene Subzone P3b occurs in Holes 1052A and 1052E. In Hole 1052A, a moderately preserved Zone P12 assemblage, which includes *Morozovella lehneri*, *M. spinulosa*, and *Hantkenina dumblei*, but no *M. aragonensis*, occurs in Cores 171B-1052A-18X and 19X. This zone is recognized only in Core 171B-1052E-2R. Subzone P3b occurs immediately below in Samples 171B-1052A-20X-CC, 24–26 cm (163.4 mbsf), and 171B-1052E-4R-CC (165.75 mbsf) and is characterized by poorly preserved *Subbotina triloculinoides*, *M. pseudobulloides*, *M. velascoensis*, and *M. angulata*. Below Subzone P3b, the upper Paleocene Subzone P3a and the lower Paleocene Zones P2, P1c, P1b, and P α were identified. Foraminifers from Zone P α are remarkably well preserved and include *Parvulorugoglobigerina eugubina*, *Woodringina claytonensis*, *W. hornerstownensis*, and *Parasubbotina pseudobulloides*. Assemblages from this interval include reworked Cretaceous species (e.g., *Globotruncanita stuarti*, *Heterohelix globulosa*) and downhole contaminants from Subzone P1b.

Foraminifers are common to abundant and well preserved in the Maastrichtian *Abathomphalus mayaroensis* Zone and *Racemiguembelina fructifera* Zone. The nominate species of the *A. mayaroensis* Zone is very rare in nearly all samples, and its occurrence is sporadic in the middle of its range. The base of this zone, which is determined by the FO of *A. mayaroensis*, is placed in Section 171B-1052E-25R-CC (368.85 mbsf). *Racemiguembelina fructifera* occurs consistently in low to moderate abundance throughout its range. The FO of this species, which denotes the base of the *R. fructifera* Zone, is identified in Sample 171B-1052E-28R-3, 37–39 cm (399.67 mbsf). The

Table 4. Calcareous nannofossil datums for Site 1052, derived from the composite section of Holes 1052A and 1052E.

Datum	Species	Age (Ma)	Minimum depth (mbsf)	Maximum depth (mbsf)
B	<i>I. recurvus</i>	36.0	14.9	24.4
B	<i>C. oamaruensis</i>	37.0	78.4	79.8
T	<i>C. grandis</i>	37.1	78.4	79.86
B	<i>D. bisecta</i>	38.0	117.9	127.6
T	<i>C. solitus</i>	40.4	127.6	129.7
B	<i>C. reticulatum</i>	42.0	147.8	150.9
T	<i>N. fulgens</i>	43.1	155.9	158.7
B	<i>R. umbilica</i>	43.7	160.5	161.9
B	<i>N. fulgens</i>	47.3	160.5	161.9
B	<i>R. inflata</i>	48.5	162.7	163.3
B	<i>D. sublodoensis</i>	49.7	162.7	163.3
T	<i>C. danicus</i>	58.6	162.7	163.3
B	<i>E. macellus/E. bollii</i>	62.6	274.2	289.1
B	<i>C. danicus</i>	63.8	289.1	300.3
B	<i>C. tenuis</i>	64.5	300.3	302.1
B	<i>C. primus</i>	64.8	300.3	302.1
T	<i>E. turriseiffelli</i>	65.0	302.1	302.8
B	<i>M. prinsii</i>	66.0	327.7	329.2
B	<i>C. kampfmeri</i>	67.2	351.8	352.9
B	<i>M. murus</i>	68.5	377.1	379.2
T	<i>R. levis</i>	69.4	415.6	418.5
T	<i>T. phacelosus</i>	71.6	474.0	474.4
T	<i>R. asper</i>	93.9	474.0	474.4
T	<i>M. chistiatus</i>	94.4	474.0	474.4
B	<i>C. kennedyi</i>	97.4	491.4	492.5
T	<i>R. irregularis</i>	99.0	529.6	538.4
T	<i>H. albiensis</i>	99.0	516.8	529.6
B	<i>E. turriseiffelli</i>	101.7	655.8	675.5

Notes: Bases of age datums are represented as B; tops of age datums are represented as T.

FOs of *Contusotruncana contusa* and *C. plicata* occur just above the base of the *R. fructifera* Zone in Sample 171B-1052E-26R-4, 16–18 cm (381.76 mbsf). The LO of inoceramid prisms occurs near the base of the *R. fructifera* Zone, as was observed at Site 1049.

The *Gansserina gansseri* Zone and *Globotruncana falsostuarti* Zone could not be differentiated in Hole 1052E. This interval extends from Sample 171B-1052E-28R-CC, 0–4 cm (400.1 mbsf), to 36R-5, 110–111 cm (480.3 mbsf), and includes abundant and well-preserved assemblages in the upper part and moderately abundant and moderately preserved assemblages in the lower part. The *Radotruncana calcarata* Zone was not identified in Hole 1052E sediment. Hence, it is not possible to determine whether the lowermost part of *G. gansseri*–*G. falsostuarti* Zone is in the Campanian or Maastrichtian stage, based on planktonic foraminifers.

The hiatus separating the lower Cenomanian from younger Cretaceous sediments occurs at the base of a 4-m-thick slumped sequence in the upper part of Core 171B-1052E-36R. Within the slumped interval are specimens of poorly preserved *Contusotruncana fornicata*, *Globotruncana arca*, and other Campanian–Maastrichtian species, along with abundant rotaliporids and other taxa that have been reworked from the lower Cenomanian. Below this level, from Samples 171B-1052E-36R-6, 68–70 cm (481.3 mbsf), to 39R-2, 23–27 cm (503.7 mbsf), foraminifer assemblages are dominated by *Rotalipora brotzeni* and yield primitive morphotypes of *R. greenhornensis*, *R. appenninica*, *Praeglobotruncana delrioensis*, and other species that are characteristic of the *R. greenhornensis* Zone (lower Cenomanian).

Samples 171B-1052E-39R-6, 89–95 cm (509.8 mbsf), through 43R-CC, 30–33 cm (549.5 mbsf), are assigned to the *Rotalipora appenninica* Zone (upper Albian), based on the absence of *R. greenhornensis* and *R. brotzeni* and the presence of *R. appenninica*. The LOs of *R. ticinensis* and *Ticinella roberti* are at the top of this zone, the LO of *Favusella washitensis* is in the middle of this zone, and the LO of *Biticinella breggiensis* is in the lower part of this zone. The FOs of *Planomalina buxtorfi*, *Costellagerina libyca*, *Guembelina cenomana*, and *Shackoina cenomana* are near the base of this zone. The finely laminated dark green claystones in the *R. appenninica*

Zone yield beautifully preserved foraminifer assemblages and include some forms that have not been described previously.

The *Rotalipora ticinensis* Zone (upper Albian) ranges from the FO of *R. appenninica* in Sample 171B-1052E-44R-CC, 16–19 cm (558.0 mbsf), to the bottom of the hole. This zone is characterized by consistent occurrences of *Biticinella breggiensis* and *R. ticinensis*. The FOs of *Ticinella roberti* and *Favusella washitensis* are in the lower part of this zone, and the FOs of *Hedbergella simplex* and *Planomalina praebuxtorfi* are in the middle of this zone.

Radiolarians

Radiolarians were recovered from Eocene and Paleocene intervals at Site 1052. All core-catcher samples from Holes 1052A, 1052C, 1052D, and nearly all from 1052E were processed and examined. Core-catcher Samples 171B-1052B-4H-CC to 14H-CC were not processed because of time constraints. Many of the faunas from the upper half of Hole 1052A were well preserved, but the intervals from Samples 171B-1052A-16X-CC to 21X-CC contained poorly preserved faunas. The Paleocene samples in the upper part of Hole 1052E were, for the most part, diluted and poorly preserved because of high clay input and radiolarian test dissolution, respectively. The zonal numbers R1, R2, and R10 through R13 (see “Explanatory Notes” chapter, this volume) are used in the biostratigraphic correlation shown in Figure 20. Occurrence, abundance, and preservation of the radiolarian taxa are shown in Tables 8 and 9.

The youngest radiolarian faunas recovered thus far during Leg 171B were from the uppermost cores in Holes 1052A through 1052D. The youngest faunas, assignable to the *Calocyclus bandyca* Zone (Zone R13), were found in five cores, which included Samples 171B-1052A-3H-CC; 171B-1052B-2H-3, 85–88 cm; 171B-1052B-3H-CC; 171B-1052C-2H-CC; and 171B-1052D-2H-CC. The base and top of the zone are defined by the morphotypic first and last appearances, respectively, of the taxon *C. bandyca*. Although the taxa *Eusyringium fistuligerum* and *Thyrsocyrtis triacantha* make their last appearance within the zone, a large number of species become extinct at the upper boundary including *C. hispada*, *Lychnocanoma bellum*, *Podocyrtis papalis*, and *Thyrsocyrtis tetracantha*.

Samples 171B-1052A-5H-CC, 6H-CC, and 8H-CC contained radiolarians indicative of the upper middle to upper Eocene *Cryptocarpium azyx* Zone (Zone R12). The base of this zone is defined by the first appearance of the species *C. azyx*. The easily recognizable taxon *Calocyclus turris* makes its first appearance and *Podocyrtis chalara* makes its last appearance within the zone. Inflated forms of *Eusyringium fistuligerum* are common throughout the zone. Sample 171B-1052A-4H-CC contained poorly preserved, middle to late Eocene taxa assignable to the radiolarian Zones R11 (*P. goetheana* Zone) to R13 (*Calocyclus bandyca* Zone). Sample 171B-1052A-7H-CC also contained a poorly preserved fauna, placing it in Zones R12–R13.

Core-catcher Samples 171B-1052A-9H-CC through 13H-CC contained moderately to well-preserved faunas that are assigned to the *Podocyrtis goetheana* Zone (Zone R11). The bottom of the zone is characterized by the first appearance of *P. goetheana*, which, however, was very rare and was found only in Sample 171B-1052A-6H-CC. The taxa *Dictyopora pirum* and *Thyrsocyrtis tetracantha* make their first appearances within the zone, and *Spongatractus pachystylus* has its last occurrence at the top. The lower limit of the zone is also synchronous with the evolutionary transition of the *Lithocyclus ocellus* group to the *L. aristotelis* group. *Eusyringium fistuligerum* is present within Samples 9H-CC through 13H-CC and is represented by two morphotypes: one that is slender with a narrow thorax and distally prolonged with a long, porous tube, and a shorter one with an inflated thorax and shorter distal tube.

Two samples, 171B-1052A-14H-CC and 15H-CC, were assigned to the *Podocyrtis chalara* Zone (Zone R10) and are the last samples

Table 5. Planktonic foraminifer datum list for Site 1052.

Datum	Species	Zone	Age (Ma)	Core, section, interval (cm)	Minimum depth (mbsf)	Maximum depth (mbsf)
				171B-1052A-		
T	<i>M. spinulosa</i>		38.10	10H-CC, 12-15	83.37	89.37
B	<i>P. semiinvoluta</i>	b P15	38.40	9H-CC, 0-4	79.82	83.35
T	<i>O. beckmanni</i>	b P14	40.10	15H-CC, 14-16	127.62	129.34
B	<i>O. beckmanni</i>	b P13	40.50	17X-CC, 16-18	142.47	149.39
B	<i>T. pomeroli</i>		42.40	19X-CC, 37-39	162.90	163.43
B	<i>G. index</i>		42.90	19X-CC, 37-39	162.90	163.43
B	<i>M. lehneri</i>		43.50	17X-3, 33-35	139.33	142.47
B	<i>M. velascoensis</i>	b P3b	60.00	20X-CC, 16-18	163.43	168.64
				171B-1052E-		
B	<i>O. beckmanni</i>	b P13	40.50	1R-CC, 16-19	142.15	148.14
B	<i>T. pomeroli</i>		42.40	2R-CC, 18-21	148.14	159.46
B	<i>G. index</i>		42.90	2R-CC, 18-21	148.14	159.46
B	<i>M. velascoensis</i>	b P3b	60.00	4R-CC, 0-3	165.75	175.27
B	<i>M. conicotruncata</i>	b P3a	60.90	5R-1, 7-8	175.27	185.50
B	<i>I. pusilla</i>		61.00	8R-CC 14-17	210.39	215.97
B	<i>M. praeangulata</i>	b P2	61.20	12R-CC, 4-7	248.17	256.05
B	<i>P. uncinata</i>	b P2	61.20	12R-CC, 4-7	248.17	256.05
B	<i>G. compressa</i>	b P1c	63.00	15R-CC, 24-26	274.16	289.11
B	<i>P. inconstans</i>	b P1c	63.00	16R-6, 75-76	289.11	300.33
B	<i>S. triloculinoides</i>	b P1b	64.30	17R-CC, 18-20	300.33	302.19
T	<i>P. eugubina</i>		64.70	18R-2, 48.5-49	300.33	302.09
B	<i>P. eugubina</i>	b P α	64.97	18R-2, 48.5-49	302.09	302.19
B	<i>A. mayaroensis</i>	b A. mayaroensis	68.25	25R-CC, 0-4	368.85	379.16
B	<i>R. fructicosa</i>	b R. fructicosa	69.60	28R-3, 37-39	399.67	400.12
B	<i>C. contusa</i>		69.60	26R-4, 16-18	381.76	385.00
T	<i>R. cushmani</i>	b R. cushmani	93.90	36R-5, 110-111	473.57	480.31
B	<i>R. greenhornensis</i>	b R. greenhornensis	98.90	37R-CC, 0-1	492.45	496.38
B	<i>R. appenninica</i>	b R. appenninica	100.40	41R-CC 20-23	529.52	538.33

Notes: Bases of age and biozonal datums are represented by B and b; tops of age and biozonal datums are represented by T and t.

downhole in Hole 1052A that contain well-preserved radiolarians. The base of the zone is defined by the evolutionary transition of *P. mitra* to *P. chalara*, and *P. trachodes* makes its last appearance in the top of the zone. The lower limit of the zone is also synchronous with the extinction of the key marker *Phormocyrtis striata striata*. However, a more inflated, undescribed morphotype similar to *Phormocyrtis s. striata* first appears in the lower part of the *P. chalara* Zone and ranges into the overlying *P. goetheana* Zone. Sample 171B-1052A-17X-CC contains only fragments of three long-ranging species (Table 8) that are indicative of a general late middle to late Eocene age.

Samples from both Holes 1052A and 1052E contain mostly poorly preserved radiolarian faunas of Paleocene age (Tables 8, 9). Faunas from core-catcher Samples 171B-1052A-20X-CC and 21X-CC are from the early Eocene/late Paleocene *Bekoma bidartensis* Zone (Zone R2) and the Paleocene *B. campechensis* Zone (Zone R1). The same zonal ages were assigned to poorly preserved Samples 171B-1052E-4R-CC and 9R-CC.

A number of samples from Hole 1052E yielded Paleocene radiolarians. Core-catcher Samples 171B-1052E-7R-CC, 8R-CC, and 10R-CC to 13R-CC contain moderately to poorly preserved faunas belonging to the *Bekoma campechensis* Zone (Zone R1). This zone is defined by the first appearance of *B. campechensis* and contains the common form *Buryella tetradica*, which ranges down into the unzoned Paleocene. Another *Buryella* species, *B. pentadica*, although generally rare, is restricted to this zone.

Samples 171B-1052E-14R-CC and 15R-CC contain faunas that are older than the *Bekoma campechensis* Zone of Riedel and Sanfilippo (1978) and therefore are not assignable to any formal radiolarian faunal zone. However, both Blome (1992) and Nishimura (1992) have shown that some taxa can be biostratigraphically useful in dating the lower part of the Paleocene. Specific examples include the taxa *Entapium regulare* and *Phormocyrtis striata prexquisita*.

Few Cretaceous radiolarians were found in samples from any of the holes at Site 1052. Several poorly preserved forms of *Lychnocanoma* sp. were found in core-catcher Sample 171B-1052E-19X-CC, and several forms belonging to the Cretaceous genus *Dictyomitra* were found in Core 171B-1052E-30R. Also, core-catcher Sample

171B-1052E-33R-CC contained one form similar to *Orbiculiforma* sp. of unknown age.

Benthic Foraminifers

Hole 1052A was analyzed for benthic foraminifers of middle to late Eocene age, and Hole 1052E was analyzed for those of late Paleocene to early Maastrichtian and early Cenomanian to late Albian age (Table 10). Preservation of benthic foraminifers is very good to moderate throughout the examined samples, with the exception of Sample 171B-1052E-8R-CC, 14–17 cm, in which preservation is poor. The abundance of benthic foraminifers is high throughout both holes, except for Sample 171B-1052E-41R-1, 98.5–101 cm (Table 10). This sample was taken from the late Albian laminated dark green claystones and provided very few benthic foraminifers in the routinely examined (>125 μ m) fraction. However, the smaller (63–125 μ m) fraction of this sample contained high abundances of benthic foraminifers (see below).

Paleodepth estimates based on benthic foraminifers reveal a deepening-upward trend through time. The presence of shallow-water taxa, such as miolinids and robust *Lenticulina*, and the absence of certain bathyal forms (e.g., *Osangularia* spp. and *Gavelinella* spp.) suggest middle–outer neritic depths (~100–200 m) during late Albian–early Cenomanian times. Middle bathyal depths (~600–1000 m) are suggested for the latest Cretaceous (Maastrichtian) and Paleogene (Paleocene–late Eocene), based on low abundances of *Nuttalides truempyi* and rare occurrences of *Aragonia* throughout this interval.

The late to middle Eocene fauna from Hole 1052A is characterized by *Bulimina alazanensis*, *B. macilenta*, *B. impendens*, *B. semicostata*, *B. tuxpamensis*, *Buliminella grata spinosa*, *Cibicoides grimsdalei*, *C. laurissae*, *C. mexicanus*, *C. tuxpamensis*, *Gavelinella capitata*, *Globocassidulina subglobosa*, *Gyrodinoides girardanus*, *Hanzawaia cushmani*, *Hanzawaia?* sp., *Karrerella chapapotensis*, *K. subglabra*, *Planulina costata*, *Pullenia eoacenaica*, *Vulvulina mexicana*, and *V. spinosa*. In addition, several taxa are present that range throughout the Maastrichtian and Paleocene in Hole 1052E, including

Table 7 (continued).

Age	Zone	Core, section, interval (cm)	Depth (mbsf)	Abundance	Preservation	<i>Globotruncana limicina</i>	<i>Globotruncana petaloides</i>	<i>Planoglobulina acervulinoides</i>	<i>Heterohelix globulosa</i>	<i>Contusotruncana patelliformis</i>	<i>Globotruncana orientalis</i>	<i>Globotruncana falsostuarti</i>	<i>Rugoglobigerina rugosa</i>	<i>Contusotruncana walfischensis</i>	<i>Globigerinelloides alvarezii</i>	<i>Globotruncamita stuarti</i>	<i>Heterohelix navarroensis</i>	<i>Laeviheterohelix glabrans</i>	<i>Planoglobulina multicamerata</i>	<i>Globotruncana aegyptiaca</i>	<i>Globotruncana esnehensis</i>	<i>Globotruncanella havanensis</i>	<i>Racemiguembelina fructicosa</i>	<i>Globotruncana dupeblei</i>	<i>Contusotruncana comtusa</i>	<i>Contusotruncana plicata</i>	<i>Globotruncana rosetta</i>	<i>Pseudoguembelina excolata</i>	<i>Pseudoguembelina palpebra</i>	<i>Abathomphalus intermedius</i>	<i>Abathomphalus mayaroensis</i>	<i>Gublerina cuvillieri</i>		
middle Eocene	P13	171B-1052E-1R-CC, 16-19	142.15	A	G																													
middle Eocene	P12	2R-CC, 18-21	148.14	A	G																													
?		3R-CC, 12-15	159.46	T	P																													
late Paleocene	P3b	4R-CC, 0-3	165.75	R	M																													
late Paleocene	P3a	5R-1 7-8	175.27	F	P																													
late Paleocene	P3a	6R-CC, 20-23	185.50	R	P																													
late Paleocene	P3a	7R-CC, 5-8	194.45	R	P																													
late Paleocene	P3a	8R-CC, 14-17	210.39	R	P																													
late Paleocene	P3a	9R-CC, 17-19	215.97	R	P																													
late Paleocene	P3a	10R-CC, 11-13	230.90	R	P																													
early Paleocene	P2	11R-CC, 16-18	234.80	R	P																													
early Paleocene	P2	12R-CC, 4-7	248.17	F	M																													
early Paleocene	P1c	13R-CC, 20-22	256.05	F	M																													
early Paleocene	P1c	14R-CC, 17-20	263.41	F	M																													
early Paleocene	P1c	15R-CC, 24-26	274.16	F	M																													
early Paleocene	P1c	16R-6, 75-76	289.11	T	P																													
early Paleocene	P1b	17R-CC, 18-20	300.33	R	M																													
early Paleocene	P0x	18R-2, 48.5-49	302.09	A	VG																													
Maastrichtian	<i>A. mayaroensis</i>	18R-2, 59-61	302.19	C	M								R									F												
Maastrichtian	<i>A. mayaroensis</i>	18R-3, 56-58	302.77	A	G								R									F												
Maastrichtian	<i>A. mayaroensis</i>	19R-CC, 9-11	311.76	A	G	P							R									F												
Maastrichtian	<i>A. mayaroensis</i>	20R-CC, 19-21	329.15	A	G								R									F												
Maastrichtian	<i>A. mayaroensis</i>	21R-CC, 20-22	336.17	A	G								R									F												
Maastrichtian	<i>A. mayaroensis</i>	22R-CC, 20-23	343.98	A	G								R									F												
Maastrichtian	<i>A. mayaroensis</i>	23R-CC, 18-21	354.72	A	G		F						R									F												
Maastrichtian	<i>A. mayaroensis</i>	24R-CC, 9-12	362.57	A	G								R									F												
Maastrichtian	<i>A. mayaroensis</i>	25R-CC, 0-4	368.85	A	G								R									F												
Maastrichtian	<i>R. fructicosa</i>	26R-2, 56-59	379.16	A	G		R	F					R									F												
Maastrichtian	<i>R. fructicosa</i>	26R-4, 16-18	381.76	C	G								R									F												
Maastrichtian	<i>R. fructicosa</i>	26R-6, 40-43	385.00	A	G								R									F												
Maastrichtian	<i>R. fructicosa</i>	26R-CC, 35-38	387.01	A	G	R							R									F												
Maastrichtian	<i>R. fructicosa</i>	27R-CC, 15-17	395.36	A	G								R									F												
Maastrichtian	<i>R. fructicosa</i>	28R-3, 37-39	399.67	R	M								R									F												
Campanian-Maastrichtian	<i>G. gansseri-G. falsostuarti</i>	28R-CC, 0-4	400.12	A	G								R									F												
Campanian-Maastrichtian	<i>G. gansseri-G. falsostuarti</i>	29R-CC, 0-3	414.52	A	G								R									F												
Campanian-Maastrichtian	<i>G. gansseri-G. falsostuarti</i>	30R-6, 122-125	424.22	A	G								R									F												
Campanian-Maastrichtian	<i>G. gansseri-G. falsostuarti</i>	31R-CC, 12-15	434.89	C	M	R		F					R									F												
Campanian-Maastrichtian	<i>G. gansseri-G. falsostuarti</i>	33R-CC, 13-15	445.93	C	M	R	R						R									F												
Campanian-Maastrichtian	<i>G. gansseri-G. falsostuarti</i>	34R-2, 57-58	455.97	A	G	R	R						R									F												
Campanian-Maastrichtian	<i>G. gansseri-G. falsostuarti</i>	35R-CC, 19-21	468.66	F	G	R	R						R									F												
Campanian-Maastrichtian	<i>G. gansseri-G. falsostuarti</i>	36R-1, 35-37	473.55	C	M	F	P	R	F				R									F												
Campanian-Maastrichtian	<i>G. gansseri-G. falsostuarti</i>	36R-1, 110-112	474.30	R	M								R									F												
Cenomanian	<i>R. greenhornensis</i>	36R-6, 68-70	481.38	A	G								R									F												
Cenomanian	<i>R. greenhornensis</i>	36R-CC, 0-1	482.55	R	P								R									F												
Cenomanian	<i>R. greenhornensis</i>	37R-2, 32-35	484.13	A	G								R									F												
Cenomanian	<i>R. greenhornensis</i>	37R-6, 74-78	490.55	F	M								R									F												
Cenomanian	<i>R. greenhornensis</i>	37R-CC, 0-1	492.45	C	G								R									F												
Cenomanian	<i>R. greenhornensis</i>	38R-3, 98-103	496.38	F	G								R									F												
Cenomanian	<i>R. greenhornensis</i>	38R-5, 103-111	499.43	F	G								R									F												
Cenomanian	<i>R. greenhornensis</i>	38R-CC, 0-1	501.08	F	G								R									F												
Cenomanian	<i>R. greenhornensis</i>	39R-2, 23-27	503.73	R	G								R									F												
Albian	<i>R. appenninica</i>	39R-6, 89-95	509.89	C	VG								R									F												
Albian	<i>R. appenninica</i>	39R-CC, 24-25	511.37	C	VG								R									F												
Albian	<i>R. appenninica</i>	40R-2, 90-92	513.00	F	M								R					</																

Table 7 (continued).

Age	Zone	Core, section, interval (cm)	Depth (mbsf)	Abundance	Preservation	<i>Morozovella velascoensis</i>	<i>Muricella albeari</i>	<i>Acarina bullbrooki</i>	<i>Catapsydrax dissimilis</i>	<i>Globigerinatheka index</i>	<i>Hankenina dumblei</i>	<i>Morozovella spinulosa</i>	<i>Subbotina venezuelana</i>	<i>Truncorotaloides rohri</i>	<i>Turborotalia pomeroli</i>	<i>Turborotalia pseudomayeri</i>	<i>Acarina primitiva</i>	<i>Orbulinoides beckhami</i>	<i>Pseudohastigerina micra</i>	<i>Subbotina linaperta</i>	<i>Turborotalia cerroazulensis</i>	
middle Eocene	P13	171B-1052E-1R-CC, 16-19	142.15	A G				F R F		F		R R R										
middle Eocene	P12	2R-CC, 18-21	148.14	A G				F R F		F		R R R					P	R R R			F P	
?	?	3R-CC, 12-15	159.46	T P																		
late Paleocene	P3b	4R-CC, 0-3	165.75	R M	P R																	
late Paleocene	P3a	5R-1, 7-8	175.27	F P																		
late Paleocene	P3a	6R-CC, 20-23	185.50	R P																		
late Paleocene	P3a	7R-CC, 5-8	194.45	R P																		
late Paleocene	P3a	8R-CC, 14-17	210.39	R P																		
late Paleocene	P3a	9R-CC, 17-19	215.97	R P																		
late Paleocene	P3a	10R-CC, 11-13	230.90	R P																		
early Paleocene	P2	11R-CC, 16-18	234.80	R P																		
early Paleocene	P2	12R-CC, 4-7	248.17	F M																		
early Paleocene	P1c	13R-CC, 20-22	256.05	F M																		
early Paleocene	P1c	14R-CC, 17-20	263.41	F M																		
early Paleocene	P1c	15R-CC, 24-26	274.16	F M																		
early Paleocene	P1c	16R-6, 75-76	289.11	T P																		
early Paleocene	P1b	17R-CC, 18-20	300.33	R M																		
early Paleocene	Pα	18R-2, 48.5-49	302.09	A VG																		
Maastrichtian	<i>A. mayaroensis</i>	18R-2, 59-61	302.19	C M																		
Maastrichtian	<i>A. mayaroensis</i>	18R-3, 56-58	302.77	A G																		
Maastrichtian	<i>A. mayaroensis</i>	19R-CC, 9-11	311.76	A G																		
Maastrichtian	<i>A. mayaroensis</i>	20R-CC, 19-21	329.15	A G																		
Maastrichtian	<i>A. mayaroensis</i>	21R-CC, 20-22	336.17	A G																		
Maastrichtian	<i>A. mayaroensis</i>	22R-CC, 20-23	343.98	A G																		
Maastrichtian	<i>A. mayaroensis</i>	23R-CC, 18-21	354.72	A G																		
Maastrichtian	<i>A. mayaroensis</i>	24R-CC, 9-12	362.57	A G																		
Maastrichtian	<i>A. mayaroensis</i>	25R-CC, 0-4	368.85	A G																		
Maastrichtian	<i>R. fructicosa</i>	26R-2, 56-59	379.16	A G																		
Maastrichtian	<i>R. fructicosa</i>	26R-4, 16-18	381.76	C G																		
Maastrichtian	<i>R. fructicosa</i>	26R-6, 40-43	385.00	A G																		
Maastrichtian	<i>R. fructicosa</i>	26R-CC, 35-38	387.01	A G																		
Maastrichtian	<i>R. fructicosa</i>	27R-CC, 15-17	395.36	A G																		
Maastrichtian	<i>R. fructicosa</i>	28R-3, 37-39	399.67	R M																		
Campanian-Maastrichtian	<i>G. gansseri-G. falsostuarti</i>	28R-CC, 0-4	400.12	A G																		
Campanian-Maastrichtian	<i>G. gansseri-G. falsostuarti</i>	29R-CC, 0-3	414.52	A G																		
Campanian-Maastrichtian	<i>G. gansseri-G. falsostuarti</i>	30R-6, 122-125	424.22	A G																		
Campanian-Maastrichtian	<i>G. gansseri-G. falsostuarti</i>	31R-CC, 12-15	434.89	C M																		
Campanian-Maastrichtian	<i>G. gansseri-G. falsostuarti</i>	33R-CC, 13-15	445.93	C M																		
Campanian-Maastrichtian	<i>G. gansseri-G. falsostuarti</i>	34R-2, 57-58	455.97	A G																		
Campanian-Maastrichtian	<i>G. gansseri-G. falsostuarti</i>	35R-CC, 19-21	468.66	F G																		
Campanian-Maastrichtian	<i>G. gansseri-G. falsostuarti</i>	36R-1, 35-37	473.55	C M																		
Campanian-Maastrichtian	<i>G. gansseri-G. falsostuarti</i>	36R-1, 110-112	474.30	R M																		
Cenomanian	<i>R. greenhornensis</i>	36R-6, 68-70	481.38	A G																		
Cenomanian	<i>R. greenhornensis</i>	36R-CC, 0-1	482.55	R P																		
Cenomanian	<i>R. greenhornensis</i>	37R-2, 32-35	484.13	A G																		
Cenomanian	<i>R. greenhornensis</i>	37R-6, 74-78	490.55	F M																		
Cenomanian	<i>R. greenhornensis</i>	37R-CC, 0-1	492.45	C G																		
Cenomanian	<i>R. greenhornensis</i>	38R-3, 98-103	496.38	F G																		
Cenomanian	<i>R. greenhornensis</i>	38R-5, 103-111	499.43	F G																		
Cenomanian	<i>R. greenhornensis</i>	38R-CC, 0-1	501.08	F G																		
Cenomanian	<i>R. greenhornensis</i>	39R-2, 23-27	503.73	R G																		
Albian	<i>R. appenninica</i>	39R-6, 89-95	509.89	C VG																		
Albian	<i>R. appenninica</i>	39R-CC, 24-25	511.37	C VG																		
Albian	<i>R. appenninica</i>	40R-2, 90-92	513.00	F M																		
Albian	<i>R. appenninica</i>	40R-5, 69-71	516.79	A VG																		
Albian	<i>R. appenninica</i>	41R-1, 98.5-101	521.29	A VG																		
Albian	<i>R. appenninica</i>	41R-3, 49-52	523.79	A G																		
Albian	<i>R. appenninica</i>	41R-CC, 20-23	529.52	A VG																		
Albian	<i>R. appenninica</i>	42R-CC, 10-14	538.33	A VG																		
Albian	<i>R. appenninica</i>	43R-CC, 30-33	549.51	F M																		
Albian	<i>R. ticinensis</i>	44R-CC, 16-19	558.07	A G																		
Albian	<i>R. ticinensis</i>	45R-CC, 0-4	561.06	F G																		
Albian	<i>R. ticinensis</i>	46R-CC, 8-10	575.66	R M																		
Albian	<i>R. ticinensis</i>	47R-7, 42-43	587.42	R M																		
Albian	<i>R. ticinensis</i>	48R-CC, 19-21	597.41	R M																		
Albian	<i>R. ticinensis</i>	49R-CC, 0-2	604.39	R G																		
Albian	<i>R. ticinensis</i>	50R-CC, 0-2	610.73	R M																		
Albian	<i>R. ticinensis</i>	51R-CC, 13-16	619.31	R M																		
Albian	<i>R. ticinensis</i>	52R-CC, 22-24	627.66	R M																		
Albian	<i>R. ticinensis</i>	53R-CC, 0-2	635.18	R G																		
Albian	<i>R. ticinensis</i>	54R-CC, 0-3	640.39	B																		
Albian	<i>R. ticinensis</i>	55R-7, 39-41	655.79	R G																		
Albian	<i>R. ticinensis</i>	57R-CC, 23-26	675.48	R G																		
Albian	<i>R. ticinensis</i>	58R-CC, 17-20	682.57	F G																		

Table 8. Radiolarian abundance and preservation in Hole 1052A.

Age	Zone	Core, section, interval (cm)	Depth (mbsf)	Abundance	Preservation	<i>Baryella tetratica</i>	<i>Enapium regulare</i>	<i>Sylosphaera coronatus coronatus</i>	<i>Calocyclus hispida</i>	<i>Dicropora mongolfieri</i>	<i>Eusyringium fistuligerum</i>	<i>Lithocyclia aristata</i> group	<i>Lychnocanoma bellum</i>	<i>Podocyrtis (Lampertium) chalara</i>	<i>Podocyrtis (Lampertium) trachodes</i>	<i>Podocyrtis (Podocyrtis) papalis</i>	<i>Theocopylissa ficus</i>	<i>Thyrocyrtilis (Pentalacorys) triacantha</i>	<i>Thyrocyrtilis (Thyrocyrtilis) rhizodon</i>	<i>Dicropora pirum</i>	<i>Serthocyrtilis triconicus</i>	<i>Tristylolypis triceros</i>	<i>Thyrocyrtilis (Pentalacorys) tetracantha</i>	<i>Cryptocarpium azyx</i>	<i>Dicropora armadillo</i>	<i>Calocyclus turris</i>	<i>Podocyrtis (Lampertium) goetheana</i>	<i>Artophormis barbadiensis</i>	<i>Calocyclus bandyca</i>	<i>Theocyrtilis tuberosa</i>			
late Eocene	<i>Calocyclus bandyca</i>	171B-1052A	0.84	B																													
late Eocene-middle Eocene	<i>Calocyclus bandyca-Podocyrtis goetheana</i>	1X-CC, 7-9	11.96	B																													
late Eocene-middle Eocene	<i>Cryptocarpium azyx</i>	3H-CC, 9-12	22.65	C	VG			F	C	R	R						R	F			F	F	R	C		C		R	R				
late Eocene-middle Eocene	<i>Cryptocarpium azyx</i>	4H-CC, 14-17	32.59	R	P												T					T											
late Eocene-middle Eocene	<i>Calocyclus bandyca-Cryptocarpium azyx</i>	5H-CC, 14-16	41.97	A	VG			F	C	R	R							F	F	R		F	F	R	F	F	R	C					
late Eocene-middle Eocene	<i>Cryptocarpium azyx</i>	6H-CC, 11-13	51.4	C	G			F	R	F	R						C		R	R		F	R	F	R	F	F	R					
late Eocene-middle Eocene	<i>Cryptocarpium azyx</i>	7H-CC, 19-21	61.18	R	P																												
middle Eocene	<i>Podocyrtis goetheana</i>	8H-CC, 21-23	70.39	C	G			F	C	F	R											F	C	F	F								
middle Eocene	<i>Podocyrtis goetheana</i>	9H-CC, 0-4	79.82	C	G			F	A	F	R	F	F				F	R	F	F	F	R	F	F									
middle Eocene	<i>Podocyrtis goetheana</i>	10H-CC, 12-15	89.34	C	M			C	C	C	F	F					F	R	F	F	F												
middle Eocene	<i>Podocyrtis goetheana</i>	11H-CC, 21-24	99.04	F	M			F	A	F	F											C	F	C	R		F						
middle Eocene	<i>Podocyrtis goetheana</i>	12H-7, 52-54	108.22	C	VG			C	C	F	F	F									C	R	F	F	R	R							
middle Eocene	<i>Podocyrtis goetheana</i>	13H-CC, 16-18	117.9	A	VG			F	A	C	R	F	F								C	F	R	R	R								
middle Eocene	<i>Podocyrtis chalara</i>	14H-CC, 22-25	127.59	C	M			A	F	R	F	F									C	F	F										
middle Eocene	<i>Podocyrtis chalara</i>	15H-CC, 14-16	129.67	C	VG			C	C	F	R	C	F	F							C	R	F	F									
middle Eocene	<i>Calocyclus bandyca-Thyrocyrtilis triacantha</i>	16X-CC, 17-19	134.95	B																													
middle Eocene	<i>Calocyclus bandyca-Thyrocyrtilis triacantha</i>	17X-CC, 16-18	142.47	R	P			T	T	T																							
Paleocene	<i>Bekoma bidartensis-Bekoma campechensis</i>	18X-CC, 16-18	154.76	B																													
Paleocene	<i>Bekoma bidartensis-Bekoma campechensis</i>	20X-CC, 16-18	163.29	T	P	T																											
Paleocene	<i>Bekoma bidartensis-Bekoma campechensis</i>	19X-CC, 37-39	164.36	B																													
Paleocene	<i>Bekoma bidartensis-Bekoma campechensis</i>	21X-CC, 24-26	168.64	T	P	T	T	T																									

Notes: Abundance: B = barren; C = common; R = rare; F = few; A = abundant; T = trace. Preservation: VG = very good; P = poor; G = good; M = moderate.

pleurostomellids, *Bulimina trinitatis*, *Nodogenerina* spp., *Nuttallides truempyi*, *Oridorsalis* spp., and *Spiroplectammina spectabilis*.

The majority of taxa present in the Paleocene sequence from Hole 1052E consist of species that survived the K/T boundary event, including *Alabama* sp. A, *Allomorphina trochoides*, *Aragonia velascoensis*, *Bolivinoidea delicatulus*, *B. paleocenica*, *Bulimina trinitatis*, *Cibicoides hyphalus*, *C. velascoensis*, *Gaudryina pyramidata*, *Gavelinella beccariiformis*, *Gyroidinoides depressus*, *G. globosus*, *Nuttallides truempyi*, *Oridorsalis* spp., *Pyramidina rudita*, *Quadrinophina allomorphinoides*, and *Spiroplectammina spectabilis*. Relatively few taxa emerged in the Paleocene, including *Anomalinoidea praespissiformis*, *Bulimina* sp. (triangular), *Buliminella beaumonti*, *B. grata*, *Charltonia*? sp., *Cibicoides dayi*, *Coryphostoma midwayensis*, *Globorotalites* sp. A, *Neoflabellina semireticulata*, *Nodogenerina* spp., and *Pyramidina*? sp.

The Maastrichtian interval is characterized by a number of taxa that do not occur in the Paleocene sequence in Hole 1052E, including *Coryphostoma incrassata*, *Eowigerina subsculptura*, *Marssonella oxycona*, *Nuttallinella florealis*, *Osangularia navarroana*, *O. velascoensis*, *Paralabamina lunata*, *Praebulimina reussi*, *Pseudowigerina plummerae*, *Reussella szajnochae*, *Sitella* sp. cf. *S. plana*, *Sliteria varsoviensis*, *Spiroplectammina* spp., and *Stensioina pommerana*. All of the Upper Cretaceous samples (except the uppermost Maastrichtian Sample 171B-1052E-18R-2, 59–61 cm) are represented by oligotaxic faunas, of which *E. subsculptura* constitutes 20%–40%. Such oligotaxic faunas have not been reported in deep-sea material before. The occurrence of *Eowigerina subsculptura* (together with *Sliteria varsoviensis*) provides evidence for high productivity over the Blake Nose during latest Cretaceous times (Widmark and Speijer, in press).

A fragmented, but otherwise well-preserved, Lower Cretaceous (early Cenomanian to late Albian) benthic foraminifer fauna was found in Hole 1052E (Table 10). The assemblage indicates shallow (neritic) depths of deposition (see above). Shipboard examination of a sample from the upper Albian laminated dark green claystones

(Sample 171B-1052E-41R-1, 98.5–101.0 cm) found only a very few benthic foraminifers in the >125- μ m fraction. Examination of the 63- to 125- μ m fraction, however, revealed a well-preserved fauna consisting of small, delicate, thin-walled lagenids (e.g., *Lenticulina* and *Dentalina*), buliminids, and pleurostomellids, all of which are indicative of low-oxygen conditions. Further investigations based on benthic foraminifers in these laminated dark green claystones will provide a unique opportunity to study population dynamics and structures of faunal alteration between “normal,” well-oxygenated conditions and oxygen-stressed environments during the Early Cretaceous.

Sediment Accumulation Rates

Ages and sub-bottom depths for calcareous nannofossil and planktonic foraminifer datums used to calculate sediment accumulation rates in Holes 1052A and 1052E are listed in Tables 4 and 5 and are plotted in Figure 21. The 684.8-m total interval cored at these two holes ranges in age from 36 to 102 Ma. The sediment accumulation rate during the middle and late Eocene was moderately high for an open-ocean pelagic setting, averaging 18 m/m.y. (Fig. 21). This slightly elevated rate reflects the contribution of both calcareous and siliceous plankton productivity. The early middle Eocene, early Eocene, and late Paleocene are represented largely by a disconformity, although microfossils from these ages are reworked into the foraminifer packstones of the basal middle Eocene section.

The sediment accumulation rate for the Danian through Maastrichtian interval is similar, with an average value of ~22 m/m.y. This sequence is separated from the underlying mid-Cretaceous sequence by a substantial disconformity with a hiatus of ~26 m.y. Hemipelagic sediment accumulation during the early Cenomanian and the late Albian was almost twice this fast, with an average rate of ~43 m/m.y. This reflects a much higher dominance of clastic sedimentation as the neritic facies became more proximal to the drilling site.

A hiatus spanning ~17 m.y. occurs between the middle Eocene (~44 Ma) and upper Paleocene (~61 Ma), and another hiatus span-

Table 9. Radiolarian abundance and preservation at Hole 1052E.

Age	Zone	Core, section, interval (cm)	Depth (mbsf)	Abundance	Preservation	<i>Buryellateradica</i>	<i>Entapium regulare</i>	<i>Lychnocamona</i> sp. B	<i>Stylosphaera coronatus coronatus</i>	<i>Stylosphaera goruna</i>	<i>Stylotrichus alveatus</i>	<i>Xiphosphaera circularis</i>	<i>Ampliyemium splendiaratum</i>	<i>Dorcadospyrus</i> sp. cf. <i>D. platycantha</i>	<i>Lychnocamona</i> (?) <i>pileus</i>	<i>Buryella pentadica</i>	<i>Clathrocyclomma parvum</i>	<i>Phormocypris striata praesquisita</i>	
Paleocene	<i>B. bidartensis</i> - <i>B. campechensis</i>	171B-1052E-1R-CC, 16-19	142.15	B															
		2R-CC, 18-21	148.14	B															
		3R-CC, 12-15	159.46	B															
		4R-CC, 0-3	165.75	R	P	R				R									
		6R-CC, 20-23	185.5	B															
		7R-CC, 5-8	194.45	T	M	T				T									
		8R-CC, 14-17	210.39	T	P	T				T									
		9R-CC, 17-19	215.97	T	P	T													
		10R-CC, 11-13	230.9	F	P	R				F			R						
		11R-CC, 16-18	234.8	R	P	R				R			R		R				
		12R-CC, 4-7	248.17	R	P	R				R		R	R		R				
		13R-CC, 20-22	256.05	F	M	F	R			C		R	C	F	R	F			
		14R-CC, 17-20	263.41	F	P	F	R			F			F	F	F	F			
		15R-CC, 24-26	274.16	F	M	F	R	C		F	R		R						
		17R-CC, 18-20	300.33	B	P														
		19R-CC, 9-11	311.76	T	P														
		20R-CC, 19-21	329.15	B															
		21R-CC, 20-22	336.17	B															
		22R-CC, 20-23	343.98	B															
		23R-CC, 18-21	354.72	B															
24R-CC, 9-12	362.57	B																	
25R-CC, 0-4	368.85	B																	
26R-CC, 35-38	387.01	B																	
27R-CC, 15-17	395.36	B																	
28R-CC, 0-4	400.12	B																	
29R-CC, 0-3	414.52	B																	
30R-6, 122-125	424.22	T																	
31R-CC, 12-15	434.89	B																	
33R-CC, 13-15	445.93	T	P																
35R-CC, 19-21	468.66	B																	
36R-CC, 0-1	482.55	B																	
37R-CC, 0-1	492.45	B																	
38R-CC, 0-1	501.08	B																	
39R-CC, 24-25	511.37	B																	
40R-5, 69-71	516.79	B																	
41R-CC, 20-23	529.52	B																	
42R-CC, 10-14	538.33	B																	
44R-CC, 16-19	558.07	B																	
46R-CC, 8-10	575.66	B																	
48R-CC, 19-21	597.41	B																	
50R-CC, 0-2	610.73	B																	
51R-CC, 13-16	619.31	B																	
52R-CC, 22-24	627.66	B																	
55R-7, 39-41	655.79	B																	
57R-CC, 23-26	675.48	B																	

Notes: Abundance: B = barren; R = rare; T = trace; F = few; C = common. Preservation: P = poor; M = moderate.

ning ~26 m.y. occurs between the Maastrichtian (~71 Ma) and lower Cenomanian (~97 Ma) sediments. This is a considerably broader expanse of missing stratigraphic record than at the deeper water sites of the Leg 171B depth transect.

PALEOMAGNETISM

Laboratory Procedures and Interpretations

Portions from nearly all cores yielded high-quality magnetostratigraphic data, and the polarity intervals were reproduced at similar depth intervals in Holes 1052A, 1052B, and 1052F. The composite polarity pattern was enhanced by the post-cruise thermal demagnetization of 215 minicores. The upper Eocene polarity chron succession from Chrons C18r through C15r was resolved at high resolution. Inclination data from the Albian through Cenomanian sediments indicate a paleolatitude of 23°N for this site.

Measurements were made using the pass-through cryogenic magnetometer on the archive half of all core sections >40 cm long. Most sections were measured at 5-cm intervals at natural remanent magnetization (NRM) and then either at a 20- or 15-mT AF demagnetization step. Higher resolution (3-cm intervals) or multiple demagnetization steps were employed for some intervals. The tensor tool was used to obtain the orientation of APC Cores 171B-1052A-4H through 15H. Discrete samples taken (typically six oriented cylinders or plastic cubes per core) to enhance the magnetostratigraphic reliability were analyzed post cruise, using progressive thermal and AF demagnetization.

Thermal demagnetization of 60 discrete minicores from Hole 1052A and 155 minicores from Hole 1052E was completed at the paleomagnetism laboratories at the University of Oxford and the University of Michigan. These analyses and associated polarity interpretations are included in this volume (see Tables 11–14 [11, 13 in ASCII format; 12, 14 in PDF format] on CD-ROM, back pocket, this

Table 10. Benthic foraminifers found in samples from Holes 1052A and 1052E.

Age	Core, section, interval (cm)	Depth (mbsf)	Abundance	Preservation
	171B-1052A-			
late Eocene	1X-CC, 7-9	0.84	Abundant	Very good
late Eocene	4H-CC, 14-17	32.59	Abundant	Good
middle Eocene	11H-CC, 21-24	99.04	Abundant	Good
middle Eocene	17X-CC, 16-18	142.47	Abundant	Good
middle Eocene	18X-CC, 16-18	154.76	Abundant	Moderate
	171B-1052E-			
late Paleocene	4R-CC, 0-3	165.75	Abundant	Moderate
late Paleocene	8R-CC, 14-17	210.39	Common	Poor
early Paleocene	12R-CC, 4-7	248.17	Abundant	Moderate
early Paleocene	15R-CC, 24-26	274.16	Abundant	Moderate
early Paleocene	17R-CC, 18-20	300.33	Abundant	Moderate
late Maastrichtian	18R-CC, 59-61	302.19	Abundant	Good
late Maastrichtian	22R-CC, 20-23	343.98	Abundant	Good
late Maastrichtian	25R-CC, 0-4	368.85	Abundant	Good
late Maastrichtian	28R-CC, 0-4	400.12	Abundant	Good
early Maastrichtian	31R-CC, 12-15	434.89	Abundant	Moderate
early Maastrichtian	34R-2, 57-58	455.97	Abundant	Good
early Cenomanian	37R-CC, 0-1	492.45	Abundant	Good
late Albian	39R-CC, 24-25	511.37	Abundant	Very good
late Albian	41R-1, 98.5-101	521.29	Trace, abundant*	Very good
late Albian	41R-CC, 20-23	529.52	Abundant	Very good
late Albian	45R-CC, 0-4	561.06	Abundant	Good
late Albian	48R-CC, 19-21	597.41	Abundant	Moderate
late Albian	52R-CC, 22-24	627.66	Abundant	Moderate
late Albian	58R-CC, 17-20	682.57	Abundant	Good

Note: * = the routinely larger (>125 μm) fraction examined and the smaller (63-125 μm) fraction, respectively.

volume). Progressive thermal demagnetization was generally at 30°C increments from ~140° through 360°C, with continuation to higher thermal steps for the more stable samples. A thermal demagnetization step of 200°C was generally adequate to remove overprints. Most sediments from Hole 1052A and the Maastrichtian portion of Hole 1052E lost nearly all of their magnetization or became magnetically unstable at thermal steps exceeding 330°C.

The bioturbated oozes and chalks of Site 1052 exhibit a significant drilling-induced overprint (radially inward and dipping steeply downward) that was usually removed by the 20 mT AF demagnetization step. This drilling-induced overprint is not significant in the more cemented Cretaceous rocks, and a present-day, normal-polarity overprint was removed upon AF demagnetization either at 15 or 20 mT. The only portions of the section that yielded ambiguous paleomagnetic results are Maastrichtian chalks with magnetizations after 15 mT that were typically $<1 \times 10^{-2}$ mA/m, which is near the noise level of the pass-through cryogenic magnetometer, and lower Eocene and Paleocene sediments recovered in Hole 1052A by XCB coring, which produced biscuits or blocks embedded in drilling slurry. Other than these intervals, the polarity zonation within each hole is apparent from the clustering of inclination data (Figs. 22–25).

The demagnetized data from the pass-through cryogenic magnetometer were filtered before being plotting by removing the few measurements with inclinations $>80^\circ$ that were assumed to be dominated by a steep-downward drilling overprint, the intervals of anomalously high intensity (these are usually associated with fragments broken off the drill bit or rust particles within the drilling slurry), and data from the uppermost 20 cm of the disturbed top of each core. We also omitted all samples with magnetizations $<5 \times 10^{-3}$ mA/m after 20 mT AF demagnetization, presuming that these would contain an unacceptably high component of noise. A three-point moving average was applied to the inclination record to smooth artifacts before plotting the data (Figs. 22–25).

Careful cross-comparison of the data with the observed disturbances in the cored sediments and occurrences of anomalous intensity spikes would probably remove additional artifacts. However, the

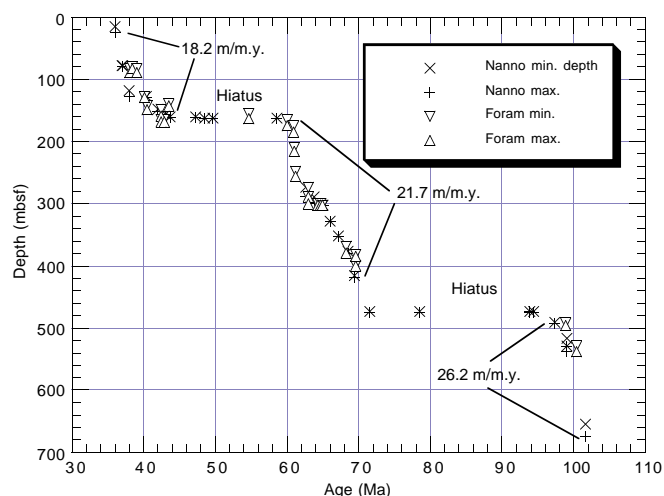


Figure 21. Age-depth relationship at Site 1052 based on calcareous nannofossil and planktonic foraminifer data from Holes 1052A and 1052E.

post-cruise thermal demagnetization and independent polarity interpretation of suites of minicores from Holes 1052A and 1052E verified the majority of the polarity zones described on the ship (Figs. 22, 24A, B).

Biomagnetostratigraphy

Polarity Zones and Chron Assignments

Assignment of polarity chrons to the polarity intervals relies on the shipboard micropaleontology datums (especially nannofossil zones) and the chronostratigraphy of Berggren et al. (1995) and Gradstein et al. (1995; Fig. 26).

Middle and Upper Eocene

The sediments cored with the APC in Holes 1052A, 1052B, and 1052F yielded nearly identical polarity patterns, with a precise match of polarity Chrons C18r through C16n of the Bartonian and lower Priabonian (upper middle Eocene–lower upper Eocene; Fig. 26). The high-resolution measurements with the pass-through magnetometer, coupled with the expanded sedimentary sequence and augmented by post-cruise analysis of minicores from Hole 1052A, also enable recognition of the brief Subchrons C16n.1r, C17n.1r, and C17.2r (Figs. 22, 26).

The polarity chron assignments for Holes 1052C and 1052D, consisting of only two cores each, are less certain but appear to show Chron C15r overlying Chron C16n. These assignments assume that the core recovery at these two holes began at a slightly higher stratigraphic level relative to Holes 1052A and 1052B; this assumption is supported by the splicing of color scanner data (see “Core-Core Integration” section, this chapter).

At 120 mbsf, we correlate a pair of thin, reversed-polarity zones, indicated in the pass-through magnetometer data, with the brief Chron C18n.1r based on their placement within Chron C18n and their biostratigraphic age (Figs. 22, 26). Coring at Hole 1052A continued with the XCB below ~130 mbsf to the uppermost Paleocene.

Maastrichtian, Paleocene, and Lower Eocene

The XCB biscuit slurry in the lower 20 m of Hole 1052A precluded unambiguous recognition of polarity zones in the pass-through cryogenic measurements, and there was limited recovery of the Paleocene/Eocene boundary interval by rotary coring in Hole

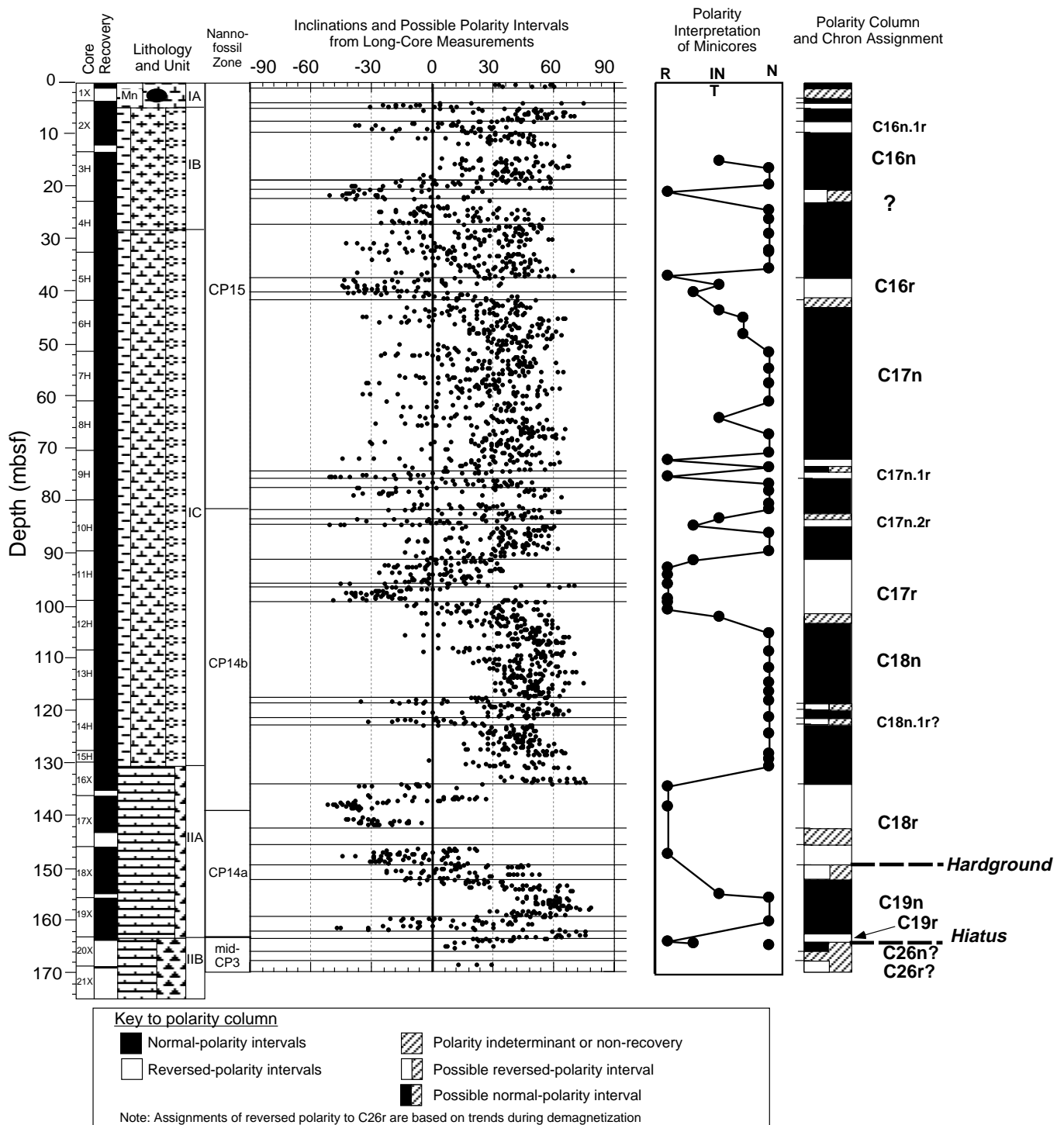


Figure 22. Magnetostratigraphy of Hole 1052A. Magnetic inclinations from long-core measurements are after AF demagnetization at 20 mT and were filtered using a three-point moving average. Measurements from the uppermost 20 cm of each core and those having anomalously high or low magnetic intensities were removed. Horizontal lines delineate clusters of predominantly positive, negative, or equally mixed magnetic inclinations that were used for a preliminary ship-board polarity column. Polarity of discrete minicores are from interpretation of progressive thermal demagnetization and are assigned relative degrees of certainty. These polarity interpretations from discrete samples are given priority in the compilation of the summary polarity column. Polarity chron assignments are based on the polarity zone pattern and nannofossil biostratigraphy.

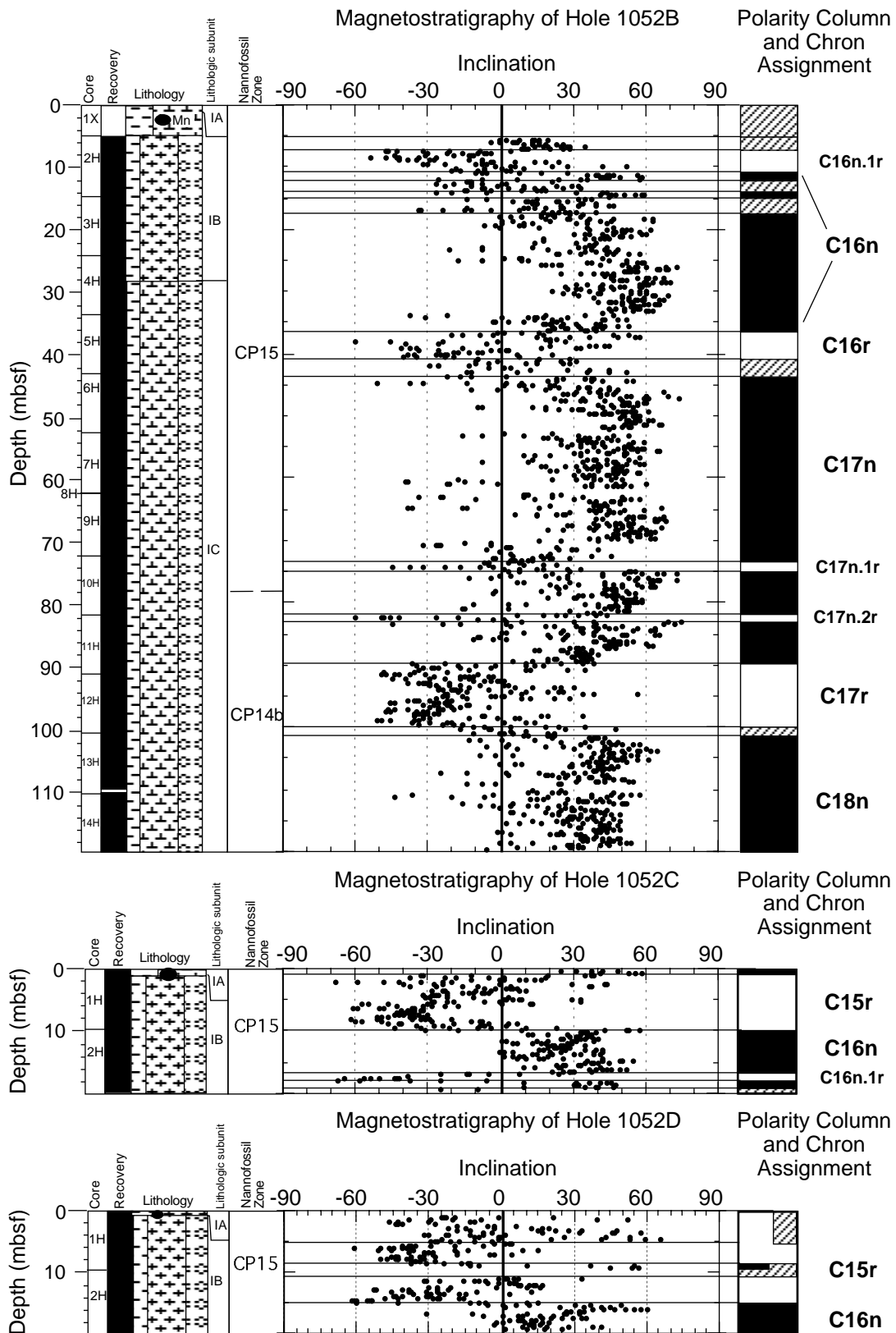


Figure 23. Magnetostratigraphy of Holes 1052B, 1052C, and 1052D. Magnetic inclinations from long-core measurements are after AF demagnetization at 20 mT and were filtered using a three-point moving average. Measurements from the uppermost 20 cm of each core and those having anomalously high or low magnetic intensities were removed. Horizontal lines delineate clusters of predominantly positive, negative, or equally mixed magnetic inclinations that were used for a preliminary shipboard polarity column. Polarity chron assignments are based upon the polarity zone pattern and nannofossil biostratigraphy.

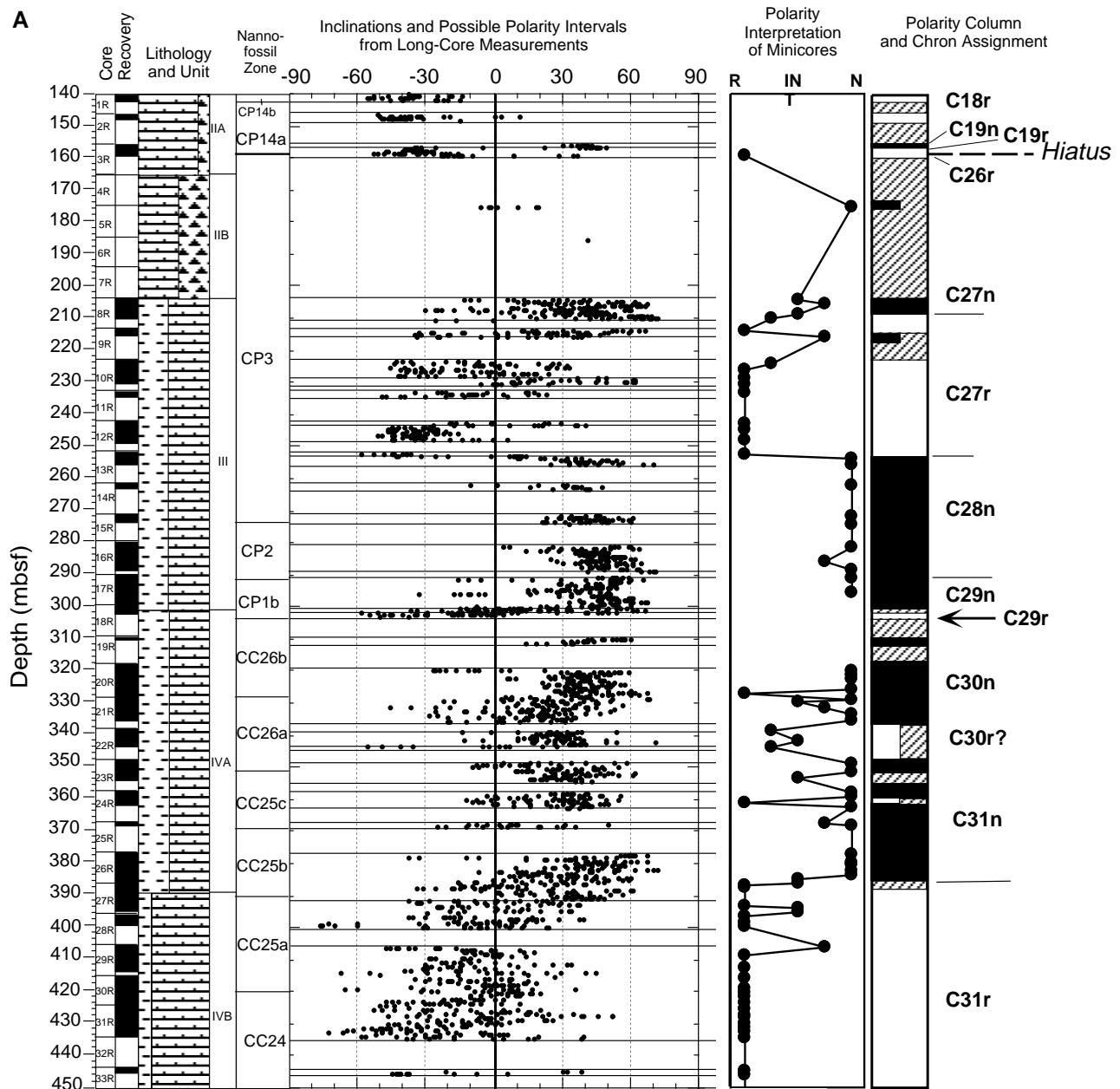


Figure 24. A. Magnetostratigraphy of the upper half of Hole 1052E. Magnetic inclinations from long-core measurements are after AF demagnetization at 20 mT and were filtered using a three-point moving average. Measurements from the uppermost 20 cm of each core and those having anomalously high or low magnetic intensities were removed. Horizontal lines delineate clusters of predominantly positive, negative, or equally mixed magnetic inclinations that were used for a preliminary shipboard polarity column. Polarities of discrete minicores are from interpretation of progressive thermal demagnetization and are assigned relative degrees of certainty. These polarity interpretations from discrete samples are given priority in the compilation of the summary polarity column. Polarity chron assignments are based on the polarity zone pattern and nannofossil biostratigraphy.

1052E. The available polarity results from post-cruise analysis of discrete samples combined with biostratigraphic data, suggest a stratigraphy of (1) Chron C18r shortened in relative thickness by a hard-ground coincident with the Lutetian/Bartonian stage boundary (middle middle Eocene); (2) a complete Chron C19n; (3) uppermost Chron C19r juxtaposed with lower Chron C26n or C26r at a major unconformity that encompasses the entire lower Eocene and the Thanetian stage of the upper Paleocene; and (4) portions of Chrons C27n and C27r of middle Paleocene age (Fig. 26).

The Danian (lower Paleocene) succession of Chrons C29r through C27n is represented in Hole 1052E, with the possible exception of the brief Chron C28r (Fig. 24A). Chron C29r is thin (2.5 m), but it may be thicker because there is a significant drilling gap (7 m)

below it. If Chron C29r is only 2.5 m thick, this suggests that the uppermost Maastrichtian and lowermost Paleocene sequences are condensed relative to adjacent strata.

Upper Maastrichtian Chrons C30n and C31n are separated by a narrow, reversed-polarity zone at 340 mbsf, interpreted to be the brief Chron C30r. Lower Maastrichtian Chron C31r continues downward to the major unconformity truncating the Cenomanian limestones (Fig. 24B).

Albian and Cenomanian

All cores of late Albian and Cenomanian age yielded normal polarity that is within Cretaceous Long Normal Chron C34n (Fig.

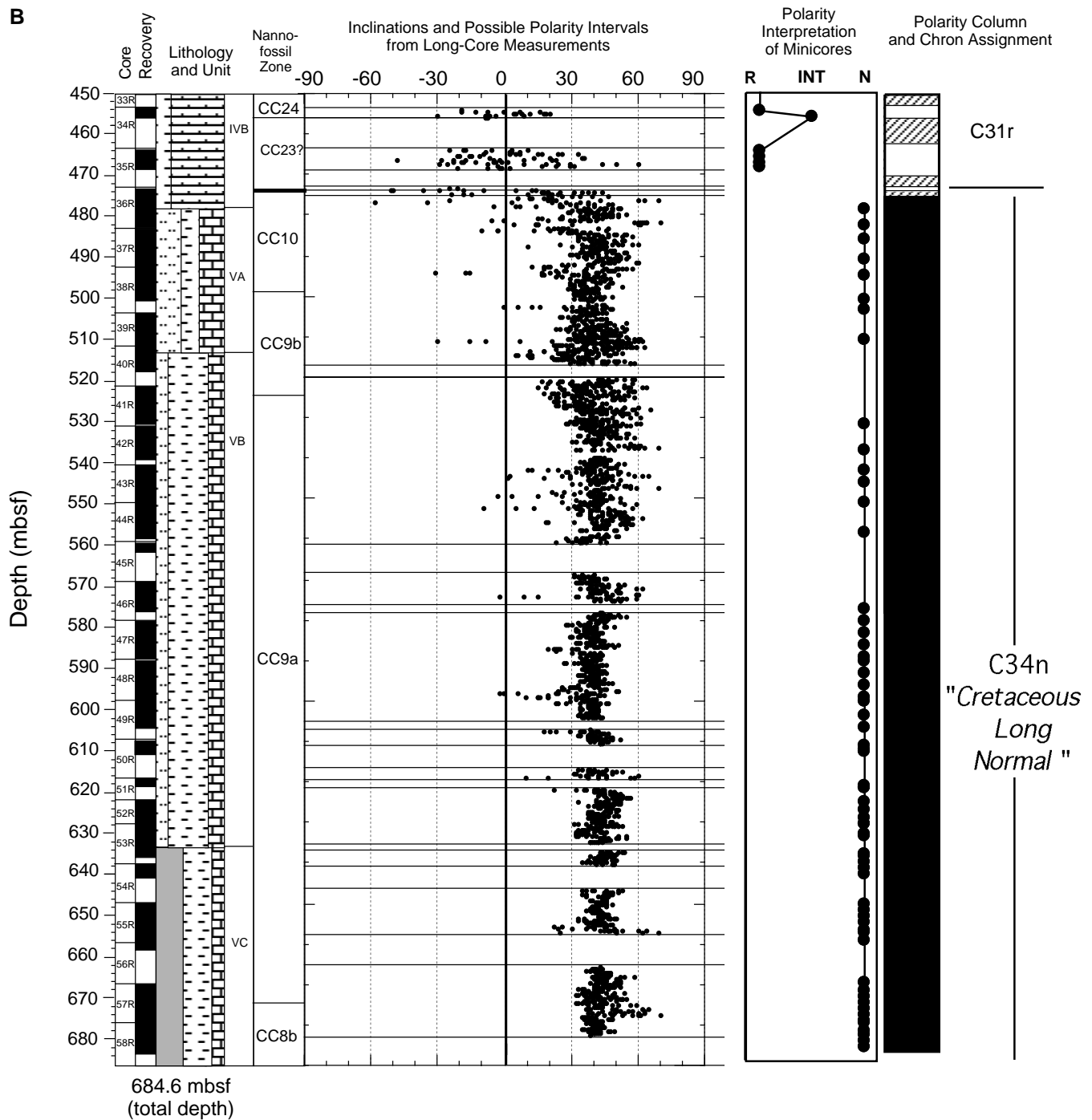


Figure 24 (continued). **B.** Magnetostratigraphy of the lower half of Hole 1052E. Magnetic inclinations from long-core measurements are after AF demagnetization at 20 mT and were filtered using a three-point moving average. Measurements from the uppermost 20 cm of each core and those having anomalously high or low magnetic intensities were removed. Horizontal lines delineate clusters of predominantly positive, negative, or equally mixed magnetic inclinations that were used for a preliminary shipboard polarity column. Polarity of discrete minicores are from interpretation of progressive thermal demagnetization and are assigned relative degrees of certainty. These polarity interpretations from discrete samples are given priority in the compilation of the summary polarity column. Polarity chron assignments are based upon the polarity zone pattern and nannofossil biostratigraphy.

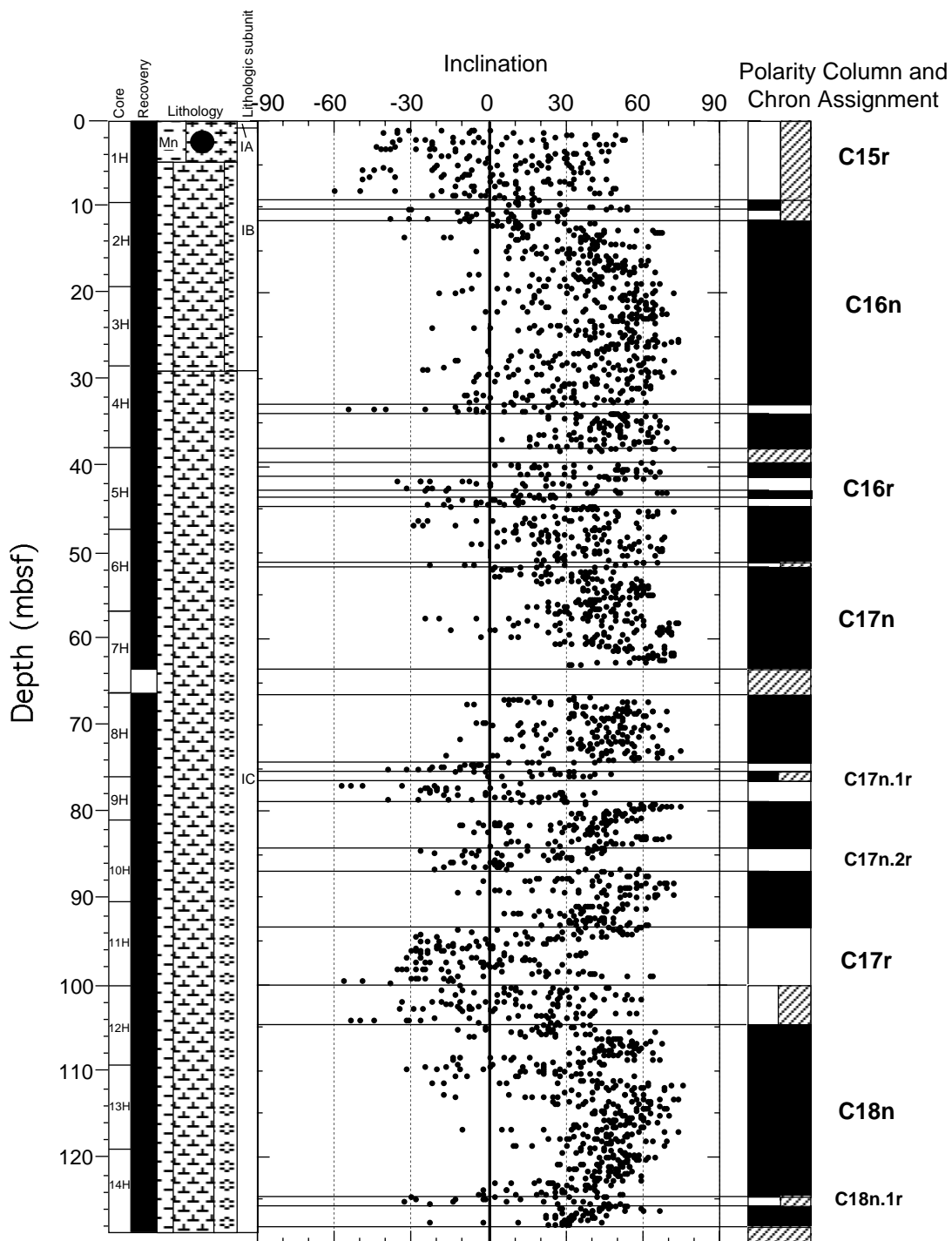


Figure 25. Magnetostratigraphy of Hole 1052F. Magnetic inclinations from long-core measurements are after AF demagnetization at 20 mT and were filtered using a three-point moving average. Measurements from the uppermost 20 cm of each core and those having anomalously high or low magnetic intensities were removed. Horizontal lines delineate clusters of predominantly positive, negative, or equally mixed magnetic inclinations that were used for a preliminary ship-board polarity column. Polarity chron assignments are based upon correlation to polarity zones at similar depths in Hole 1052A.

24B). Drilling did not penetrate the uppermost middle Albian strata to test the validity of and to accurately date the elusive reversed-polarity Subchron “M-3” (e.g., Ryan et al., 1978; Gradstein et al., 1995).

Paleolatitude

The upper Albian dark silty claystones and lower Cenomanian clayey limestones generally were recovered in long (~100 cm) coher-

ent sections of core and do not contain significant drilling slurry. Upon AF demagnetization, these facies yielded highly stable magnetic directions within any single intact section of core. For the computation of paleolatitude, we selected a subset of the Albian–Cenomanian data from at least 5 cm of the ends of coherent core pieces (720 data points from the ~2500 measurements from the Albian–Cenomanian) and then smoothed the data with a moving three-point mean. The mean NRM inclination of these data is $56.7^{\circ} \pm 10.8^{\circ}$, with a median value of 50.9° for the set. The mean NRM inclination would

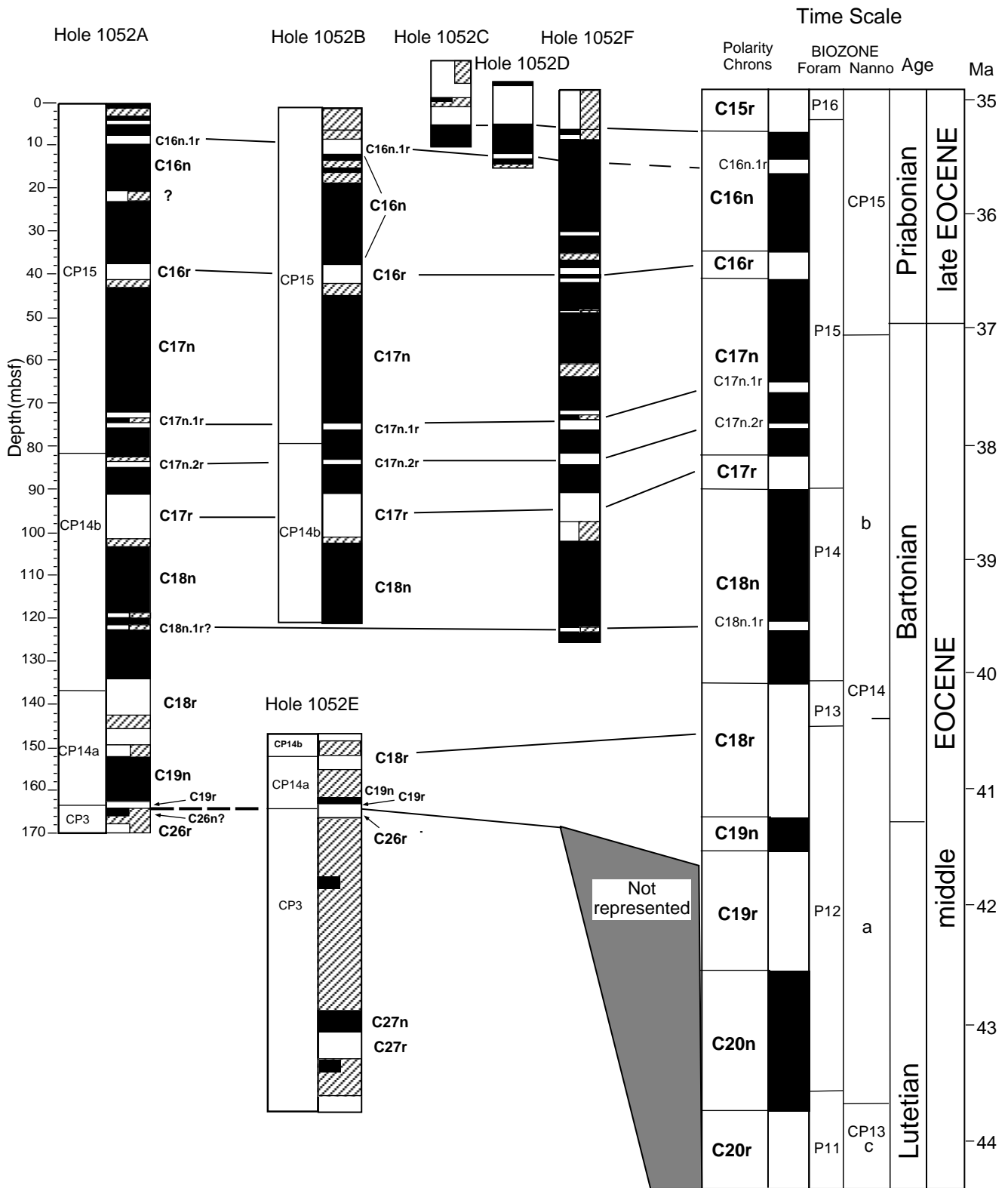


Figure 26. Eocene–Paleocene composite magnetostratigraphy of Site 1052. Comparison of polarity interpretations from the six holes at Site 1052 where Eocene sediments were recovered with Eocene chronostratigraphy, and correlation of the two holes (Holes 1052A and 1052E) penetrated by Paleocene sediments. The lower Paleocene and Cretaceous continuation of Hole 1052E is shown in Figure 24A, B.

imply a paleolatitude of 37.2°N, whereas Site 1052 is located at ~32°N. Therefore, the NRM is oversteepened, presumably by a component of downward-directed drilling overprint.

The mean inclination for these 720 measurements after AF demagnetization either at 20 or 25 mT is $40.4^\circ \pm 4.8^\circ$, with a median value of 40.9°. This inclination corresponds to a paleolatitude of 23.0°N for the late Albian–early Cenomanian. Kono (1980) derived an alternate method for the statistical treatment of inclination-only data from ocean drilling cores, but his results imply that there will be a significant difference between his method and the method used in this study only at high latitudes, and therefore at this low-latitude site, the difference in the corresponding paleolatitude would probably be <1°.

Most current models of Cretaceous–Tertiary plate motion assume that North America remained stationary throughout most of the Cretaceous period, which was preceded and followed by rapid spurts of continental drift (e.g., Cretaceous compilation by Irving et al., 1993). Such a concept may be partially an artifact of poor age constraints on magnetically suitable sediments within the North American craton, but it may also indicate incorporation of unsuitable paleomagnetic material. Poles derived from Aptian–Albian intrusions in New England suggest that the compiled North American Cretaceous path may have episodes of rapid motion (McEnroe, 1996). According to the generalized Cretaceous compilation (Irving et al., 1993), the sites drilled during Leg 171B have a predicted mid-Cretaceous (Hauterivian to Santonian) paleolatitude of 30°N, followed by a rapid northward drift to a Campanian–Maastrichtian position at 40°N in the latest Cretaceous, and then a return southward to reach the present 32°N position in the late Tertiary. In addition, our sites are projected to have rotated counterclockwise ~20° to 30° from the Late Cretaceous to the present.

In contrast to the generalized Cretaceous compilation of Irving et al. (1993), the 23°N paleolatitude obtained at Site 1052 for the late Albian–early Cenomanian represents the first well-dated paleolatitude from marine sediments and the first Cretaceous paleolatitude incorporating more than 100 data points. The implication from the Site 1052 result is that the “mid-Cretaceous North American pole” has been placed ~7° (or 1000 km) too far south with respect to the southeastern United States. Within the late Albian to Cenomanian, there were no statistically significant changes in the mean paleolatitude.

CORE-CORE INTEGRATION

At Site 1052, magnetic susceptibility and gamma-ray attenuation porosity evaluator (GRAPE) density data from the multisensor track (MST) and output from the Minolta color spectrophotometer were available for precise core-core integration (Tables 15–20 on CD-ROM, back pocket, this volume). APC coring of Holes 1052A, 1052B, 1052C, 1052D, and 1052F reached a maximum depth of 129.7 mbsf, and a composite section was constructed down to the base of Core 171B-1052A-14H, below which there is no overlap of cored holes. Only two cores were taken in each of Holes 1052C and 1052D, and correlation among the uppermost cores recovered at this site was initially more difficult than among cores deeper in the section. The GRAPE density records, which are of negligible value for hole-to-hole correlation at the previous sites drilled during Leg 171B, proved invaluable in this interval. A series of correlative density reductions that are probably caused by intervals of higher biogenic silica content characterize the upper part of the section at Site 1052 (Fig. 27).

Figure 27 demonstrates the base level for constructing a composite section and illustrates how a composite section may be constructed with an eye to its subsequent use to construct a splice. The minor GRAPE density minima marked “a” and “b” in the records for Holes 1052C, 1052D, and 1052E appear to be correlative. Among these three holes, the distance between these events and the top of the re-

covered sediment is greatest in Hole 1052F, and for this reason, the top of this core (171B-1052F-1H) is assigned zero depth on the mcd scale. Tying Core 171B-1052C-2H to Core 171B-1052F-1H at event b may be used to determine the depth of event c, which is also observed in Cores 171B-1052B-2H, 1052D-2H, and 1052F-2H. Events d and e (with a subsidiary minimum event f that is associated with a volcanic ash layer) occur in these same cores, so the decision to tie the cores at event c precludes their being perfectly aligned at event f. It was possible to align Core 171B-1052C-2H at event f, but it was aligned to Core 171B-1052F-2H at about 18 mcd, so that the lower part of Core 171B-1052C-2H could be utilized in the sampling splice to bridge the gap between Cores 171B-1052F-2H and 3H. The data from Core 171B-1052A-2X are also illustrated in Figure 27. This core appears to contain both the high-density surface layer that is present at the top of Core 171B-1052F-1H and also low-density events c through e; obviously, Core 171B-1052A-2X should be used only with caution, and it would not provide a good measure of the position of events in the sediment with respect to the seafloor. Note also that an overlap of almost 3 m is indicated between Cores 171B-1052D-1H and 2H. One-half of this section has a low apparent density and is obviously highly disturbed; the remainder may represent true overlap (as is also implied by the magnetic susceptibility data), because it is possible for the drill bit to move laterally in the soft upper part of the sediment column.

The magnetic susceptibility data are quite reliable at Site 1052; the spikes were almost invariably found to have been caused by volcanic ash and provided useful ties among holes. The color data are also of good quality. Holes 1052A and 1052B were cored with almost no overlap between the cores in one hole and with the gaps between cores in the other. Hole 1052F was cored after it became apparent that the signal in the data provided an excellent opportunity for precise

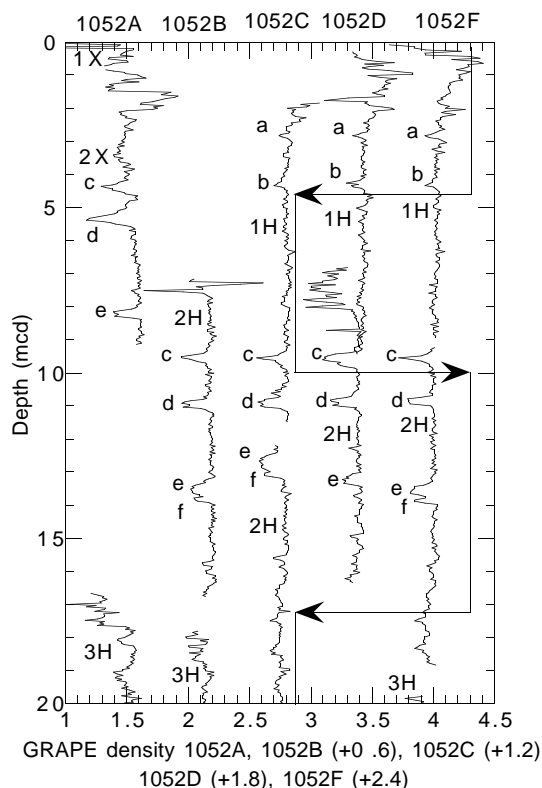


Figure 27. GRAPE density data from 0 to 20 mcd in Holes 1052A, 1052B, 1052C, 1052D, and 1052F. Events marked a–f are discussed in the text. Arrows mark the track of the splice (see text).

hole-to-hole correlation, although the cores in Holes 1052A and 1052B did not provide a complete sedimentary section. Hole 1052F was intended to bridge these intercore gaps, but this was not entirely successful in the upper part of the section. An adjustment to the drilling depth was made for the deepest cores in Hole 1052F, which provided a better overlap with the gaps between cores in Holes 1052A and 1052B. Table 21 lists the depth offsets applied to successive cores to produce the composite depth scale. The depth on the composite depth scale of any sample from a particular core is obtained by adding the offset (in meters [m]) for that core to the depth of the sample on the mbsf scale.

Coring at both Holes 1052B and 1052F was interrupted by limited recovery and a damaged core liner at about 65 mcd in Hole 1052B. The section is probably not complete at that point, but it is not clear exactly how much is missing.

Site 1052 may be the first Paleogene site at which a fully successful composite section was constructed. The composite section ends at 127 mbsf (133 mcd), so the composite section is about 5% longer than the true sedimentary section. In previously studied Pliocene–Pleistocene sections, the expansion of the composite section is almost invariably between 10% and 15%, and this has been attributed to rebound following pressure release (Moran, 1997). Additional work is required to establish whether the smaller expansion of the composite section observed at Site 1052 is consistent with this explanation.

In Table 21 it is evident that the cores from Hole 1052F were adjusted in depth by about 3 m less than those from Holes 1052A and 1052B. The reason for this is that depth mbsf was judged from the depth at which the driller observed a reduction in drill-string weight when spudding in the absence of an obvious mudline in the first core recovered. This has the unlikely implication that the seafloor depth changes from one hole to another, although the holes were drilled about 10 m from one another. Holes 1052A, 1052B, and 1052F were drilled at nominal seafloor depths of 1356.0, 1356.5, and 1353.5 mbrf, respectively; these differences explain the systematic differences among the offsets in Table 21.

Offsets for the shallowest cores are much more erratic than those for cores deeper in the section. This explains both why it was initially difficult to align the shallowest cores taken and why neither the mudline nor the depth at which weight reduction on the drill string is observed is a reliable means of judging water depth or assigning mbsf.

The magnetic susceptibility and color data for Holes 1052A, 1052B, and 1052F are illustrated on the mcd scale in Figures 28 through 34. In each figure, the left panel shows the magnetic susceptibility for the three holes, and the right panel shows color. Figure 28 (0–20 mcd) shows that the upper part of the section lacks distinctive features for correlation. It is possible that the diagenetic color change from greenish to yellowish that is observed at about 29 mcd (Fig. 29) has obscured some of the original color variability. Notice in Figure 29 that the color change does not appear at precisely the same mcd depth in Hole 1052F as in the other two holes. The reason is that in Hole 1052F, as in several other places, the cores were correlated with an eye to the optimal means of sampling a complete section in good material, rather than being correlated at the most prominent points. Similarly, the prominent magnetic susceptibility spike, caused by a volcanic ash layer at about 72 mcd (Fig. 31), does not appear precisely aligned, although the ash layers at about 88.5 mcd (Fig. 32) and 101.5 mcd (Fig. 33) do. Significant coring distortion of the distance between prominent common features is evident throughout the interval. For example, the three cores are perfectly aligned at the 88.5 mcd ash layer, yet the cyclic variations in susceptibility and color are out of phase at 91 mcd. The spliced magnetic susceptibility record illustrated in Figure 35 is intended to represent a complete record of the material cored at Site 1052, and Table 22 gives the tie points for constructing this spliced section at Site 1052. The operation of this table is also illustrated in Figure 27, in which a vertical line is drawn along the core interval included in the splice, and the horizontal line with an arrow shows where the section is tied to a point at the same depth (mcd) in another hole. The chief purpose of Table 22 is to provide

Table 21. Offsets applied to the depths (mbsf) of individual cores at Site 1052 to generate a composite section and a composite depth scale (mcd).

Core	Offset (m)
171B-1052A-	
1X	0.00
2X	-2.70
3H	3.40
4H	1.83
5H	3.33
6H	5.92
7H	5.04
8H	3.77
9H	3.79
10H	4.02
11H	5.18
12H	5.73
13H	5.63
14H	6.02
15H	6.02
16X	5.62
17X	5.62
18X	5.62
19X	5.62
20X	5.62
21X	5.79
171B-1052B-	
2H	2.08
3H	3.24
4H	2.58
5H	2.97
6H	4.87
7H	4.12
8H	4.18
9H	5.09
10H	4.43
11H	5.62
12H	6.70
13H	7.05
14H	6.55
171B-1052C-	
1H	1.76
2H	2.61
171B-1052D-	
1H	0.22
2H	-3.02
171B-1052F-	
1H	0.00
2H	-0.35
3H	0.70
4H	0.71
5H	1.92
6H	2.47
7H	1.60
8H	1.35
9H	0.03
10H	1.76
11H	2.48
12H	2.91
13H	2.91
14H	3.46

some guidance to scientists who want to sample parts of the site at high resolution to construct a continuous record. The splice is based mostly on material from Holes 1052B and 1052F. Relative distortion in records from parallel holes invariably is observed when a composite section is constructed; as discussed in the “Explanatory Notes” chapter (this volume), it may be desirable to make an even more precise post-cruise correlation among the cores by allowing relative stretching and/or compression.

ORGANIC GEOCHEMISTRY

Gas Analyses

In Holes 1052A and 1052E, gas chromatographic analysis of the headspace samples detected methane (C_1) with traces of ethane (C_2), ethylene ($C_2=$), propane (C_3), and propylene ($C_3=$; Table 23). At the FO of ethane at 140 mbsf, the $C_1/(C_2 + C_3)$ ratios were in the potentially hazardous range of <100 (Table 23; Fig. 36). No action was taken because the total gas content remained below 0.01 vol% C_1 . Be-

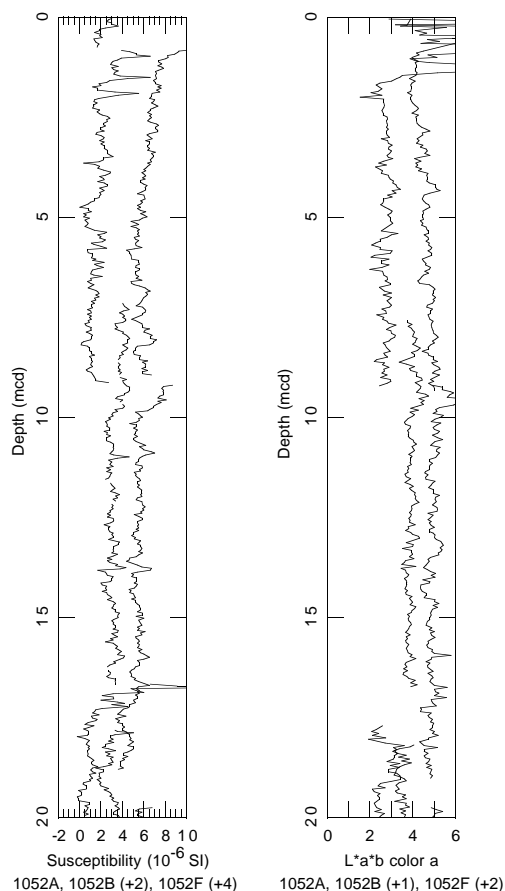


Figure 28. Magnetic susceptibility data and L*a*b code a from 0 to 20 mcd in Holes 1052A, 1052B, and 1052F. The magnetic susceptibility and color data are available on CD-ROM (back pocket, this volume).

cause no hazardous levels of gas were detected in Holes 1052A and 1052E, gases were not monitored in the other holes drilled at Site 1052.

Two gas zones were recognized in Holes 1052A and 1052E (Fig. 36). The surface gas zone, which averages 3 ppm C_1 , shows a generally increasing gas content of 2 to 4 ppm C_1 from 0 to 130 mbsf. Below 130 mbsf, the lithologic change related to the transition from Unit I to Unit II may form a seal that has trapped C_1 and C_{2+} gases below it. This lithologic transition forms the upper boundary of the deep gas zone at 130 mbsf. The deep gas zone has a low gas content overall, averaging 6 ppm C_1 and ranging from 2 to 18 ppm C_1 . Within the deep gas zone, from 130 mbsf to the bottom of Hole 1052E at 685 mbsf, the trend of the C_1 content is to increase slightly with depth (Fig. 36). Minor amounts of C_{2+} gases appear in the sediment from the deeper portion of Hole 1052E.

Elemental Analyses

Three samples were taken from each core for carbonate-carbon and total carbon, hydrogen, nitrogen, and sulfur (CHNS) analyses.

At Site 1052, total organic carbon (TOC) averages 0.2 wt% and ranges from below the detection limit to 0.91 wt% TOC (Table 24; Fig. 37). The reported TOC value of 3.1 wt% at 287.6 mbsf was not confirmed by subsequent Rock-Eval analysis (Sample 171B-1052E-16R-5, 71.5–72 cm; Table 25), and the data from this sample are considered unreliable. The average TOC content is greater at this site than at the other 171B sites along the Blake Nose—particularly from

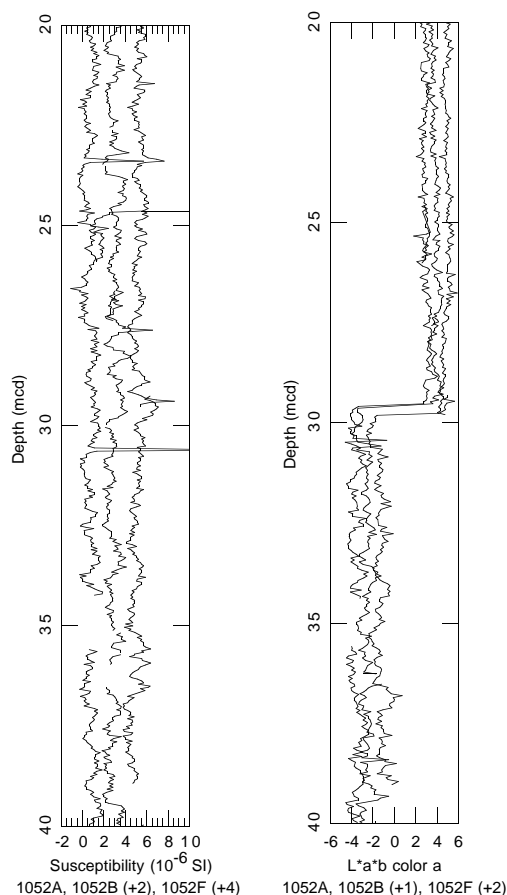


Figure 29. Magnetic susceptibility data and L*a*b code a from 20 to 40 mcd in Holes 1052A, 1052B, and 1052F.

520 to 640 mbsf, which corresponds to late Albian-aged sediments of lithologic Subunit VB.

Carbonate and TOC contents show a crude inverse relationship (Fig. 37). As carbonate decreases, TOC generally increases. In particular, the clay-rich beds in lithologic Units III and V have higher TOC contents than the other units in this hole (Fig. 38).

The sulfur content is generally below detection limits, but moderate levels occur in claystone-rich intervals in Units III and V (Table 24; Fig. 38).

Nitrogen is generally low, averaging 0.05 wt% and ranging from below the detection limit to 0.18 wt%. Nitrogen does not vary much between lithologic units (Fig. 38). Hydrogen content averages 0.24 wt% and ranges from below the detection limit to 0.8 wt% (Table 24). An altered humic kerogen type is consistent with the overall low hydrogen content of these samples. The presence of woody terrestrial organic matter in the claystone-rich beds, shown by smear slides and paleontology reports, supports this possibility.

Rock-Eval Analyses

Rock-Eval results show that the sediment has a low to moderate kerogen content, with TOC averaging 0.57 wt% and ranging from below the detection limit to 1.4 wt% (Table 25). Only samples with a TOC content >0.4 wt% are discussed because samples below this level gave unreliable results at this site. At Site 1052, the kerogen is immature, as shown by the low average T_{max} value of 420°C. The T_{max} value of 593°C from Sample 171B-1052E-44R-6, 117–118 cm, is spurious and seems to be caused by the difficulty in accurately deter-

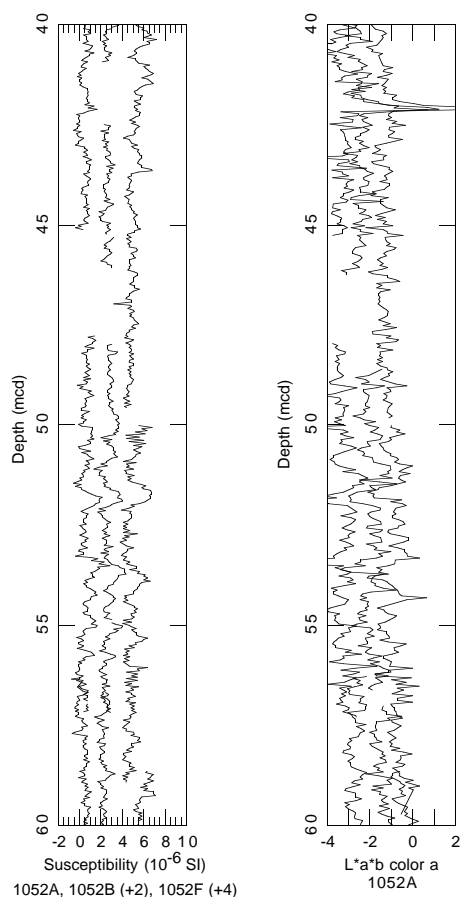


Figure 30. Magnetic susceptibility data and L*a*b code a from 40 to 60 mcd in Holes 1052A, 1052B, and 1052F.

mining the S₂ peak of samples with very low S₂ yield (Table 25). The immaturity indicated by the low average T_{max} is corroborated by the lack of increased thermogenic (C₂₊) hydrocarbons detected in head-space samples taken from Cores 171B-1052E-40R through 52R (411–625 mbsf) that sampled the greenish dark gray laminated claystone beds of lithologic Subunits IV and V (Table 23). Hydrogen indices (HIs) of the kerogen are low, ranging from 9 to 97 mg hydrocarbons (HC)/g rock with a mean of 48 mg HC/g rock. The oxygen content of the kerogen is moderate to high, with oxygen indices (OIs) ranging from 116 to 325 mg CO₂/g rock with a mean of 211 mg CO₂/g rock. The HC index (S₂/S₃) of the kerogen ranges from 0.02 to 0.52 mg HC/mg CO₂ with a mean of 0.24 mg HC/mg CO₂, indicating that the kerogen is dry-gas prone. The genetic potential (S₁ + S₂) of the kerogen is poor, ranging from 0.05 to 0.79 mg HC/g rock and averaging 0.37 mg HC/g rock.

The upper Albian to Cenomanian greenish dark gray laminated claystone beds at Site 1052 contain an altered terrestrial (type IV) kerogen similar to that found in some large fluvial-deltaic depositional systems (Fig. 39). Type IV kerogen is produced either by alteration in environments undergoing intense weathering or by organic matter oxidation during a long terrestrial residence time. This type of kerogen is not geochemically related to the marine sapropel found at Site 1049. Rather, the kerogen at Site 1052 is more like that reported from upper Albian to Cenomanian greenish dark gray laminated claystones of the Hatteras Formation in the nearby Blake-Bahama Basin (Herbin et al., 1983; Katz, 1983; Summerhayes and Masran, 1983). The carbonaceous laminated claystones within the Blake-Bahama

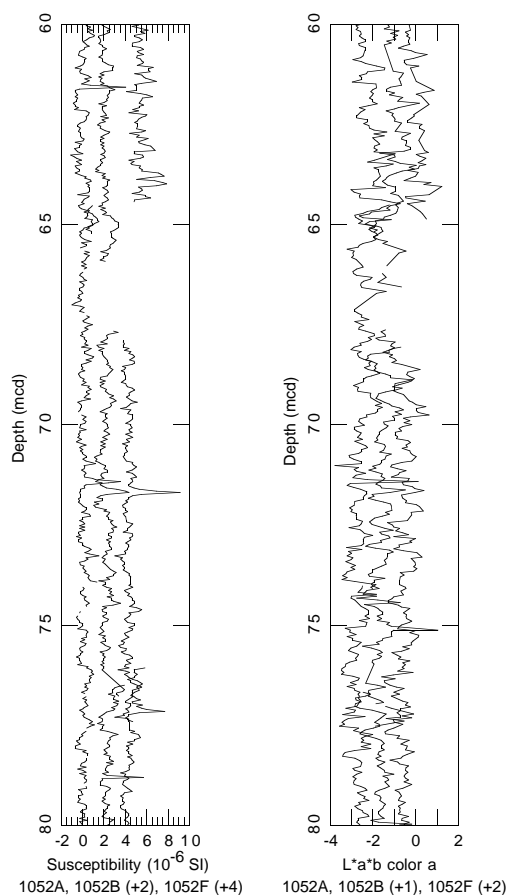


Figure 31. Magnetic susceptibility data and L*a*b code a from 60 to 80 mcd in Holes 1052A, 1052B, and 1052F.

Basin contain low to moderate amounts of TOC (about 0.8–4 wt%) consisting of both type III and type IV kerogen, typically with HIs <150.

INORGANIC GEOCHEMISTRY

Analytical Results

Interstitial waters were taken from 28 core samples at Site 1052 (Holes 1052A and 1052E; Table 26). Pore-water salinities in this hole show a steady increase (36.0–41.5) from the top to the bottom (~678 mbsf) of the section (Fig. 40A). Similarly, pore-water chloride and sodium concentrations show a steady increase from near seawater concentrations (Cl⁻, ~560 mM; Na⁺, ~475 mM) in the upper 80 m of the section to significantly higher values (Cl⁻, ~700 mM; Na⁺, >565 mM) at the base of the section (Fig. 40B).

Pore-water alkalinity shows a steady increase from ~3 mM at the top of the section to 4.35 mM at ~113 mbsf (Fig. 40C). This steady increase is followed by a general decrease to ~1 mM in the lower 500 m of the section, except for higher values (2.55–2.75 mM) in two samples between ~410 and 445 mbsf (Fig. 40C). The pH of pore waters shows an overall increase (7.67–8.55) with depth from the top of the section to ~650 mbsf (Fig. 40C).

Pore-water calcium concentrations are always higher than standard seawater (10.55 mM) and increase steadily from a minimum of 11.09 mM in the shallowest sample (7.95 mbsf) to 33.16 mM at the bottom of the section (Fig. 40A). Pore-water magnesium concentra-

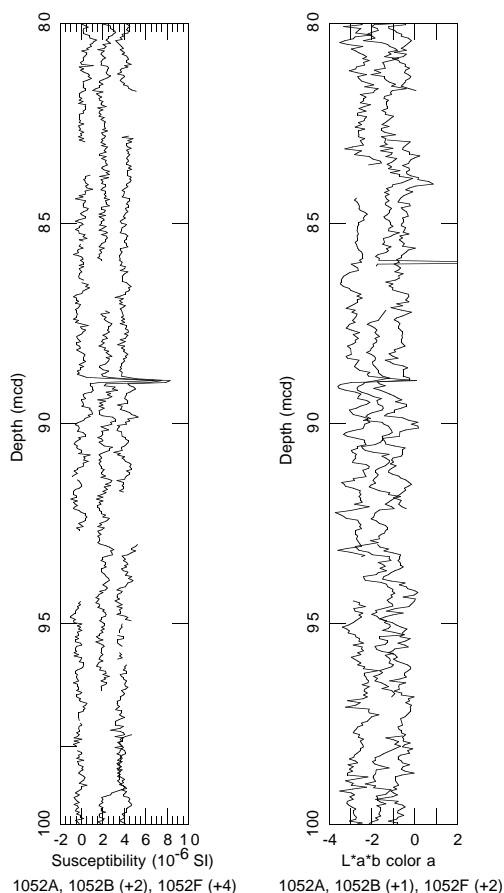


Figure 32. Magnetic susceptibility data and L*a*b code a from 80 to 100 mcd in Holes 1052A, 1052B, and 1052F.

tions at the site are always lower than standard seawater (54 mM) and decrease steadily from a maximum of 52.99 mM in the shallowest sample to 32.61 at the bottom of the section (Fig. 40A).

Pore-water potassium concentrations in the upper 150 m of the section at Site 1052 are significantly higher than standard seawater (10.44 mM; Fig. 40D) and show an overall decrease from 12.6 mM in the shallowest sample (7.95 mbsf) to 3.57 mM at the base of the section. Pore-water rubidium concentrations show a general decrease from 2.25 μM in the shallowest sample to 0.35 μM at the base of the section (Fig. 40E).

Pore-water strontium concentrations at Site 1052 are always higher than standard seawater (90 μM) and increase sharply from a minimum of 100 μM in the shallowest sample (7.95 mbsf) to 566 μM at ~200 mbsf (Fig. 40F). This sharp increase is followed by a more gradual increase to 860 μM at ~445 mbsf. Strontium values then continue to increase sharply to 1665 μM at ~603 mbsf, decrease to 1559 μM at ~625 mbsf, and then increase to 1766 μM at the bottom of the hole. In general, calculated $\text{Sr}^{2+}/\text{Ca}^{2+}$ ($\mu\text{M}/\text{mM}$) values show a pattern similar to the Sr^{2+} concentration depth profile, except for two decreases over two intervals (~225–275 and 350–450 mbsf; Fig. 40G, F, respectively).

Pore-water lithium concentrations increase gradually with depth from near seawater values (~30 μM) at the top of the section to 191 μM at ~410 mbsf and then decrease gradually to 161 μM at 678.03 mbsf (Fig. 40F).

In general, dissolved silica concentrations of the interstitial-water samples from Site 1052 are relatively high (~400–800 μM) in the upper 300 m of the section and are relatively low (~50–300 μM) in the lower 400 m of the section (Fig. 40H).

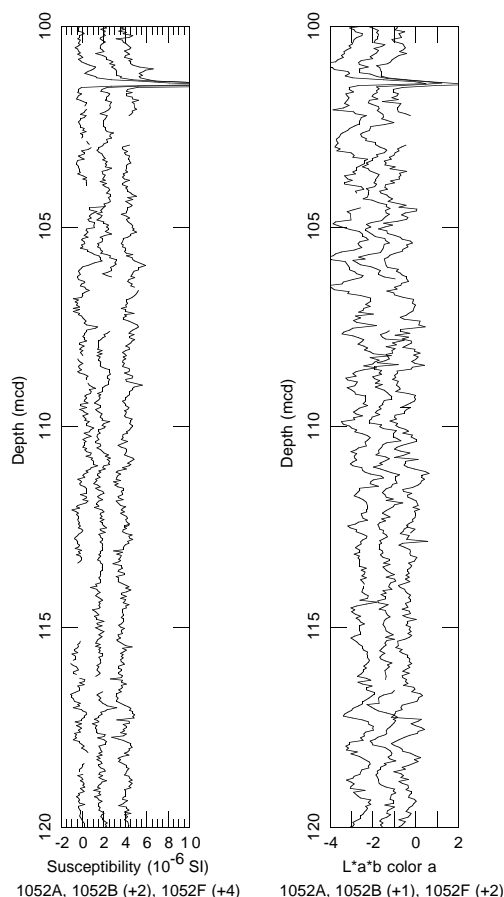


Figure 33. Magnetic susceptibility data and L*a*b code a from 100 to 120 mcd in Holes 1052A, 1052B, and 1052F.

Pore-water sulfate concentrations at Site 1052 show a relatively gradual decrease with depth from 28.5 mM at the top of the section to 26.4 mM at ~150 mbsf and show a more abrupt decrease to 15.5 mM at ~325 mbsf (Fig. 40I). These decreases are followed by an interval (~325–500 mbsf) with little change in sulfate concentration and by an interval of sharp decrease to ~6 mM at the base of the section (Fig. 40I). Pore-water ammonium concentrations show a sharp increase with depth from 14.6 μM at the top of the section to 574 μM at ~200 mbsf (Fig. 40I). This is followed by a more gradual increase to more than 1000 μM at ~410 mbsf. Ammonium concentrations further increase to ~1600 μM at 678.03 mbsf.

Pore-water boron concentrations at Site 1052 range between 109 and 723 μM and show a general decrease with depth (Fig. 40J).

Discussion

Two significant differences in pore-water chemistry exist between Site 1052 and the other sites previously occupied during Leg 171B. First, the Site 1052 waters show significant downsection increases in salinity, chloride, and sodium concentrations (Fig. 40A, B). Such increases at Site 1052 may indicate the presence of an evaporite sequence in the underlying Cretaceous and Jurassic sediments. Second, the Site 1052 waters show a significant increase in ammonium and a decrease in sulfate concentrations with depth (Fig. 40I). Such data are consistent with the partial degradation of organic matter within the sediments at Site 1052 (see “Organic Geochemistry” section, this chapter).

Pore-water calcium and magnesium concentration depth gradients at Site 1052 are broadly similar to those at the sites previously

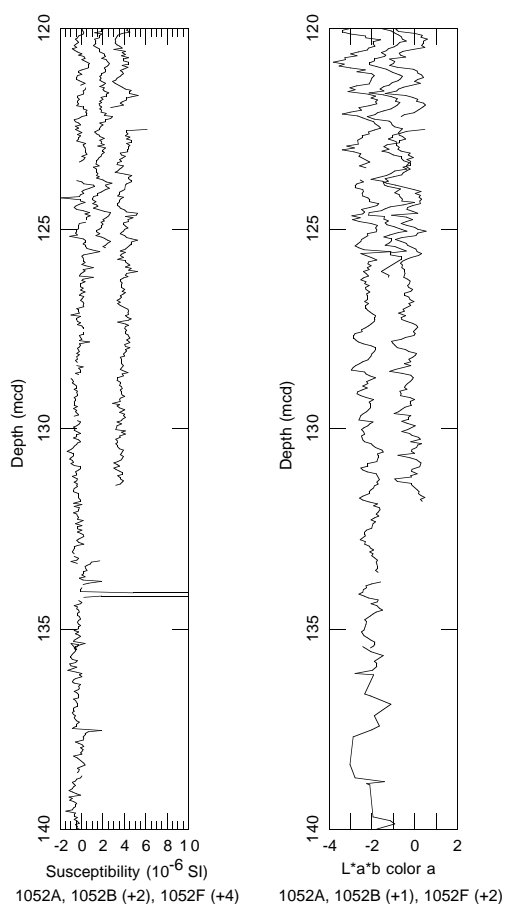


Figure 34. Magnetic susceptibility data and L*a*b code a from 120 to 140 mcd in Holes 1052A, 1052B, and 1052F.

occupied during Leg 171B, except that magnesium is slightly further depleted (by ~ 2.75 mM) toward the base (~ 600 mbsf) of the section at Site 1052 than at an equivalent depth within Hole 1051A (Figs. 40A, 32A, “Site 1051” chapter, this volume). These data are consistent with the extreme distance (>5 km; see “Introduction” chapter, this volume) to basement at the Blake Nose and suggest that regional pore-water concentrations of these cations are influenced by seawater interaction with volcanoclastic sediments and/or dolomitization. Such an interpretation is consistent with the occurrence of authigenic dolomite and smectite within the Site 1052 sediments (see “Lithostratigraphy” section, this chapter) and supports the probable contribution to the kinetic hindrance of dolomite formation played by complexing between magnesium and sulfate ions in seawater (Baker and Kastner, 1981).

The potassium and rubidium depth profiles at Site 1052 are consistent with the alteration of volcanic ash (particularly in the upper 300 m) and possible reverse-weathering reactions with clay minerals (particularly in the lower 150 m) of Hole 1052E (see “Lithostratigraphy” section, this chapter). Dissolved silica concentrations at Site 1052 are relatively low; this is consistent with the overall low silica content of the sediment at this site (see “Lithostratigraphy” section, this chapter). Siliceous nanofossil ooze and volcanic ash layers in the upper 100 m of this site (see “Lithostratigraphy” section, this chapter) are potential sources for the higher dissolved silica concentrations in the pore waters of the upper 300 m of the section (Fig. 40H).

The overall increase in strontium concentrations and calculated Sr/Ca values at Site 1052 is consistent with the recrystallization of biogenic calcite in the sediment column and with the alteration of

volcanoclastic sediments. The relatively steep increase in strontium with depth may be caused partially by proximity to underlying carbonate periplatform and/or evaporite sediments. The depth profile of pore-water lithium concentrations at Site 1052 indicates that lithium-rich sediments are less abundant at Site 1052 than at Sites 1050 and 1051.

PHYSICAL PROPERTIES

Physical properties at Site 1052 were measured on both whole-round sections and discrete samples from split-core sections. Whole-round measurements included the determination of GRAPE bulk density, magnetic susceptibility, compressional P -wave velocity, and natural gamma radiation, as well as measurements of thermal conductivity. Index properties, compressional P -wave velocity, shear strength, and resistivity were measured on discrete samples from split-core and minicore sections at a frequency of three measurements per core.

MST Measurements

GRAPE and MST P -wave velocity data were filtered to remove anomalous values that are artifacts of section-end and void or crack effects. The data sets were filtered to remove values outside the 10% error band of a reference curve, which was calculated from a 10-point running mean of the data. This filtering of the data set significantly improves visual presentation and aids interpretation of the data.

GRAPE bulk density was measured on all cores from Site 1052 (Holes 1052A, 1052B, and 1052E are shown in Fig. 41; data for Holes 1052A–1052F are in Tables 27–32 on CD-ROM, back pocket, this volume). These data, along with magnetic susceptibility and color reflectance, were used to form a Site 1052 composite stratigraphic section (see “Core-Core Integration” section, this chapter).

GRAPE bulk density shows an increase in magnitude from 1.55 to 1.9 g/cm³ in the interval cored with the APC and XCB between 0 and 165 mbsf, which corresponds to the nanofossil ooze of lithologic Subunits IB, IC, and ID and chalk and chert in the uppermost part of lithologic Unit II. Below 165 mbsf, Hole 1052E was cored with the RCB, and these GRAPE bulk density data are less accurate because the GRAPE is sensitive to the core volume. Between 165 and 300 mbsf, which corresponds with the nanofossil chalk and claystones of lithologic Unit III, GRAPE bulk density fluctuates about an approximate average of 1.55 g/cm³. Between 300 and 470 mbsf, which corresponds with the nanofossil chalk and clays of lithologic Subunits IVA and IVB, GRAPE bulk density fluctuates about an approximate average of 1.7 g/cm³. GRAPE bulk density fluctuates about an approximate average of 1.91 g/cm³ between 470 mbsf and total depth, which corresponds with the siltstones of lithologic Subunit VA, laminated black shales of Subunit VB, and sandstones, siltstones, and claystones of Subunit VC. The magnitude of the fluctuations in GRAPE bulk density is greater below 470 mbsf in comparison with the fluctuations above this depth. This pattern is also seen in the downhole logging bulk density data (see “Downhole Logging” section, this chapter).

MST measurements of magnetic susceptibility from Holes 1052A, 1052B, and 1052E are shown in Figure 42 (data for Holes 1052A–1052F are in Tables 33–38 on CD-ROM, back pocket, this volume). Above 150 mbsf, magnetic susceptibility fluctuations cannot be distinguished from background levels, except for a number of magnetic susceptibility “spikes,” some of which correlate with ash layers. At 160 mbsf, corresponding to the cherty claystone in lithologic Unit II, there is a peak in magnetic susceptibility to 20×10^{-5} SI units. Magnetic susceptibility fluctuates between 5×10^{-5} and 0 SI units between 200 and 300 mbsf in Hole 1052E, which corresponds to the nanofossil chalk and claystones of lithologic Unit III. Between 300 and 390 mbsf within the nanofossil chalk and chalky clay

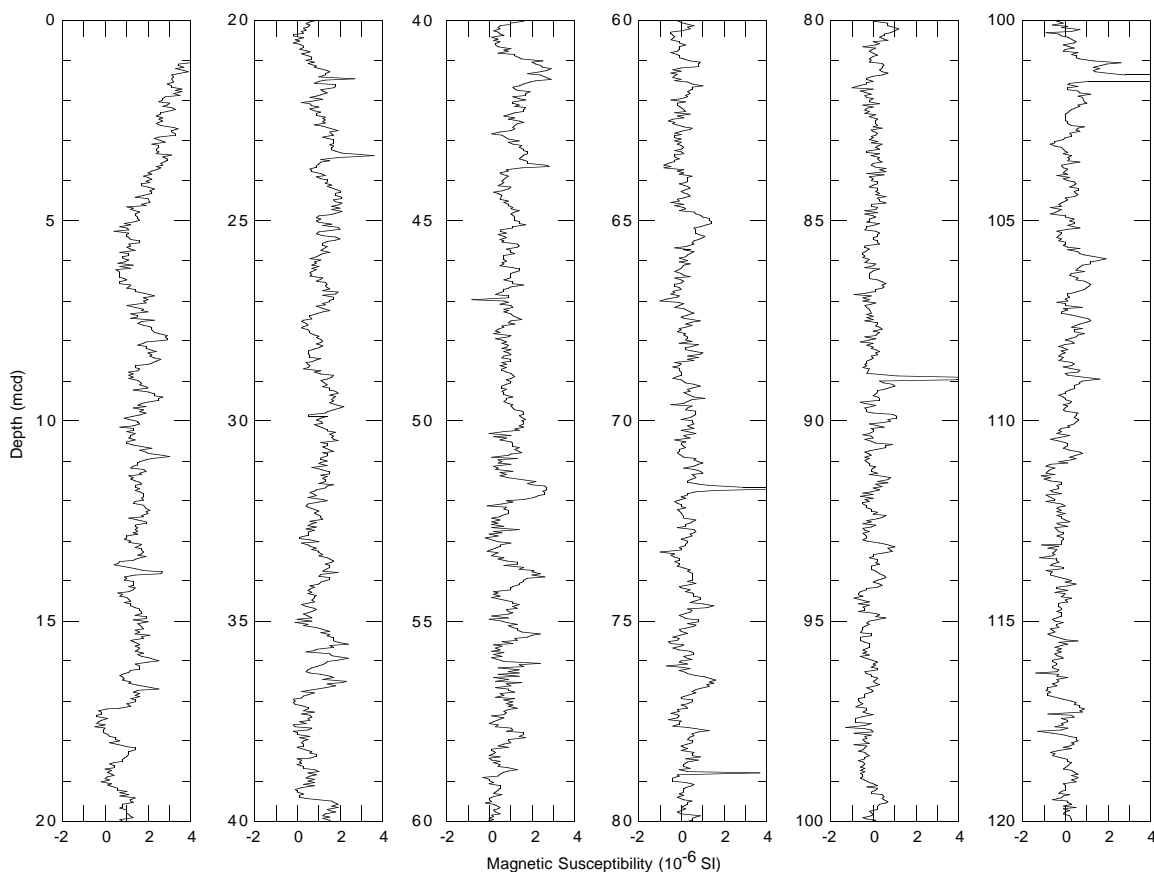


Figure 35. Spliced magnetic susceptibility record for Site 1052 from 0 to 120 mcd, using the intervals in Table 22.

Table 22. Splice table for Site 1052.

Hole, core, section, interval (cm)	Depth (mbsf)	Depth (mcd)	Whether tied	Hole, core, section, interval (cm)	Depth (mbsf)	Depth (mcd)
171B-				171B-		
1052F-1H-1, 0.00-0.00	0.00	0.00	Start	1052C-1H-2, 136.00-136.00	2.87	4.63
1052F-1H-4, 13.00-13.00	4.63	4.63	Tie to	1052F-2H-1, 84.50-84.50	10.36	10.01
1052C-1H-6, 75.00-75.00	8.25	10.01	Tie to	1052C-2H-4, 56.00-56.00	14.57	17.18
1052F-2H-6, 53.00-53.00	17.53	17.18	Tie to	1052F-3H-1, 148.00-148.00	20.48	21.18
1052C-2H-7, 7.00-7.00	18.57	21.18	Tie to	1052B-4H-2, 44.00-44.00	25.95	28.53
1052F-3H-6, 133.00-133.00	27.83	28.53	Tie to	1052F-4H-1, 67.50-67.50	29.18	29.89
1052B-4H-3, 31.00-31.00	27.31	29.89	Tie to	1052B-5H-2, 44.00-44.00	35.45	38.42
1052F-4H-7, 21.00-21.00	37.71	38.42	Tie to	1052F-5H-1, 88.50-88.50	38.90	40.82
1052B-5H-3, 135.00-135.00	37.85	40.82	Tie to	1052B-6H-1, 82.50-82.50	43.84	48.71
1052F-5H-6, 129.00-129.00	46.79	48.71	Tie to	1052F-6H-1, 86.00-86.00	48.37	50.84
1052B-6H-2, 147.00-147.00	45.97	50.84	Tie to	1052B-7H-2, 26.50-26.50	54.28	58.40
1052F-6H-6, 93.00-93.00	55.93	58.40	Tie to	1052A-8H-1, 125.50-125.50	61.96	65.73
1052B-7H-7, 11.00-11.00	61.61	65.73	Tie to	1052F-8H-1, 61.00-61.00	67.11	68.46
1052A-8H-3, 99.00-99.00	64.69	68.46	Tie to	1052B-10H-1, 83.00-83.00	72.83	77.26
1052F-8H-7, 41.00-41.00	75.91	77.26	Tie to	1052F-10H-2, 84.50-84.50	83.36	85.12
1052B-10H-6, 119.00-119.00	80.69	85.12	Tie to	1052B-11H-2, 91.00-91.00	83.91	89.53
1052F-10H-5, 77.00-77.00	87.77	89.53	Tie to	1052F-11H-1, 121.00-121.00	91.71	94.19
1052B-11H-5, 107.00-107.00	88.57	94.19	Tie to	1052B-12H-4, 2.50-2.50	95.49	102.19
1052F-11H-7, 21.00-21.00	99.71	102.19	Tie to	1052F-12H-2, 85.00-85.00	102.35	105.26
1052B-12H-6, 11.00-11.00	98.56	105.26	Tie to	1052B-13H-3, 140.00-140.00	104.91	111.96
1052F-12H-7, 5.00-5.00	109.05	111.96	Tie to	1052F-13H-1, 66.00-66.00	110.17	113.08
1052B-13H-4, 103.00-103.00	106.03	113.08	Tie to	1052B-14H-3, 108.00-108.00	114.09	120.64
1052F-13H-6, 73.00-73.00	117.73	120.64	Tie to	1052F-14H-2, 123.50-123.50	121.74	125.20
1052B-14H-6, 115.00-115.00	118.65	125.20	Tie to	1052A-14H-6, 11.00-11.00	125.31	131.33
1052F-14H-6, 137.00-137.00	127.87	131.33	Tie to			
1052A-14H-7, 63.00-63.00	127.33	133.35	Continue in 1052A			

of lithologic Subunit IVA, magnetic susceptibility fluctuates about an approximate average of 5×10^{-5} SI units. Magnetic susceptibility cannot be distinguished from background levels between 390 and 480 mbsf, which corresponds to the nannofossil chalk of lithologic Subunit IVB. Between 480 and 510 mbsf, which corresponds to the siltstones and chalk of lithologic Subunit VA, magnetic susceptibility

increases from background levels to $\sim 7 \times 10^{-5}$ SI units. The highest average magnetic susceptibility in Hole 1052E, averaging about 12×10^{-5} SI units, is observed in the interval from 510 mbsf to total depth, which corresponds to the laminated black shales and sandstones, siltstones, and claystones of lithologic Subunits VB and VC, respectively.

Table 23. Holes 1052A and 1052E headspace gas composition.

Depth (mbsf)	Gas zone	C ₁ (ppm)	C ₂ (ppm)	C ₂ = (ppm)	C ₃ (ppm)	C ₃ = (ppm)	C ₁ /(C ₂ +C ₃)
171B-1052A-							
0.72	Surface	1.8					
8.00	Surface	1.8					
17.70	Surface	1.9					
27.20	Surface	1.9					
36.70	Surface	2.1					
46.20	Surface	2.4					
55.70	Surface	3.1					
65.20	Surface	2.6					
74.70	Surface	2.8					
84.20	Surface	3.2					
93.70	Surface	2.7					
103.20	Surface	3.6					
112.70	Surface	2.9					
122.20	Surface	4.0					
128.70	Surface	3.3					
132.70	Surface	3.2					
139.00	Surface	3.7					
171B-1052E-							
141.50	Deep	7.2	0.5	0.3			9.0
146.40	Deep	2.8					
171B-1052A-							
150.20	Deep	3.6					
171B-1052E-							
157.50	Deep	2.8		0.3			9.3
171B-1052A-							
159.80	Deep	3.2					
162.90	Deep	2.2					
168.62	Deep	18.0	1.4	1.5			6.2
171B-1052E-							
207.00	Deep	5.1					
215.11	Deep	5.0					
227.70	Deep	5.7					
234.30	Deep	5.7					
245.19	Deep	4.4					
255.00	Deep	3.1					
262.90	Deep	3.9					
294.87	Deep	5.5		0.2			27.5
311.20	Deep	3.9					
323.80	Deep	4.2		0.2			21.0
333.40	Deep	7.1	0.2	0.5			10.1
341.60	Deep	6.8		0.8			8.5
351.30	Deep	4.1					
359.40	Deep	4.3		0.2			20.0
368.84	Deep	6.1					
381.60	Deep	6.7					
389.70	Deep	5.6					
397.80	Deep	5.5					
418.50	Deep	5.1					
429.60	Deep	3.4					
444.62	Deep	8.0					
455.40	Deep	3.7					
466.60	Deep	8.6	0.2	0.3			17.2
476.20	Deep	5.0					
486.81	Deep	6.5					
496.90	Deep	4.3					
506.50	Deep	7.1	0.2	0.3			14.2
513.60	Deep	12.0	1.0	0.7			7.1
524.80	Deep	5.6	0.3	0.2			11.2
534.40	Deep	4.8					
543.94	Deep	9.7	0.6				16.2
553.60	Deep	5.3	0.5	0.4		0.1	5.9
558.70	Deep	9.1	1.1	0.2			7.0
569.25	Deep	7.4	0.6	1.0			4.6
582.50	Deep	8.4		0.5			16.8
592.10	Deep	5.7					
600.30	Deep	5.7					
609.90	Deep	6.1	0.2				30.5
618.10	Deep	7.1	0.5	0.3	0.3		64.5
624.70	Deep	6.4					
628.70	Deep	5.6					
639.80	Deep	3.2					
649.40	Deep	5.7		0.5			11.4
671.11	Deep	4.0	0.2	0.5			5.7
678.18	Deep	4.8		0.5			9.6

Notes: In all cases, the injected sample size was 5 cm³. Concentration of gas is in parts per million by volume. Where no values are reported, concentrations are below detection limits.

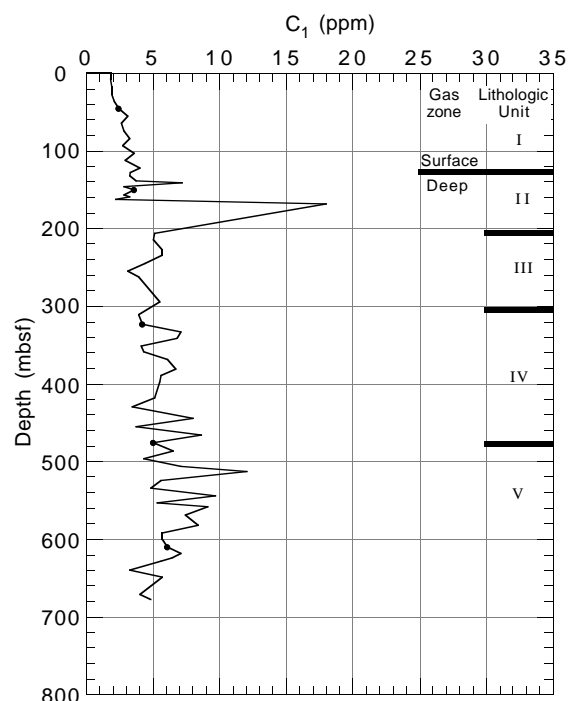


Figure 36. Methane (C₁) content vs. depth in Holes 1052A and 1052E. Lithologic units are described in the "Lithostratigraphy" section (this chapter).

MST *P*-wave velocity data from Hole 1052A APC cores are shown in Figure 43 (also see Table 39 on CD-ROM, back pocket, this volume). Despite the apparent scatter in this data set, which may be the result of sediment cracking or poor liner/sediment contact, it can be observed that *P*-wave velocity increases slightly with depth from ~1.45 to 1.50 km/s across the depth range 25 to 125 mbsf.

Natural gamma-radiation counts measured on the MST for Holes 1052A and 1052E are shown in Figure 44 (also see Tables 40, 41 on CD-ROM, back pocket, this volume). Natural gamma-radiation fluctuates about background levels in the upper 165 m of the sediment column. Between 200 and 470 mbsf, natural gamma radiation fluctuates between background levels and 11.5 counts per second (cps), with maxima observed at 205 and 325 mbsf within claystone intervals. Natural gamma radiation increases from background counts at 470 mbsf to ~14 cps at 525 mbsf, and it fluctuates about an approximate average of 12 cps between 525 mbsf and total depth. The natural gamma-radiation and magnetic susceptibility records show similar trends that reflect an increase in clastic sediment flux in the upper part of lithologic Unit III and also in lithologic Subunits VA and VB.

Index Properties

Index properties were determined for Holes 1052A and 1052E (Table 42; Fig. 45). Index properties data suggest that progressive sediment compaction and fluid expulsion with depth are the dominant factors contributing to the physical nature of the sediments, although there are discrete intervals with anomalous index properties values. Bulk and dry density values show a steady increase between the seafloor and total depth at Site 1052, from average values of 1.65 to 2.15 g/cm³ and 0.9 to 1.8 g/cm³, respectively. Grain density decreases between 0 and 130 mbsf from an average value of 2.66 to 2.62 g/cm³ and shows a sharp increase to 2.68 g/cm³ at the ooze to chalk transition at 130 mbsf. A small increase in bulk and dry density values occurs at the transition between lithologic Subunits IB and IC, which was defined on the basis of a yellow to green color change (see

Table 24. Holes 1052A and 1052E total inorganic carbon, carbonate, total carbon, total organic carbon, nitrogen, sulfur, and hydrogen analyses.

Core, section, interval (cm)	Depth interval (mbsf)	TIC (wt%)	CaCO ₃ (wt%)	TC (wt%)	TOC (wt%)	N (wt%)	S (wt%)	H (wt%)
171B-1052A-								
1X-1, 63-64	0.63-0.64	9.88	82.27	9.91	0.03			0.19
3H-1, 125-126	14.45-14.46	10.15	84.53	10.15	0.00			0.12
3H-3, 134-139	17.54-17.59	8.94	74.45	8.99	0.05			0.27
3H-5, 92-93	20.12-20.13	9.55	79.54	9.90	0.35			0.19
4H-1, 93-94	23.63-23.64	9.11	75.90	9.14	0.03			0.2
4H-3, 134-139	27.04-27.09	8.59	71.53	8.68	0.09			0.26
4H-5, 78-79	29.48-29.49	9.36	77.98	9.46	0.10	0.002		0.2
5H-1, 77-78	32.97-32.98	9.22	76.83	9.31	0.09			0.24
5H-3, 135-140	36.55-36.60	8.83	73.55	8.67	0.00	0.003		0.35
5H-5, 64-65	38.84-38.85	9.34	77.77	9.29	0.00			0.22
6H-1, 78-79	42.48-42.49	9.43	78.53	9.37	0.00			0.22
6H-3, 133-138	46.03-46.08	8.26	68.78	8.24	0.00	0.07		0.32
6H-5, 78-79	48.48-48.49	9.65	80.41	9.70	0.05	0.004		0.18
7H-1, 77-78	51.97-51.98	9.92	82.64	9.90	0.00			0.15
7H-3, 133-138	55.53-55.58	9.88	82.30	9.87	0.00	0.11		0.17
7H-5, 78-79	57.98-57.99	9.95	82.84	10.02	0.07			0.13
8H-1, 77-78	61.47-61.48	10.45	87.08	10.42	0.00			0.11
8H-3, 134-139	65.04-65.09	10.18	84.78	10.22	0.04			0.13
8H-5, 62-63	67.32-67.33	9.85	82.01	9.81	0.00			0.17
9H-1, 78-79	70.98-70.99	9.96	82.99	9.92	0.00			0.16
9H-3, 134-139	74.54-74.59	9.22	76.76	9.37	0.15	0.13		0.23
9H-5, 78-80	76.98-77.00	9.67	80.58	9.77	0.10			0.19
10H-1, 80-81	80.50-80.51	9.46	78.80	9.43	0.00			0.21
10H-3, 134-139	84.04-84.09	9.79	81.52	9.77	0.00	0.09		0.17
10H-5, 78-79	86.48-86.49	9.87	82.23	9.88	0.01	0.18		0.18
11H-1, 77-78	89.97-89.98	9.69	80.71	9.71	0.02			0.18
11H-3, 134-139	93.54-93.59	9.33	77.74	9.28	0.00			0.26
11H-5, 77-78	95.97-95.98	9.03	75.21	8.98	0.00			0.23
12H-1, 78-79	99.48-99.49	9.64	80.27	9.73	0.09			0.2
12H-3, 135-140	103.05-103.10	9.17	76.35	9.18	0.01			0.26
12H-5, 78-79	105.48-105.49	9.57	79.74	9.65	0.08			0.21
13H-1, 78-79	108.98-108.99	9.66	80.46	9.70	0.04			0.22
13H-3, 129-134	112.49-112.54	9.26	77.17	9.36	0.10	0.01		0.24
13H-5, 78-79	114.98-114.99	9.69	80.75	9.74	0.05			0.2
14H-1, 73-74	118.43-118.44	9.88	82.31	9.96	0.08			0.17
14H-3, 134-137	122.04-122.07	9.90	82.46	9.99	0.09			0.18
14H-5, 73-74	124.43-124.44	9.83	81.92	9.89	0.06			0.19
15H-1, 77-78	127.97-127.98	10.22	85.17	10.27	0.05			0.14
15H-1, 135-140	128.55-128.60	10.72	89.28	10.72	0.00			0.1
16X-1, 74-75	130.44-130.45	10.46	87.17	10.39	0.00	0.008		0.13
16X-3, 135-139	134.05-134.09	10.93	91.01	11.00	0.07			0.08
17X-1, 70-71	136.70-136.71	10.68	88.95	10.72	0.04	0.006		0.11
17X-3, 132-137	140.32-140.37	10.96	91.30	11.08	0.12	0.003		0.09
18X-2, 92-93	148.12-148.13	11.00	91.65	10.94	0.00			0.07
18X-3, 130-135	150.00-150.05	10.50	87.43	10.71	0.21			0.09
18X-5, 82-83	152.52-152.53	10.67	88.92	10.62	0.00	0.001		0.09
19X-1, 82-83	156.12-156.13	10.34	86.09	10.43	0.09	0.002		0.13
19X-3, 130-134	159.60-159.64	10.03	83.53	10.38	0.35			0.12
19X-5, 85-86	162.15-162.16	11.01	91.68	11.12	0.11	0.01		0.07
19X-6, 89-90	163.69-163.70	4.50	37.49	4.51	0.01			0.39
21X-CC, 25-27	168.65-168.67	2.68	22.31	2.93	0.25			0.43
21X-CC, 32-33	168.72-168.73	2.18	18.18	2.39	0.21			0.4
171B-1052E-								
3R-1, 77-78	156.77-156.78	10.39	86.56	10.43	0.04	0.11		0.13
3R-1, 144-147	157.44-157.47	9.97	83.08	9.98	0.01	0.09		0.16
5R-1, 18-21	175.38-175.41	9.67	80.59	9.87	0.2	0.1		0.16
5R-1, 23-24	175.43-175.44	9.53	79.35	9.71	0.18			0.14
6R-1, 19-19	184.99-184.99	7.72	64.29	8.03	0.31			0.24
8R-1, 19-20	204.19-204.20	9.73	81.07	9.84	0.11	0.1		0.15
8R-4, 64-65	209.14-209.15	4.12	34.33	4.52	0.4	0.03		0.55
8R-4, 114-118	209.64-209.68	3.98	33.17	4.35	0.37	0.08		0.57
9R-1, 36-37	213.96-213.97	9.80	81.67	9.9	0.1	0.11		0.14
9R-2, 26-27	215.37-215.38	5.16	43.01	5.42	0.26	0.12		0.44
9R-2, 42-46	215.53-215.57	3.34	27.83	3.77	0.43	0.08		0.45
10R-1, 7-10	223.27-223.30	3.82	31.85	4.13	0.31	0.08		0.51
10R-1, 44-47	223.64-223.67	2.97	24.73	3.1	0.13	0.08		0.46
10R-1, 123-124	224.43-224.44	5.79	48.25	6.1	0.31	0.11		0.41
10R-3, 130-134	227.50-227.54	6.73	56.05	6.88	0.15	0.1		0.32
10R-5, 87-88	230.07-230.08	4.48	37.32	4.64	0.16			0.38
11R-1, 46-49	233.26-233.29	3.76	31.31	4.08	0.32	0.07		0.38
11R-1, 57-58	233.37-233.38	6.89	57.37	7.15	0.26	0.008		0.3
12R-1, 17-20	242.57-242.60	5.24	43.67	5.38	0.14	0.13		0.41
12R-1, 64-67	243.04-243.07	4.02	33.47	4.24	0.22	0.08		0.4
12R-3, 138-141	246.57-246.60	7.00	58.28	6.94	0	0.09		0.18
12R-4, 11-12	246.80-246.81	7.42	61.77	7.64	0.22	0.002		0.21
13R-1, 44-45	252.44-252.45	8.74	72.84	9.06	0.32	0.01		0.25
13R-3, 62-63	255.62-255.63	8.62	71.79	8.74	0.12	0.01		0.19
14R-1, 75-76	262.45-262.46	9.26	77.16	9.31	0.05	0.13		0.15
14R-1, 106-109	262.76-262.79	9.00	74.97	9.19	0.19	0.09		0.13
14R-2, 32-33	263.22-263.23	9.33	77.69	9.38	0.05	0.007		0.14
15R-1, 78-79	272.08-272.09	7.95	66.25	7.98	0.03			0.16
15R-2, 45-46	273.15-273.16	8.27	68.86	8.27	0	0.09		0.16
15R-2, 76-80	273.46-273.50	8.35	69.57	8.53	0.18	0.002		0.19
16R-1, 96.5-97.5	281.87-281.88	8.23	68.58	8.31	0.08	0.03		0.18
16R-4, 93-97	286.29-286.33	8.05	67.06	8.21	0.16	0.11		0.25
16R-5, 71.5-72	287.58-287.58	3.20	26.67	6.37	3.17	0.007		0.22
17R-1, 77-78	291.27-291.28	8.55	71.22	8.62	0.07	0.11		0.21
17R-5, 116-117	297.53-297.54	5.96	49.65	6.06	0.1			0.44

Table 24 (continued).

Core, section, interval (cm)	Depth interval (mbsf)	TIC (wt%)	CaCO ₃ (wt%)	TC (wt%)	TOC (wt%)	N (wt%)	S (wt%)	H (wt%)
17R-6, 21-24	298.08-298.11	6.06	50.47	6.31	0.25	0.12		0.47
20R-1, 57-58	319.87-319.88	8.89	74.08	9.15	0.26	0.12		0.2
20R-3, 127-130	323.57-323.60	8.35	69.58	8.34	0	0.14		0.28
20R-5, 79-80	326.09-326.10	9.02	75.16	9.03	0.01	0.1		0.2
21R-1, 75-76	329.65-329.66	8.48	70.61	8.49	0.01	0.12		0.25
21R-4, 143-146	334.83-334.86	8.52	70.97	8.45	0	0.02		0.25
21R-5, 77-78	335.67-335.68	9.28	77.28	9.33	0.05	0.12		0.19
22R-1, 115-116	339.75-339.76	9.10	75.82	9.24	0.14	0.005		0.2
22R-2, 143-146	341.53-341.56	8.62	71.82	8.6	0	0.09		0.26
22R-4, 65-66	343.75-343.76	8.27	68.9	8.36	0.09	0.12		0.27
23R-1, 128-129	349.58-349.59	7.71	64.21	7.78	0.07			0.33
23R-2, 129-131	351.09-351.11	8.46	70.43	8.36	0	0.1		0.3
23R-4, 98-99	353.78-353.79	9.40	78.34	9.39	0	0.11		0.19
24R-1, 108-109	358.98-358.99	9.33	77.76	9.44	0.11			0.19
24R-3, 110-112	362.00-362.02	9.19	76.54	9.31	0.12	0.005		0.2
24R-3, 124-127	362.14-362.17	8.80	73.27	8.74	0	0.07	0.02	0.23
25R-1, 41-44	367.91-367.94	8.88	73.96	8.83	0	0.02		0.25
25R-1, 77-78	368.27-368.28	8.66	72.1	8.85	0.19	0.11		0.21
26R-2, 125-126	379.85-379.86	8.01	66.69	8.36	0.35	0.11		0.27
26R-4, 93-94	382.53-382.54	8.88	73.99	9.23	0.35	0.11		0.21
26R-CC, 30-33	386.96-386.99	7.48	62.32	7.59	0.11	0.02		0.35
27R-1, 64-65	387.34-387.35	8.52	70.95	8.68	0.16	0.00		0.26
27R-1, 110-112	387.80-387.82	7.93	66.03	7.99	0.06	0.08		0.28
27R-1, 149-150	388.19-388.20	8.85	73.7	8.89	0.04	0.09		0.19
27R-4, 105-106	392.25-392.26	10.70	89.09	10.87	0.17			0.13
27R-5, 37-38	393.07-393.08	10.53	87.75	10.61	0.08			0.1
27R-CC, 1-4	395.22-395.25	10.14	84.5	10	0	0.01		0.15
28R-1, 22-23	396.52-396.53	10.82	90.16	10.59	0	0.09	0.009	0.1
28R-2, 136-139	399.16-399.19	10.48	87.28	10.58	0.1	0.007		0.11
28R-3, 67-68	399.97-399.98	10.42	86.8	10.77	0.35	0.008		0.1
29R-1, 68-69	406.58-406.59	10.90	90.77	10.21	0	0.11		0.15
29R-3, 128-131	410.18-410.21	11.12	92.67	10.81	0	0.004		0.1
29R-5, 75-76	412.65-412.66	10.45	87.04	10.2	0	0.1		0.14
30R-1, 72-73	416.22-416.23	10.46	87.13	10.25	0	0.11		0.15
30R-3, 69-72	419.19-419.22	10.34	86.13	10.17	0	0.007		0.14
30R-5, 75-76	422.25-422.26	10.71	89.24	10.47	0	0.07		0.12
31R-3, 35-39	428.45-428.49	9.91	82.57	9.76	0	0.11		0.2
31R-3, 84-85	428.94-428.95	10.22	85.17	9.95	0	0.1	0.13	0.17
31R-5, 81-82	431.91-431.92	11.00	91.65	10.78	0	0.09		0.11
33R-1, 72-75	445.02-445.05	9.67	80.51	9.44	0	0.01	0.22	0.19
33R-1, 143-144	445.73-445.74	11.21	93.37	10.9	0	0.007		0.08
34R-1, 125-128	455.15-455.18	10.15	84.52	9.98	0	0.01		0.15
34R-1, 144-145	455.34-455.35	11.02	91.82	10.74	0	0.14		0.1
35R-1, 76-77	464.36-464.37	10.99	91.56	10.88	0	0.11	0.01	0.08
35R-3, 4-7	466.64-466.67	10.58	88.11	10.4	0	0.009		0.11
36R-3, 143-144	477.63-477.64	8.83	73.57	0	0			
36R-4, 98-99	478.68-478.69	9.16	76.33	9.53	0.37	0.04	0.11	0.25
36R-4, 138-139	479.08-479.09	11.30	94.14	11.2	0	0.1		0.06
36R-6, 82-83	481.52-481.53	6.55	54.59	0	0			
37R-2, 31-32	484.12-484.13	7.14	59.52	7.39	0.25	0.02	0.27	0.34
37R-6, 73-74	490.54-490.55	8.10	67.51	8.12	0.02	0.02		0.29
38R-3, 54-55	495.94-495.95	10.10	84.16	9.96	0	0.08		0.12
38R-4, 134-135	498.24-498.25	4.61	38.37	4.97	0.36	0.08		0.57
39R-4, 11-12	506.61-506.62	7.34	61.1	7.5	0.17	0.1	0.05	0.29
39R-5, 142-143	508.92-508.93	10.99	91.51	11.08	0.09	0.005		0.06
40R-1, 44-45	511.04-511.05	6.21	51.76	0	0			
40R-1, 55-58	511.15-511.18	5.20	43.33	0	0			
40R-1, 125-126	511.85-511.86	3.24	27.01	0	0			
40R-2, 3.5-4.5	512.14-512.15	2.89	24.06	0	0			
40R-2, 23.5-24.5	512.34-512.35	3.23	26.91	0	0			
40R-2, 69-70	512.79-512.80	4.62	38.52	0	0			
40R-2, 111-112	513.21-513.22	4.69	39.05	0	0			
40R-2, 148-149	513.58-513.59	2.69	22.4	0	0			
40R-3, 9-9.5	513.69-513.70	2.35	19.55	3.26	0.91	0.12	0.29	0.8
40R-CC, 3-4	516.84-516.85	10.84	90.26	10.8	0	0.1		0.09
41R-1, 101-102	521.31-521.32	3.48	29	4.21	0.73	0.11	0.74	0.6
41R-1, 131-132	521.61-521.62	3.30	27.46	4.11	0.81	0.06	0.26	0.72
41R-2, 77-78	522.57-522.58	10.61	88.34	10.52	0	0.09		0.09
41R-3, 48-53	523.78-523.83	5.65	47.1	6.15	0.5	0.1		0.36
41R-3, 118-119	524.48-524.49	3.16	26.3	0	0			
41R-4, 24.5-25.5	525.05-525.06	4.26	35.49	4.87	0.61	0.14		0.51
41R-4, 67-69	525.47-525.49	3.99	33.21	4.66	0.67	0.12		0.55
41R-4, 99-100.5	525.79-525.81	3.53	29.4	4.3	0.77	0.12		0.63
41R-5, 13-14	526.43-526.44	5.35	44.59	0	0			
41R-7, 23.5-24.5	529.04-529.05	3.79	31.54	0	0			
42R-2, 75-77	532.15-532.17	4.49	37.37	4.93	0.44	0.1		0.46
42R-5, 77-78	536.67-536.68	4.03	33.53	4.41	0.38	0.08	0.81	0.5
43R-1, 139-140	540.89-540.90	3.13	26.09	3.65	0.52	0.13		0.6
43R-3, 35-36	542.79-542.80	5.47	45.52	5.77	0.31	0.02	0.45	0.41
43R-5, 115-116	546.59-546.60	3.18	26.49	3.83	0.65	0.04	0.47	0.58
43R-7, 14-15	548.58-548.59	3.38	28.15	0	0			
43R-7, 58-59	549.02-549.03	3.48	28.98	4.01	0.53	0.11		0.52
44R-1, 75-76	549.85-549.86	5.98	49.84	6.15	0.17	0.1		0.34
44R-2, 1-3	550.61-550.63	4.70	39.11	0	0			
44R-2, 98-99	551.58-551.59	7.24	60.27	0	0			
44R-3, 2-3	552.12-552.13	5.46	45.51	5.82	0.36	0.11		0.36
44R-3, 130-132	553.40-553.42	4.07	33.88	0	0			
44R-4, 143-144	555.03-555.04	3.21	26.74	0	0			
44R-6, 117-118	557.77-557.78	3.12	26	3.67	0.55	0.13		0.67
45R-1, 89-90	559.59-559.60	4.23	35.26	4.6	0.37	0.1		0.43
45R-2, 55-57	560.75-560.77	3.10	25.82	3.67	0.57	0.11		0.65

Table 24 (continued).

Core, section, interval (cm)	Depth interval (mbsf)	TIC (wt%)	CaCO ₃ (wt%)	TC (wt%)	TOC (wt%)	N (wt%)	S (wt%)	H (wt%)
45R-2, 85-86	561.05-561.06	3.00	24.95		0			
46R-1, 77-78	569.07-569.08	3.64	30.3	4.14	0.5	0.13		0.56
46R-4, 53-54	572.79-572.80	3.57	29.76	4.19	0.62	0.04		0.45
47R-1, 50-51	578.50-578.51	4.65	38.71	5.02	0.37	0.13		0.36
47R-4, 49-50	582.99-583.00	3.92	32.66	4.43	0.51	0.12		0.36
47R-6, 131-132	586.81-586.82	3.07	25.57	3.69	0.62	0.13		0.5
48R-1, 67-68	588.27-588.28	3.26	27.12	3.96	0.7	0.14	0.22	0.47
48R-5, 102-103	594.62-594.63	4.15	34.54	4.58	0.43	0.17		0.39
48R-6, 84-85	595.94-595.95	3.52	29.36	4.12	0.6	0.12		0.42
49R-1, 20-21	597.50-597.51	3.31	27.59	3.85	0.54	0.1		0.44
49R-1, 61-62	597.91-597.92	3.42	28.49	3.89	0.47	0.13		0.36
49R-1, 119-120	598.49-598.50	4.97	41.44	5.16	0.19	0.12		0.29
49R-3, 15-16	600.45-600.46	2.83	23.61	3.68	0.85	0.1	0.26	0.63
49R-4, 54-55	602.34-602.35	3.74	31.19	4.18	0.44	0.1		0.44
49R-4, 87-88	602.67-602.68	3.84	31.95	4.39	0.55	0.14		0.51
49R-5, 50-51	603.80-603.81	2.90	24.13	3.41	0.51	0.11		0.46
50R-1, 8-9	606.98-606.99	3.48	28.95	4.01	0.53	0.14		0.55
50R-1, 56-57	607.46-607.47	2.63	21.91	3.32	0.69	0.11	0.08	0.59
50R-3, 7-8	609.97-609.98	4.03	33.54	4.57	0.54	0.15	0.3	0.42
50R-3, 23-24	610.13-610.14	3.87	32.24	4.58	0.71	0.12		0.51
51R-1, 138-139	617.98-617.99	3.62	30.19	4.23	0.61	0.14		0.42
51R-2, 101-104	619.11-619.14	5.14	42.79	5.57	0.43	0.12		0.39
52R-1, 20-21	621.90-621.91	4.89	40.74	5.16	0.27	0.11		0.31
52R-2, 129-133	624.49-624.53	1.52	12.66	2.03	0.51	0.11		0.47
52R-3, 114-115	625.84-625.85	1.40	11.67	2.16	0.76	0.12		0.62
53R-5, 137-138	634.57-634.58	4.51	37.58		0			
53R-6, 34-36	635.04-635.06	6.61	55.05		0			
54R-2, 138-139	639.68-639.69	2.60	21.68		0			
55R-1, 54-55	646.94-646.95	6.30	52.48		0			
55R-6, 4-5	653.94-653.95	5.52	46.01		0			
56R-1, 26-27	656.26-656.27	11.45	95.4		0			
57R-3, 139-140	669.50-669.51	3.68	30.64		0			
57R-6, 132-133	673.93-673.94	2.19	18.23		0			
58R-1, 54-55	675.74-675.75	2.09	17.44		0			
58R-3, 131.5-132.5	679.50-679.51	2.27	18.95		0			
Maximum		11.45	95.40	11.20	3.17	0.18	0.81	0.80
Minimum		1.40	11.67		0.00			
Mean		7.24	60.33	6.78	0.19	0.05	0.02	0.24
Standard deviation		2.94	24.46	3.62	0.30	0.05	0.10	0.18

Notes: TIC = total inorganic carbon; TC = total carbon; TOC = total organic carbon computed by difference (TC - TIC). Negative TOC values are reported as 0.00. wt% = weight percent. Where no values are reported, concentrations are below detection limits.

“Lithostratigraphy” section, this chapter). There is an additional small increase in bulk and dry densities at 130 mbsf, which again correlates with the ooze to chalk transition between lithologic Subunit IC and Unit II. Grain density data are widely scattered between 2.55 and 2.75 g/cm³ in the interval 130–300 mbsf, which possibly reflects the variable siliceous content of lithologic Units II and III. Between 300 mbsf and total depth, grain density remains relatively constant about an average of 2.72 g/cm³. In intervals at 160–220, 490–525, and 630–680 mbsf, significant excursions of peak bulk and dry densities are apparent. These intervals correlate, respectively, with the massive calcareous claystones in lithologic Unit II, cemented limestones in lithologic Subunit VA, and cemented sandstones and limestones in lithologic Subunit VC.

Sediment porosity, water content, and void ratio (Fig. 45) show complementary inverse trends with depth to the trends observed for bulk and dry densities. Excursions of low porosity and water content are observed for the three intervals with peak bulk and dry densities. The index properties data from these intervals suggest that diagenesis decreased sediment porosity and water content by secondary cementation of the lithology. These intervals of elevated density and low porosity may also act to inhibit fluid flow.

Discrete bulk density measurements show good agreement with GRAPE bulk density estimates for the APC cored interval between 0 and 160 mbsf at Site 1052 (Fig. 46). Between 160 mbsf and total depth, which was cored with the RCB, GRAPE bulk density significantly underestimates the values obtained by discrete measurements. GRAPE bulk densities significantly underestimate true values of bulk density because RCB coring generally results in a much reduced sediment core diameter.

P-wave Velocity

Discrete measurements of *P*-wave velocity were obtained on split-core sections from Hole 1052A and minicores from Hole 1052E using the Hamilton Frame velocimeter (Table 43; Fig. 47). Comparison of discrete measurements of *P*-wave velocity with MST PWL values (Fig. 43) shows that the MST PWL significantly underestimates true *P*-wave velocity.

P-wave velocity shows a general increase in value with depth from 1.5 to 2.25 km/s, with discrete intervals of significantly higher velocities. Between 0 and 150 mbsf, *P*-wave velocity shows a linear increase from 1.5 to 1.75 km/s. No change in *P*-wave velocity is observed between lithologic Subunits IB and IC, for which the contact is defined by a color change. Conversely, a small, stepped increase in velocity occurs at the ooze to chalk transition at ~140 mbsf, which is at the contact between lithologic Subunit IC and Unit II. In the interval between 160 and 220 mbsf, *P*-wave velocity values as much as 4 km/s correspond with the claystones in lithologic Unit II that forced us to terminate XCB coring in Hole 1052A. Between 150 and 470 mbsf, *P*-wave velocity shows a more irregular increase with depth from ~1.75 to 2.5 km/s. *P*-wave velocity is relatively constant at about 2.25 km/s between 470 mbsf and total depth. Between ~490 and 525 mbsf and 630 and 680 mbsf, there are peak values of *P*-wave velocity as much as 5.7 km/s. These elevated velocities are associated with the cemented limestones in lithologic Subunit VA and cemented sandstones and limestones in lithologic Subunit VC, respectively.

Acoustic anisotropy, the ratio of *P*-wave velocity measured perpendicular to the split-core surface (*x*-direction) to that measured parallel to the core axis (*z*-direction), is plotted for Hole 1052E in Figure

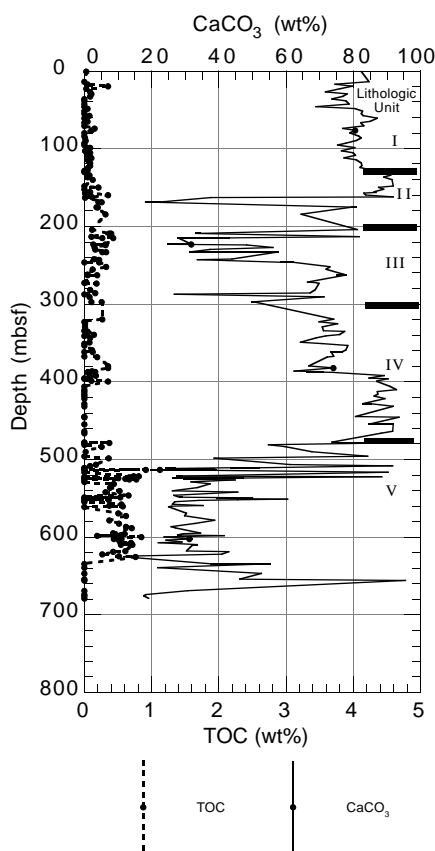


Figure 37. TOC and carbonate contents vs. depth in Holes 1052A and 1052E. TOC values, except those values >0.4 wt%, are considered unreliable at this site. Lithologic units are described in the “Lithostratigraphy” section (this chapter).

47. The acoustic anisotropy data show that P -wave velocity is faster in the transverse direction (x) than in the longitudinal direction (z) and that this ratio increases with depth. The relatively higher transverse velocity suggests that there may be evidence for pressure solution, recrystallization, and grain growth parallel to bedding planes.

Figure 48 illustrates the general positive relationship between P -wave velocity and bulk density. This relationship is most significant for data from the interval 0–150 mbsf and for data from the discrete intervals of elevated P -wave velocity and bulk density, as discussed previously.

Undrained Shear Strength

Undrained shear strength was measured on sediments recovered from Hole 1052A using both the miniature vane-shear device and, when the sediment became too indurated to insert the vane-shear device, a pocket penetrometer (Table 44; Fig. 49). There is no systematic relationship between shear strength and depth in Hole 1052A, although pocket penetrometer measurements are biased toward higher values than those obtained with the vane-shear device.

Normalized shear strength, the ratio of shear strength (S_u) to effective overburden pressure (P_o'), can be used to assess the stress history of a sediment column. Normalized shear strength ratios (S_u/P_o') determined for Hole 1052A are plotted against depth in Figure 50. A normally consolidated sediment has an S_u/P_o' between 0.2 and 0.22 (Ladd et al., 1977). Sediments above 45 mbsf in Hole 1052A have $S_u/P_o' > 0.22$ and are overconsolidated. Below 45 mbsf in Hole 1052A,

S_u/P_o' are generally ≤ 0.22 , suggesting that sediments below this depth are underconsolidated. Estimation of the overburden thickness—assuming that the sediment at 5.78 mbsf where the maximum value of S_u was measured was normally consolidated at maximum overburden thickness and that no changes in shear strength have occurred—suggests that 11 m of sediment may have accumulated and been removed in Hole 1052A between the late Eocene and the present.

Resistivity

The resistivity data from Hole 1052A were measured using the Scripps Institution of Oceanography probe (Table 45; Fig. 51). Resistivity values show a general increase in magnitude from 0.51 to 0.61 Ωm between 0 and 130 mbsf. Resistivity measurements were made only in the APC cores above the ooze to chalk transition at Site 1052, and thus miss the change in resistivity associated with this transition at Site 1051 (see “Physical Properties” section, “Site 1051” chapter, this volume). Resistivity and porosity are well correlated (Fig. 52), reflecting progressive reduction of porosity with depth because of compaction and cementation processes.

Thermal Conductivity

Thermal conductivity data from the APC cores of Hole 1052A are listed in Table 46 and are shown in Figure 53. Thermal conductivity measurements for Hole 1052A were obtained using the TK-04 instrument, and they display less scatter than measurements obtained for Holes 1049B and 1050B using the Thermcon-85 unit. Three measurements <1.0 W/(m·K) may be spurious data points resulting from poor thermal contact between the needle probe and the sediment during data collection. Thermal conductivity shows a slight increase with depth between the seafloor and ~35 mbsf, where a color change defines the contact between lithologic Subunits IB and IC. Below 35 mbsf, thermal conductivity remains relatively constant. An average thermal conductivity of 1.23 ± 0.09 W/(m·K) is a representative estimate for the depth interval 35 to 128 mbsf.

Interval Velocities and Identification of Seismic Reflectors

Interval velocities were calculated from P -wave velocity measurements on discrete samples from Holes 1052A and 1052E to correlate prominent seismic reflectors in U.S. Geological Survey (USGS) MCS Line TD-5 (Hutchinson et al., 1995) with major lithologic units and boundaries identified during core description (see “Lithostratigraphy” section, this chapter). Measured P -wave velocity values are listed in Table 20, and the calculated interval velocities are listed in Table 47. Average velocities were tabulated for all intervals, except for the interval between 215 and 500 mbsf. Between 215 and 300 mbsf, a linear regression was fit to the P -wave velocity data, where

$$V = 1500 + 1.818 \times \text{depth}.$$

Average interval velocities in the intervals between 500 and 525 mbsf and between 630 and 660 mbsf were computed as weighted sums of a low-velocity component and a high-velocity component calculated from measured values (see Fig. 47), where

$$V = 0.33 (4700 \text{ m/s}) + 0.67 (2150 \text{ m/s}).$$

Two-way traveltimes calculated from measured depths (mbsf) for lithologic units and boundaries identified during core description and interval velocities are listed in Table 48 and identified in Figure 54.

Table 25. Rock-Eval analysis data for Hole 1052E.

Core, section, interval (cm)	T _{max} (°C)	S ₁ (mg HC/g rock)	S ₂ (mg HC/g rock)	S ₃ (mg HC/g rock)	PI	S ₂ /S ₃	PC	TOC (wt%)	HI (mg HC/g TOC)	OI (mg CO ₂ /g TOC)
171B-1052E-										
16-5, 71.5-72.0	415		0.01	1.39		0.00	0.00	0.08	12	1737
38-3, 54.0-55.0	393	0.03	0.03	0.45	0.50	0.06	0.00	0.05	60	900
38-4, 134.0-135.0	412	0.05	0.45	1.22	0.10	0.36	0.04	0.46	97	265
39-4, 11.0-12.0	407	0.09	0.09	1.03	0.50	0.08	0.01	0.17	52	605
39-5, 142.0-143.0		0.06	0.00	0.08	1.00	0.00	0.00	0.03	0	600
40-1, 44.0-45.0	402	0.04	0.17	0.87	0.20	0.19	0.01	0.42	40	207
40-1, 55.0-58.0	406	0.02	0.24	1.56	0.08	0.15	0.02	0.52	46	300
40-1, 125.0-126.0	416	0.04	0.52	1.66	0.07	0.31	0.04	0.94	55	176
40-2, 23.5-24.5	411	0.07	0.61	1.59	0.10	0.38	0.05	1.37	44	116
40-2, 148.0-149.0	417	0.05	0.52	1.51	0.09	0.34	0.04	0.94	55	160
40-2, 69.0-70.0	402	0.02	0.13	1.52	0.14	0.08	0.01	0.53	24	286
40-3, 9.0-9.5	421	0.10	0.69	1.32	0.13	0.52	0.06	0.98	70	134
41-1, 131.0-132.0	454	0.11	0.63	0.02	0.15	31.50	0.06	0.07	900	28
41-1, 100.0-102.0	418	0.07	0.59	1.35	0.11	0.43	0.05	0.88	67	153
41-3, 48.0-53.0	409	0.09	0.45	1.15	0.17	0.39	0.04	0.46	97	250
41-3, 118.0-119.0	414	0.02	0.37	1.49	0.05	0.24	0.03	0.77	48	193
41-7, 23.5-24.5	374	0.01	0.04	1.40	0.25	0.02	0.00	0.43	9	325
42-2, 75.0-77.0	413	0.01	0.36	1.24	0.03	0.29	0.03	0.63	57	196
42-5, 77.0-78.0	403	0.06	0.23	4.17	0.21	0.19	0.02	0.52	44	225
43-5, 115.0-116.0	484	0.03	0.30	1.52	0.09	0.19	0.02	0.64	46	237
44-6, 117.0-118.0	593	0.04	0.46	1.51	0.08	0.30	0.04	0.68	67	222
45-1, 89.0-90.0	417	0.04	0.38	1.15	0.10	0.33	0.03	0.50	76	230
45-5, 13.0-14.0	403	0.02	0.21	1.38	0.09	0.15	0.01	0.47	44	293
49-5, 50.0-51.0	412	0.02	0.10	1.31	0.17	0.07	0.01	0.54	18	242
52-2, 129.0-133.0	414	0.01	0.07	0.98	0.12	0.07	0.00	0.54	12	181
58-1, 54.0-55.0	415	0.04	0.09	1.04	0.33	0.08	0.01	0.83	10	125
58-3, 131.5-132.5	413	0.01	0.19	1.09	0.05	0.17	0.01	0.92	20	118

Notes: The definitions of the reported values are given in the “Explanatory Notes” chapter (this volume). Blank cells indicate that no value was reported from the Rock-Eval analysis. The 0.00 values in the S₁, S₂, and S₃ columns indicate concentrations that are below detection limits.

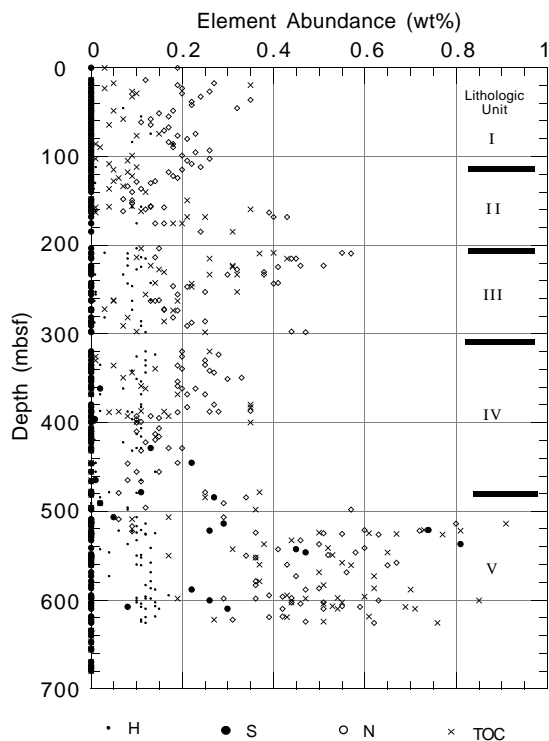


Figure 38. Elemental abundance vs. depth in Holes 1052A and 1052E. Lithologic units are described in the “Lithostratigraphy” section (this chapter).

Figure 54 is a short segment of USGS reflection seismic Line TD-5 (see Fig. 3, “Introduction” chapter, back-pocket foldout, this volume) that is split vertically at the location of Hole 1052E. Near the bottom of Hole 1052E, clastic-rich interbeds contained in the Albian clinoform stack form weak, discontinuous reflectors in the vicinity of Hole 1052E. One of these interbeds was penetrated before reaching total depth for the hole. The top of the Albian is a well-defined regional

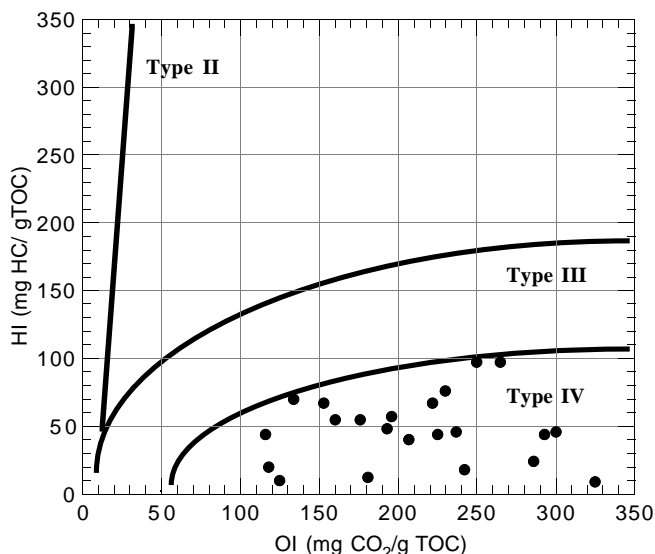


Figure 39. Hydrogen index vs. oxygen index labeled with kerogen type fields. Data from samples with TOC values <0.4 wt% (Table 25) are considered unreliable at this site and are not shown.

reflector that truncates an underlying clinoform stack of Albian sediments. The Cenomanian/Maastrichtian (C/M) unconformity forms an identifiable, but weak, reflector. Above the C/M unconformity, thick intervals of soft-sediment deformation and slumping are expressed as weak to moderate patchy reflectors. Although the K/T boundary is a strong reflector locally, it is discontinuous over a regional scale. Above the K/T boundary reflector are several strong reflectors caused by sharp velocity and lithologic contrasts in upper Paleocene claystones, located at the Paleocene/Eocene unconformity, and in middle Eocene cherts. Because core recovery was relatively poor in this interval, the correlation between lithology and reflectors is less certain.

Table 26. Interstitial-water geochemical data for Site 1052.

Core, section, interval (cm)	Depth (mbsf)	pH	Alkalinity (mM)	Salinity (g/kg)	Cl (mM)	Na (mM)	Mg (mm)	Ca (mM)	SO ₄ (mM)	NH ₄ (μM)	H ₄ SiO ₄ (μM)	K (mM)	Sr (μM)	Li (μM)	Rb (μM)	B (μM)
171B-1052A-																
2X-3, 145-150	7.95	7.67	3.15	36.0	553	472	52.99	11.09	28.5	14.6	398	12.6	100	36.6	2.25	416
3H-3, 145-150	17.65	7.51	3.19	36.0	560	478	52.85	11.79	28.5	8.7	680	13.4	115	37.4	2.44	495
4H-3, 145-150	27.15	7.53	3.42	36.0	557	476	52.73	12.31	28.8	11.7	720	12.0	129	42.3	2.30	516
5H-3, 145-150	36.65	7.72	3.56	36.0	562	477	52.26	13.02	27.8	29.2	744	13.8	145	48.6	2.41	509
6H-3, 145-150	46.15	7.65	3.81	36.0	562	475	51.95	13.50	27.0	48.2	722	13.5	163	48.3	2.37	502
7H-3, 145-150	55.65	7.26	3.90	36.0	561	474	51.77	13.92	26.9	68.7	702	13.7	176	52.4	2.44	452
10H-3, 145-150	84.15	7.59	4.30	36.0	564	479	50.83	15.18	26.7	106.7	780	10.8	215	66.4	2.08	516
13H-3, 145-150	112.65	7.42	4.35	36.0	577	490	50.40	16.10	26.1	170	791	10.6	254	75.5	2.03	537
16X-2, 145-150	132.65	7.85	3.62	36.0	571	486	49.57	16.03	27.3	239.6	691	12.0	289	82.5	2.19	423
18X-3, 145-150	150.15	7.54	3.42	36.0	577	490	48.63	17.22	26.4	340.5	568	11.4	348	95.7	2.02	573
171B-1052E-																
2R-1, 93-100	147.33	7.63	3.46	36.0	582	493	48.77	17.24	25.4	341.9	515	11.1	353	97.7	2.08	723
8R-2, 135-145	206.85	7.61	2.80	36.0	592	497	43.92	20.64	20.4	574.3	612	9.40	566	142	1.66	559
10R-3, 140-150	227.60	7.74	1.74	36.0	597	501	42.51	20.76	19.0	618.2	497	9.21	628	152	1.62	537
12R-2, 119-129	245.09				602		42.31	20.88	20.3	697.1	638	9.28	619	153	1.74	594
14R-1, 109-120	262.79			38.0	613		42.18	22.62	17.8	748.2	667	8.47	669	162	1.6	559
16R-3, 131-146	285.21			36.5	617		41.30	22.21	18.9	799.4	585	8.45	695	167	1.52	559
20R-3, 135-150	323.65	7.83	1.34	36.5	616	515	39.33	22.89	15.5	853.4	91	8.79	770	181	1.74	338
23R-2, 138-150	351.18	7.85	1.04	36.8	630	529	39.04	23.42	15.3	928	85	8.15	812	188	1.52	366
26R-3, 135-150	381.45	8.01	0.86	38.0	631	529	39.00	24.03	15.5	970.4	94	7.43	824	184	1.27	188
29R-3, 135-150	410.25	7.48	2.73	38.0	635	530	39.48	26.53	15.3	1030	292	6.09	878	191	1.05	573
33R-1, 33-45	444.63	7.53	2.55	38.0	634	529	39.60	26.17	15.0	1070	272	6.32	860	181	1.03	616
36R-2, 135-150	476.05			38.3	643		39.69	25.59	15.1			7.31	1019.3	182	0.73	352
39R-3, 135-150	506.35				652		35.82	26.27	12.8	1407		7.66	1079	166	0.74	109
46R-4, 135-150	573.61	8.15	0.68	40.0	683	571	37.06	28.87	11.9	1441	54	4.69	1555	179	0.88	280
49R-4, 137-150	603.17	8.20	0.93	40.5	712	595	34.21	32.45	10.1	1466	61	4.87	1665	176	0.82	202
52R-2, 135-150	624.55	8.57	1.13	40.5	682	566	33.26	31.47	8.75	1695	46	4.73	1559	164	0.61	209
55R-2, 135-150	649.25	8.55		40.0	685		34.78	31.64	7.57	1573	55	3.99	1618	171	0.38	252
58R-2, 135-150	678.03			41.5	699		32.61	33.16	6.02	1626	39	3.57	1766	161	0.35	252

Note: Where no values are reported, data are absent.

Summary

Physical properties data at Site 1052 indicate that compaction and fluid expulsion are the controlling factors on general sediment properties. Discrete intervals with peak bulk and dry densities and *P*-wave velocity values and with complementary decreases in water content and porosity (between 160 and 220, 490 and 525, and 638 and 680 mbsf) indicate that certain layers have undergone preferential diagenesis and cementation processes. These intervals may act to inhibit fluid flow, and they forced us to change from XCB to RCB coring to penetrate them.

DOWNHOLE LOGGING

Logging Operations

After Hole 1052E was drilled to a total depth of 684.8 mbsf, the borehole and drilling equipment were prepared for wireline logging. Upon the completion of coring operations, a complete wiper trip was made to condition the borehole for logging. With the pipe set near the bottom of the hole, the bit was released, and a pill of sepiolite mud was pumped down the drill pipe to sweep the hole of cuttings not removed by circulating seawater. Because major washouts were detected in the upper part of the hole during these operations, the BHA was positioned at 222 mbsf to maintain stable hole conditions.

Three logging tool strings were deployed in Hole 1052E, in the following order: triple-combo, FMS, and geological high-sensitivity magnetometer tool (see "Downhole Logging" section, "Explanatory Notes" chapter, this volume). The Lamont-Doherty temperature-logging tool was attached at the bottom of the first logging run. Each tool string was lowered to the bottom of the hole and pulled up at a rate between 300 and 600 m/hr. All three tool strings reached the total depth drilled. A repeat interval was also run with each logging tool string to provide data quality control.

The wireline heave compensator was not available for use during logging operations during Leg 171B. Fortunately, sea-state conditions were good (~1-m swells) and did not appear to seriously degrade the logging data. Table 49 shows the logging schedule and intervals logged with each tool string in Hole 1052E.

Data Quality

Overall, the data recorded in Hole 1052E are of good quality and compare well with discrete measurements made on core samples (see "Comparison of Core-Log Physical Properties Data" section, this chapter). Some post-cruise reprocessing, however, of the log data is required to remove any effects of ship heave and "stick-and-slip" logging tool motion. Results from the general purpose inclinometry tool indicate that the borehole is deviated between 0° and 1.5°, whereas the direction of borehole dip (borehole azimuth) gradually rotates downhole from 190° to 270°N.

Borehole diameter, measured by the Litho-Density sonde (HLDT) caliper, typically varied between 10.4 and 11.2 in (26.4 and 28.5 cm). The bit used to drill this hole was 25 cm (9.875 in). The FMS calipers indicate that the borehole was "in gauge," or round, with a maximum difference of 2 cm between the caliper readings.

Depth shifts for each of the logging runs were determined by correlating the natural gamma-ray logs and were made relative to the NGT on the triple-combo tool string. The depth to the end of pipe, determined by wireline measurements, was 2.0 m shallower than that given by drill-pipe measurement. All logs were depth shifted from meters below rig floor to meters below seafloor by subtracting 1355 m (the distance from rig floor to the bottom of the BHA). These preliminary adjustments will be replaced by more accurate depth shifts during post-cruise processing (post-cruise processed log data are available on CD-ROM, back pocket, this volume). The FMS microresistivity data have undergone shipboard image processing, thereby improving the image for preliminary shipboard interpretation and integration with core observations. Post-cruise processing of the array sonic (SDT) logs from Hole 1052E is necessary before useful velocity data can be obtained. Selected unprocessed sonic data are presented in Figure 55.

Logging Units

Excellent hole conditions and a strong signal in the wireline logs allow clear identification of six logging units. The boundaries between adjacent logging units were placed at major changes in log characteristics. The main lithologic units, as determined from the re-

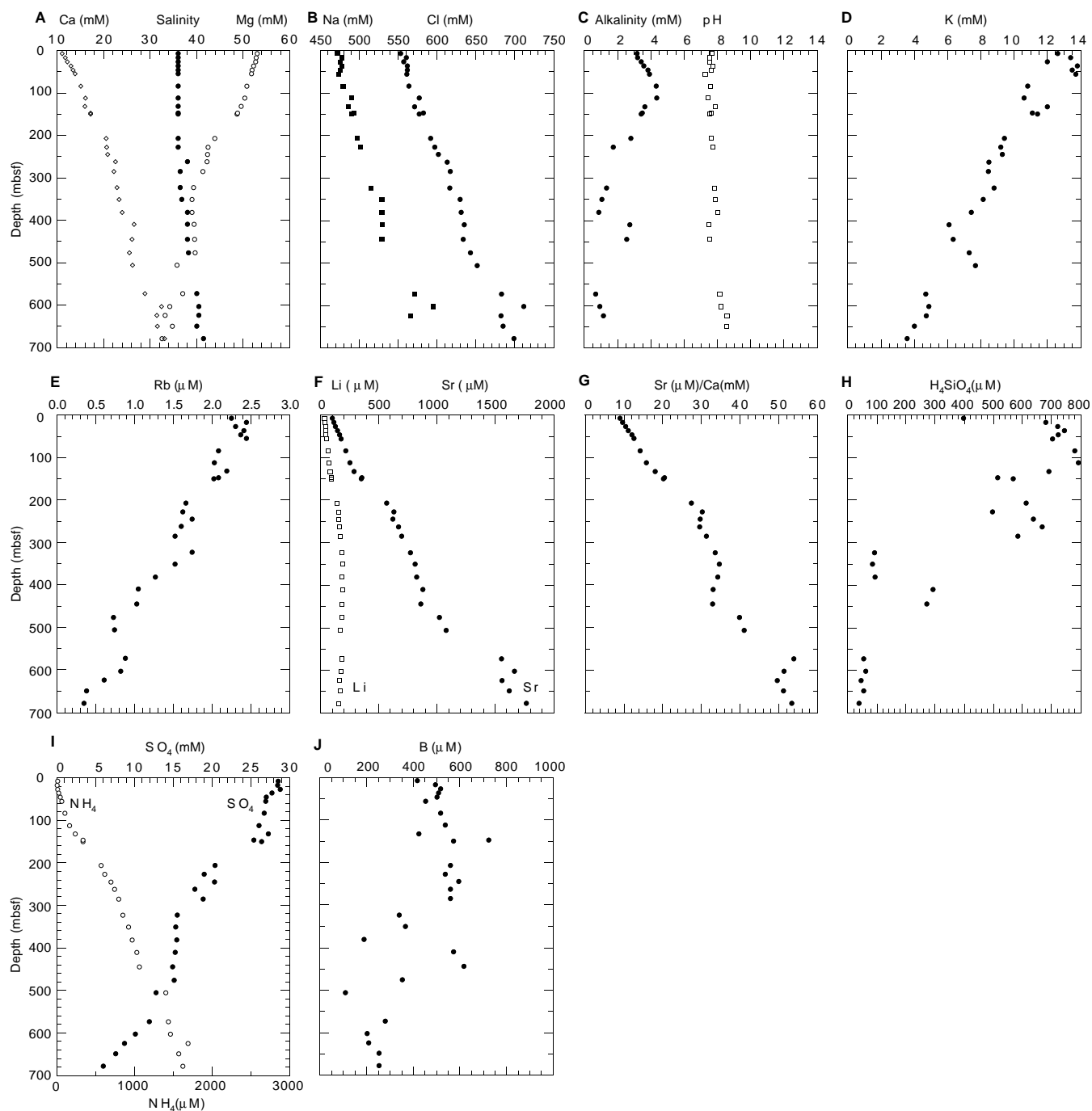


Figure 40. Interstitial-water geochemical data for Hole 1052A vs. depth. **A.** Calcium, salinity, and magnesium. **B.** Sodium and chloride. **C.** Alkalinity and pH. **D.** Potassium. **E.** Rubidium. **F.** Lithium and strontium. **G.** Strontium/calcium ratio. **H.** Silica. **I.** Sulfate and ammonium. **J.** Boron.

covered cores (see “Lithostratigraphy” section, this chapter), are recognizable on all of the downhole measurement logs.

Logging Unit 1 (220–295 mbsf)

The interval between 220.0 mbsf (the base of the drill pipe) and 295 mbsf is characterized by increasing mean bulk density (RHOB) and photoelectric factor (PEF) and variable decreasing porosity (APLC; Fig. 56). Resistivity values are typically low (<1.25 Ωm), except for the interval between 240 and 260 mbsf where they reach a maximum for the unit (>4 Ωm). In addition, magnetic susceptibility

values are low (<240 × 10⁻⁶ SI) and exhibit little variability (Fig. 57). Total gamma-ray counts (HSGR) are variable but typically low (<36 GAPI) throughout the unit. Finally, the uranium concentration is generally higher relative to thorium and potassium and is greater than the concentration recorded in Hole 1051A (Fig. 58).

Logging Unit 1 corresponds to lithologic Unit III (204.0–301.6 mbsf). The low gamma-ray counts and relatively low density and PEF values are consistent with the relatively high carbonate content (i.e., low clay content) of the predominantly nannofossil claystones, calcareous claystones, nannofossil and calcareous chinks with clay, and foraminifer chalk of lithologic Unit III. The upper boundary of

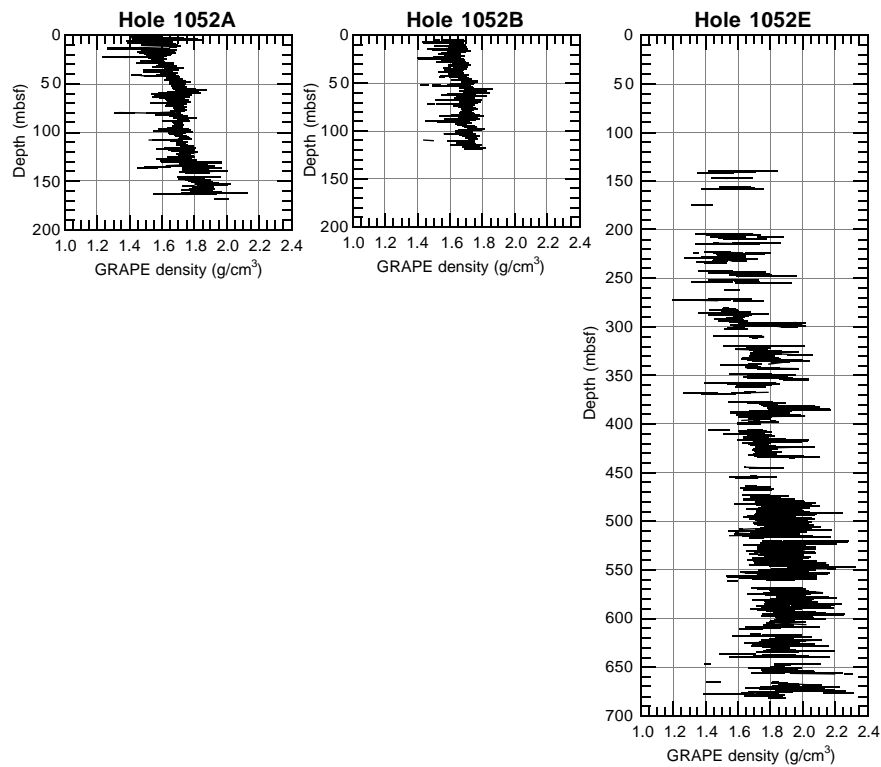


Figure 41. GRAPE bulk density for Holes 1052A, 1052B, and 1052E (see Tables 27, 28, and 31 [CD-ROM, back pocket, this volume] for data). Data for Holes 1052C, 1052D, and 1052F are not plotted but are included in Tables 29, 30, and 32, respectively, on CD-ROM, back pocket, this volume.

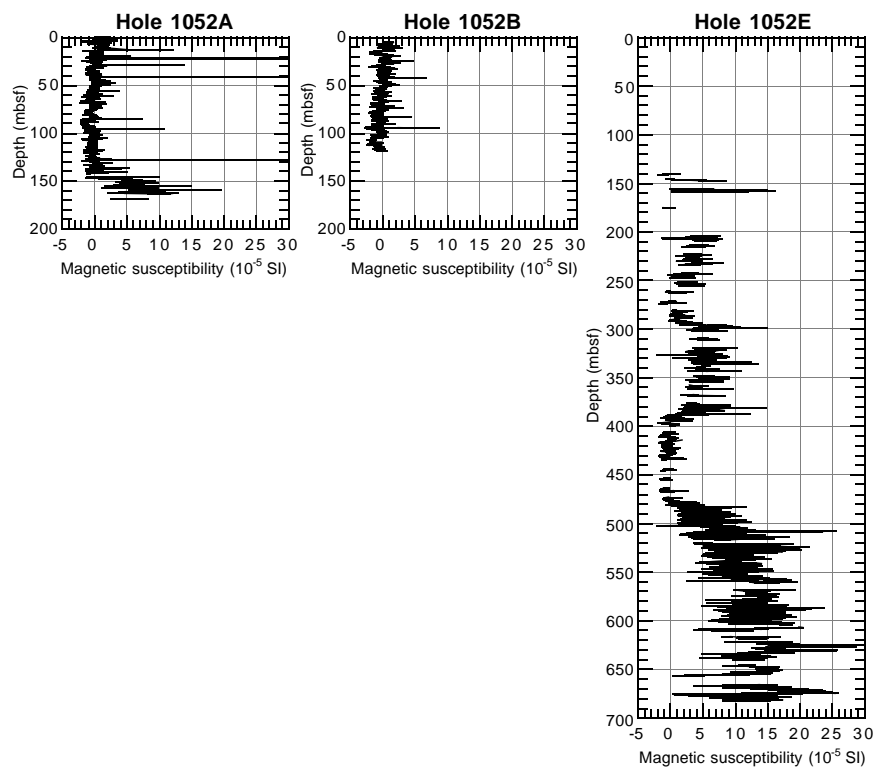


Figure 42. Magnetic susceptibility for Holes 1052A, 1052B, and 1052E (see Tables 33, 34, and 37 [CD-ROM, back pocket, this volume] for data). Data for Holes 1052C, 1052D, and 1052F are not plotted but are included in Tables 35, 36, and 38, respectively, on CD-ROM, back pocket, this volume.

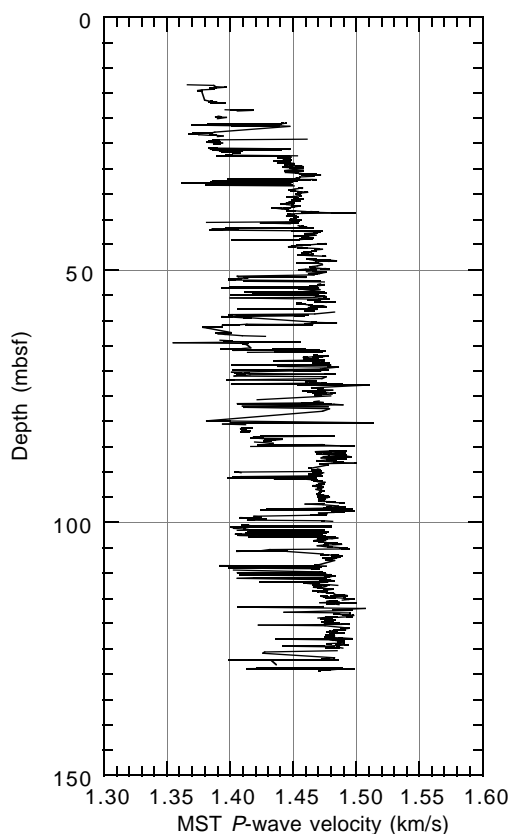


Figure 43. MST *P*-wave velocity for Hole 1052A (see Table 39 [CD-ROM, back pocket, this volume] for data). *P*-wave velocity was measured on APC cores only.

logging Unit 2 marks the position of the K/T boundary, and it can be clearly seen on the FMS images as a shift toward more conductive lithology.

Logging Unit 2 (295–350 mbsf)

Logging Unit 2 is distinguished by an abrupt and sustained increase in average magnetic susceptibility values from $\sim 230 \times 10^{-6}$ to 260×10^{-6} SI (Fig. 57). Unit 2 is also characterized by gradually increasing bulk density and PEF values and slightly decreasing mean porosity toward the boundary of logging Units 2 and 3 (Fig. 56). The natural gamma-ray counts are consistently higher than those measured in Unit 1 and show greater amplitude variations (Fig. 58). Resistivity is uniformly low and ranges from about 1.75 Ωm at the top of the unit to 1.1 Ωm at the base.

Logging Unit 2 corresponds to lithologic Subunit IVA (301.6–388.6 mbsf), which consists of nanofossil chalk with clay to clayey nanofossil chalk with subtle meter-scale alternations between lighter (relatively carbonate-poor) and darker (relatively carbonate-rich) intervals (see “Lithostratigraphy” section, this chapter). FMS micro-resistivity images clearly show this cyclicity.

Logging Unit 3 (350–390 mbsf)

Logging Unit 3 is defined by an abrupt increase in resistivity (1.1–1.7 Ωm) and a step decrease in magnetic susceptibility (282×10^{-6} to 212×10^{-6} SI; Fig. 57). Unit 3 is further characterized by moderately high bulk density ($>2.06 \text{ g/cm}^3$) and PEF ($>5.5 \text{ barns/e}^-$) values, low and decreasing porosity ($<0.5 \text{ p.u.}$), and increasing resistivity toward the base of the unit (Fig. 58).

Logging Unit 3 corresponds to the upper portion (34 m) of lithologic Subunit IVB (388.6–477.4 mbsf), which is composed mostly of

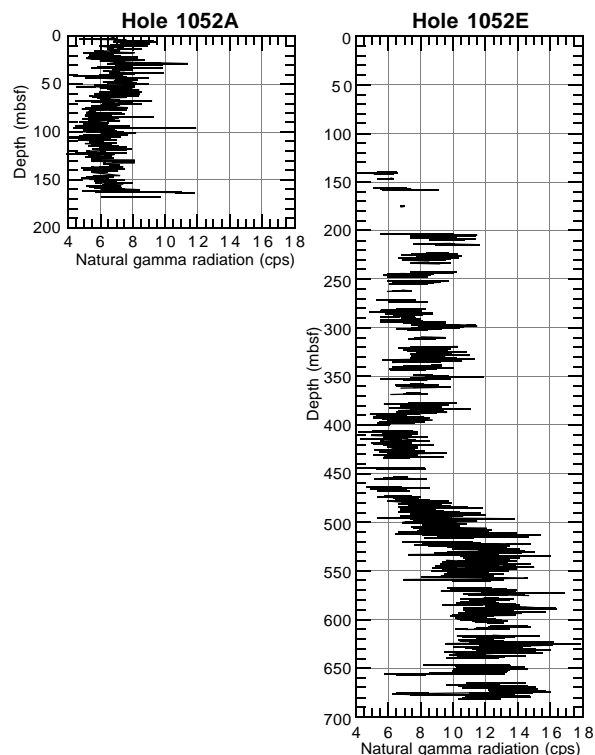


Figure 44. Natural gamma radiation for Holes 1052A and 1052E (see Tables 40, 41 [CD-ROM, back pocket, this volume] for data).

nanofossil chalk and nanofossil chalk with clay (see “Lithostratigraphy” section, this chapter). The lower boundary of logging Unit 3 corresponds to a lithologic hardground.

Logging Unit 4 (390–470 mbsf)

Unit 4 is characterized by uniformly low magnetic susceptibility ($<215 \times 10^{-6}$ SI) and resistivity ($<1.9 \Omega\text{m}$), high Earth’s conductivity (MAGC $>400 \text{ ppm}$), and variable, slightly elevated porosity ($>0.42 \text{ p.u.}$) values. Unit 4 is also distinguished by an abrupt decrease in average bulk density values (from about 1.94 to 2.08 g/cm^3). Gamma-ray counts are low ($<16 \text{ GAPI}$) throughout Unit 4, primarily as a result of decreases in potassium and thorium concentrations (Fig. 58). Uranium values are variable and show a slight decrease in mean concentration.

Logging Unit 4 corresponds to lithologic Subunit IVB (388.6–477.4 mbsf), which contains mostly clayey nanofossil chalk and nanofossil chalk with clay. This subunit is further distinguished by subtle meter-scale alternations between carbonate-rich and carbonate-poor intervals (see “Lithostratigraphy” section, this chapter). Uniformly low gamma-ray counts are consistent with the high carbonate content (i.e., low clay content) of lithologic Subunit IVB.

Logging Unit 5 (470–512 mbsf)

Logging Unit 5 is characterized by an abrupt increase in bulk density, PEF, and resistivity (SFLU), and a decrease in porosity and Earth’s conductivity values (Figs. 56, 58). Bulk density typically ranges between 2.2 and 2.6 g/cm^3 . This unit is also distinguished by variable but gradually increasing natural gamma-ray counts and magnetic susceptibility values (Figs. 57, 58).

Logging Unit 5 corresponds to lithologic Subunit VA (477.4–511.8 mbsf). The generally high gamma-ray counts, high bulk density and resistivity, and low porosity are consistent with the silty claystone, calcareous claystone, and laminated dark claystones (see

Table 42. Discrete index properties measurements for Holes 1052A and 1052E.

Core, section, interval (cm)	Depth (mbsf)	Water content (total mass wt%)	Water content (solid mass wt%)	Bulk density (g/cm ³)	Grain density (g/cm ³)	Dry density (g/cm ³)	Porosity (%)	Void ratio
171B-1052A-								
2X-2, 75-77	5.75	60.8	37.8	1.66	2.65	1.03	61.2	1.57
2X-3, 75-77	7.25	63.5	38.8	1.64	2.66	1.00	62.2	1.65
2X-5, 75-77	10.25	59.2	37.2	1.68	2.69	1.05	60.8	1.55
3H-1, 122-124	14.42	67.1	40.2	1.63	2.68	0.97	63.7	1.76
3H-3, 124-126	16.95	69.9	41.2	1.61	2.68	0.95	64.6	1.83
3H-5, 89-91	20.09	70.2	41.3	1.60	2.66	0.94	64.6	1.83
4H-1, 94-96	23.64	71.5	41.7	1.60	2.66	0.93	65.0	1.86
4H-3, 74-76	26.44	73.3	42.3	1.58	2.63	0.91	65.3	1.88
4H-5, 75-77	29.45	59.9	37.4	1.66	2.66	1.04	60.8	1.55
5H-1, 75-77	32.95	73.2	42.3	1.59	2.65	0.92	65.4	1.89
5H-3, 51-53	35.71	56.8	36.2	1.69	2.67	1.08	59.7	1.48
5H-6, 65-67	40.35	59.5	37.3	1.66	2.63	1.04	60.4	1.53
6H-1, 75-77	42.45	60.3	37.6	1.66	2.65	1.04	61.0	1.56
6H-3, 54-56	45.24	60.3	37.6	1.66	2.66	1.04	61.0	1.57
6H-5, 75-77	48.45	52.7	34.5	1.72	2.65	1.12	57.8	1.37
7H-1, 75-77	51.95	55.2	35.6	1.69	2.62	1.09	58.6	1.41
7H-3, 75-77	54.95	55.2	35.6	1.69	2.65	1.09	58.8	1.43
7H-5, 75-77	57.95	52.8	34.6	1.72	2.67	1.12	57.9	1.38
8H-1, 74-76	61.44	56.8	36.2	1.69	2.69	1.08	59.8	1.49
8H-2, 48-50	62.68	58.1	36.8	1.68	2.68	1.06	60.4	1.52
8H-3, 65-67	64.35	55.3	35.6	1.69	2.64	1.09	58.8	1.43
8H-5, 60-62	67.30	53.8	35.0	1.70	2.64	1.11	58.1	1.39
9H-1, 75-77	70.95	51.8	34.1	1.72	2.64	1.13	57.2	1.33
9H-3, 75-77	73.95	51.5	34.0	1.72	2.64	1.13	57.0	1.33
9H-5, 75-77	76.95	51.2	33.9	1.72	2.64	1.14	56.9	1.32
10H-1, 75-77	80.45	56.6	36.2	1.68	2.65	1.07	59.4	1.46
10H-3, 75-77	83.45	50.7	33.6	1.72	2.64	1.14	56.6	1.31
10H-5, 75-77	86.45	52.0	34.2	1.71	2.63	1.13	57.2	1.34
11H-1, 75-77	89.95	52.0	34.2	1.72	2.64	1.13	57.3	1.34
11H-3, 75-77	92.95	51.2	33.8	1.72	2.64	1.14	56.9	1.32
11H-6, 75-77	97.45	50.9	33.7	1.71	2.61	1.14	56.4	1.29
12H-1, 75-77	99.45	51.4	34.0	1.71	2.62	1.13	56.8	1.32
12H-3, 75-77	102.45	55.0	35.5	1.69	2.62	1.09	58.5	1.41
12H-5, 75-77	105.45	50.1	33.4	1.72	2.61	1.15	56.1	1.28
13H-1, 75-77	108.95	54.0	35.0	1.69	2.60	1.10	57.8	1.37
13H-3, 75-77	111.95	55.8	35.8	1.68	2.63	1.08	58.9	1.43
13H-5, 75-77	114.95	47.7	32.3	1.74	2.63	1.18	55.0	1.22
14H-1, 75-77	118.45	43.8	30.4	1.78	2.62	1.24	52.9	1.12
14H-3, 75-77	121.45	47.7	32.3	1.74	2.60	1.18	54.7	1.21
14H-5, 75-77	124.45	48.4	32.6	1.74	2.62	1.17	55.3	1.24
15H-1, 75-77	127.95	49.8	33.2	1.73	2.63	1.15	56.1	1.28
16X-1, 76-78	130.46	49.6	33.2	1.73	2.64	1.16	56.1	1.28
16X-3, 37-39	133.07	45.8	31.4	1.78	2.68	1.22	54.5	1.20
17X-1, 66-68	136.66	42.8	30.0	1.81	2.68	1.26	52.9	1.12
17X-2, 115-117	138.65	46.5	31.7	1.77	2.69	1.21	55.0	1.22
17X-4, 93-95	141.43	44.2	30.6	1.80	2.69	1.25	53.7	1.16
18X-1, 69-71	146.39	48.2	32.5	1.76	2.69	1.19	55.8	1.27
18X-4, 61-63	150.81	46.7	31.8	1.78	2.71	1.21	55.3	1.24
19X-1, 80-82	156.10	42.1	29.6	1.81	2.66	1.27	52.2	1.09
19X-3, 82-84	159.12	42.7	29.9	1.80	2.67	1.26	52.6	1.11
19X-7, 2-4	164.01	22.2	18.2	2.02	2.58	1.65	35.9	0.56
171B-1052E-								
3R-1, 75-77	156.75	40.8	29.0	1.82	2.66	1.29	51.5	1.06
4R-1, 6-7	165.66	10.0	9.1	2.14	2.40	1.94	19.0	0.24
4R-1, 7-8	165.67	9.8	8.9	2.12	2.37	1.93	18.4	0.23
5R-1, 24-26	175.44	31.7	24.1	1.94	2.71	1.47	45.6	0.84
8R-1, 9-11	204.09	11.2	10.1	2.76	3.41	2.49	27.2	0.37
8R-1, 101-103	205.01	41.8	29.5	1.79	2.60	1.26	51.5	1.06
8R-4, 60-62	209.10	43.1	30.1	1.78	2.60	1.24	52.2	1.09
9R-1, 36-38	213.96	12.5	11.1	2.31	2.74	2.05	25.1	0.34
9R-2, 27-29	215.38	45.1	31.1	1.75	2.59	1.21	53.3	1.14
10R-1, 35-37	223.55	36.1	26.5	1.79	2.45	1.31	46.3	0.86
10R-1, 119-121	224.39	39.0	28.1	1.83	2.63	1.31	50.1	1.00
10R-5, 92-94	230.12	41.8	29.5	1.79	2.59	1.26	51.4	1.06
11R-1, 54-56	233.34	37.8	27.4	1.84	2.64	1.34	49.3	0.97
12R-1, 55-57	242.95	41.8	29.5	1.78	2.58	1.26	51.2	1.05
12R-2, 75-77	244.65	33.9	25.3	1.88	2.63	1.41	46.5	0.87
12R-3, 65-67	245.84	37.3	27.1	1.86	2.68	1.36	49.4	0.98
12R-4, 134-136	248.03	34.5	25.6	1.91	2.71	1.42	47.7	0.91
13R-1, 74-76	252.74	33.8	25.2	1.91	2.71	1.43	47.1	0.89
13R-3, 45-47	255.45	29.5	22.8	1.96	2.69	1.52	43.7	0.78
14R-1, 73-75	262.43	34.1	25.4	1.90	2.68	1.42	47.1	0.89
15R-1, 75-77	272.05	39.8	28.5	1.01	2.01	0.72	28.2	0.39
15R-2, 43-45	273.13	32.9	24.8	1.87	2.58	1.41	45.3	0.83
16R-1, 94-96	281.84	36.9	27.0	1.84	2.61	1.34	48.5	0.94
16R-3, 74.5-76.5	284.65	34.6	25.7	1.88	2.65	1.40	47.3	0.90
16R-5, 72-74	287.58	34.3	25.5	1.85	2.56	1.38	46.1	0.86
17R-1, 75-77	291.25	34.7	25.8	1.88	2.65	1.40	47.4	0.90
17R-3, 75-77	294.12	35.9	26.4	1.84	2.58	1.35	47.5	0.91
17R-4, 69.5-71.5	295.57	35.3	26.1	1.88	2.66	1.39	47.8	0.92
17R-5, 114-116	297.51	39.0	28.1	1.84	2.68	1.33	50.5	1.02
20R-1, 59-61	319.89	32.9	24.8	1.93	2.72	1.45	46.7	0.88
20R-3, 70-72	323.00	28.2	22.0	1.99	2.72	1.56	42.9	0.75
20R-5, 77-79	326.07	31.3	23.8	1.94	2.69	1.48	45.1	0.82
21R-1, 75-77	329.65	29.0	22.5	1.97	2.70	1.53	43.4	0.77
21R-3, 125-127	333.15	34.0	25.4	1.91	2.72	1.43	47.5	0.90

Table 42 (continued).

Core, section, interval (cm)	Depth (mbsf)	Water content (total mass wt%)	Water content (solid mass wt%)	Bulk density (g/cm ³)	Grain density (g/cm ³)	Dry density (g/cm ³)	Porosity (%)	Void ratio
21R-5, 75-77	335.65	34.2	25.5	1.91	2.72	1.42	47.5	0.91
22R-1, 120-122	339.80	32.5	24.5	1.93	2.70	1.46	46.1	0.86
22R-4, 62-64	343.72	27.0	21.2	2.00	2.70	1.58	41.5	0.71
23R-1, 107-109	349.37	24.2	19.5	2.06	2.72	1.66	39.1	0.64
23R-3, 59-61	351.89	27.6	21.6	2.00	2.71	1.57	42.2	0.73
23R-4, 67-69	353.47	29.8	22.9	1.96	2.70	1.51	44.0	0.78
24R-1, 106-108	358.96	25.0	20.0	2.04	2.70	1.63	39.8	0.66
24R-3, 108-110	361.98	25.3	20.2	2.04	2.72	1.63	40.1	0.67
25R-1, 75-77	368.25	27.3	21.4	2.01	2.72	1.58	42.0	0.73
26R-2, 126-128	379.86	23.4	18.9	2.08	2.73	1.68	38.4	0.62
26R-4, 94-96	382.54	23.4	19.0	2.06	2.70	1.67	38.2	0.62
26R-6, 60-62	385.20	23.5	19.0	2.06	2.70	1.67	38.2	0.62
27R-1, 91-93	387.61	26.6	21.0	2.00	2.69	1.58	41.2	0.70
27R-3, 84-86	390.54	29.0	22.5	1.97	2.70	1.53	43.3	0.76
27R-5, 91-93	393.61	27.8	21.7	2.02	2.76	1.58	42.8	0.75
28R-1, 70-72	397.00	25.4	20.3	2.05	2.75	1.63	40.6	0.68
28R-3, 75-77	400.05	30.9	23.6	1.94	2.67	1.48	44.6	0.81
29R-1, 68-70	406.58	29.0	22.5	1.98	2.71	1.53	43.4	0.77
29R-3, 70-72	409.60	31.0	23.7	1.95	2.71	1.49	45.1	0.82
29R-5, 64-66	412.54	25.3	20.2	2.03	2.71	1.62	40.1	0.67
30R-1, 70-72	416.20	27.5	21.5	2.02	2.76	1.59	42.5	0.74
30R-3, 66-68	419.16	26.7	21.1	2.00	2.67	1.58	41.1	0.70
30R-5, 72.5-74.5	422.23	27.5	21.6	1.98	2.67	1.56	41.7	0.72
31R-1, 75-77	425.85	24.3	19.5	2.04	2.70	1.65	39.0	0.64
31R-3, 82-84	428.92	20.9	17.3	2.11	2.71	1.75	35.5	0.55
31R-5, 83-85	431.93	24.9	20.0	2.03	2.68	1.62	39.5	0.65
33R-1, 143.5-145.5	445.74	28.8	22.3	1.97	2.69	1.53	43.0	0.76
34R-1, 144-146	455.34	28.6	22.3	1.98	2.70	1.54	43.0	0.76
35R-1, 77-79	464.37	31.7	24.1	1.94	2.72	1.48	45.7	0.84
35R-3, 95-97	467.55	25.6	20.4	2.02	2.69	1.61	40.2	0.67
36R-3, 84-86	477.04	23.7	19.2	2.05	2.69	1.66	38.4	0.62
36R-4, 97-99	478.67	20.7	17.1	2.11	2.70	1.75	35.3	0.55
37R-3, 117-119	486.48	19.9	16.6	2.13	2.72	1.78	34.5	0.53
38R-3, 54-56	495.94	9.7	8.8	2.36	2.71	2.15	20.4	0.26
38R-4, 134-136	498.24	22.3	18.3	2.08	2.70	1.70	37.1	0.59
39R-4, 11-13	506.61	21.8	17.9	2.11	2.74	1.73	36.8	0.58
39R-5, 142-144	508.92	4.5	4.3	2.55	2.73	2.44	10.7	0.12
40R-3, 9.5-11.5	513.70	24.7	19.8	2.03	2.69	1.63	39.4	0.65
40R-6, 3-5	516.84	4.5	4.3	2.54	2.72	2.44	10.6	0.12
41R-1, 131-133	521.61	3.7	3.6	2.58	2.73	2.48	9.0	0.10
41R-2, 77-79	522.57	24.2	19.5	2.05	2.70	1.65	39.0	0.64
42R-2, 76-78	532.16	24.8	19.8	2.04	2.70	1.63	39.5	0.65
42R-5, 78-80	536.68	23.4	19.0	2.07	2.73	1.68	38.4	0.62
43R-3, 36-38	542.80	19.6	16.4	2.15	2.73	1.80	34.3	0.52
43R-5, 116-118	546.60	24.7	19.8	2.05	2.72	1.64	39.6	0.66
44R-1, 76-78	549.86	16.5	14.2	2.22	2.75	1.90	30.7	0.44
44R-6, 115-117	557.75	23.7	19.1	2.07	2.72	1.67	38.6	0.63
45R-1, 90-92	559.60	21.1	17.4	2.11	2.71	1.74	35.8	0.56
46R-1, 78-80	569.08	23.4	19.0	2.06	2.69	1.67	38.2	0.62
46R-4, 51-53	572.77	21.6	17.8	2.09	2.71	1.72	36.3	0.57
47R-1, 51-53	578.51	18.5	15.6	2.16	2.72	1.83	33.0	0.49
47R-4, 50-52	583.00	20.1	16.7	2.13	2.71	1.77	34.7	0.53
48R-1, 67-69	588.27	18.8	15.9	2.16	2.73	1.82	33.4	0.50
48R-5, 103-105	594.63	22.5	18.3	2.09	2.73	1.71	37.5	0.60
49R-1, 59-61	597.89	21.7	17.8	2.11	2.73	1.73	36.6	0.58
49R-4, 51.5-53.5	602.32	17.7	15.1	2.18	2.72	1.85	32.0	0.47
50R-3, 7-9	609.97	23.5	19.0	2.06	2.71	1.67	38.3	0.62
51R-1, 137-139	617.97	23.4	18.9	2.06	2.70	1.67	38.1	0.62
52R-1, 20-22	621.90	13.7	12.0	2.27	2.72	2.00	26.6	0.36
52R-3, 114-116	625.84	19.5	16.3	2.14	2.72	1.79	34.1	0.52
53R-5, 137-139	634.57	16.5	14.2	2.20	2.72	1.89	30.5	0.44
53R-6, 34-36	635.04	10.6	9.6	2.35	2.72	2.13	21.9	0.28
54R-2, 138-140	639.68	19.4	16.3	2.13	2.70	1.79	33.9	0.51
55R-1, 54-56	646.94	6.4	6.0	2.47	2.72	2.32	14.5	0.17
55R-6, 4-6	653.94	12.2	10.9	2.31	2.73	2.06	24.6	0.33
56R-1, 26-28	656.26	1.8	1.8	2.66	2.74	2.61	4.7	0.05
57R-3, 139-141	669.50	19.0	16.0	2.15	2.71	1.80	33.5	0.50
57R-6, 132-134	673.93	20.0	16.7	2.12	2.69	1.77	34.5	0.53
58R-1, 123-125	676.43	4.9	4.7	2.54	2.73	2.42	11.5	0.13
58R-3, 54-56	678.72	19.3	16.2	2.15	2.73	1.80	34.0	0.52
58R-5, 100-102	682.18	20.3	16.8	2.12	2.70	1.76	34.8	0.54

“Lithostratigraphy” section, this chapter) of lithologic Subunit VA. The FMS data show an interval of strongly contrasting high- and low-resistivity beds, consistent with the occurrence of calcareous intervals alternating with more terrigenous-rich zones.

Logging Unit 6 (512–684 mbsf)

Logging Unit 6 is characterized by a distinct increase in the amplitude and frequency of variation in bulk density, porosity, resistivity, natural gamma-ray counts, and magnetic susceptibility values. Total gamma-ray counts are elevated (>30 GAPI), and the shape of the gamma-ray curve is dominated by significant variations in uranium,

which generally vary inversely with thorium and potassium (Fig. 58). Thorium vs. potassium concentrations in the interval 480–512 mbsf fall largely within the montmorillonite (smectite) clay field (Fig. 59).

The boundary between logging Units 5 and 6 is gradational and occurs over slightly different depths, depending on which logging data are used. For example, an abrupt increase in magnetic susceptibility and the Earth’s conductivity is observed at 514 mbsf, whereas an interval of reduced natural gamma-ray counts occurs between 505 and 510 mbsf (Figs. 57, 58).

Logging Unit 6 corresponds to lithologic Subunit VB (511.8–633.50 mbsf), which is distinguished by the occurrence of laminated

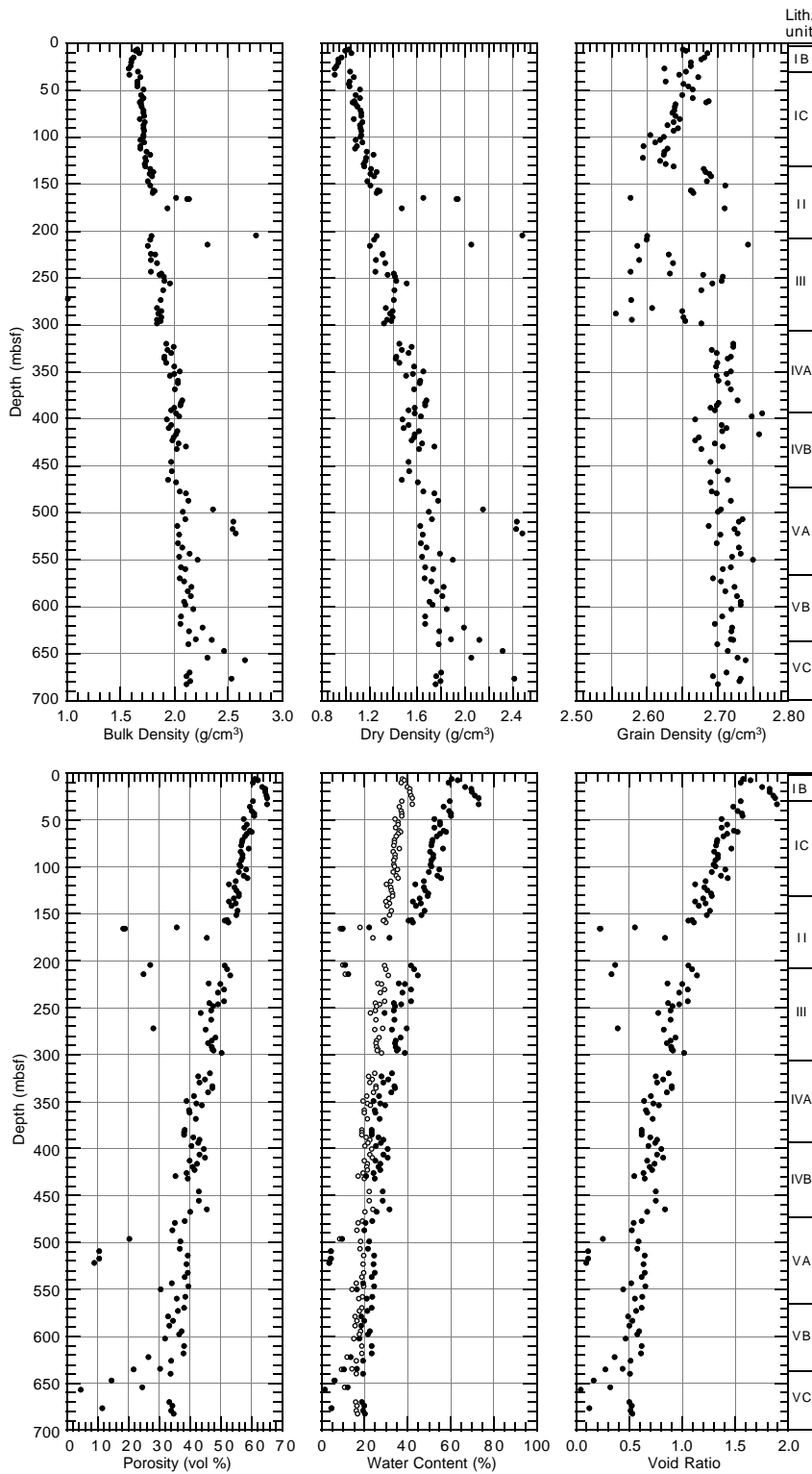


Figure 45. Discrete measurements of bulk, dry, and grain densities, porosity, water content, and void ratio for Holes 1052A and 1052E. Lithologic units (see “Lithostratigraphy” section, this chapter) are included for comparative purposes. In the water content plot, open circles = values expressed in terms of total mass; solid circles = values expressed in terms of the total mass of solids.

dark claystone with varying amounts of calcareous nannoplankton and foraminifers, terrigenous clastic material (mainly quartz and feldspar), as well as laminated claystone (black shale; see “Lithostratigraphy” section, this chapter).

Downhole Temperatures

The TLT was run with the triple-combo tool string (see “Explanatory Notes” chapter, this volume). TLT measurements were linked

to the actual logging depths using a time-depth log that is recorded in the logging unit. These data are available on CD-ROM (back pocket, this volume).

Comparison of Core-Log Physical Properties Data

In general, there is good agreement between the logging data and core measurements (see “Physical Properties” section, this chapter) collected in Hole 1052E. Figure 60 shows the comparison between

log magnetic susceptibility and MST core measurements. The core (GRAPE) and logging (RHOB) measurements of sediment bulk density and porosity also show good agreement despite the lower resolution of the discrete core data (see Figs. 61, 62).

REFERENCES

- Baker, P.A., and Kastner, M., 1981. Constraints on the formation of sedimentary dolomite. *Science*, 213:215–216.
- Berggren, W.A., Kent, D.V., Swisher, C.C., III, and Aubry, M.-P., 1995. A revised Cenozoic geochronology and chronostratigraphy. In Berggren, W.A., Kent, D.V., Aubry, M.-P., and Hardenbol, J. (Eds.), *Geochronology, Time Scales and Global Stratigraphic Correlation*. Spec. Publ.—Soc. Econ. Paleontol. Mineral., 54:129–212.
- Blome, C.D., 1992. Radiolarians from Leg 122, Exmouth and Wombat Plateaus, Indian Ocean. In von Rad, U., Haq, B.U., et al., *Proc. ODP, Sci. Results*, 122: College Station, TX (Ocean Drilling Program), 633–652.
- Br  h  ret, J.G., 1994. The mid-Cretaceous organic-rich sediments from the Vocontian Zone of the French Southeast Basin. In Mascle, A. (Ed.), *Hydrocarbon and Petroleum Geology of France*: New York (Springer Verlag), 295–320.
- Christopher, R.A., Owens, J.P., and Sohl, N.F., 1979. Cretaceous palynomorphs from the Cape Fear Formation of North Carolina. *Southeastern Geol.*, 20:145–149.
- Erbacher, J., and Thurow, J., 1997. Influence of oceanic anoxic events on the evolution of mid-Cretaceous radiolaria in the North Atlantic and western Tethys. *Mar. Micropaleontol.*, 37.
- Glaser, J.D., 1969. Petrology and origin of Potomac and Magothy (Cretaceous) sediments, middle Atlantic Coastal Plain. *Maryland Geol. Surv. Rept. Invest.*, 11.
- Gradstein, F.M., Agterberg, F.P., Ogg, J.G., Hardenbol, J., van Veen, P., Thierry, J., and Huang, Z., 1995. A Triassic, Jurassic and Cretaceous time scale. In Berggren, W.A., Kent, D.V., Aubry, M.-P., and Hardenbol, J. (Eds.), *Geochronology, Time Scales and Global Stratigraphic Correlation*, Spec. Publ.—Soc. Econ. Paleontol. Mineral., 54: 95–126.
- Hallam, A., 1984. Continental humid and arid zones during the Jurassic and Cretaceous. *Palaeogeogr., Palaeoclimatol., Palaeoecol.*, 47:195–223.
- Haq, B.U., Hardenbol, J., and Vail, P.R., 1987. Chronology of fluctuating sea levels since the Triassic. *Science*, 235:1156–1167.
- Herbin, J.P., Deroo, G., Roucach  , J., 1983. Organic geochemistry in the Mesozoic and Cenozoic formations of Site 534, Leg 76, Blake Bahama Basin, and comparison with Site 391, Leg 44. In Sheridan, R.E., and Gradstein, F.M., et al., *Init. Repts. DSDP*, 76: Washington (U.S. Govt. Printing Office), 481–493.
- Holmes, M.A., Breza, J.R., and Wise, S.W., Jr., 1987. Provenance and deposition of Lower Cretaceous turbidite sands at Deep Sea Drilling Project Site 603, lower continental rise off North Carolina. In Van Hinte, J.E., Wise, S.W., Jr., et al., *DSDP Init. Repts.*, 93: Washington (U.S. Govt. Printing Office), 941–960.
- Hutchinson, D.R., Poag, C.W., and Popenoe, P., 1995. Geophysical database of the East Coast of the United States: Southern Atlantic margin—stratigraphy and velocity from multichannel seismic profiles. *Open-File Rep.—U.S. Geol. Surv.*, 95–27.
- Irving, E., Wynne, P.J., and Globberman, B.R., 1993. Cretaceous paleolatitudes and overprints of North American Craton. In Caldwell, W.G.E., and Kauffman, E.G. (Eds.), *Evolution of the Western Interior Basin. Geol. Assoc. Can. Spec. Rep.*, 39:91–96.
- Katz, B.K., 1983. Organic geochemical character of some Deep Sea Drilling Project cores from Legs 76 and 44. In Sheridan, R.E., Gradstein, F.M., et al., *Init. Repts. DSDP*, 76: Washington (U.S. Govt. Printing Office), 463–468.
- Kono, M., 1980. Statistics of paleomagnetic inclination data. *J. Geophys. Res.*, 85:3878–3882.
- Ladd, D.D., Foott, R., Ishihara, K., Schlosser, F., and Poulos, H.G., 1977. Stress-deformation and strength characteristics: state-of-the-art report. *Proc. 9th Int. Conf. Soil Mechanics Foundation Engineering*, Tokyo, 2:421–482.
- Macleod, K.G., 1994. Bioturbation, inoceramid extinction, and mid-Maastriichtian ecological change. *Geology*, 22:139–142.
- McEnroe, S.A., 1996. North America during the Lower Cretaceous: new palaeomagnetic constraints from intrusions in New England. *Geophys. J. Int.*, 126: 494.
- Moran, K., 1997. Elastic property corrections applied to Leg 154 sediment, Ceara Rise. In Shackleton, N.J., Curry, W.B., Richter, C., and Bralower, T.J. (Eds.), *Proc. ODP, Sci. Results*, 154: College Station, TX (Ocean Drilling Program), 151–155.
- Nishimura, A., 1992. Paleocene radiolarian biostratigraphy in the northwest Atlantic at Site 384, Leg 43, of the Deep Sea Drilling Project. *Micropaleontology*, 38:317–362.
- Quirein, J.A., Garden, J.S., and Watson, J.T., 1982. Combined natural gamma-ray spectral/litho-density measurements applied to complex lithology. *SPE of AIME, 57th Annual Fall Technical Conf. and Exhibit.*, New Orleans, paper SPE 11143:1–14.
- Riedel, W.R., and Sanfilippo, A., 1978. Stratigraphy and evolution of tropical Cenozoic radiolarians. *Micropaleontology*, 24:61–96.
- Ryan, W.B.F., Bolli, H.M., Foss, G.N., Natland, J.H., Hottman, W.E., and Foresman, J.B., 1978. Objectives, principle results, operations, and explanatory notes of Leg 40, South Atlantic. In Bolli, H.M., Ryan, W.B.F., et al., *Init. Repts. DSDP*, 40: Washington (U.S. Govt. Printing Office), 5–26.
- Sarti, M., and von Rad, U., 1987. Early Cretaceous turbidite sedimentation at Deep Sea Drilling Project Site 603, off Cape Hatteras (Leg 93). In Van Hinte, J.E., Wise, S.W., Jr., et al., *DSDP Init. Repts.*, 93: Washington (U.S. Govt. Printing Office), 891–940.
- Sohl, N.F., and Owens, J.P., 1991. Cretaceous stratigraphy of the Carolina Coastal Plain. In Horton, J.W., Jr., and Zullo, V.A. (Eds.), *The Geology of the Carolinas*. Carolina Geol. Soc. 50th Ann. Vol., Knoxville (Univ. Tenn. Press), 191–220.
- Summerhayes, C.P., and Masran, T.C., 1983. Organic facies of Cretaceous and Jurassic sediments from Deep Sea Drilling Project Site 534 in the Blake Bahama Basin, Western North Atlantic. In Sheridan, R.E., and Gradstein, F.M., et al., *Init. Repts. DSDP*, 76: Washington (U.S. Govt. Printing Office), 469–480.
- Widmark, J.G.V., and Speijer, R.P., in press. Benthic foraminiferal ecomarker species of the terminal Cretaceous deep-sea Tethys. *Mar. Micropaleontol.*

Ms 171BIR-106

NOTE: Core-description forms (“barrel sheets”) and core photographs can be found in Section 4, beginning on page 363. Forms containing smear-slide data, thin-section descriptions, and shore-based log processing data can be found on CD-ROM. See Table of Contents for material contained on CD-ROM.

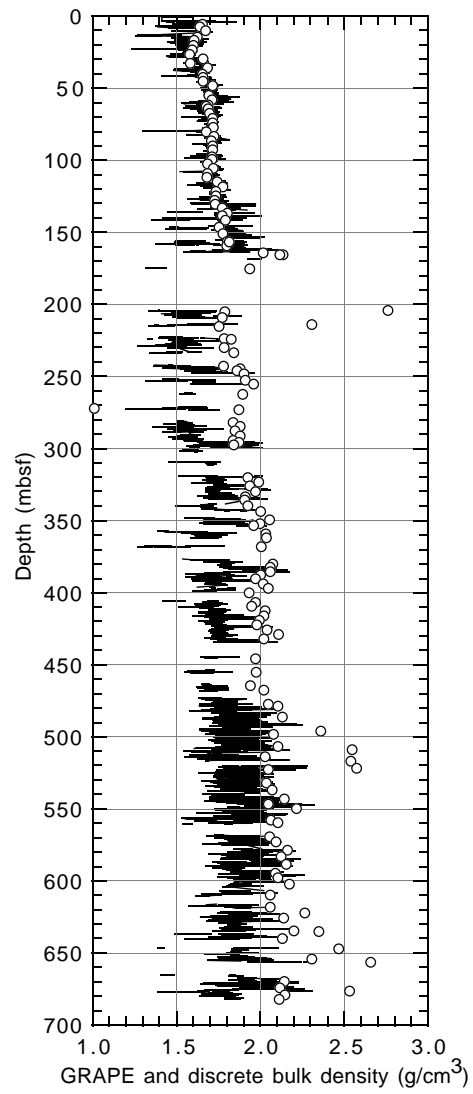


Figure 46. Comparison of composite GRAPE bulk density (line) with discrete measurements of bulk density (open circles) for Holes 1052A and 1052E.

Table 43. Discrete measurements of uncorrected *P*-wave velocity for Holes 1052A and 1052E.

Core, section, interval (cm)	Depth (mbsf)	Transverse <i>P</i> -wave velocity (km/s)	Longitudinal <i>P</i> -wave velocity (km/s)	Acoustic anisotropy (x/z)
171B-1052A-				
2X-2, 74-76	5.75	1.559		
2X-3, 74.2-76.2	7.25	1.559		
2X-5, 74-76	10.25	1.566		
3H-1, 121.3-123.3	14.42	1.552		
3H-3, 74-76	16.95	1.555		
3H-5, 88.2-90.2	20.09	1.555		
4H-1, 94.2-96.2	23.65	1.546		
4H-3, 74-76	26.45	1.547		
4H-5, 74.2-76.2	29.45	1.574		
5H-1, 74-76	32.95	1.554		
5H-3, 50.7-52.7	35.72	1.577		
5H-6, 64.1-66.1	40.35	1.566		
6H-1, 74-76	42.45	1.571		
6H-3, 54.1-56.1	45.25	1.575		
6H-5, 74.1-76.1	48.45	1.598		
7H-1, 74-76	51.95	1.584		
7H-3, 74-76	54.95	1.594		
7H-5, 74-76	57.95	1.596		
8H-1, 74.1-76.1	61.45	1.573		
8H-3, 64-66	64.35	1.579		
8H-5, 59.3-61.3	67.30	1.582		
9H-1, 74.3-76.3	70.95	1.586		
9H-3, 74-76	73.95	1.584		
9H-5, 79.5-81.5	77.01	1.594		
10H-1, 74-76	80.45	1.576		
10H-3, 72.5-74.5	83.44	1.594		
10H-5, 74-76	86.45	1.605		
11H-1, 74-76	89.95	1.587		
11H-3, 74-76	92.95	1.593		
11H-6, 82.3-84.3	97.53	1.607		
12H-1, 74-76	99.45	1.605		
12H-3, 74.2-76.2	102.45	1.592		
12H-5, 74.1-76.1	105.45	1.615		
13H-1, 74-76	108.95	1.603		
13H-3, 74-76	111.95	1.602		
13H-5, 74.1-76.1	114.95	1.643		
14H-1, 74-76	118.45	1.634		
14H-3, 74.3-76.3	121.45	1.632		
14H-5, 74-76	124.45	1.621		
15H-1, 74.1-76.1	127.95	1.628		
16X-1, 78.7-80.7	130.50	1.713		
16X-3, 39-41	133.10	1.701		
17X-1, 66.7-68.7	136.68	1.764		
17X-2, 62.9-64.9	138.14	1.679		
17X-4, 32.1-34.1	140.83	1.754		
18X-1, 67.9-69.9	146.39	1.745		
19X-1, 80.5-82.5	156.12	1.932		
19X-3, 71.7-73.7	159.03	2.084		
19X-6, 59.5-61.5	163.41	1.734		
20X-1, 7.4-9.4	162.98	3.344		
20X-CC, 24-26	163.38	3.790		
171B-1052E-				
4R-1, 6-8	165.68	3.517	3.211	1.095
5R-1, 24-26	175.46		1.937	
5R-1, 32-34	175.54	1.906		
5R-1, 43-45	175.65	4.089	4.017	1.018
6R-CC, 3-5	185.35	3.086		
8R-1, 9-11	204.11	2.990	2.932	1.020
8R-1, 101-103	205.03	1.813	1.756	1.033
8R-4, 60-62	209.12	1.786	1.751	1.020
9R-1, 36-38	213.98	2.910	2.833	1.027
9R-2, 27-29	215.40	1.823	1.779	1.025
10R-1, 35-37	223.57	2.542	2.203	1.154
10R-1, 119-121	224.41	1.918	1.945	0.986
10R-5, 95-97	230.17	1.914	1.869	1.024
11R-1, 54-56	233.36	1.937	1.927	1.005
12R-1, 54-56	242.96	2.244	1.996	1.124
12R-2, 74-76	244.66	2.095		
12R-3, 65-67	245.86	2.027		
12R-4, 134-136	248.86	2.140	2.094	1.022
13R-1, 74-76	252.76	2.078	2.100	0.990
13R-3, 45-47	255.47	2.109	2.177	0.968
14R-1, 73-75	262.44	1.999	2.054	0.973
15R-1, 75-77	272.07	2.252	2.127	1.059
15R-2, 43-45	273.15	2.440	2.493	0.979
16R-1, 94-96	281.86	2.122	2.131	0.996
16R-3, 74.5-76.5	284.67	1.988	2.075	0.958
16R-5, 72-74	287.60	2.422	2.271	1.066
17R-1, 75-77	291.27	2.090	2.128	0.982
17R-3, 75-77	294.14		2.207	
17R-4, 69.5-71.5	295.59	2.165	2.182	0.992
17R-5, 114-116	297.53	1.953	1.903	1.026
20R-1, 59-61	319.91	1.856	1.924	0.965
20R-3, 70-72	323.02	1.967	1.939	1.015
20R-5, 77-79	326.09	1.912	1.963	0.974
21R-1, 75-77	329.67	1.975	1.911	1.034

Table 43 (continued).

Core, section, interval (cm)	Depth (mbsf)	Transverse <i>P</i> -wave velocity (km/s)	Longitudinal <i>P</i> -wave velocity (km/s)	Acoustic anisotropy (x/z)
21R-3, 125-127	333.17	1.929	1.827	1.055
21R-5, 75-77	335.67	1.864	1.856	1.004
22R-1, 120-122	339.82	1.923	1.853	1.038
22R-4, 62-64	343.74	2.082	2.023	1.029
23R-1, 107-109	349.39	2.195	2.150	1.021
23R-3, 59-61	351.91	2.021	1.952	1.036
23R-4, 67-69	353.49	2.157	2.071	1.041
24R-1, 106-108	358.98	2.215	2.092	1.059
24R-3, 108-110	362.00	2.196	2.070	1.061
25R-1, 75-77	368.27	1.864	1.774	1.051
26R-2, 126-128	379.88	2.121	2.021	1.050
26R-4, 94-96	382.56	2.320	2.211	1.049
26R-6, 60-62	385.22	2.083	2.055	1.013
27R-1, 91-93	387.63	2.218	2.164	1.025
27R-3, 84-86	390.56	2.580	2.502	1.031
27R-5, 91-93	393.63	2.228	2.186	1.019
28R-1, 70-72	397.02	2.214	2.184	1.013
28R-3, 75-77	400.07	2.163	2.112	1.024
29R-1, 68-70	406.60	2.202	2.130	1.034
29R-3, 70-72	409.62	1.524	2.058	0.740
29R-5, 64-66	412.56	2.298	2.230	1.030
30R-1, 70-72	416.22	1.749	2.057	0.850
30R-3, 66-68	419.18	2.216	2.117	1.047
30R-5, 72.5-74.5	422.25	2.149	2.135	1.007
31R-1, 75-77	425.87	2.260	2.108	1.072
31R-3, 82-84	428.94	2.338	2.285	1.023
31R-5, 83-85	431.95	2.332	2.240	1.041
33R-1, 143.5-145.5	445.76	2.283	2.202	1.037
34R-1, 144-146	455.36	2.420	2.193	1.103
35R-1, 77-79	464.39	2.260	2.072	1.091
35R-3, 95-97	467.39	2.368	2.254	1.051
36R-3, 84-86	477.06	2.578	2.507	1.028
36R-4, 97-99	478.69	2.269	2.092	1.085
37R-3, 117-119	486.50	2.145	2.025	1.059
38R-3, 54-56	495.96	3.132	2.911	1.076
38R-4, 134-136	498.26	2.064	1.907	1.082
39R-4, 11-13	506.63	2.251	2.122	1.061
39R-5, 142-144	508.94	4.734	4.886	0.969
40R-3, 9.5-11.5	513.72	2.063	1.799	1.147
40R-CC, 3-5	516.86	4.587	4.389	1.045
41R-1, 131-133	521.63	4.680	4.876	0.960
41R-2, 77-79	522.59	2.060	1.830	1.126
42R-2, 76-78	532.18	2.026	1.858	1.090
42R-5, 78-80	536.70	1.932	1.862	1.037
43R-3, 36-38	542.82	2.204	2.039	1.081
44R-1, 76-78	549.88	2.302	2.136	1.078
44R-6, 115-117	557.77	1.984	1.897	1.046
45R-1, 90-92	559.62	2.081	1.996	1.043
46R-1, 78-80	569.10	2.114	1.973	1.072
46R-4, 51-53	572.79	2.130	2.071	1.029
47R-1, 51-53	578.53	2.058	1.997	1.030
47R-4, 50-52	583.02	2.148	2.086	1.030
48R-1, 67-69	588.29	1.976	1.932	1.023
48R-4, 103-105	593.15	2.080	2.008	1.036
49R-1, 59-61	597.91	2.012	1.926	1.045
49R-3, 51.5-53.5	600.84	2.398	2.141	1.120
50R-3, 7-9	609.99	2.003	1.924	1.041
51R-1, 137-139	617.99	1.852		
52R-1, 20-22	621.92	2.602	2.506	1.038
52R-3, 114-116	625.86	2.204	2.057	1.071
53R-5, 137-139	634.59	2.268	2.141	1.059
53R-6, 34-36	635.06	3.685	3.277	1.124
54R-2, 138-140	639.70	2.061	2.029	1.016
55R-1, 54-56	646.96	4.153	3.682	1.128
55R-6, 4-6	653.96	2.720	2.458	1.107
56R-1, 26-28	656.28	5.634	5.413	1.041
57R-3, 139-141	669.52	2.168	2.087	1.039
57R-6, 132-134	673.95	2.131	2.010	1.060
58R-1, 123-125	676.45	5.035	4.829	1.043
58R-3, 54-56	678.74	2.230	2.058	1.084
58R-5, 100-102	682.20	2.160	2.120	1.019

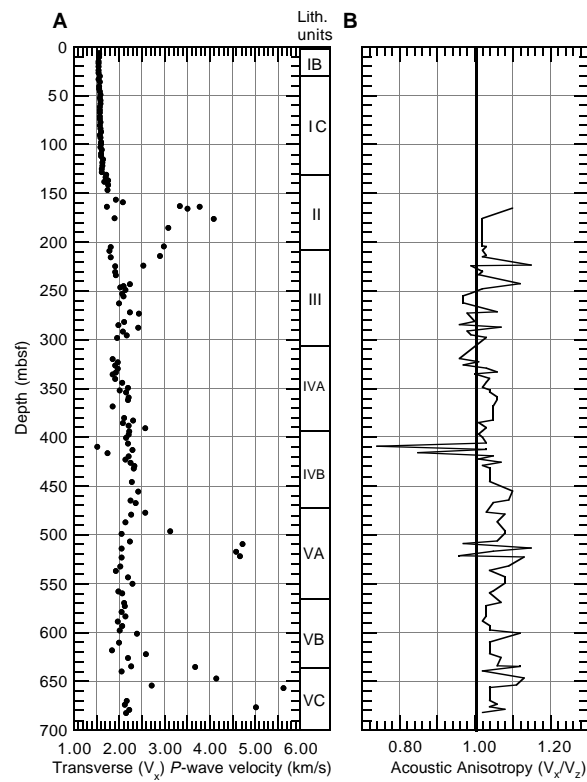


Figure 47. **A.** Discrete transverse *P*-wave velocity measured perpendicular to the split-core surface (x-direction) for Holes 1052A and 1052E. **B.** Acoustic anisotropy (x-direction/z-direction) for Holes 1052A and 1052E. The z-direction is oriented parallel to the core axis. Lithologic units (see “Lithostratigraphy” section, this chapter) are included for comparative purposes.

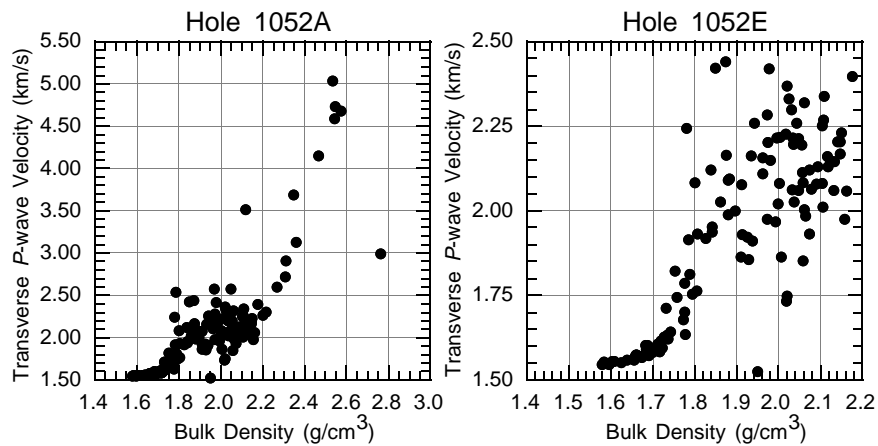


Figure 48. Comparison of discrete transverse *P*-wave velocity (x-direction) and discrete bulk density for Holes 1052A and 1052E. The *P*-wave velocity values are uncorrected for in situ pressure and temperature conditions. The Hole 1052E data are plotted on an expanded scale.

Table 44. Discrete measurements of shear strength for Hole 1052A.

Core, section, interval (cm)	Depth (mbsf)	Peak (kPa)	Residual (kPa)	Penetrometer (kPa)
171B-1052A-				
2X-2, 77-78	5.78	20.92	10.74	
2X-3, 77.6-78.6	7.28	23.03	10.21	
2X-5, 77.1-78.1	10.28	30.50	9.15	
3H-1, 125.3-126.3	14.46	15.61	8.48	
3H-3, 78-79	16.99	17.57	5.86	
3H-5, 92.4-93.4	20.13	32.46	8.33	
4H-1, 98.2-99.2	23.69	36.51	13.15	
4H-3, 77.5-78.5	26.48	54.76	18.71	
4H-5, 78.1-79.1	29.49	85.26	35.08	
5H-1, 77.4-78.4	32.98	42.32	16.17	
5H-3, 54.6-55.6	35.75	55.91	19.62	
5H-6, 67.4-68.4	40.38	63.75	21.28	
6H-1, 78.4-79.4	42.49	88.34	33.46	
6H-3, 57.4-58.4	45.28	31.45	14.36	
6H-5, 77.8-78.8	48.48	67.05	26.50	
7H-1, 78.4-79.4	51.99	29.22	10.62	
7H-3, 77.6-78.6	54.98	51.83	17.63	
7H-5, 77.4-78.4	57.98	21.43	11.64	
8H-1, 79-80	61.50	16.02	7.74	
8H-3, 67.9-68.9	64.38	25.75	13.57	
8H-5, 62.9-63.9	67.33	54.32	26.99	
9H-1, 77.6-78.6	70.98	27.27	10.46	
9H-3, 76.9-77.9	73.97	21.75	11.10	
9H-5, 82.7-83.7	77.03	38.52	19.01	
10H-1, 77.7-78.7	80.48	52.27	20.91	
10H-3, 77.1-78.1	83.48	38.31	17.11	
10H-5, 77.5-78.5	86.48	38.20	16.93	
11H-1, 77.6-78.6	89.98	56.49	19.96	107.9
11H-3, 77.2-78.2	92.98	43.83	17.53	83.4
11H-6, 85.7-86.7	97.56	48.48	20.36	
12H-1, 77.6-78.6	99.48	30.95	9.08	66.2
12H-3, 76.8-77.8	102.47	33.11	15.43	80.9
12H-5, 77.8-78.8	105.48	45.23	18.25	103.0
13H-1, 77.4-78.4	108.98	37.23	14.02	83.4
13H-3, 77.9-78.9	111.98	31.71	12.37	61.3
13H-5, 76.7-77.7	114.97	55.41	24.94	
14H-1, 76.7-77.7	118.47	35.93	16.05	93.2
14H-3, 77-78	121.48	44.58	19.92	88.3
14H-5, 77.1-78.1	124.48	28.57	11.62	
15H-1, 78.3-79.3	127.99	15.58	6.86	

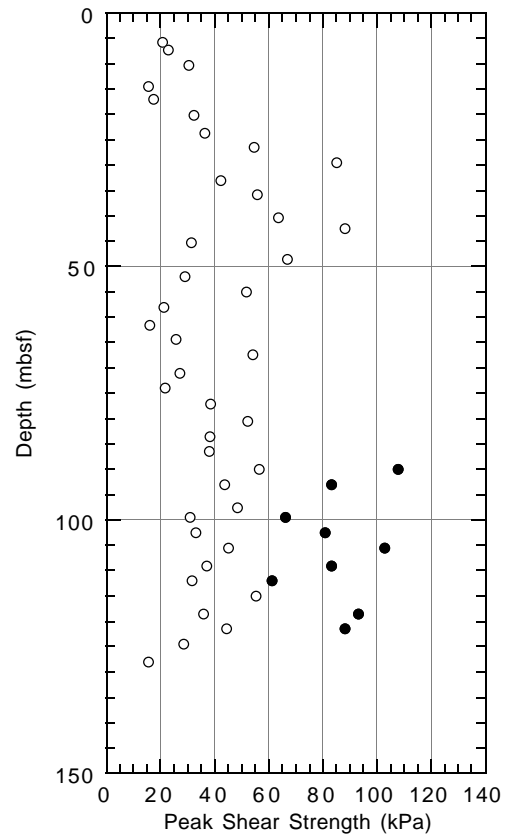


Figure 49. Shear strength for Hole 1052A. Open circles = vane-shear device measurements; solid circles = pocket penetrometer measurements.

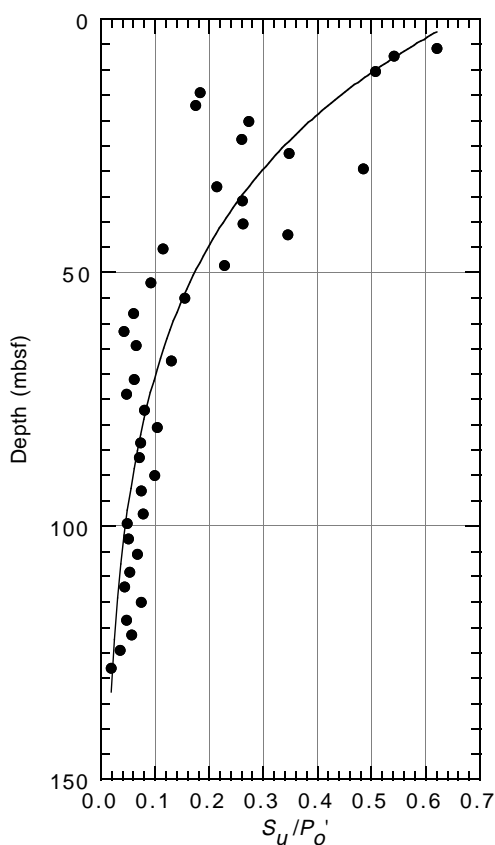


Figure 50. S_u/P_o' for Hole 1052A. The S_u/P_o' are calculated from bulk density and undrained shear strength data (see “Physical Properties” section [this chapter] for further details). The line is a logarithmic fit to the data.

Table 45. Discrete measurements of resistivity for Hole 1052A.

Core, section, interval (cm)	Depth (mbsf)	Longitudinal resistivity (Ω m)	Transverse resistivity (Ω m)
171B-1052A-			
2X-2, 70.5-73.5	5.71	0.547	0.528
2X-3, 70.5-73.5	7.21	0.505	0.499
2X-5, 80.5-83.5	10.31	0.538	0.553
3H-1, 127.5-130.5	14.48	0.476	0.472
3H-3, 80.5-83.5	17.01	0.528	0.515
3H-5, 95.5-98.5	20.16	0.971	0.552
4H-1, 102.5-105.5	23.73	0.510	0.478
4H-3, 83.5-86.5	26.54	0.971	0.553
4H-5, 81.5-84.5	29.52	0.603	0.556
5H-1, 81.5-84.5	33.02	0.484	0.478
5H-3, 57.5-60.5	35.78	0.566	0.561
5H-6, 71.5-74.5	40.42	0.542	0.527
6H-1, 84.5-87.5	42.55	0.618	0.581
6H-3, 61.5-64.5	45.32	0.543	0.533
6H-5, 82.5-85.5	48.53	0.586	0.560
7H-1, 94.5-97.5	52.15	0.549	0.528
7H-3, 83.5-86.5	55.04	0.566	0.540
7H-5, 81.5-84.5	58.02	0.622	0.595
8H-1, 85.5-88.5	61.56	0.537	0.511
8H-3, 73.5-76.5	64.44	0.756	0.5802
8H-5, 68.5-71.5	67.39	0.562	0.542
9H-1, 69.5-72.5	70.90	0.53	0.540
9H-3, 80.5-83.5	74.01	0.542	0.557
9H-5, 88-91	77.08	0.691	0.750
10H-1, 81.5-84.5	80.52	0.527	0.574
10H-3, 70-73	83.40	0.592	0.564
10H-5, 79.5-82.5	86.50	0.635	0.669
11H-1, 81-84	90.01	0.560	0.575
11H-3, 81.5-84.5	93.02	0.574	0.582
11H-6, 89.5-92.5	97.60	0.628	0.660
12H-1, 80.5-83.5	99.51	0.555	0.571
12H-3, 80-83	102.50	0.511	0.541
12H-5, 82-85	105.52	0.606	0.605
13H-1, 80.5-83.5	109.01	0.624	0.606
13H-3, 82.5-85.5	112.03	0.564	0.569
13H-5, 79-82	114.99	0.670	0.606
14H-1, 81-84	118.51	0.619	0.642
14H-3, 81-84	121.51	0.598	0.606
14H-5, 80-83	124.50	0.575	0.595
15H-1, 83.5-86.5	128.04	0.562	0.568

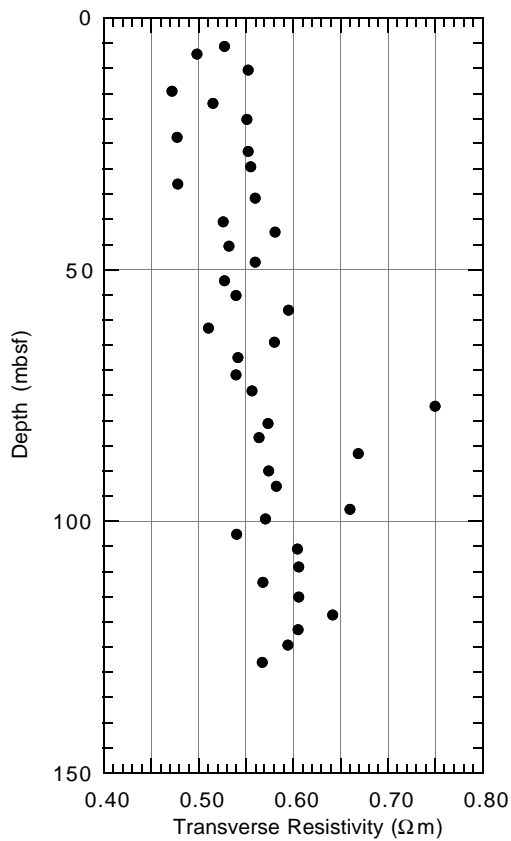


Figure 51. Sediment resistivity for Hole 1052A. Transverse resistivity measurements are considered more reliable than longitudinal measurements because planar unloading cracks that are perpendicular to the core axis bias longitudinal resistivity measurements to higher values.

Table 46. Discrete measurements of thermal conductivity for Hole 1052A.

Core, section, interval (cm)	Depth (mbsf)	Thermal conductivity (W/[m-K])
171B-1052A-		
2X-1, 89-91	4.39	1.38
2X-3, 69-71	7.19	0.34
2X-5, 69-71	10.19	1.09
3H-1, 69-71	13.89	1.04
3H-3, 69-71	16.89	1.20
3H-5, 69-71	19.89	1.11
4H-1, 69-71	23.39	1.16
4H-3, 69-71	26.39	1.11
4H-5, 69-71	29.39	1.27
5H-1, 69-71	32.89	0.90
5H-3, 69-71	35.89	0.52
5H-5, 69-71	38.89	1.24
6H-1, 69-71	42.39	1.17
6H-3, 69-71	45.39	1.24
6H-5, 69-71	48.39	1.37
7H-1, 69-71	51.89	1.12
7H-3, 69-71	54.89	1.24
7H-5, 69-71	57.89	1.19
8H-1, 69-71	61.39	1.32
8H-3, 69-71	64.39	1.21
8H-5, 69-71	67.39	1.29
9H-1, 69-71	70.89	1.27
9H-3, 69-71	73.89	1.26
9H-5, 69-71	76.89	1.29
10H-1, 69-71	80.39	1.24
10H-3, 69-71	83.39	1.23
10H-5, 69-71	86.39	1.25
11H-1, 69-71	89.89	1.20
11H-3, 69-71	92.89	1.24
11H-5, 69-71	95.89	1.20
12H-1, 69-71	99.39	1.26
12H-3, 69-71	102.39	1.28
12H-5, 69-71	105.39	1.21
13H-1, 69-71	108.89	1.22
13H-3, 69-71	111.89	1.21
13H-5, 69-71	114.89	1.30
14H-1, 69-71	118.39	0.82
14H-3, 69-71	121.39	1.23
14H-5, 69-71	124.39	1.28
15H-1, 69-71	127.89	1.23

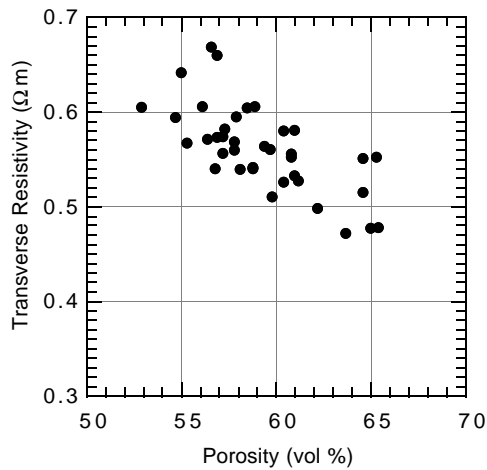


Figure 52. Comparison of transverse resistivity and sediment porosity for Hole 1052A.

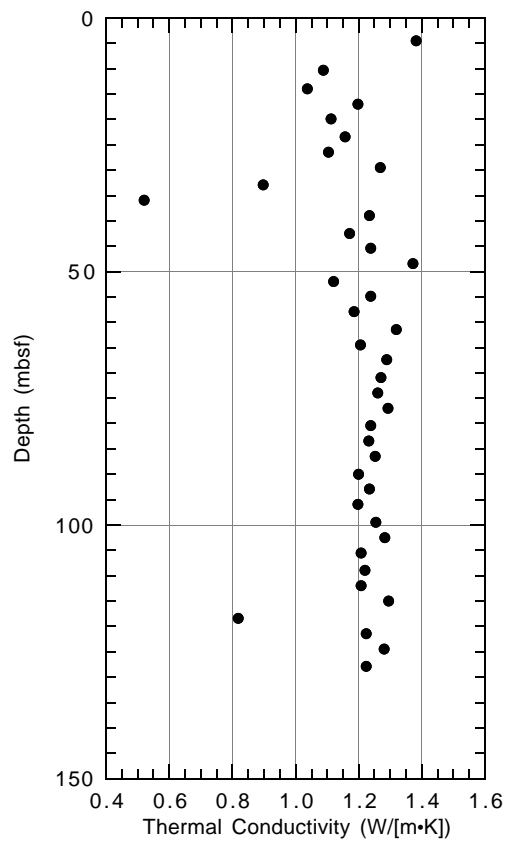


Figure 53. Thermal conductivity for Hole 1052A.

Table 47. Interval velocities for Site 1052 calculated from discrete measurements of P-wave velocity.

Depth interval (mbsf)	Interval velocity (m/s)
0-146	1605
146-215	2629
215-500	2175
500-525	2850
525-630	2200
630-660	2850

Table 48. Two-way traveltimes calculated for major lithologic features at Site 1052.

Depth (mbsf)	Two-way traveltme (s)	Lithologic feature
130	0.162	middle Eocene cherts
160	0.193	Paleocene/Eocene unconformity
215	0.234	late Paleocene claystones
300	0.32	Cretaceous/Tertiary boundary
476	0.474	Cenomanian/Maastrichtian unconformity
500-525	0.496-0.514	Top of Albian; limestone-black shale interval
630-660	0.609-0.630	late Albian clastic interbeds

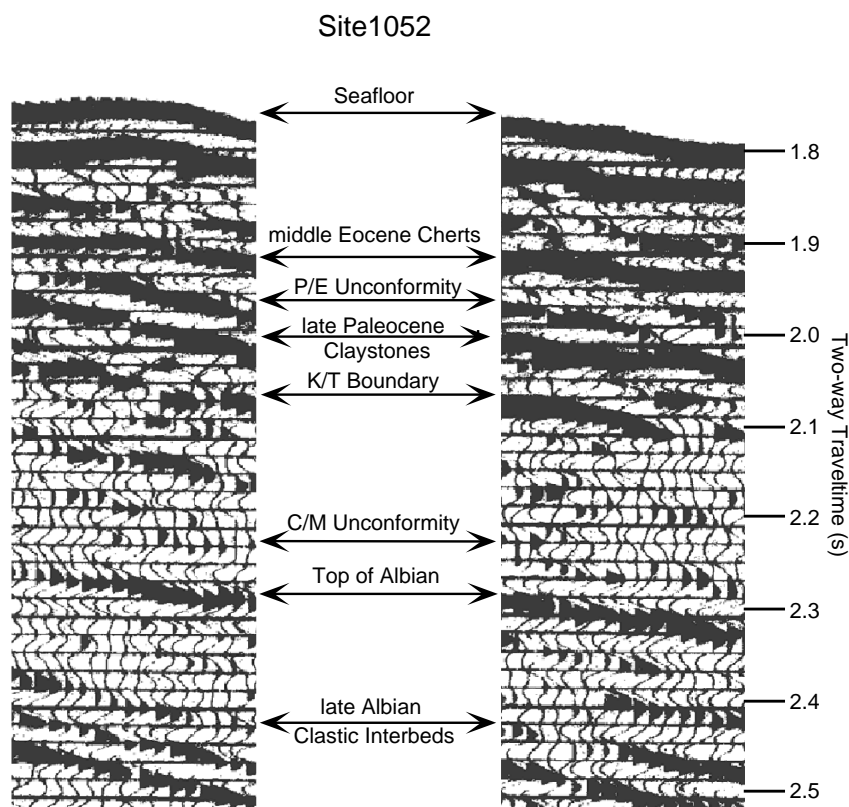


Figure 54. Major lithologic features identified on a scanned version of the seismic Line TD-5 reflection profile at Site 1052. Two-way traveltimes are from the original reflection seismic record.

Table 49. Logging operations in Hole 1052A.

Time	Operation
5 February 1997	
10:30	Triple combo assembled and prepared for logging.
11:30	Run in hole with triple combo.
12:19	Stop at mudline to equilibrate TLT.
12:22	Run down to bottom of hole (680.3 mbsf).
12:59	Stop at bottom of hole to equilibrate TLT.
13:00	Begin logging first upward pass (680.3-0 mbsf) at 1800 ft/hr.
13:56	Enter pipe (222 mbsf).
14:06	Drop back down into hole and log repeat section corresponding to the Cretaceous/Tertiary (K/T) boundary (339.5-235.7 mbsf).
14:28	Triple Combo pulled out of pipe, disassembled, and removed from rig floor.
15:15	FMS-SDT assembled and prepared for logging.
16:45	Run in hole with FMS-SDT.
17:22	Exit pipe and run down to bottom of hole (682.1 mbsf).
17:40	Begin logging first upward pass (681.3-215.2 mbsf) at 900 ft/hr.
19:11	Enter pipe.
19:13	Drop back down into hole and log K/T interval.
19:40	FMS-SDT pulled out of pipe, disassembled, and removed from rig floor.
20:45	Run in hole with GHMT.
21:40	Exit pipe and run down to bottom of hole (680 mbsf).
22:00	Begin logging first upward pass (680-215 mbsf) at 900 ft/hr.
22:36	Enter pipe.
23:44	Drop back down into hole and log K/T interval.
6 February 1997	
00:05	GHMT pulled out of pipe, disassembled, and removed from rig floor.
01:30	Rig-down finished.

Notes: Drillers total depth = 2039 mbrf (684 mbsf). Water depth = 1355 mbrf.

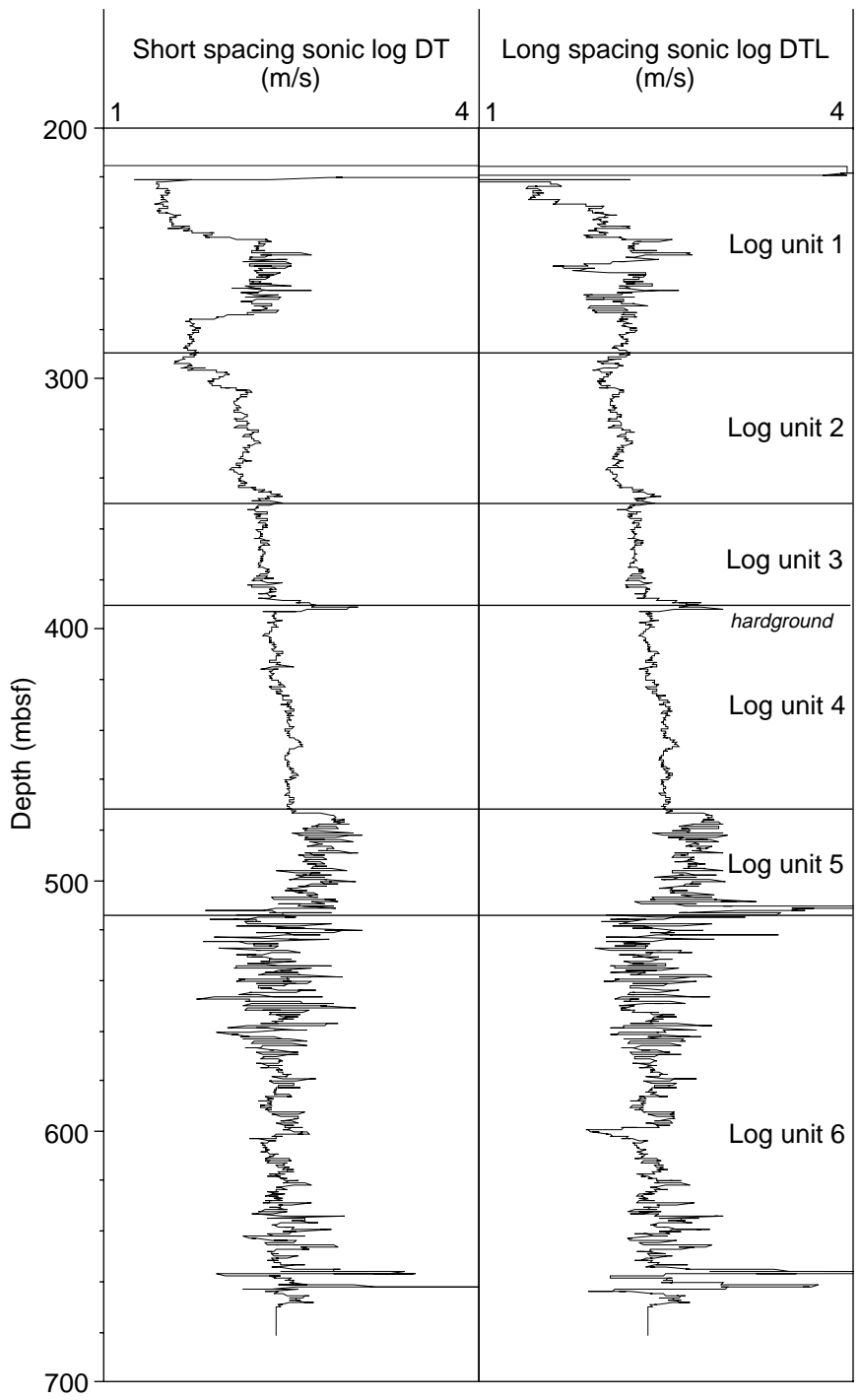


Figure 55. Comparison of short- (DT) and long- (DTL) spacing sonic logs for Hole 1052E. Lines = logging unit boundaries.

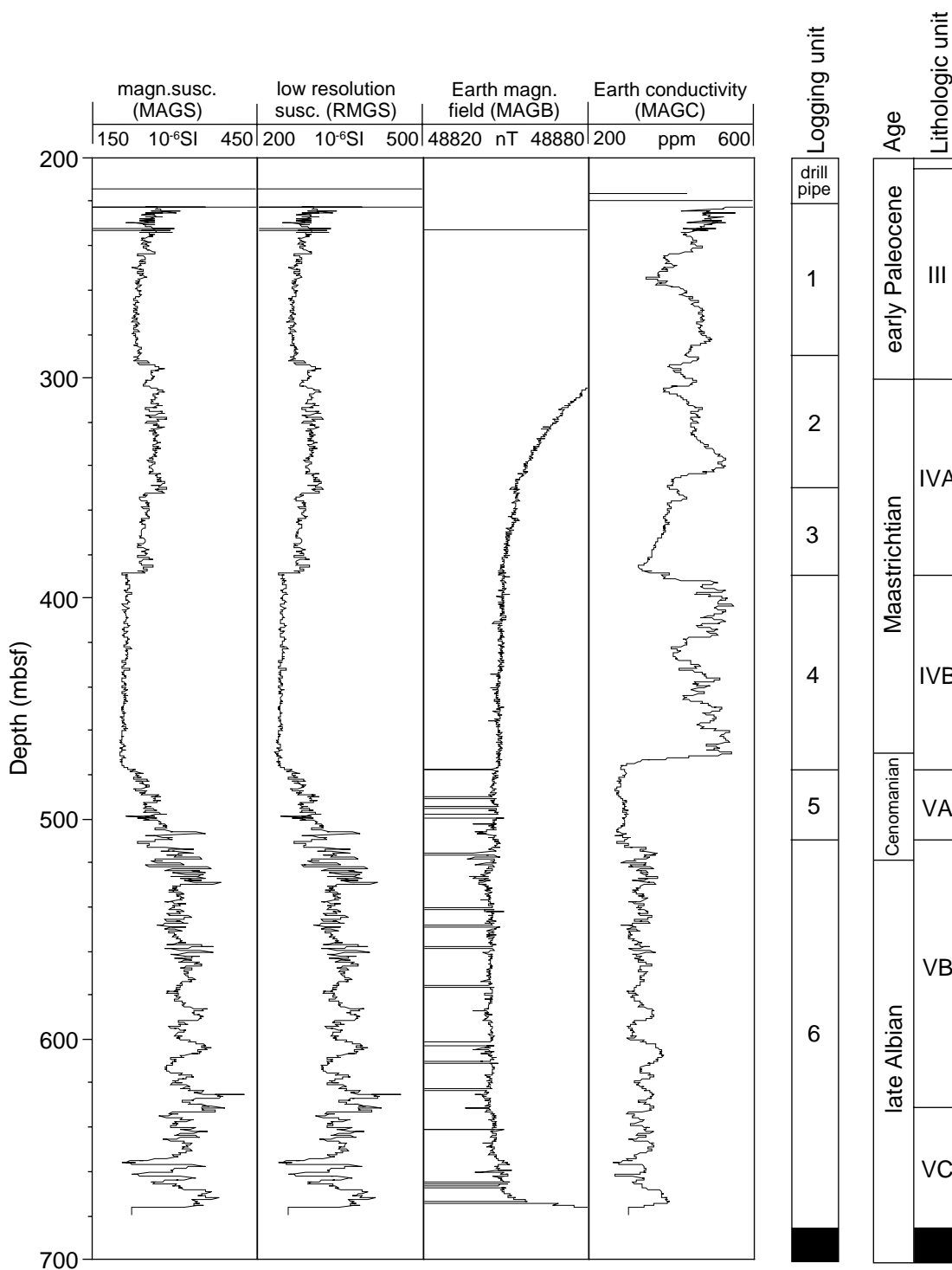


Figure 57. Selected downhole logs from the GHMT tool string for the interval 220 to 680 mbsf in Hole 1052E. From left to right, the tracks are magnetic susceptibility (MAGS), low-resolution susceptibility (RMS), Earth's magnetic field (MAGB), and Earth's conductivity (MAGC). The logging units are discussed in the "Downhole Logging" section (this chapter); the lithologic units and ages are discussed in the "Lithostratigraphy" section (this chapter).

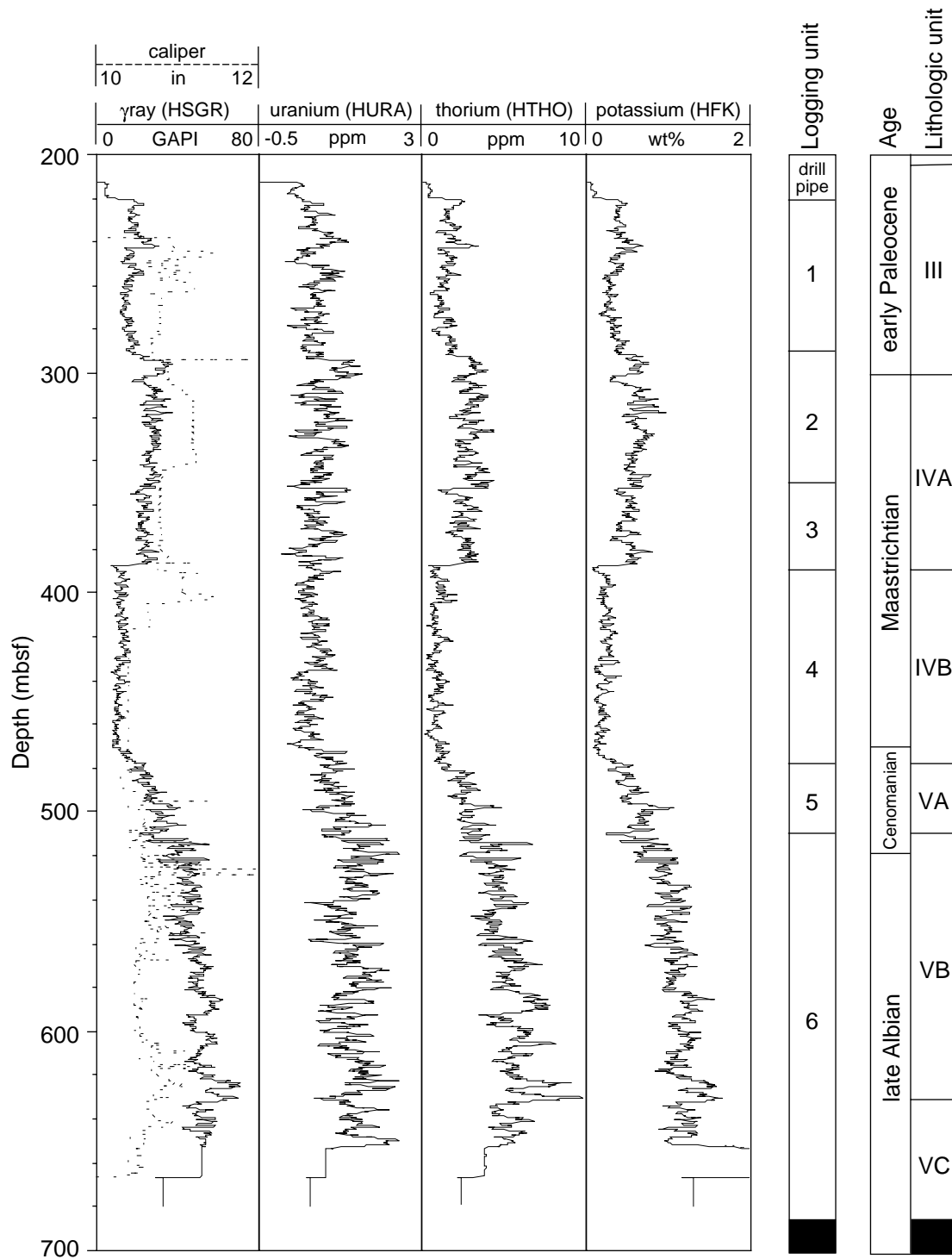


Figure 58. Spectral natural gamma-ray results for the interval 215–665 mbsf (using the HNGT tool on the triple-combo tool string), logging units, and a lithologic summary column in Hole 1052E (see “Lithostratigraphy” section, this chapter).

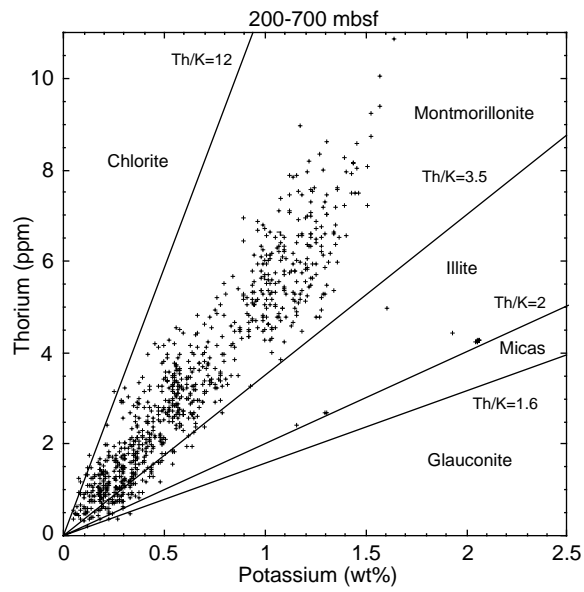


Figure 59. Identification of clay minerals as a function of thorium and potassium concentrations, as recorded by the natural gamma-ray spectrometry tool. Graph modified after Quirein et al. (1982).

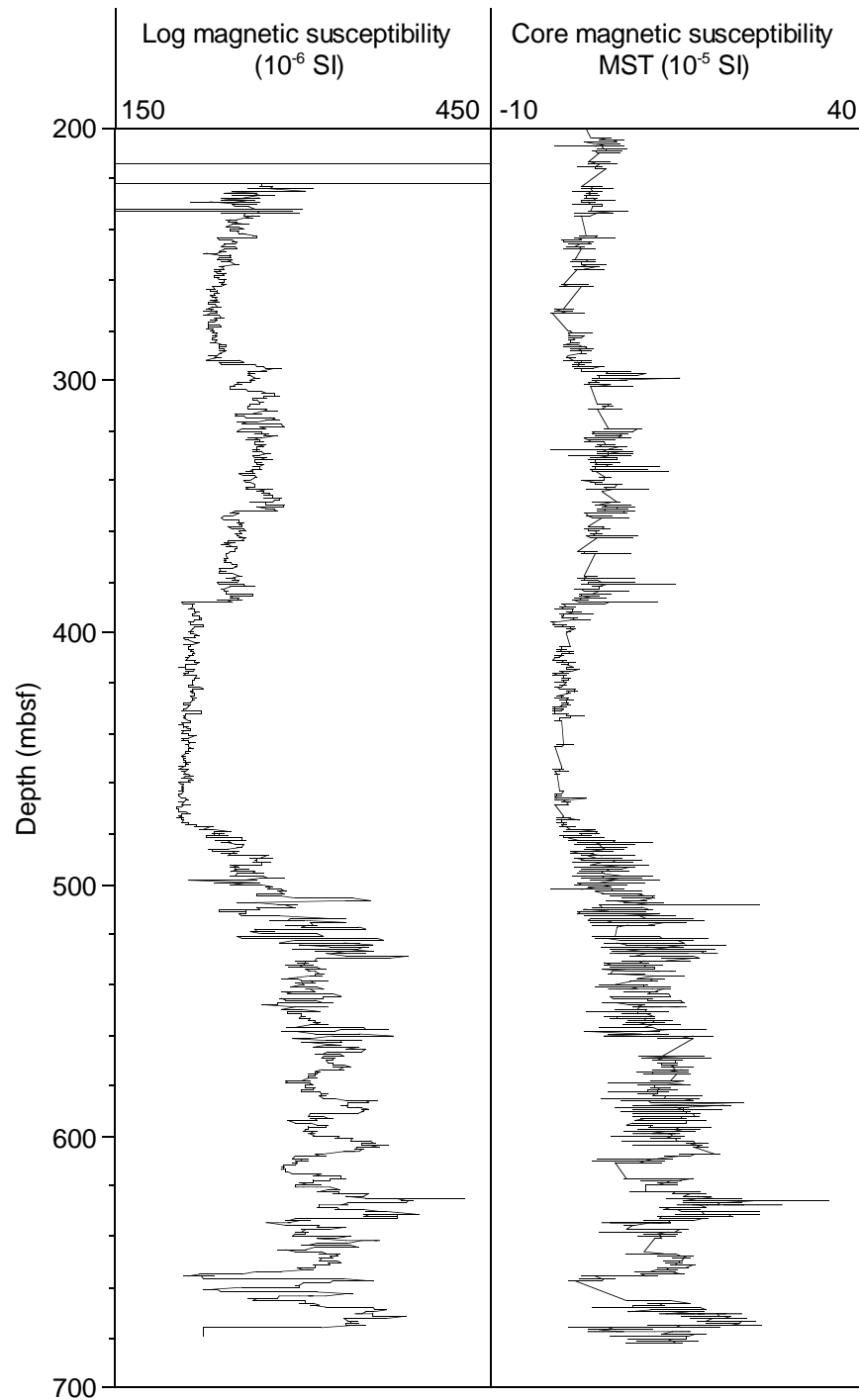


Figure 60. Comparison of log magnetic susceptibility data and discrete core susceptibility measurements (MST; see “Physical Properties” section, this chapter) for Hole 1052E.

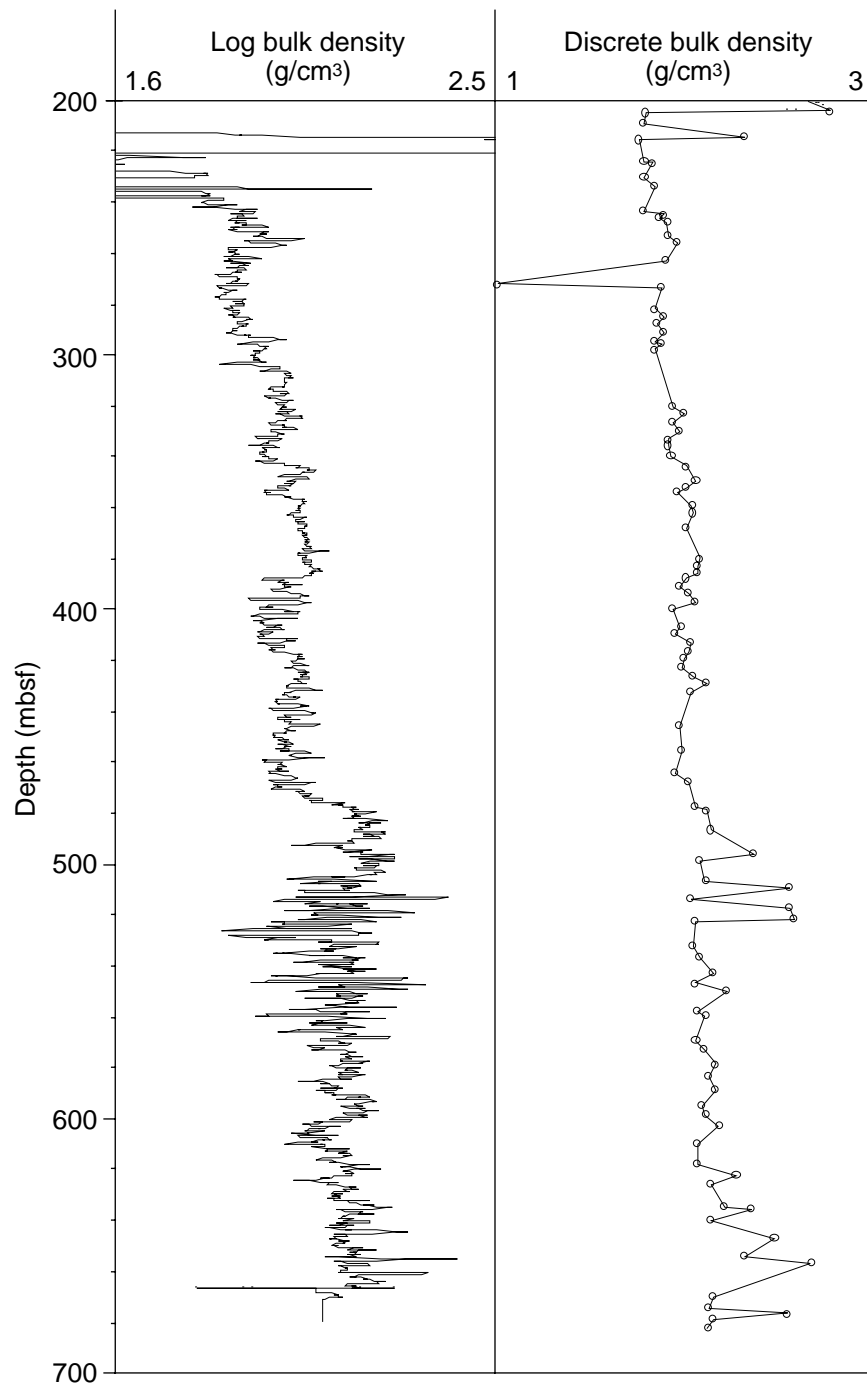


Figure 61. Comparison of log bulk density and core discrete bulk density (see "Physical Properties" section, this chapter) for Hole 1052E.

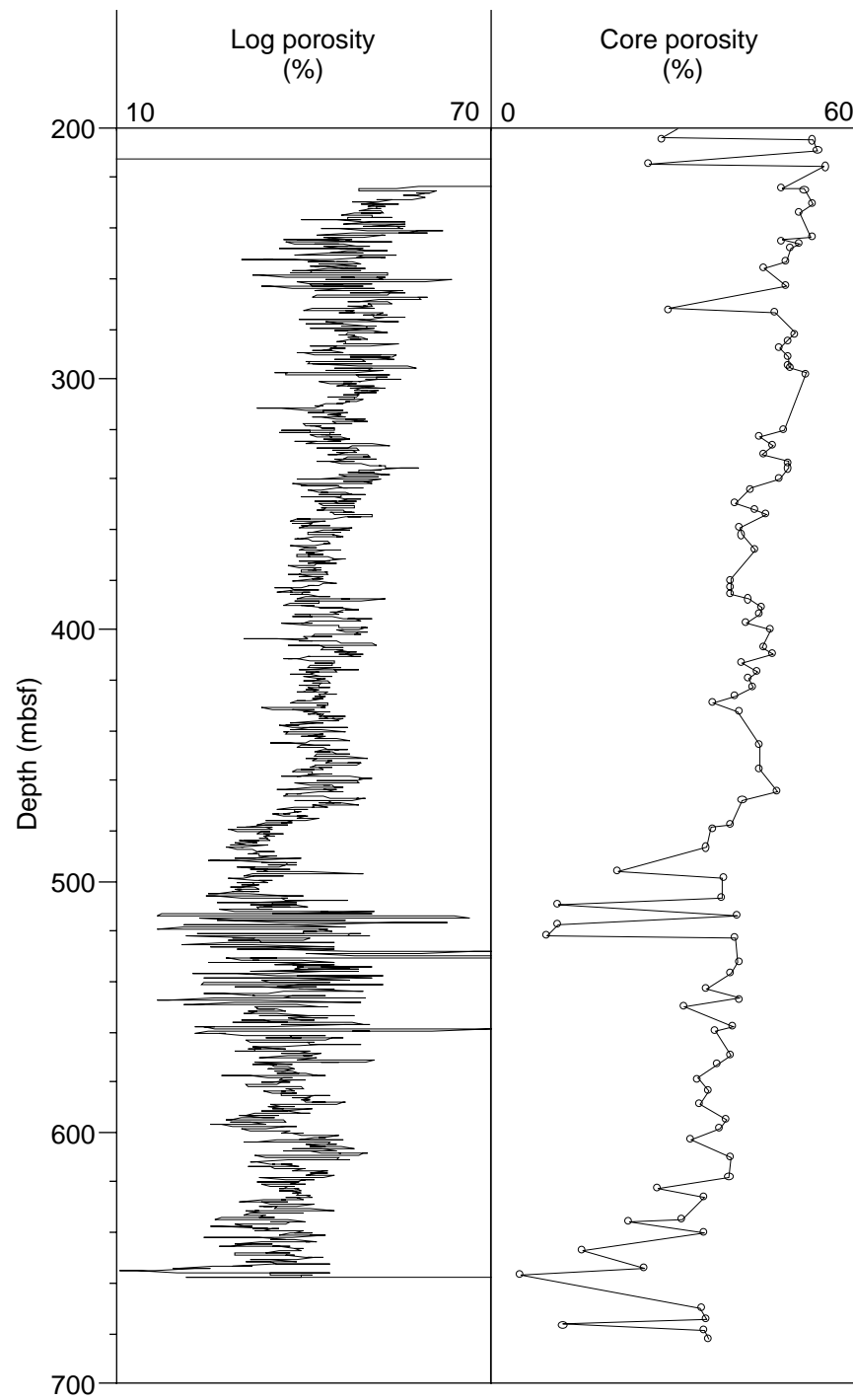


Figure 62. Comparison of log and core physical properties data. The higher variability indicated by the neutron (APLC) log is caused partly by the influence of molecular-bound water associated with clay mineral content in the Hole 1052E sediments.